Development of a Computational Framework for the Prediction of Free–Ion Activities, Ionic Equilibria and Solubility in Dairy Liquids

---

A thesis submitted in fulfilment

of the requirements for the

degree of Doctor of Philosophy

in Chemical and Process Engineering

University of Canterbury

New Zealand

Pariya Noeparvar

November 2018

ABSTRACT

The electrolytes in milk are essential as nutrients and for osmotic balance and have been well characterised at normal milk concentrations. When milk is concentrated by evaporation or reverse osmosis, the concentration of ions can easily exceed solubility limits. Hence, it seems necessary to deeply understand the ion partitioning in milk and milk–like solutions at various concentrations either at equilibrium or in a dynamic state.

An ion speciation model was proposed to comprehensively consider principal milk components such as calcium, magnesium, sodium, potassium, and hydrogen as the main cations, and citrate, phosphate, carbonate, sulphate, chloride, phosphate esters, carboxylate, and hydroxide as the main anions in serum milk. The dissociable side groups of amino acids in αs_1–, αs_2–, β–, and κ–casein were incorporated into the model as well as the calcium phosphate nanoclusters (CPN) and phosphoserine residues in the bovine casein. The saturation of potential solid salts such as calcium phosphate in different phases and calcium citrate were obtained. The Mean Spherical Approximation (MSA) method was used to calculate free–ion activity coefficients as it contained terms that enhanced accuracy at higher concentrations. Further, it allows the addition of non–electrolyte components such as lactose. This approach led to a system of over 180 non–linear equations for equilibria, electroneutrality and conservation, that were scaled and then solved using Newton's method.

The dynamic calculation of ion speciation was also implemented using Euler's method to solve differential equations for precipitation kinetics. This enabled the monitoring of pH, saturation, and the concentration of calcium salts formed over time. The model was first applied to the binary solutions of calcium chloride, sodium chloride, buffer solutions of citrate and phosphate with and without lactose, calcium carbonate, calcium phosphate, and calcium citrate solid phases, and milk serum both at equilibrium and dynamically. Moreover, the model was applied to milk as the main system including serum and casein proteins with and without CPN, for which net charge of the molecule was calculated as the means of validation. The model could satisfactorily predict pH and saturation of calcium solid salts in concentrated milk up to four times its normal concentration.

The calcium phosphate precipitation was studied experimentally at various concentrations under varied and controlled pH values. The experiments were carried out at 23 ˚C with various concentrations of calcium and phosphate solutions without and with 9.5%w/w lactose. pH was

a key factor to determine the amount of calcium phosphate precipitation. Zetasizer analysis showed that lactose strongly influenced the calcium phosphate solution by forming nanoparticles with a size of about 1 nm. The role of lactose in enabling the formation of nanoparticles was previously unknown but is likely to be an important property of milk.

ACKNOWLEDGMENTS

I would like to express my gratitude to my supervisor, Associate Professor Ken Morison, for his invaluable guidance, enthusiasm, generous support, and most importantly to develop and encourage me as a researcher in the best possible way. I am very thankful for your warm supervision throughout the journey. I am really grateful to a number of people who have helped me during my research:

- Dr Aaron Marshall for his support as postgraduate coordinator.
- CAPE technical staff, especially Glen Wilson, Stephen Beuzenberg, Michael Sandridge, Rayleen Fredericks, and Graham Furniss for their technical help and being so approachable.
- Master student Elisabeth Scheungrab from Technical University of Munich, not only for her assistance during the running of experiments, but also speaking in German language in the lab after 3 years of having no practice. She has become one of my very closest friend. Eli, thank you for your encouraging and heart–warming messages.
- CAPE undergraduate students, Hassan Ahmed and Hope Neeson, for their assistance and ideas during the experimentation.
- CAPE administrative staff, Ranee Hearst and Joanne Pollard for their kindness and help.
- To my CAPE friends, Balaji and Wasim for the funny discussions we had during the study breaks.
- Mr and Mrs Stanbury, my landlords. I really appreciate you because of being so kind and considerate. The words cannot describe my feelings to you. You are angels.
- My parents for their unconditional support and kindness. I could have never done my PhD without your love to pursue this path. Dad, wish you could remember me, call me, and sing my favourite song for your daughter. You both are always in my heart and mind.
- My sisters, Vida and Diana, my beloved niece, Andia, my brother in law, Peyman, and my families in law.

Lastly, Hani, my husband and my best friend. Thank you for your love, kindness, and patience. I love you.

Table of Contents

ABBREVIATIONS

ACP	Amorphous calcium phosphate
Ala	Alanine
Arg	Arginine
Asn	Asparagine
BMCSL	Boublik–Mansoori–Carnahan–Starling–Leyland
Asp	Aspartic acid
BSA	Bovine serum albumin
CCP	Colloidal calcium phosphate
CDA	Calcium–deficient apatite
CPN	Calcium phosphate nanoclusters
Cys	Cysteine
DCPA	Dicalcium phosphate anhydrous
DCPD	Dicalcium phosphate dihydrate
DLS	Dynamic light scattering
es	Electrostatic
EXAFS	Extended x–ray absorption fine structure
FTIR	Fourier–transform infrared spectroscopy
Gln	Glutamine
Glu	Glutamic acid
Gly	Glycine
HAP	Hydroxyapatite
His	Histidine
hs	Hard sphere
IAP	Ion activity product
IEP	Isoelectric point
Ile	Isoleucine
IM	Immunoglobulin
K_a	Association constant
K_{ac}	Acidity constant
K_d	Dissociation constant
K_{sp}	Solubility product

$K_{sp,C}$	Thermodynamic solubility product
K_w	water constant
Lact	lactate
Leu	Leucine
Lys	Lysine
MCP	Micellar calcium phosphate
Met	Methionine
MPC	Milk protein concentrate
MSA	Mean Spherical Approximation
NPMSA	Non–Primitive Mean Spherical Approximation
OCP	Octacalcium phosphate
Phe	Phenylalanine
prec	Precipitation
Pro	Proline
SAXS	Small angle x–ray scattering
SEM	Scanning electron microscope
Ser	Serine
SerP	Phosphoserine
SI	Saturation index
SMUF	Simulated milk ultrafiltrate
TCCH	Tricalcium citrate hexahydrate
TCCT	Tricalcium citrate tetrahydrate
Thr	Threonine
Trp	Tryptophan
Tyr	Tyrosine
UHT	Ultra high temperature
Val	Valine
WH	Whitlockite
XRD	X–ray powder refraction
α–la	α–lactalbumin
β–lg	β–lactoglobulin

1 Introduction

1.1 Overview

Evaporation and reverse osmosis have been widely used to concentrate raw milk by dairy producers to decrease costs of transportation from farms to factories or by factories for further processing (Grandison and Lewis, 1996). When bovine milk is concentrated by any means of concentration, the activity of ions can easily exceed solubility limits leading to fouling and changes in the solubility of the dried milk products. Hence, saturation is of great importance to avoid any undesirable precipitation of the dissolution of dried milk products.

Some of the milk minerals are soluble at concentrations below their solubility limits, although some of them such as calcium phosphate exceed their solubility limits at room temperature milk (Holt, 1997). Different phases of calcium phosphate and citrate can be formed under different conditions and it is suggested that casein micelles prevent their uncontrolled precipitation (Mekmene and Gaucheron, 2011). Hence, the ion partitioning of milk in presence of the casein micelles and other salts seem significant to determine the behaviour of casein during milk processing (Holt, 1997).

Calcium, magnesium, sodium, and potassium ions are the primary cations, and phosphate, citrate, carbonate, and chloride are the main anions in milk (Davies and White, 1960; Holt, 1997). The milk minerals distribute differently between both the serum and casein milk, i.e. about 70% of calcium, 50% of inorganic phosphate, 40% of magnesium, and 10% of citrate are partially associated to the casein micelles as undissolved ion complexes called micellar calcium phosphate (Holt, 1997; Mekmene et al., 2010). In milk serum, the minerals are present either as free ions or as ion–pairs, e.g. sodium and potassium ions have weak affinities with chloride, citrate, and inorganic phosphate, thus are mainly present as free ions. The calcium and magnesium ions form ion–pairs primarily with citrate and to a lower degree with the hydrogen phosphate ion. However, $CaHPO_4$ is calculated to be supersaturated in milk serum but precipitation is prevented by its low activity in the serum (Walstra and Jenness, 1984; Mekmene, Le Graet, et al., 2009).

The ion–pairs and free ions are in a rapid and dynamic equilibrium in milk serum, while there is a slow and dynamic salt equilibrium between both serum and casein milk (Walstra and

Jenness, 1984). The alteration of ion equilibria can alter the salts distribution and ions concentrations in both phases of milk leading to changes in the physicochemical features of the casein micelles (Walstra et al., 2006). This affects the product stability during both processing and storage. Therefore, it is very useful to deeply understand the ion partitioning in milk by considering casein and serum proteins under various conditions (Gao, 2010).

Several ion speciation models have been proposed for the ion equilibria calculation in milk and milk–like systems based on the ions interaction through the association constants. Wood et al. (1981) proposed an ion equilibria model for the calculation of milk ions concentrations. Since then, multiple computational models, which are useful for the improvement of relevant works, have been developed under various conditions by considering different components. Almost all of the models have used either Debye–Hückel or Davies theories to predict the activity coefficients of ions. The main drawback with these theories is that the activity coefficient of zero–charged species is ignored due to the presence of a charge parameter in their formulas leading to zero value for the species with zero charge.

Nevertheless, a generalised model seems essential to predict ions activity, activity coefficient, and solubility for any dairy liquid even at high concentration. The Mean Spherical Approximation (MSA) theory can determine the activity coefficient of zero–charged values by incorporating a size variable as well as charge.

Several investigations have been done on the ions equilibria calculation at equilibrium, but no model has been proposed for the dynamic prediction of ions partitioning in milk. The concentration and saturation of potential solid phases of milk can be calculated over time.

1.2 Objectives and outcomes

The main objective of this study was to improve the understanding of the ions speciation and solubility by considering almost all principal components of milk or dairy liquids, as to be able to model the milk partitioning especially at high concentration. To achieve this, another objective was to predict activity coefficients of all ions, ion–pairs, and non–electrolytes regardless of their charges.

It was hoped that the outcomes of this study provide insight into the influence of the state of the components on the properties of milk–based liquids over a range of concentration. The

results might also be helpful for the prediction of fouling in reverse osmosis, mineral precipitation in whey processing, solubility of concentrates and dried milk products in dairy industry.

1.3 Outline of thesis

A literature review is provided in Chapter 2, including the description of principal milk components and ion equilibria, in which the fundamental definitions of activity, activity coefficient, solubility, and association constants are given.

The proposed model is given in Chapter 3 for the calculation of ion equilibria both at equilibrium and dynamically. It is then applied to different systems such as the binary solutions of sodium chloride and calcium chloride, the buffer solutions of citrate and phosphate with and without lactose, the potential solid salts in milk, and milk serum. The experimental data from literature, water activity, and reproducing of other methods are used for the validation. This chapter provides the confidence to apply the model to milk in Chapter 5.

Chapter 4 covers the effect of lactose on the precipitation of calcium phosphate solutions experimentally under various and controlled pH values. Solutions of calcium chloride, sodium phosphate, and sodium hydroxide were mixed with no and 9.5%w/w lactose with Ca/P of unity, pH, and conductivity of which were measured over time to monitor the precipitation of solution. The particles size of solution was analysed by the Zetasizer instrument to determine if any nanoparticles were formed.

In Chapter 5, the proposed model is applied to different milk–like solutions by considering dissociable side groups of amino acids in the serum and casein proteins. Net charge is calculated for the solution as a mean of validation. Calcium phosphate nanoclusters (CPN) and phosphoserine residues of casein were incorporated into the model.

An overall discussion is given in Chapter 6. The conclusions and recommendation for future work are provided on Chapter 7.

2 Literature Review

2.1 Principal constituents of milk

Milk is one of the most significant foods in human history and is a complex liquid including numerous components in several states of dispersion. It can be defined as the excretion of the mammary glands of all female mammals including humans, cows, buffaloes, goats, etc. (Walstra and Jenness, 1984; Fox and McSweeney, 1998; Walstra et al., 2006). The term '*milk*' is sometimes used specifically for the healthy cow's milk, which is white, opaque, and can be a yellowish fluid especially in summer when the cows are grazed on pasture (Spreer, 1998).

The principal constituents of milk are water, lipids, sugar (lactose), proteins, and minerals, which are categorised as shown in Table 2.1. Several factors have a significant effect on the composition of milk such as lactation stage, nutritional, genetic and environmental conditions of the cow, which cause a wide change in the concentration of various minerals; however, this variation is partly due to contamination and analytical errors happening during collection, multiple processing units, and operational procedures (Flynn and Cashman, 1997). The concentrations of the main components, as well as minor constituents, differs widely for various mammals e.g. lipids, 2–55%; proteins, 1–20%; lactose, 0–10%, primarily depending on the energy needs and growth rates of the neonate. The fat and protein content of cow's milk varies among different breeds. In contrast, the osmotic pressure of milk is much more constant so the total concentrations of molecules and ions are also relatively constant (Fox, 2009).

Table 2.1 Composition of cow's milk (Walstra and Jenness, 1984).

Component	Average value in milk (%w/w)	Approximate range (%w/w)
Water	87.3	85.5–88.7
Solids excluding fat	8.8	7.9–10.0
Lactose	4.6	3.8–5.3
Protein	3.25	2.4–5.5
Casein	2.6	2.3–4.4
Mineral elements	0.65	0.53–0.80
Organic ions	0.18	0.13–0.2
Others	0.14	–
Fat	3.9	2.4–5.5

The knowledge of milk components and their influences on each other are required to understand physical characteristics, nutritive quality, and the several changes that can happen in milk (Walstra and Jenness, 1984). In addition to the major components, there are plentiful minor components such as minerals, vitamins, hormones, enzymes, and several compounds that are chemically alike in various species (Fox, 2009).

2.1.1 Lactose

2.1.1.1 General overview

The primary carbohydrate of most mammals' milk is lactose (4–*O*–β–D–galactopyranosyl–D–glucose) comprising galactose and glucose bound by a β1–4 glycosidic bond. Almost all of mammals' milk contains lactose, whose concentration can vary from zero to around 100 g L^{-1} depending on the mammal species, e.g. no lactose has been found in the milk of California sea lions and other Pacific seals (Kuhn and Low, 1949; Trucco et al., 1954; Reithel and Venkataraman, 1956; Walstra and Jenness, 1984; Holsinger, 1997; Walstra et al., 2006; Fox, 2009). There are two isomers of lactose, α and β, that are equilibrated in an aqueous solution depending on the temperature (Spreer, 1998).

Bovine milk contains lactose 4.6% (Renner, 1983; Holsinger, 1997), but several dairy products such as evaporated, condensed, and dried milk have higher quantities of lactose. Dried skim milk has 50–53% lactose, whereas the higher level of fat in dry whole milk reduces its lactose content to 36–38% (Freeley et al., 1975; Nickerson, 1978; Morrissey, 1985).

The concentration of lactose in bovine milk is affected by various factors, among which the cow's breed and health condition have the most significant impacts. The content of lactose reduces during lactation (Figure 2.1), although this trend is in contrast to the increase in fat and protein content of milk (Fox and McSweeney, 1998).

Sugars has been commonly added to foods to improve and modify physicochemical, microbial, sensorial features of food like decreasing activity of water, viscosity, texture, and softness improvement (Fennema, 1996; Lindsay, 1996). Several researchers claimed that sugars could alter properties of protein such as casein hydration, thermal stability, its surface activity (Mora-Gutierrez et al., 1997; Mora-Gutierrez and Farrell, 2000). At high concentrations of lactose or other sugars, such as in sweetened condensed milk, the stability of casein micelles can be affected by 'salt partitioning'. Accordingly, sugars such as lactose

considerably transform the ion equilibria in milk–like systems (Gao, van Leeuwen, et al., 2010).

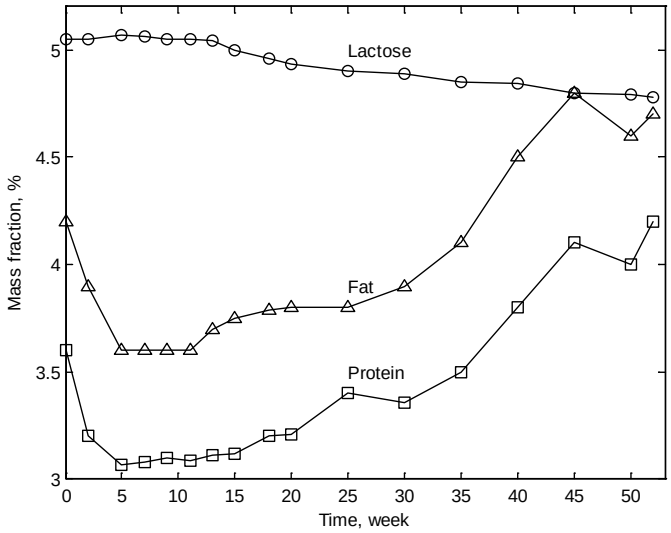

Figure 2.1 Variations of the fat, protein, and lactose concentration in the bovine milk during lactation; data from Fox and McSweeney (1998).

There are similarities between the characteristics of milk lactose and other sugars, but some of the properties of lactose are:

1. Lactose has no carbonyl group in its structure unlike most sugars; hence, it is classified as a reducing sugar (Fox, 2009).
2. Lactose has a molecular weight of 342.3 g mol^{-1}, which is small enough to contribute to activities of water and ions.
3. Lactose dissociates only to a very small extent in solution and thus does not produce a significant number of ions.
4. The properties of two lactose isomers are quite different, e.g. optical rotation and solubility (Fox, 2009).
5. Lactose can be used as a substrate for fermentation of dairy products, in which it is converted to lactic acid (Fox, 2009).

2.1.1.2 Some lactose applications in food industry

Lactose is widely used in many industries such as food and pharmaceutical industries, as an additive because of low cost, low sweetness, and good compatibility with other compounds. It has an effective role as a substrate in several fermented food products, e.g. yoghurt, but

yeast, as one of the essential ingredients of beer industry cannot ferment lactose. Hence, lactose improves mouth feel taste, and smoothness of the final product (Holsinger, 1997; Illanes et al., 2016).

Other similar applications of lactose are in the dairy industry where lactose is used as an additive for milk, in particular, skimmed milk, buttermilk, chocolate milk etc. (Reimerdes, 1990; Zadow, 1991). Cheese and casein whey used to be a waste substance given to farm animals or applied to land with water, but nowadays they are used more effectively. Lactose is crystallised in large quantities from concentrated and/or ultrafiltrated whey, which is additionally the primary source for producing different kinds of whey proteins and whey powders. About 400,000 tonnes crystals of lactose are produced annually (Holsinger, 1997; Walstra et al., 2006).

2.1.1.3 Lactose phosphate

Production of lactose containing products with high and consistent qualities has been a challenge for dairy industries where a comprehensive understanding of the production processing is sought in either long or short process such as double crystallisation of lactose or production of lactose powders from whey permeate (Zadow, 2005). Lactose phosphate was found as a contaminant in pharmaceutical grade lactose for the first time by Visser (1980), who later claimed that lactose phosphate slows down lactose crystal formation in solution (Visser, 1984, 1988). This impurity can strongly influence on the solubility of the component being crystallised preventing crystal growth. This retarding behaviour of lactose phosphate was originated by two factors, one of which is due to molecular resemblance of lactose phosphate to lactose. Another factor is that lactose phosphate acts as an anion at most of pH ranges except in very pH lower than 1 (Visser, 1988).

Some research was done on lactose phosphate mainly by Visser (1980, 1984, 1988), Pigman and Horton (1972), and Lifran (2007). Lactose phosphate has an extra monophosphate, which is the only difference between lactose and lactose phosphate in terms of structure. The phosphate group of 90% of lactose phosphate is linked to the galactose part of the lactose (Berg et al., 1988; Visser, 1988).

2.1.1.4 Lactose and calcium phosphate

Mammalian milk and milk products are able to hold calcium and phosphate ions at concentrations over 20 times greater than their solubility in water, thus enabling the key role of carrying calcium phosphate to the infants for bone growth. For over half a century it has been considered that lactose in milk does not influence the solubility of calcium phosphate (Wasserman, 1964; Guéguen and Pointillart, 2000). Lactose is known to associate with calcium (Herrington, 1934), and possibly enhances calcium absorption in the gut (Ghishan et al., 1982), but no association with calcium phosphate is known. Kezia et al. (2017) found that lactose increased the solubility of calcium and phosphate ions from calcium hydrogen phosphate dehydrate (also known as dicalcium phosphate), but they did not investigate the mechanism.

Casein micelles within milk are considered the primary carrier of calcium phosphate as amorphous nanoclusters formed by interaction with β–casein phosphopeptide (Holt et al., 1982; Holt et al., 1996; Holt, 2004). Lactose has not been considered to be involved at all. In an area closely related to this study, there has been considerable research into the chemistry of calcium and phosphate ions within simulated artificial body fluids (without lactose) for the biomimetic fabrication of bone–like materials (Posner and Betts, 1975; Dey et al., 2010; Holt et al., 2014; Park et al., 2017). It is thought that ions form nanoparticles, then clusters and solid materials but the form of the nanoparticles in these systems is still under debate (Lin and Chiu, 2017).

2.1.2 Milk fat

Milk fat is primarily composed of triacylglycerides (previous referred to as triglycerides), which are esters of glycerol (propanetriol), and monocarboxylic acids (fatty acids). Fat exists in milk as droplets, so–called milk fat globules with diameters in the range of 1–5 μm (Spreer, 1998; El-Loly, 2011). Lipids are normally soluble in nonpolar solvents and insoluble in polar ones such as water. Milk fat was in the past the most valuable component of milk, hence the value of milk paid to farmers was based on the fat content. The milk lipids have long appealed to researchers who have investigated many studies on milk fat as a complex compound with particular features (Fox and McSweeney, 1998; Fox, 2009).

Lipids exist in the milk of all mammals with various concentration of 2–50% depending on many factors such as breed, lactation stage, nutritional conditions, the animal age, health,

feed, and season within cows (Auldist et al., 1998; Fox and McSweeney, 1998; Mansson, 2008; Heck et al., 2009). The highest concentration of milk fat in cows is from Jersey cows with nearly 5% fat, whereas the lowest one is from Holstein/Friesians cows (Fox and McSweeney, 1998).

Lipids are normally categorised into two groups: neutral lipids, which are a combination of glycerol esters, mono–, di–, and triglycerides, comprise 98.5% of total milk lipids that are the main type of lipids available in all foods. Another class of lipids is polar lipids, which are a varied combination of esters of fatty acids, with either glycerol or other. Polar lipids mainly contain phosphoric acid, a nitrogen compound, or a sugar comprising about 1% of total milk lipids approximately; however, they have significant roles in milk by forming the membrane around globules of milk lipids (Fox, 2009).

2.1.2.1 Membrane of milk fat globule

Almost all of lipids are insoluble in aqueous solutions, but in milk, lipids are contained within fat globules, which are surrounded by a thin layer that is called the 'milk fat globule membrane'. The membrane comprises phospholipids, lipoproteins, cerebrosides, nucleic acids, enzymes, trace components, and water (Fox and McSweeney, 1998; Fox, 2009).

Natural milk fat globule membrane does not contain milk proteins, which are casein and whey protein; thus, the interaction between fat globules and milk protein is either weak or even noninteractive. In addition, no hydrophobic interaction can occur between the milk fat globule membrane and whey protein. Both milk fat globule membrane and casein micelles carry negative charges with pH of 6 preventing any interactions between ions (Volkov, 2001). But, Corredig and Dalgleish (1996) found that β–lactoglobulin interacts with milk fat globules at temperature higher than 65 ˚C when whole milk is either heated by UHT or direct steam injection.

2.1.3 Milk proteins

Proteins are made up of amino acids that are bound into different structures. Each amino acid has an amino (–NH_2) group and a carboxyl (–COOH) group. The α–amino acids are those whose NH_2 group is attached to the second carbon atom. Since nine amino acids cannot be formed by the human digestion system, they must be consumed for human sustenance. There is an internal transfer of a hydrogen ion from the –COOH group to the –NH_2 group to leave

an ion with both a negative charge and a positive charge. This is called a zwitterion. The electrical charge of proteins is strongly dependent on the pH of the solution and the accessibility of the free amino or carboxyl groups (Spreer, 1998). The amino acids of bovine milk can be classified by their side chains as uncharged and nonpolar such as alanine, glycine, isoleucine, leucine, methionine, phenylalanine, proline, and tryptophan; polar side chains such as asparagine, cysteine, glutamine, serine, threonine, and tyrosine; and charged side chains such as arginine, aspartic acid, glutamic acid, histidine, and lysine. Table 2.2 shows the composition of various amino acids as a proportion of total protein and of casein protein in cow's milk (Belitz and Grosch, 1999).

Table 2.2 The composition of amino acids in different protein fractions (%w/w) of bovine milk (Walstra and Jenness, 1984; Belitz and Grosch, 1999; Mekmene et al., 2010).

Amino acid	Symbol	Total protein	Whole casein
Alanine	Ala	2.53	3.21
Arginine	Arg	3.02	3.83
Asparagine	Asn	3.23	4.10
Aspartic acid	Asp	2.31	2.93
Cysteine	Cys	0.19	0.24
Glutamine	Gln	8.52	10.81
Glutamic acid	Glu	9.74	12.36
Glycine	Gly	1.48	1.88
Histidine	His	2.32	2.95
Isoleucine	Ile	4.86	6.17
Leucine	Leu	7.65	9.71
Lysine	Lys	6.45	8.19
Methionine	Met	2.47	3.13
Phenylalanine	Phe	4.30	5.45
Proline	Pro	9.25	11.74
Serine	Ser	5.63	7.15
Phosphoserine	SerP	4.06	5.16
Threonine	Thr	3.57	4.53
Tryptophan	Trp	0.97	1.23
Tyrosine	Tyr	4.85	6.16
Valine	Val	5.73	7.27

Milk can be transformed into a wide range of dairy products leading to it becoming a very important food source with proteins. Thus, in this aspect, milk proteins are likely the most significant components because of their particular features. Several investigations have been done on milk proteins since the 19th Century making them the best described among all food proteins (Fox and McSweeney, 2003; Huppertz et al., 2006). Milk proteins are classified into two categories with respect to their solubility at pH 4.6: the insoluble casein proteins

comprising around 80% of total milk proteins; and soluble whey proteins, which constitute 20% of the total (Huppertz et al., 2006).

2.1.3.1 The caseins

The caseins are a part of phosphoproteins formed in the mammary gland as quite large colloidal particles so–called '*casein micelles'*. Casein micelles are mainly composed of thousands of casein molecules, calcium ions, inorganic phosphate ions, and citrate ions. The casein micelles exist as a stable colloidal dispersion in milk, and cause the turbidity of skim milk. They can tolerate the heat up to 100 ˚C and the pressure up to 100 MPa without losing their structure and stability. Casein micelle properties, which are shown in Table 2.3, have been widely investigated by many scientists (Swaisgood, 2003; Dalgleish, 2011; Holt et al., 2013).

Table 2.3 Main physico-chemical features of the casein micelles (Broyard and Gaucheron, 2015).

Feature	Typical value
Surface area	8×10^{-14} m^2
Volume	2.1×10^{-21} m^3
Density (hydrated)	1063.2 kg m^{-3}
Mass	2.2×10^{-18} kg
Hydration	3.7 g H_2O g^{-1}
Molecular weight (hydrated)	1.3×10^9 g mol^{-1}
Molecular weight (dehydrated)	5×10^8 g mol^{-1}
Number of peptide chains	5×10^3
Number of particles per m^3 of milk	10^{20}–10^{22}
Surface of micelles per m^3 of milk	5×10^6 m^2

Caseins were first introduced as a homogenous element, but it was then presented as a two discrete parts; the calcium–sensitive caseins, which are precipitated in the presence of calcium, and the calcium–insensitive caseins (Ginger and Grigor, 1999). It is now known that casein is a combination of several individual proteins, including α_{s1}–, α_{s2}–, β–, κ–, and γ–casein, each of which has quite different features (Southward, 1986; Belitz and Grosch, 1999).

α_{s1}–casein is the main fraction of bovine milk protein that makes up around 38% of the whole casein source (Eigel et al., 1984; Fox, 2009). The B variant of α_{s1}–casein comprises a chain of peptide containing 199 amino acid residues, among which 8 phosphoserine residues are situated in positions 43–80 attached to highly polar regions of carboxyl groups. The polarity of amino acid residues 100–199 is high leading to a strong linkage; however, phosphate groups decrease the association by making repulsive forces (Belitz and Grosch, 1999).

α_{s2}–casein has a dipolar structure, anionic and cationic groups of which are located at the N– and C–terminal regions, respectively. Both α_{s1}–and α_{s2}–casein are phosphorylated peptides. In the presence of Ca^{2+}, α_{s2}–casein solubility is less than that of α_{s1}–casein (Belitz and Grosch, 1999; Broyard and Gaucheron, 2015).

β–casein is the second most plentiful protein among all the proteins in serum milk, leading to the formation of colloidal aggregates in the aqueous solution with a concentration higher than 0.5 mg mL^{-1} (Leclerc and Calmettes, 1997; Dickinson, 1999). β–casein is a peptide chain comprising 209 residues with a molar mass of 24.5 kDa. Bovine β–casein contains five phosphoserine residues, where all ionising positions of the molecule are located. The amino acid residues of β–casein are usually less hydrophobic than that of a normal globular protein and more than that of an unfolded protein. The charged and phosphorylated sites of β–casein is mostly localised at the N–terminal 21 residues, whilst the uncharged part of structure is mainly made up of the hydrophobic residues (Follows et al., 2011). The precipitation of the protein normally occur in the range of the bovine Ca^{2+} concentration (Belitz and Grosch, 1999; Ginger and Grigor, 1999).

Bovine κ–casein comprises 10% of the total casein content, and consists of 169 amino acid residues helping to increase the colloidal stability of α_{s1}–, α_{s2}–, and β–caseins by the formation of casein micelles. It can be mostly found on the outer surface of the micelle creating a hairy structure, composed of macropeptides that stretch out from the micelle. It has a key role in the stabilisation of the structure of casein micelles by making a hydrophilic coating preventing the association and the aggregation of the micelles (de Kruif, 1999; Swaisgood, 2003; Johansson et al., 2009; Palmer et al., 2013).

2.1.3.2 The serum

The precipitation of casein occurs when the pH of milk decreases to about 4.6 at 20˚C. The supernatant residue is called milk whey or serum and contains 20% of the whole milk protein (Walstra and Jenness, 1984). It is also called as 'diffusate phase' by Holt et al. (1981), whereas micellar phase sometimes referred to 'non–diffusible phase'.

Unlike caseins, the whey proteins are globular and contain more organised and consistent structures (Ng-Kwai-Hang, 2003). They are bound to each other by disulfide crosslinks. Whey proteins are more sensitive to heat than casein proteins, but are less sensitive to calcium (Kinsella, 1984).

β–lactoglobulin (β–lg), α–lactalbumin (α–la), bovine serum albumin (BSA), immunoglobulin (IM), and proteose–peptone are considered the main characterised components of the whey proteins. They represent more than 95% of the non–casein proteins (Ng-Kwai-Hang, 2003; Farrell et al., 2004). Table 2.4 shows the composition of milk serum proteins.

Table 2.4 Composition of milk serum proteins (Walstra and Jenness, 1984).

Protein	Concentration in skimmed milk, mM	Mass fraction in total protein, %w/w
β–lactoglobulin	180	9.8
α–lactalbumin	90	3.7
Bovine serum albumin	6	1.2
Immunoglobulin	4	2.1
Miscellaneous	40	2.4

β–lactoglobulin represents about 50% of the total whey protein, and 10% of the total protein of bovine milk (Creamer and Sawyer, 2003). The monomeric molecular weight of β–lactoglobulin is 18,300 Da (Kinsella, 1984). It has 162 amino acids, among which 5 cysteine residues are able to form disulphide bonds between various positions (Ng-Kwai-Hang, 2003). It can also interacts with other proteins, in particular κ–casein and α–lactalbumin (Walstra and Jenness, 1984).

Dimerisation of β–lactoglobulin normally occurs in the pH range 3.5–7.5 depending on the protein concentration, pH, temperature, and ionic strength. There are strong electrostatic repulsions at pH below 3.5 where the dimer dissociates; however, octamers are formed for

pH between 3.5–5.2. The dimer becomes stable at pH between 5.5–7.5, and unstable at pH above 8.0 where the aggregations of denatured proteins usually occur (Lyster, 1972).

The second most plentiful of the whey proteins is α–lactalbumin representing 20% of the total whey protein and 2–5% of the total skim milk protein (Wong et al., 1996). It has a compact globular structure with a molecular weight of 14,175 Da and 123 amino acids. There are 4 disulphide bonds connecting 8 cysteine residues in different positions (Kinsella, 1984; Ng-Kwai-Hang, 2003).

According to Zhang and Brew (2003), the stability and structure of α–lactalbumin is highly affected by ionic calcium (Ca^{2+}); however, the protein becomes unstable as the pH reduces due to removal of ionic calcium. Besides, α–lactalbumin has other cationic binding with other divalent ions such as Zn^{2+}, Mn^{2+}, Hg^{2+}, and Pb^{2+}.

Bovine serum albumin (BSA) is a polypeptide consisting of 582 amino acids with a molecular weight of 66,433 Da approximately. It constitutes 5% of the total bovine whey proteins (Walstra and Jenness, 1984; Haggarty, 2003). Bovine serum albumin contains 1 free thiol and 17 disulphide linkages which hold the structure as a multiloop. The function of serum albumin is probably limited in cow's milk but it can bind to metals and fatty acids (Fox and McSweeney, 1998; Ng-Kwai-Hang, 2003).

The largest and the most heterogeneous protein of the whey proteins are immunoglobulins with molecular weights over 1000 kDa. They are usually 10% of the bovine whey proteins and are available as either monomer or light and heavy polymers of polypeptide chains, which are attached by disulphide linkages leading to the immunoglobulin basic structure (Walstra and Jenness, 1984).

Lactoferrin and transferrin, β_2–microglobulin, and proteose–peptone form a small fraction of the bovine whey proteins (Walstra and Jenness, 1984).

2.1.4 Milk salts

The term '*minerals*' was previously used in the field of dairy science to describe milk salts; however, it is nowadays considered to be an incorrect word, since the minerals are not naturally occurring in the milk salts. The bovine milk salt fraction, which is 8–9 g L^{-1} of the total skimmed milk, contains several cations (calcium, magnesium, sodium, and potassium)

and anions (citrate, inorganic phosphate, chloride, carbonate, sulphate, phosphate esters, carboxylate, and hydroxide) (Holt, 1997). Table 2.5 indicates the composition of the bovine milk salts in mass and molar concentrations; however, there is a slight change in some cases among the species.

Table 2.5 The composition of the bovine milk salts (Walstra and Jenness, 1984; Gaucheron, 2005).

Milk salt	Concentration	
	mg kg^{-1}	mmol kg^{-1}
Calcium (Ca)	1042–1283	26–32
Magnesium (Mg)	97–146	4–6
Sodium (Na)	390–643	17–28
Potassium (K)	1212–1681	31–43
Citrate (Cit)	1323–2080	7–11
Inorganic phosphate (PO_4)	1804–2184	19–23
Carbonate (CO_3)	~120	~2
Sulphate (SO_4)	~96	~1
Chloride (Cl)	780–1205	22–34
Phosphate esters (Glc–1–P)	418–836	2–4
Carboxylate (RCOO)	15044–60176	1–4

The macro–elements of bovine milk are dispersed into two phases referred to as diffusible (milk serum) and non–diffusible (casein). The serum components are potassium, sodium, and chloride, whereas calcium, inorganic phosphate, and magnesium strongly interact with casein micelles, whose structure and stability are highly affected by the milk ions. Therefore, it is very useful to have a good understanding of milk salts properties (Holt, 1997; Gaucheron, 2005). Milk serum contains about 30% of the total calcium, 50% of the total inorganic phosphate, and 60% of the magnesium. A small quantity of calcium is also connected to α–lactalbumin, while the remainder is associated with the casein micelles (Hiraoka et al., 1980). According to Gaucheron (2005), the milk salts have negligible binding to lactose.

2.1.4.1 Preparation of milk serum

Dialysis, ultrafiltration, ultracentrifugation, and rennet coagulation are four common methods for segregation of the aqueous phase of milk. It is essential to control physico–chemical factors such as pH and temperature during the sample preparation, as they highly affect the salt equilibria of the phases. The results of each method can be slightly different due to the type of sample preparation, e.g. the concentration of species in the ultracentrifuge supernatant is higher than that of ultrafiltrate. This is because the ultracentrifuge supernatant contains whey proteins and soluble casein that have the ability to bind calcium and magnesium ions,

whereas the ultrafiltrate does not have the soluble proteins (Gaucheron, 2005). The method of milk serum preparation can affect experimental results.

2.1.4.2 Salt concentration and association in the milk serum

Free ions are not the only ions of the solution, but there are various associations among the ions that interact with each other depending on the association constants and the solubilities (Holt et al., 1981; Walstra and Jenness, 1984; Holt, 1985).

Generally, calcium is present in the serum as free calcium (Ca^{2+}) and several complexes mostly with trivalent citrate (Cit^{3-}) e.g. $CaCit^{-}$, to a lesser level with mono valent and divalent inorganic phosphates ($H_2PO_4^{-}$, HPO_4^{2-}), and chloride (Cl^{-}) i.e. $CaCl^{+}$. The solubility of calcium phosphate salts is rather low. Potassium and sodium are mostly available as free ions in milk serum; however, there is a small affinity with citrate, inorganic phosphate, and chloride (Gaucheron, 2005).

2.1.4.3 Micellar calcium phosphate and CPN

According to Gaucheron (2005), the casein molecules contains phosphoserine residues in their structures. The cations can mainly bind to the casein through the phosphate groups of the phosphoserine residues of the casein molecules. There is a decrease in the order of cation binding capacity of the casein proteins as α_{s2}– > α_{s1}– > β– > κ–casein due to the number of phosphoserine groups. However, the phosphoserine residues are not the only amino acid group within the casein proteins, but other amino acids existing in the milk solution can be associated to the cations, which will be discussed in the Chapter 5 in detail.

Multiple undissolved complexes named colloidal calcium phosphate (CCP) or micellar calcium phosphate (MCP) or calcium phosphate nanoclusters (CPN) constitute the salts in the casein micelles and include 70% of the total calcium, 30% of the total magnesium, 50% of the total inorganic phosphate, and 10% of the total citrate (Holt, 1997). The micellar calcium phosphate can have several compositions with various Ca/P ratios due to its complex physico–chemical properties, various crystallised forms, and a very slow thermodynamic equilibrium. The definition of micellar calcium phosphate is quite complicated because calcium is not only associated with inorganic phosphate in the casein micelles, but also has a strong affinity with phosphoserine residues. Hence, the calcium in the micellar phase can be described as a combination of calcium caseinate and calcium phosphate containing organic and inorganic

phosphate, respectively, but the composition of each cannot be calculated individually because they are inseparable. However, several approaches have been used to specify the composition, the structure, and Ca/P ratio of the micellar calcium phosphate (Gaucheron, 2005).

When the calcium phosphate matrix incorporates the bound calcium and the casein ester phosphate, it is assumed that the ratio of Ca/P is approximately 1.5 representing the tri–calcium phosphate ($Ca_3(PO_4)_2$). Brushite (DCPD, $CaHPO_4.2H_2O$) is another proposed form of micellar calcium phosphate assumed as an essential part of the calcium phosphate structure. The analyses of X–ray absorption and infrared spectroscopy were used to verify that the micellar calcium phosphate structure is similar to brushite (Gaucheron, 2005).

However, Holt (1992) suggested the dicalcium phosphate anhydrous (DCPA, $CaHPO_4$) for the brushite structure by using the solubility product of the salt.

McGann et al. (1983) and Lyster et al. (1984) proposed an amorphous structure for the micellar calcium phosphate by the methods of diffraction and high resolution transmission electron microscopy.

A chemical formula was suggested by van Dijk (1990) representing the affinity between the casein and the micellar calcium phosphate containing a couple of phosphoserine residues, 4 inorganic phosphate, and 8 divalent cations mainly calcium; however, the formula does not adapt to the existence of clusters with nanometre diameter.

Micellar calcium phosphate strongly interacts with the milk serum through calcium citrate, calcium phosphate, and negatively charged citrate and phosphate anions at the pH of milk as shown in Figure 2.2. According to Gaucheron (2005), approximately one minute is needed to exchange all calcium to the colloidal phase.

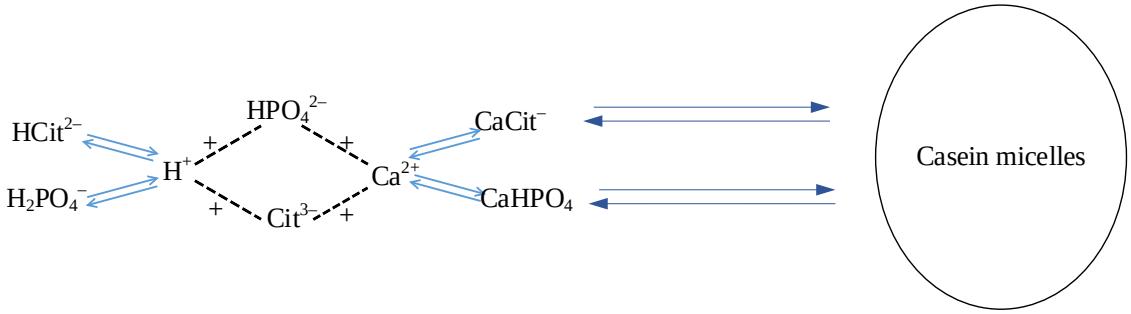

Figure 2.2 The interaction between the calcium phosphate and citrate of serum and casein micelles (Gaucheron, 2005).

Calcium phosphate nanoclusters are thought to be equilibrated particles with a certain composition, in which a shell of casein phosphopeptides with 1.6 nm thickness surrounds a core of acidic and hydrated amorphous calcium phosphate (Holt et al., 2009). The spontaneous formation of calcium phosphate nanoclusters occurs by adding the phosphopeptide to amorphous calcium phosphate, which was confirmed by several characterisation analyses. The core of calcium phosphate nanoclusters is believed to have resemblance with the micellar calcium phosphate in respect to structure, solubility, and dynamics (Holt et al., 2009). Holt et al. (1998) prepared calcium phosphate nanoclusters using 10 mg mL^{-1} of the β–casein 25–amino–acid N–terminal tryptic phosphopeptide as a stabilised component. The mathematical model estimated a spherical core of 355±20 units of dicalcium phosphate dihydrate for nanoparticles with density of 2.31 g mL^{-1} and radius of 2.30±0.05 nm covered by a shell comprising 49±4 peptide chains. They also suggested that the phosphopeptide inhibits the growth process of calcium phosphate precipitate.

Holt et al. (1996) tested the idea of calcium phosphate nanoclusters formation by a short phosphopeptide at roughly 1 mM concentration that prevent the solution from precipitating and lead to a stable phase of solution even for a supersaturated solution. The nanoparticles have been found to be stable for months.

Holt (1997) claimed that the nanoparticles composition is very similar to that of dicalcium phosphate containing tiny amounts of citrate and magnesium ions with identical solubility to that of colloidal calcium phosphate. They also found that the nanoparticles were coated by the phosphopeptides, structure of which seemed to be unclear.

Later on, the formation of nanoparticles in the preventing or reducing the precipitation of calcium phosphate was discussed by Holt (2004), and hence will add to the stability of calcium

phosphate in milk. This effect will be in addition to the role of casein in stabilising calcium phosphate in milk.

More recently, Lenton et al. (2016) applied neutron diffraction and contrast–matching methods to identify long–range order of calcium phosphate nanoparticles within phosphopeptide of milk casein and osteopontin. The results confirmed the presence of amorphous calcium phosphate in the core of nanoparticles.

It is thought that ions form nanoparticles, then clusters and solid materials but the form of the nanoparticles in these systems is still under debate (Lin and Chiu, 2017). In Chapter 4, a set of experiments was done regarding the unexpected role of lactose in the possible formation of calcium phosphate nanoparticle under varied and controlled pH and at different concentrations.

2.1.4.4 Calcium phosphate solid solutions

Calcium phosphates are formed in various amorphous and crystalline phases under different experimental conditions. The most frequent forms are categorised and shown in Table 2.6, in which some inconsistencies in the chemical formula and solubility product values were seen for different versions of calcium phosphate phases due to various conventions for ion activity product. The full description of solubility product is given in Section 2.2.5.

The precipitation of calcium phosphate are mostly dependent on temperature, phosphate and calcium concentrations, pH, and considering other ions during the precipitation (Madsen and Thorvardarson, 1984; Madsen and Christensson, 1991). Several studies have been done on the precipitation of calcium phosphate salts under different conditions using mathematical and experimental solutions.

Ferguson and McCarty (1971) studied the effect of magnesium and carbonate on calcium phosphate precipitation at the concentrations very similar to the anaerobic digestion process for phosphate removal from wastewater. They explored that the precipitation was highly influenced by magnesium and carbonate concentration, time, and pH. It was suggested that the optimum pH for phosphate removal was between 7.5 to 9.5.

Table 2.6 Calcium phosphate solid phases.

Solid phase name	Chemical formula	Ion activity product (*IAP*)	Solubility product, K_{sp}	References
Dicalcium phosphate dihydrate (brushite, DCPD)	$CaHPO_4.2H_2O$	$a_{Ca^{2+}} \times a_{HPO_4^{2-}}$	2.57×10^{-7} [mol^2 L^{-2}]	(Driessens and Verbeeck, 1990)
			1.87×10^{-7} [mol^2 L^{-2}]	(Johnsson and Nancollas, 1992)
			2.09×10^{-7} [mol^2 L^{-2}]	(Mekmene, Quillard, et al., 2009)
			1.12×10^{-7} [mol^2 L^{-2}]	(Bleek and Taubert, 2013)
Dicalcium phosphate anhydrous (monetite, DCPA)	$CaHPO_4$	$a_{Ca^{2+}} \times a_{HPO_4^{2-}}$	1.26×10^{-7} [mol^2 L^{-2}]	(Driessens and Verbeeck, 1990; Bleek and Taubert, 2013)
Octacalcium phosphate (OCP)	$Ca_8H_2(PO_4)_6.5H_2O$	$a^8_{Ca^{2+}} \times a^2_{H^+} \times a^6_{PO_4^{3-}}$	2.51×10^{-97} [mol^{16} L^{-16}]*	(Bleek and Taubert, 2013)
	$Ca_8(HPO_4)_2(PO_4)_4.5H_2O$	$a^8_{Ca^{2+}} \times a^2_{HPO_4^{2-}} \times a^4_{PO_4^{3-}}$	3.16×10^{-73} [mol^{14} L^{-14}]	(Driessens and Verbeeck, 1990)
			2.51×10^{-97} [mol^{14} L^{-14}]*	(Dorozhkin, 2014)
	$Ca_4(HPO_4)(PO_4)_2.5H_2O$	$a^4_{Ca^{2+}} \times a_{HPO_4^{2-}} \times a^2_{PO_4^{3-}}$	1.26×10^{-47} [mol^7 L^{-7}]	(Mekmene, Quillard, et al., 2009)
	$Ca_4H(PO_4)_3.5H_2O$	$a^4_{Ca^{2+}} \times a^3_{HPO_4^{2-}} \times a_{H^+}$	1.26×10^{-49} [mol^8 L^{-8}]	(Gao, van Halsema, et al., 2010)
Amorphous calcium phosphate (ACP)	$Ca_xH_y(PO_4)_z.nH_2O$; n=3–4.5	$a^x_{Ca^{2+}} \times a^y_{H^+} \times a^z_{PO_4^{3-}}$	Cannot be measured precisely	(Dorozhkin, 2014)
	$Ca_3(PO_4)_2.nH_2O$	$a^3_{Ca^{2+}} \times a^2_{PO_4^{3-}}$	1.00×10^{-26} [mol^5 L^{-5}]	(Gao, van Halsema, et al., 2010)
			1.99×10^{-33} [mol^5 L^{-5}] (pH=5) 1.26×10^{-30} [mol^5 L^{-5}] (pH=6) 1.99×10^{-33} [mol^5 L^{-5}] (pH=7.4)	(Bleek and Taubert, 2013)
Hydroxyapatite (HAP)	$Ca_{10}(PO_4)_6(OH)_2$	$a^{10}_{Ca^{2+}} \times a^6_{PO_4^{3-}} \times a^2_{OH^-}$	1.58×10^{-117} [mol^{18} L^{-18}]	(Dorozhkin, 2014)
	$Ca_5(PO_4)_3(OH)$	$a^5_{Ca^{2+}} \times a^3_{PO_4^{3-}} \times a_{OH^-}$	1.82×10^{-58} [mol^9 L^{-9}]	(McDowell et al., 1977)
Whitlockite (α–TCP)	$Ca_3(PO_4)_2$	$a^3_{Ca^{2+}} \times a^2_{PO_4^{3-}}$	3.16×10^{-26} [mol^5 L^{-5}]	(Bleek and Taubert, 2013)
	$Ca_{10}(HPO_4)(PO_4)_6$	$a^{10}_{Ca^{2+}} \times a_{HPO_4^{2-}} \times a^6_{PO_4^{3-}}$	1.99×10^{-82} [mol^{17} L^{-17}]	(Driessens and Verbeeck, 1990)
Tricalcium phosphate (β–TCP)	$Ca_3(PO_4)_2$	$a^3_{Ca^{2+}} \times a^2_{PO_4^{3-}}$	1.26×10^{-29} [mol^5 L^{-5}]	(Dorozhkin, 2014)
Calcium–deficient apatite (CDA)	$Ca_{10\text{-}x}(HPO_4)_x(PO_4)_{6\text{-}x}(OH)_{2\text{-}x}$ (0<x<1)	$a^{10-x}_{Ca^{2+}} \times a^x_{HPO_4^{2-}} \times a^{6-x}_{PO_4^{3-}}$	1.00×10^{-85}	(Dorozhkin, 2014)
	$Ca_9(HPO_4)(PO_4)_5(OH)$	$a^9_{Ca^{2+}} \times a_{HPO_4^{2-}} \times a^5_{PO_4^{3-}} \times a_{OH^-}$	7.94×10^{-86} [mol^{16} L^{-16}]	(Driessens and Verbeeck, 1990)

*Not consistent.

Boskey and Posner (1976) showed that the hydroxyapatite precipitation could occur in a relatively low supersaturation without the formation of the amorphous calcium phosphate. pH, calcium and inorganic phosphate concentrations, ionic strength and temperature are the key parameters to determine the initial precipitate in respect to the hydroxyapatite formation.

Chhettry et al. (1999) obtained the stability constants for the ion–pairs $CaH_2PO_4^+$, $CaHPO_4^\circ$, $NaHPO_4^-$, and calcium acetate ($CaAc^+$) by the Extended Debye–Hückel equation to solve the relevant equilibria of apatite dissolution systems. Dicalcium phosphate dihydrate was used as a probe to evaluate the equilibrium constants because of quick equilibration and availability of its solubility product.

Lu and Leng (2005) analysed the driving force and nucleation rate of calcium and phosphate formation in simulated body fluids by using theoretical crystallisation method. The results indicated that octacalcium phosphate has a considerable higher nucleation rate than hydroxyapatite (HAP) because of less stability of octacalcium phosphate in simulated body fluid. They also claimed that precipitation of DCPD is unlikely to occur unless calcium and phosphate concentrations increase to a higher value than the normal concentration in normal simulated body fluid.

Pan and Darvell (2009a) investigated the titration of hydroxyapatite, octacalcium phosphate, tricalcium phosphate in a 100 mmol L^{-1} KCl solution at 37 ˚C. They claimed that DCPD formation occurred above pH of 4.2, under which it can be formed a metastable phase under particular conditions. It was stated that DCPD is less stable than HAP in an acidic environment where pH is below 4.2.

Combes and Rey (2010) presented a review on fundamental formation details, physico–chemical and structure features, and characterisation of amorphous calcium phosphate. Moreover, several methods were suggested to synthesise ACP for different industrial and biomedical applications.

Lango et al. (2012) investigated dicalcium phosphate dihydrate and hydroxyapatite homogenous precipitation and seed–assisted precipitation in chloride solutions at 22 ˚C. The homogenous precipitation of DCPD was faster than that of the seed–assisted one due to low supersaturation. Calcium–deficient hydroxyapatite was formed at pH 7.6 under particular supersaturation by both methods, which were different in size of nanocrystalline and shape.

Gao, van Halsema, et al. (2010) proposed a thermodynamic model enabling ion equilibria prediction of freshly prepared and equilibrated simulated milk ultrafiltrate (SMUF) by incorporating solubility products of various calcium phosphate phases, calcium carbonate, calcium citrate, and magnesium phosphate solids. However, the model is unable to ascertain the kinetic changes for the calcium phosphate precipitation.

Holt et al. (2014) studied the precipitation of amorphous calcium phosphate in milk ultra–filtrate, artificial blood serum, urine, and saliva in terms of pH and osteopontin or casein phosphopeptide concentration. They believed that stable calcium phosphate solutions are undersaturated with amorphous calcium phosphate; however, they could be supersaturated with hydroxyapatite. A solution containing ACP nanoclusters will be stable if the saturation of solution is lower than one, or the sequestered ACP is not able to grow into larger solid particles, or there is no contact between the solution and crystalline calcium phosphate.

Kezia et al. (2017) assessed the solubility of calcium phosphate in concentrated solutions containing sodium chloride, lactose, organic acids, and anions for three different temperature. They explored that calcium activity increases by addition of more sodium chloride leading to decrease in other ions concentrations due to changes in activity coefficient values. It was stated that lactose has less but significant effect on calcium activity due to the formation of a calcium salt with lactose.

Some investigations have been conducted on the kinetics of calcium phosphate precipitation assuming conditions similar to milk solutions.

Dicalcium phosphate dihydrate, amorphous calcium phosphate, octacalcium phosphate, hydroxyapatite were formed and grown in various conditions of pH, temperature, and supersaturation (van Kemenade and de Bruyn, 1987). The kinetics of precipitation was determined by the growth rate and relaxation curve and was validated by the Ostwald rule of changes.

According to Schmidt and Both (1987), dicalcium phosphate dihydrate was obtained as the first solid phase formed in the calcium and phosphate solution at 25 and 50 ˚C in the pH range between 5.3 and 6.8.

Pouliot et al. (1991) studied the induction of amorphous calcium phosphate precipitation in cheese whey permeate using two alkalinisation methods: a simple one and the seeding combination, the second of which showed extensive crystallisation by dropping soluble calcium phosphate in the solution.

Andritsos et al. (2002) improved the crystallisation with solution aging leading to the formation of amorphous calcium phosphate followed by hydroxyapatite precipitation.

Arifuzzaman and Rohani (2004) designed a set of experiments to monitor the effect of initial calcium and phosphate concentration on the formation of solid phase, pH of solution, and distribution of particle size over time by characterisation analyses that revealed the presence of dicalcium phosphate dihydrate precipitate.

Spanos et al. (2007) and Rosmaninho et al. (2008) continued the calcium phosphate precipitation studies with mathematical modelling of simulated milk ultrafiltrate in which milk proteins was ignored. The aim of their research was to comprehend the fouling of milk in heat exchangers due to presence of calcium phosphate precipitation at 50–70 ˚C.

Mekmene, Quillard, et al. (2009) dynamically investigated the effects of calcium to phosphate ratio and constant and drifting pH on the calcium phosphate precipitation. The characterisation of precipitates ascertained the presence of brushite as the main crystalline phase followed by the formation of calcium–deficient apatite. They concluded that pH is an important parameter to determine and control the precipitation process as well as the crystalline structure of calcium phosphate precipitation.

Despite of all of this research, essential studies need to be done on this matter due several uncertainties and lack of information about the mechanism as well as the dynamic and steady state changes of calcium phosphate precipitation.

2.1.4.5 Structure of casein micelles

The large amounts of calcium phosphate and calcium citrate which are mainly bound to casein proteins help to form the structure of casein micelles. The micellar calcium phosphate was considered as the integral part of the casein micelle in all proposed models for the structure of the casein micelle (Gaucheron, 2005).

The oldest model proposed for the casein micelle molecules was presented by Waugh (1958), and later Schmidt (1982) assumed that the micellar calcium phosphate binds to a subunit structure. According to Walstra and Jenness (1984), casein micelles are composed of more diminutive submicelles which are bound to each other constantly by calcium phosphate bonds.

Horne (2003) proposed the dual–binding model, in which the polymerisation of caseins occurs via the several interactive locations in the molecules. The phosphoserine clusters in the caseins are the sites where there is a possibility to interact with calcium phosphate. The common basis of all these models was the ability of caseins to self–assemble to form micellar structures even in the absence of calcium. The protein sub–micelles are bound by the micellar calcium phosphate, which is placed at the periphery of a small sphere (sub–micelle) with the radius of 9.3 nm in both sub–micelle and the dual–binding model (Horne, 2003).

The nanocluster model, which was first presented by de Kruif and Holt (2003), was described as dispersion of the MCP in a homogeneous protein matrix as a nanogel. Phosphorylated caseins bind to the developing nanoclusters to hinder the calcification process of the mammary gland. The association of the protein tails with other proteins containing weak interactions make an almost homogeneous protein matrix. The term weak interactions expresses the hydrophobic interactions, hydrogen bonding, ion bonding, and weak electrostatic interactions (de Kruif and Grinberg, 2002; de Kruif et al., 2002; Mikheeva et al., 2003).

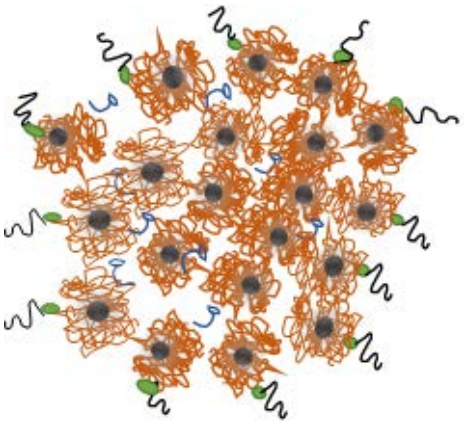

Figure 2.3 Presumptive model of casein micelles proposed after Dalgleish (2011).

The substructure of micellar calcium phosphate is very similar to that of the calcium phosphate nanoclusters, which is produced when the pH of the calcium phosphate solution and β–casein phosphopeptide 4P (f1–25) is increased up to ~ 6.7. The determinations of the

peptide nanoclusters can be done by neutron and X–ray scattering showing a nanometric calcium phosphate core covered by approximately 49 peptides producing a shell with thickness of 1.6 nm (Holt et al., 1998; de Kruif and Holt, 2003; Holt, 2004). Dalgleish (2011) proposed a model for the structure of casein micelles that described the binding of calcium phosphate nanoclusters (in black dots) to casein molecules (in orange curly shape). The outer surface has a high concentration of κ–casein with a hairy appearance shown in Figure 2.3. Water channels is shown in blue in the micelle.

2.1.5 Other milk components

The enzymes are another category of the milk components in bovine milk that are normally secreted in the secretory cells, blood, leukocytes etc. The native enzymes are localised at various regions in the cow's milk. A large amount of enzymes are correlated with the milk fat globule membrane; however, some of the enzymes are both associated with both the milk serum and the casein micelles. The milk enzymes do not seem to have a significant biological role in milk even at high concentration (Walstra et al., 2006).

A large number of milk constituents do not belong to any of the previous milk component categories having a concentration of less than 100 mg kg^{-1} (Walstra and Jenness, 1984; Walstra et al., 2006).

Carbon dioxide (CO_2), nitrogen (N_2), and oxygen (O_2) are the gases present in the milk in a very low concentrations. Carbon dioxide is associated with bicarbonate anion (HCO_3^-) in the milk solution, but the carbon dioxide concentration decreases quickly when milk is uncovered, although exposure of milk to air causes an increase in the oxygen and nitrogen concentrations. Moreover, several processes can lead to removal of carbon dioxide from the milk such as heating and vacuum stripping (Walstra and Jenness, 1984; Walstra et al., 2006).

Several trace components are present in the bovine milk in different proportions, among which zinc (Zn) is the highest one in concentration (about 3 mg kg^{-1}) having a relatively high affinity with the casein micelles. Copper is another trace element causing the autoxidation of milk fat globules. Almost 100 μg kg^{-1} of iron is found in the milk fat globule membrane (Walstra and Jenness, 1984; Walstra et al., 2006).

Other trace elements of milk with less importance are manganese (Mn), molybdenum (Mo), selenium (Se), cobalt (Co), bromine (Br), boron (B) etc. that can be variable depending on the cow's food source (Walstra and Jenness, 1984; Walstra et al., 2006).

2.2 Ion Equilibria

As mentioned in the previous section, milk serum contains both free ions as well as complexes '*ion–pairs*' that dynamically and quickly associate with each other within the aqueous phase of the milk. Although the associations among the salts of the milk serum and casein are similarly dynamic, they are relatively slow (Walstra and Jenness, 1984). The ion equilibria significantly affect the stability and the structure of casein micelles (Walstra, 1990; Horne, 1998). Any changes in the ion equilibria can lead to considerable changes in the concentration of free ions and ion–pairs within the both phases of milk. Moreover, these alterations can influence the physicochemical features of the colloidal phase as well as the products stability in various processing operations (de La Fluente, 1998; Fox and McSweeney, 1998; Huppertz and Fox, 2006). Hence, it seems necessary to determine the ion equilibria precisely in various conditions.

Generally, when a salt dissolves in water, the ions are available in various forms in solution, such as free ions, ion–pairs, or ion complexes, and undissolved species depending on the magnitude of association constant. Thus, in milk, several association and dissociation dynamic equilibria are developed with various rates depending on the activities.

There are two approaches used to determine activity coefficients and hence ion activities: free–ion and ion–pair approaches.

2.2.1 Activity based on the free–ion approach

The free–ion approach is predicated on the partial dissociation of a salt in a solvent or in a mixed solution. In other words, the salt is not totally dissociated into free ions, but also forms compounds called ion–pairs, which must be considered in the ion equilibria calculations. For example, when calcium chloride salt adds to water, it dissociates into the free ions like Ca^{2+}, Cl^{-} as well as the ion–pair $CaCl^{+}$. Although the free–ion approach does incorporate all ions into a solution including free ions and ion–pairs, it might be confusing due to the title of approach. This method was named free–ion approach, because all the ions from a dissolved salt (e.g. Na^{+} from NaCl) are free to associate independently from their initial counter ion.

The properties in a salt solution are thermodynamically specified by activities and not by concentrations (Walstra and Jenness, 1984). The activity of a free species in a solution (a_i) is defined by the mean of chemical potential depending on temperature, pressure, and salt composition in solution (Stokes, 1991):

$$\mu_i = \mu_i^\circ + RT \ln(a_i / a_i^\circ) \tag{2.1}$$

Here μ_i is chemical potential of species i in a solution; μ_i° is standard chemical potential of species i in a solution; a_i° is standard activity of species i in a solution; R is gas constant; and T is the absolute temperature in K.

The standard activity is often chosen as unity. Hence, Equation (2.1) can be rearranged as follows (Stokes, 1991):

$$\mu_i = \mu_i^\circ + RT \ln(a_i) \tag{2.2}$$

Molal activity ($a_i{}^m$) and molal concentration (m_i, moles of solute per kg of water) are generally related by the molal activity coefficient (γ_i) of species i in a solution as follows:

$$\gamma_i = \frac{a_i^m}{m_i}, \gamma_i \to 1 \; as \; m_i \to 0 \tag{2.3}$$

Molality is defined as moles of solute per kg of water (mol $kg^{-1}{}_{water}$).

$$m_i = \frac{n_i}{M_1 n_1}, \quad i = 2, C \tag{2.4}$$

Here M_1 is molar mass of water in kg mol^{-1}. Equally we could use molarity, C_i, in mol L^{-1} (or mol m^{-3}) or mole fraction, x_i.

Similarly, there is a relationship between molar activity and molar concentration (C_i, moles of solute per litre of solution) given as follows:

$$y_i = \frac{a_i^C}{C_i}, y_i \to 1 \; as \; C_i \to 0 \tag{2.5}$$

where y_i is the molar activity coefficient of species i in a solution. The activity coefficients γ_i and y_i should have the same value at equivalent concentrations, but they are often defined separately so that the basis for their calculation is clear.

Activities can have the unit of mole fraction too, so can be written in the same way:

$$f_i = \frac{a_i^x}{x_i}, f_i \to 1 \; as \; x_i \to 0 \tag{2.6}$$

Here x is mole fraction; f_i is the rational activity coefficient of species i based on mole fraction scale; $a_i{}^x$ is activity of species i based on mole fraction scale. When applied to ions some authors argue that it is not possible to measure the activity coefficient of a free ion, but the measurement of these will not concern us here.

In food systems, it would be more applicable to employ molality scale than molarity, as it is quite difficult to visualise one litre of milk products such as cheese, but molar basis can be used for solutions (van Boekel, 2008). Moreover, the molal concentration remains constant, in contrast with molar scale, when temperature varies over the time (Goel, 2006). Equilibria between the phases occurs by definition when the chemical potentials (J mol^{-1}) of the phases are equal.

Activity can be defined from chemical potential using any concentration units. By substituting Equations (2.3), (2.5), and (2.6) into the Equation (2.2), chemical potential can be written in terms of both scales (Stokes, 1991):

$$\mu_i = \mu^{\circ}_{i(m)} + RT \ln(m_i \gamma_i) \tag{2.7}$$

$$\mu_i = \mu^{\circ}_{i(C)} + RT \ln(C_i y_i) \tag{2.8}$$

$$\mu_i = \mu^{\circ}_{i(x)} + RT \ln(x_i f_i) \tag{2.9}$$

Here superscript ^{o} indicates a reference state, which can be arbitrarily chosen. The subscripts m, x, and C indicate concentration scales of molality (mol $kg^{-1}{}_{solvent}$), molarity (mol L^{-1}), and mole fraction, respectively. These equations are mathematically incorrect, as they require a logarithm of a variable with units, but there are methods of allowing this.

We can equate chemical potential and hence for a given solution:

$$\mu^{\circ}_{i(m)} + RT \ln a_i^m = \mu^{\circ}_{i(x)} + RT \ln a_i^x = \mu^{\circ}_{i(C)} + RT \ln a_i^c \tag{2.10}$$

Differentiating and dividing by RT we get

$$d \ln a_i^m = d \ln a_i^x = d \ln a_i^C \tag{2.11}$$

Now if we consider an actual change in concentration, which can be expressed as, $\Delta m_i, \Delta C_i, \Delta x_i$. It is required $\Delta \mu_i$ to be equal regardless of the activity units used. Therefore,

$$\Delta \ln a_i^m = \Delta \ln a_i^x = \Delta \ln a_i^C \tag{2.12}$$

Formally, we are considering a change from state 1 to state 2 represented by corresponding concentrations 1 and 2. Then by integrating,

$$\int_{m_1}^{m_2} dln\ a_{i,m} = \int_{x_1}^{x_2} dln\ a_{i,x} = \int_{C_1}^{C_2} dln\ a_{i,C} \tag{2.13}$$

Or in other words considering concentrations 1 and 2:

$$\ln a_{i,2}^m - \ln a_{i,1}^m = \ln a_{i,2}^x - \ln a_{i,1}^x = \ln a_{i,2}^C - \ln a_{i,1}^C \tag{2.14}$$

Hence, the activities in different units can be easily relaxed.

2.2.1.1 Setting the reference state for activity

It seems essential to set a basis for activity and activity coefficient definitions, as they are frequently used in this thesis and thus a good definition can clarify the concept. There is no requirement that the reference states are the same and hence the effective definitions of activity might be different. The reference state can essentially be defined by deciding a basis for setting an activity coefficient to 1.0. Four options are suggested here for setting a reference state:

Option 1.

It can be stated that activities represent a concentration of active component *i*:

$$a_i^x = \frac{\text{moles of active component i}}{\text{total moles in a solution}} \tag{2.15}$$

For example for pure water

$$a_i^x = \frac{\text{moles of active water}}{\text{total moles in a solution}} = \frac{\text{moles of water}}{\text{moles of water}} = 1.0 \tag{2.16}$$

If, e.g. we have a mixture of water and methanol, each component is defined as having an activity coefficient of 1.0 when it is pure.

This effectively defines the quantity of each active component. Molal and molar activity can also be expressed as

$$a_i^m = \frac{\text{moles of active component i}}{\text{kg}_{\text{water}}} \tag{2.17}$$

$$a_i^c = \frac{\text{moles of active component i}}{\text{L}} \tag{2.18}$$

It seems that this approach is normally taken for liquids and gases, for which the reference state for the chemical potential is pure component *i* at a defined pressure and temperature.

Option 2.

For electrolyte solutions, Lewis and Randall (1921) defined molal activity coefficient of the solute to be 1.0 at infinite dilution. That was because they wished it to be related to dissociation. At infinite dilution, an ionic molecule should be fully dissociated and hence it might be seen as fully active. However, the activity coefficients of many ionic molecules exceed 1.0 indicating they are not fully active at infinite dilution.

This definition seems to be common on electrolyte thermodynamics. All ion–pair activity coefficients seem to be defined on this basis.

Option 3.

For non–electrolyte solutes, Williamson (1967) used the melting point of the pure solute as the reference condition at which the activity equals 1.0. The activities of pure solute or solute in equilibrium with pure solute, at other temperatures can be found using:

$$R \ln f_i x_i = -\int_{T_m}^{T} \frac{\Delta_f H}{T^2} dT \tag{2.19}$$

where f_i is the mole fraction activity coefficient of the solute *i* in the saturated solution at temperature *T*; $\Delta_f H$ is the enthalpy change of fusion of the pure solvent; T_m is the melting point.

Option 4.

Bressan and Mathlouthi (1994) defined the activity coefficient (as mole fraction, molar or molal) of the solute to be 1 at the saturation concentration at a standard temperature. In this thesis, all of the calculations and definitions are based on Option 1.

2.2.1.2 Conversion of the scales

The aim of this section is to know the relationships between different scales of concentrations and activities in a solution expecting to have equivalent activities in the range of possible units by assuming Option 1 as reference state. Table 2.7 indicates the concentration conversion among the molar, molal, and mole fraction scales, in which the sum over *j* represents the sum of all solutes but not water.

Table 2.7 Concentration conversion of molar, molal, and mole fraction scales.

	To C_i	To m_i	To x_i
From C_i	–	$\frac{C_i/\rho_{soln}}{1-\Sigma_j C_j M_j/\rho_{soln}}$	$\frac{C_i}{\sum_j C_j}$
From m_i	$\frac{\rho_{soln} m_i}{1+\Sigma_j M_j m_j}$	–	$\frac{m_i}{1/M_1+\sum_j m_j}$
From x_i	$\frac{x_i\,\rho_{soln}}{x_1 M_1+\sum_j x_j\,M_j}$	$\frac{x_i}{M_1 x_1}=\frac{x_i}{M_1(1-\sum_j x_j)}$	–

If the density of solution (ρ_{soln}) is assumed in kg m^{-3}, then it is needed to divide by 1000 to get consistent molal activity, thus kg L^{-1} is chosen appropriate unit of density used in Table 2.7. Activities can also be converted to different scales as shown in Table 2.8.

Table 2.8 Activity conversion of molar, molal, and mole fraction scales.

	To a_i^c	To a_i^m	To a_i^x
From a_i^c	–	$\frac{a_i^C(1+\sum_j m_j M_j)}{\rho_{soln}}$	$\frac{a_i^c(x_1 M_1+\sum_j x_j M_j)}{\rho_{soln}}$
From a_i^m	$\frac{\rho_{soln} a_i^m}{1+\Sigma_j M_j m_j}$	–	$\frac{a_i^m}{\frac{1}{M_1}+\sum_j m_j}=\frac{a_i^m M_1}{1+M_1\sum_j m_j}$
From a_i^x	$\frac{a_i^x\,\rho_{soln}}{x_1 M_1+\sum_j x_j M_j}$	$\frac{a_i^x}{x_1 M_1}$	–

It is usually essential to convert free ion activity coefficients of one scale to another. For this reason, free ion activity and subsequently the free ion activity coefficient of the other scale can be obtained by multiplying the free ion activity coefficient and the concentration to get the free ion activity of the certain scale by using Table 2.8.

2.2.2 Activity based on the ion–pair approach

The ion–pair approach assumes full dissociation of a salt in a solvent. The term ion–pair is used here to refer to the pair of ions in the original solute, e.g. Ca^{2+} and Cl^{-} from $CaCl_2$. It is assumed that the ions are fully dissociated and have the same concentrations as in the solute. This approach assumes that ion–pairs, e.g. $CaCl^{+}$, do not exist in solution. Therefore, the title might be a misnomer, as the title may bring the idea that the ion–pair approach assumes ion–pairs in calculations.

It is only possible to add an electrolyte with a chemical formula of $M_{\nu_1}X_{\nu_2}$, but not an ion to a solution due to the electroneutrality requirement (Stokes, 1991; van Boekel, 2008) as follows:

$$\nu_1 z_1 = -\nu_2 z_2 \tag{2.20}$$

Here *M* and *X* represent cation and anion with charge number of z_1 and z_2; ν_1 and ν_2 are the stoichiometric number of moles of cation and anion in a one molar solution of mixed salts. Thus the total number of cations and anions moles in a one molar solution of mixed salts:

$$\nu = \nu_1 + \nu_2 \tag{2.21}$$

The chemical potential of the electrolyte $M_{\nu_1}X_{\nu_2}$ can be given by putting cation by 1 and anion by 2:

$$\mu_{M_{\nu_1}X_{\nu_2}} = \nu_1\mu_{M^{z_1}} + \nu_2\mu_{X^{z_2}} = \mu^{\circ}{}_{M_{\nu_1}X_{\nu_2}} + \nu_1 RT\ln(m_1\gamma_1) + \nu_2 RT\ln(m_2\gamma_2) \tag{2.22}$$

Here $\mu^{\circ}_{M_{\nu_1}X_{\nu_2}}$ is a combined term for the free ions. Then, it is rearranged as:

$$\mu_{M_{\nu_1}X_{\nu_2}} = \mu^{\circ}{}_{M_{\nu_1}X_{\nu_2}} + RT\ln(m_1^{\nu_1}m_2^{\nu_2}) + RT\ln(\gamma_1^{\nu_1}\gamma_2^{\nu_2}) = \mu^{\circ}{}_{M_{\nu_1}X_{\nu_2}} + \nu RT\ln(m_{\pm}\gamma_{\pm})) \tag{2.23}$$

Hence, mean molality of solution and mean ion–pair molal activity coefficient are given as:

$$m_{\pm} = \left({m_1}^{\nu_1} m_2^{\nu_2}\right)^{\frac{1}{\nu}}, \qquad \gamma_{\pm} = ({\gamma_1}^{\nu_1}{\gamma_2}^{\nu_2})^{\frac{1}{\nu}} \tag{2.24}$$

The molal activity of electrolyte $M_{\nu_1}X_{\nu_2}$ is given by using Equations (2.22) and (2.24) as follows (van Boekel, 2008):

$$a^m_{M_{\nu_1}X_{\nu_2}} = (a^m_{M^{z_1}})^{\nu_1}(a^m_{X^{z_2}})^{\nu_2} = (\gamma_{M^{z_1}})^{\nu_1}(\gamma_{X^{z_2}})^{\nu_2}(m_{M^{z_1}})^{\nu_1}(m_{X^{z_2}})^{\nu_2} \tag{2.25}$$

When the electrolyte is completely dissociated into free ions:

$$m_{M^{z_1}} = \nu_1 m_{M_{\nu_1}X_{\nu_2}}, \quad m_{X^{z_2}} = \nu_2 m_{M_{\nu_1}X_{\nu_2}} \tag{2.26}$$

By substituting Equation (2.26) into Equation (2.25):

$$a^m_{M_{\nu_1}X_{\nu_2}} = (\gamma_1)^{\nu_1}(\gamma_2)^{\nu_2}\left(\nu_1 m_{M_{\nu_1}X_{\nu_2}}\right)^{\nu_1}\left(\nu_2 m_{M_{\nu_1}X_{\nu_2}}\right)^{\nu_2} = (\gamma_1)^{\nu_1}(\gamma_2)^{\nu_2}\nu_1^{\nu_1}\nu_2^{\nu_2}\left(m_{M_{\nu_1}X_{\nu_2}}\right)^{\nu_1+\nu_2} \tag{2.27}$$

Thus, molal activity of the electrolyte can be defined by using Equations (2.25) and (2.27) as follows; however, similar equation is applicable for molar activity of the electrolyte:

$$a^m_{M_{\nu_1}X_{\nu_2}} = \nu_1^{\nu_1}\nu_2^{\nu_2}\left(\gamma_{\pm} m_{M_{\nu_1}X_{\nu_2}}\right)^{\nu_1+\nu_2} \tag{2.28}$$

The ion–pair approach has been very popular and useful for studying simple solutes in water. However, it is very difficult to extend it to multi–ion systems and hence is not used in this thesis, except when interpreting data created using this approach.

2.2.3 Water activity

In the food industry, the main solvent is water, thus the water activity is of great importance in respect to food stability (van Boekel, 2008).

The water activity of a solution can be numerically obtained by the Gibbs–Duhem relationship, in which either mean ion–pair or free ion properties can be used, but both calculations should yield similar results if they are consistent. This will be further discussed in Chapter 3.

Water activity can be expressed in terms of chemical potential. Several measurement methods such as osmotic measurements, electromotive force measurements, and ion selective electrodes can be used for estimation of activities. It is desired to ascertain how solutes can

influence water activity. The osmotic coefficient is a term by which nonideality of a solvent is specified. In other words, the osmotic coefficient can describe the deviation of the solvent from nonideality in a mixed solution (Stokes, 1991; van Boekel, 2008).

$$\phi = -\frac{\ln a_1}{M_1 \sum_k \nu_k m_k} \tag{2.29}$$

Here M_1 is molar mass of the solvent (water) in standard SI units of kg mol^{-1}, thus avoiding the need for 1000 in equations; subscript *k* represents the electrolyte.

2.2.4 Association and dissociation constants

A substance in a thermodynamically closed system proceeds through a set of metastable and unstable intermediates to reach to the lowest level of free energy. The relative partial molal free energy is a term by which the composition effect of solution on the free energy of a substance i (G_i) is expressed in an ideal solution as (Clegg and Whitfield, 1991):

$$G_i = \mu_i - \mu_i^\circ = RT \ln\left(\frac{a_i}{a_i^\circ}\right) \tag{2.30}$$

Chemical potentials are very useful for the determination of reactants and products concentrations in an equilibrated system. The overall change of the free energy (ΔG) is obtained from the subtraction of total reactants and products chemical potentials as:

$$\Delta G = \sum_i n_i \mu_i - \sum_j n_j \mu_j \tag{2.31}$$

where *n* is the moles number of the components; subscripts *i* and *j* represent the reactants and products, respectively.

The overall change of the free energy can be also shown by using the Equations (2.30) and (2.31) as follows:

$$\Delta G = \sum_i n_i \mu_i^\circ - \sum_j n_j \mu_j^\circ + RT\left(\sum_i n_i \ln a_i - \sum_j n_j \ln a_j\right) \tag{2.32}$$

It can be written $\Delta G = 0$ for the system at equilibrium:

$$\Delta G^{\circ} = \sum_i n_i \mu_i^{\circ} - \sum_j n_j \mu_j^{\circ} = -RT\left(\sum_i n_i \ln a_i - \sum_j n_j \ln a_j\right) \tag{2.33}$$

Hence, the equilibrium constant is generally defined as (Clegg and Whitfield, 1991):

$$\ln K = -\frac{\Delta G^{\circ}}{RT} \tag{2.34}$$

The dissociation and association constants are defined for the equilibria when a salt is either completely or partly dissociated to its corresponding ions or the ions are associated to its salt, respectively. For example, by the assumption of complete dissolution of a solid salt $M_{\nu_1}X_{\nu_2}$ in water, we can write (van Boekel, 2008):

$$M_{\nu_1}X_{\nu_2} \rightarrow \nu_1 M^{z_1} + \nu_2 X^{z_2} \tag{2.35}$$

Apart from the dissolved free ions remaining in the solution, some ion–pairs are formed in solution that are in a thermodynamic equilibrium with the free ions:

$$M^{z_1} + X^{z_2} \leftrightarrow MX^{(z_1+z_2)} \tag{2.36}$$

Here, there is no requirement that the ion–pair is neutral. The affinity between free ions and ion pairs is described by a term so–called '*association constant (K_a)*'(van Boekel, 2008):

$$K_a = \frac{a_{MX^{(z_1+z_2)}}}{a_{M^{z_1}} a_{X^{z_2}}} \tag{2.37}$$

Pollard (2010) defined the association constant in terms of the forward and reverse rates of Equation (2.36). The association and dissociation rate constants were then presumed equal at the equilibrium:

$$\text{binding rate} = k_+ a_{M^{z_1}} a_{X^{z_2}} = k_- a_{MX^{(z_1+z_2)}} \tag{2.38}$$

The association constant was then expressed as the ratio of forward to the reverse rate constants, or in other words, as the ratio of the product activity to the reactants activities at equilibrium with the unit of M^{-1} (Coico and Geoffrey, 2009; Pollard, 2010):

$$K_a = \frac{k_+}{k_-} = \frac{a_{MX^{(z_1+z_2)}}}{a_{M^{z_1}} a_{X^{z_2}}} \tag{2.39}$$

Similarly, the dissociation constant (K_d) is defined as the inverse of the association constant (Pollard, 2010):

$$K_d = \frac{k_-}{k_+} = \frac{a_{M^{z_1}} a_{X^{z_2}}}{a_{MX^{(z_1+z_2)}}} \tag{2.40}$$

Some authors use the terms association constant and dissociation constant without following the definitions given here.

The equilibrium constant of an acid/base system is defined as a dissociation constant (Atkins, 1990). For a standard point of view, the equilibrium for a simple acid/base system is written as follows:

$$\text{Unionised acid}_{(aq)} + \text{H}_2\text{O}_{(l)} \leftrightarrow \text{Anion} + H^+ \tag{2.41}$$

The pH of a solution by definition is:

$$\text{pH} = -\log_{10} a_{H^+} \tag{2.42}$$

The acidity constant, K_{ac}, is expressed as follows for acids:

$$K_{ac} = \frac{a_{H^+} a_{\text{Anion}}}{a_{\text{Unionised acid}}} \tag{2.43}$$

A large value of K_{ac} indicates a strong acid, e.g. the value of HCl acidity constant is quite large, hence, most of the salt dissociates to its corresponding free ions and a very tiny amount of the electrolyte remains as an undissociated ion. Lactose is a good example of weak electrolyte, which sometimes refers to a non–electrolyte with very low value of acidity constant that mostly remains as the undissociated ion in the solution.

In most of the literature, the symbol for acidity constant and association constants are the same. In this thesis, K_{ac} and K_a are used for acidity constant and association constant, respectively to avoid confusion. The acidity association constants values cover a wide range; hence, it is appropriate to use the base 10 logarithm of K_{ac}:

$$pK_{ac} = -\log_{10}(K_{ac}) \tag{2.44}$$

Equation (2.44) is combined with Equations (2.42) and (2.43) to give:

$$\mathrm{pH} = pK_{ac} + \log_{10}\frac{a_{\mathrm{Anion}}}{a_{\mathrm{Unionised\ acid}}} \tag{2.45}$$

which is also called Henderson–Hasselbach Equation.

Similarly, pK_b can be written for bases:

$$K_b = \frac{a_{OH^-}a_{Cation}}{a_{\mathrm{unionised\ acid}}} \tag{2.46}$$

And:

$$pK_b = -\log_{10}(K_b) \tag{2.47}$$

Water dissociation in aqueous solutions is expressed as:

$$K_w = a_{H^+}a_{OH^-} \tag{2.48}$$

Harned and Cook (1937) proposed a relationship between dissociation constant of water and temperature based on experiments as:

$$pK_w = -\log_{10} K_w = \frac{4787.3}{T} + 7.1321\log_{10} T + 0.010365T - 22.801 \tag{2.49}$$

At 298.15 K (25°C), pK_w is 13.9966 $\mathrm{mol}^2\ \mathrm{L}^{-2}$ but often 14 $\mathrm{mol}^2\ \mathrm{L}^{-2}$ is used.

In some literature, the term "intrinsic association constant" was used to describe the affinity between the reactants and products of equilibrium and has the same definition as association constant. According to Cruse and Lewis (2010), intrinsic association constant represents the case when a ligand is univalently bound to a special site of a protein if all sites are exactly the same. Holt et al. (1981) used the intrinsic association constant parameter using activities and not concentrations, and so the intrinsic association constant depends on the activity coefficient models. In this thesis, it is used with the same meaning as Holt et al. (1981).

2.2.5 Solubility

According to Mullin (2001), the solubility of a solid substance is described as the maximum dissolved amount of a solid substance in a solvent (water) under certain conditions. The solubility product constant, $K_{sp,}$ is a term by which the dissolution reaction is often described (Stumm and Morgan, 1996). The dissolution reaction of a solid salt can be shown as:

$$M_{\nu_1}X_{\nu_{2(s)}} \leftrightarrow \nu_1 M^{z_1} + \nu_2 X^{z_2} \tag{2.50}$$

and the solubility product constant, K_{sp}, equals the ion activity product (IAP) when the solid and ions are at equilibrium:

$$IAP = \left(a_M^{z_1}\right)^{\nu_1}\left(a_X^{z_2}\right)^{\nu_2} \tag{2.51}$$

Here *IAP* is the product chemical activities of free ions existing in the supersaturated solution.

The activity of the solid salt is not included in the solubility product equation, because the solid phase is usually presumed to be pure component with an activity of 1.0, see Section 2.2.1.1, Option 4). This might contradict with the definitions of molar, molal, and mole fraction activity shown in Equations (2.3), (2.5), and (2.6). They use different reference points and neither of the definitions is wrong.

Precipitation can happen when the *IAP* is higher than the K_{sp} of a particular salt in the aqueous phase. In contrast, dissolution occurs when the *IAP* is lower than the K_{sp}. These result in the supersaturation and undersaturation concepts and a driving force for either precipitation or dissolution. Having the knowledge of the supersaturation and undersaturation concepts is essential to predict precipitation or dissolution phenomena. The supersaturation ratio, Ω, is shown as (Mullin, 2001):

$$\Omega = \left(\frac{IAP}{K_{sp}}\right)^{\frac{1}{\nu}} = (Sat)^{\frac{1}{\nu}} \tag{2.52}$$

Here *v* is the total number of participating ions in the solid formula. The term '*Sat*' refers to saturation, which is defined as the ratio of *IAP* to K_{sp}. In some literature, the supersaturation ratio is also called the oversaturation (Mullin, 2001). Relative supersaturation is another term to describe the state of the supersaturated solution that is expressed as (Nielsen, 1984):

$$\sigma = \Omega - 1 = \left(\frac{IAP}{K_{sp}}\right)^{\frac{1}{\nu}} - 1 \tag{2.53}$$

The supersaturation value directs the equilibrium state to proceed to either precipitation or dissolution. Another parameter that can be used to determine the equilibrium state is the saturation index (*SI*):

$$SI = \log_{10} \frac{IAP}{K_{sp}} \tag{2.54}$$

For a given equilibrium containing a solid phase, one of the three below situations can occur:

- When the solution is undersaturated, i.e., the ratio of *IAP* is smaller than the K_{sp} (*SI*<0), the dissolution occurs; or
- When the solution is saturated or in equilibrium, i.e., the ratio of *IAP* equals to the K_{sp} (*SI*=0); or
- When the solution is supersaturated, i.e., the ratio of *IAP* is larger than the K_{sp} (*SI*>0), precipitation can occur (Kazadi Mbamba, 2016).

Hence, the magnitude of the *SI* as a useful parameter can establish the state of solution, but metastability and particle growth in solutions cannot be determined by the *SI* factor (Ferguson and McCarty, 1971; Reddy and Wang, 1980; Marti et al., 2008).

Nucleation is a significant process in the solid phase formation within the supersaturated solution that occurs as the first step of precipitate formation causing a basis for further precipitation to happen which is called 'growth' (Mullin, 2001).

A supersaturated solution might not precipitate even if the supersaturation ratio is larger than one (Ω>1) due to an insufficient extent of supersaturation leading to nucleation. For this case, the solution containing solid phase is metastable with the supersaturation $1< \Omega< \Omega_{\mathrm{m}}$ where Ω_{m} represents the maximum amount of supersaturation above which precipitation will always occur. Figure 2.4 shows the three potential phases of a sparingly salt of $M_{\nu_1} X_{\nu_2}$ in a solution. Nucleation can occur in the metastable solutions, and its rate increases with larger supersaturation ratio. Temperature and pH are two significant factors affecting the metastability (Mullin, 2001).

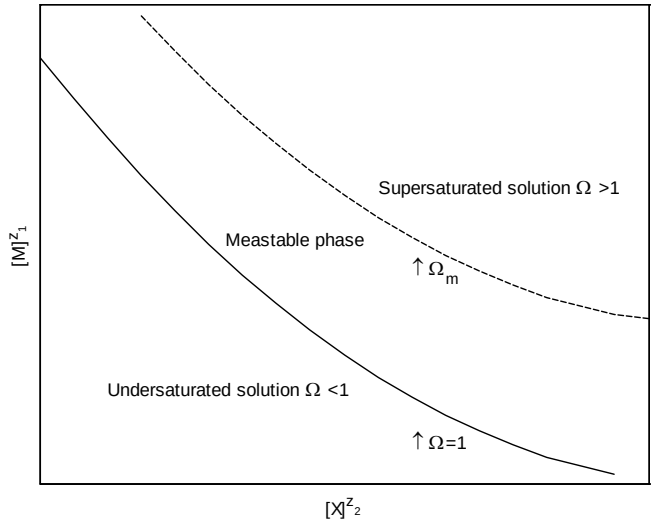

Figure 2.4 A phase scheme of a relatively insoluble salt (Kazadi Mbamba, 2016). The brackets represent the molar concentration of species.

2.2.5.1 Dynamic solubility

The precipitation or dissolution reactions of a sparingly insoluble salt can be predicted by dynamic models leading to a mathematical solution, by which the solution phase transition can be determined over time (Kazadi Mbamba, 2016).

Many researchers have worked on the solid formation mechanism of a solution by various methods (Kralj et al., 1997; Babić-Ivančić et al., 2006; Cha et al., 2013; Othman et al., 2014; Shen et al., 2014). Hanze et al. (2000) proposed a model to predict phosphate precipitation by a pseudo–equilibrium reaction, considering both precipitation and dissolution kinetic rates, in which the pH of solution is presumed neutral.

Nielsen and Toft (1984) and Wiechers et al. (1975) presented a semi–empirical kinetic rate law for a simple reaction including precipitation with a first and n^{th} orders influence on the solid phase concentration and supersaturation in the solution, respectively. The kinetic precipitation rate of the solid phase is shown as follows:

$$r_{prec} = k_{prec} C_{prec}\, \sigma^{n} \tag{2.55}$$

where r_{prec} is the rate of precipitation in mol L^{-1} h^{-1}; k_{prec} is the precipitation rate constant in h^{-1}; C_{prec} is the dynamic (time–dependent) molar concentration of precipitate; n is the order of the solid phase reaction; and σ is the relative supersaturation determines how far the solution is from precipitation or dissolution or neither. The kinetic rate law can be also

dynamically applied to dissolution (Kazadi Mbamba, 2016). The rate of precipitation becomes zero in Equation (2.55) for σ<1.

2.2.6 Activity coefficient models

Generally, association and dissociation constants pertain to activities, and only to concentrations when they are at infinite dilution. The activity coefficients of species in the solution can be significantly less than 1.0 when the molal ionic strength of the solution is larger than about 0.01 mol kg^{-1}_{water}. Several models and experimental methods have been proposed for the calculation and measurement of mean ion–pair and free ion activity coefficient. However, it is impossible to measure the activity coefficient of individual ions due to the electroneutrality principle (Gao, 2010). Hence, free ion activity coefficients need to be inferred from measurements of the same ion in multiple solutions with different counter ions.

In the following sections, various proposed models and theories are categorised based on the ion–pair and free ion approaches to be able to distinguish mean ion–pair and free ion activity coefficients.

2.2.6.1 Mean ion–pair activity coefficients models

As already discussed in Section 2.2.2, the mean ion–pair activity coefficient assumes a fully dissociated electrolyte in a solution.

Debye–Hückel theory

The Debye–Hückel theory is an empirical model, in which the electrostatic effects determine the solution deviation from non–ideality in regards to a central ion whereas other ions are considered as point charges. The general equation is a relationship between the mean molal ion–pair activity coefficient ($\gamma_{\pm}$), charge numbers of cations and anions (z_+ and z_-), and the distance of closest approach (σ, [m]) as (Zemaitis et al., 1986; van Boekel, 2008):

$$\ln \gamma_{\pm} = -\frac{|z_+ z_-| e_0^2}{8\pi\varepsilon_0\varepsilon_r k_B T} \frac{\kappa}{1+\kappa\sigma} \tag{2.56}$$

where the Debye screening parameter (κ) is defined as:

$$\kappa = \sqrt{4\pi L_B \sum_i \rho_i z_i^2} \tag{2.57}$$

Here ρ_i is the number density of component i. The Bjerrum parameter ($L_B, [\mathrm{m}]$) is the distance at which either the attractive or repulsive energies between ion charges equal to the thermal energy:

$$L_B = \frac{e_0^2}{4\pi\varepsilon_0\varepsilon_r k_B T} \tag{2.58}$$

The full details of parameters with their corresponding units are shown in Table 2.9.

Table 2.9 Full description of the Debye–Hückel parameters (van Boekel, 2008).

The Debye–Hückel parameter	The symbol	The unit in SI
Mean molal ion-pair activity coefficient	$\gamma_\pm$	Dimensionless
Charge numbers of cation and anion	z_+, z_-	Dimensionless
Boltzmann constant	k_B	1.38×10^{-23} $\mathrm{m^2 kg\, s^{-2} K^{-1}}$
Debye screening length parameter	κ	$\mathrm{m^{-1}}$
The permittivity of vacuum	ε_0	$8.854 \times 10^{-12}\,\frac{\mathrm{Farads}}{\mathrm{m}}$ or $\frac{\mathrm{C^2 s^2}}{\mathrm{m^3\ kg}}$
The elementary charge	e_0	1.602×10^{-19} coulomb
The relative permittivity of the medium*	ε_r	Dimensionless
Absolute temperature	T	K
Bjerrum parameter	L_B	m
The distance of closest approach	σ	m
The number of density of species	ρ_i	Number of particles $\mathrm{m^{-3}}$

*The old name of the relative permittivity of the medium is the dielectric constant. In this thesis, the dielectric constant is used.

Shilov and Lyashchenko (2015) extended a correlation between the dielectric constant and molar concentration of the electrolyte. However, this influence was ignored by Debye–Hückel theory, e.g. Tikanen and Fawcett (1996) and Buchner et al. (1999) showed the dependency of the dielectric constant of electrolyte with the molar concentration of sodium chloride (NaCl) and calcium chloride ($CaCl_2$) solutions as:

$$\varepsilon_{r_{NaCl}} = \varepsilon_w - 15.45C + 3.76C^{1.5} \quad (2.59)$$

$$\varepsilon_{r_{CaCl_2}} = \varepsilon_w - 34C + 10C^{1.5} \quad (2.60)$$

ε_w is dielectric constant of water which is 78.65 at 298.15 K. The density number of species and molar concentration of species i (C_i) can be expressed as (van Boekel, 2008):

$$\rho_i = 10^3 C_i \, N_{AV} \quad (2.61)$$

where N_{AV} is Avogadro's number (6.022×10^{23} mol^{-1}).

The distance of closest approach (σ or in some other literature shown as d_R) is another parameter of Debye–Hückel theory representing the sum of the interacting ions effective radii. Kielland (1937) defined it as 'the effective radii of the hydrated ions' that was estimated for various mono–, di–, and tri–valent ions. Shannon and Prewitt (1969) have carried out research on the crystal radii and the effective ionic radii. According to Debye–Hückel theory, all ions in a particular system are presumed to have identical sizes equal to the means ion diameter (van Boekel, 2008).

Debye–Hückel Limiting Law and Extended Debye–Hückel theories

The principal Debye–Hückel theory was modified relating mean molal ion–pair activity coefficient to the total molal ionic strength ($I_{m,T}$) giving the Debye–Hückel Limiting Law and the Extended Debye–Hückel equations as shown by Equations (2.62) and (2.63), respectively (van Boekel, 2008):

$$\log_{10} \gamma_{\pm} = -A_{DH} |z_+ z_-| \sqrt{I_{m,T}} \quad (2.62)$$

and

$$\log_{10} \gamma_{\pm} = -\frac{A_{DH} |z_+ z_-| \sqrt{I_{m,T}}}{1 + B_{DH} \sigma \sqrt{I_{m,T}}} \quad (2.63)$$

Lewis and Randall (1921) defined the ionic strength as a function of molal concentration and charge number of ions:

$$I_{m,T} = \frac{1}{2}\sum_i m_i z_i^2 \tag{2.64}$$

The subscripts *m* and *T* represent molal scale and total of ionic strength, respectively, due to the full dissociation of electrolyte. Equations (2.62), (2.63), and (2.64) can be similarly used for the molar scale, but they should be substituted with the total molar ionic strength ($I_{C,T}$) and mean molar ion–pair activity coefficient ($y_{\pm}$).

A_{DH} and B_{DH} are two temperature dependent parameters of the Limiting Law and Extended Debye–Hückel equations that can be used for both scales:

$$A_{DH} = \frac{\sqrt{2\pi N_{AV} \times 1000\, L_B^3}}{\ln 10} \left[\mathrm{mol}^{-\frac{1}{2}}.\mathrm{L}^{\frac{1}{2}}\right] \text{ or } \left[\mathrm{mol}^{-\frac{1}{2}}\mathrm{kg}^{\frac{1}{2}}\right] \tag{2.65}$$

$$B_{DH} = \frac{\kappa}{\sqrt{I_T}}, \left[\mathrm{mol}^{-\frac{1}{2}}.\mathrm{kg}^{\frac{1}{2}}.\mathrm{m}^{-1}\right] \text{or } [\mathrm{mol}^{-\frac{1}{2}}.\mathrm{L}^{\frac{1}{2}}.\mathrm{m}^{-1}] \tag{2.66}$$

Schmidt and Both (1987) proposed an equation for the calculation of A_{DH} in terms of temperature (˚C):

$$A_{DH} = 0.486 + 6.07 \times 10^{-4} T + 6.43 \times 10^{-6} T^2 \tag{2.67}$$

Table 2.10 indicates the values of the temperature–dependent parameters, relative permittivity, and Bjerrum length in terms of different temperature at 1 bar pressure (van Boekel, 2008).

Table 2.10 The numerical values of the Debye–Hückel equations (van Boekel, 2008).

Temperature (˚C)	$\varepsilon_r[-]$	$L_B \times 10^9[\mathrm{m}]$	A_{DH}	$B_{DH} \times 10^{-10}$
0	87.74	0.696	0.491	0.325
15	81.94	0.707	0.502	0.327
20	80.10	0.711	0.506	0.328
25	78.30	0.715	0.510	0.329
30	76.54	0.719	0.515	0.330

The effect of long–range Coulomb forces is demonstrated by the numerator of the Extended Debye–Hückel, whereas the dominator specifies the short–range interactions among the

species. Debye–Hückel theories should be used only when the solution is dilute with a maximum total molar ionic strength of 100 mmol L^{-1}. Another drawback of these theories is that the finite size of species is neglected and this causes inaccuracies when the solution becomes concentrated (Debye and Hückel, 1923; van Boekel, 2008).

Davies theory

Davies (1962) proposed an empirical extension that has been extensively applied to various systems to predict mean molal ion–pair activity coefficient. This model is a modified version of Guggenheim (1926) method, that gives a better fit to experimental values even for solutions with higher ionic strength up to 0.5 mol kg^{-1}_{water}:

$$\log_{10}\gamma_{\pm} = -A_{DH}\left(\frac{|z_+z_-|\sqrt{I_{m,T}}}{1+\sqrt{I_{m,T}}} - 0.2\, I_{m,T}\right) \tag{2.68}$$

This model has been used extensively in literature for calculation of activity coefficient because it is simple to use, requiring only concentrations and charge number of ions.

Bromley's theory

The mean molal ion–pair activity coefficient can be accurately predicted for concentrated solutions with the total molal ionic strength up to 6 mol kg^{-1}_{water} at 25 ˚C (Bromley, 1972).

$$\log_{10}\gamma_{\pm} = \frac{-A_{DH}\,|z_+z_-|\sqrt{I_{m,T}}}{1+\sqrt{I_{m,T}}} + \frac{(0.06+0.6\,B)|z_+z_-|\,I_{m,T}}{\left(1+\frac{1.5\,I_{m,T}}{|z_+z_-|}\right)^2} + BI_{m,T} \tag{2.69}$$

where B is the interaction parameter, kg mol^{-1}. Table 2.11 indicates the numerical values of B determined by the least squares methods for some electrolytes at 25˚C. The application of this model to multicomponent systems is not defined.

Table 2.11 Numerical values of B for Bromley's method at 25 ˚C (Bromley, 1972).

	HCl	$CaCl_2$	NaCl	H_2SO_4	Na_2HPO_4	NaH_2PO4
B, [kg mol^{-1}]	0.1433	0.0948	0.0574	0.0606	–0.0265	–0.0460

Pitzer theory

The Debye–Hückel theory was modified by considering the ionic strength affinity with the short–range forces influence in solutions. Pitzer (1973) included the kinetic effects of the hard core, which was not determined by the Debye–Hückel theory:

$$\ln \gamma_{\pm} = |z_+ z_-| f^{\gamma} + m B_{\pm}^{\gamma} + m^2 C_{\pm}^{\gamma} \tag{2.70}$$

Here f^{γ}, $B_{\pm}^{\gamma}$ and $C_{\pm}^{\gamma}$ are expressed by the following equations:

$$f^{\gamma} = -A_{\phi}\left[\frac{\sqrt{I_{m,T}}}{1 + b\sqrt{I_{m,T}}} + \frac{2}{b}\ln\left(1 + b\sqrt{I_{m,T}}\right)\right] \tag{2.71}$$

$$B_{\pm}^{\gamma} = 2\beta_0 + \frac{2\beta_1}{\alpha^2 I_{m,T}}\left[1 - \left(1 + \alpha\sqrt{I_{m,T}} - 0.5\alpha^2 I_{m,T}\right)\exp\left(-\alpha\sqrt{I_{m,T}}\right)\right] \tag{2.72}$$

$$C_{\pm}^{\gamma} = \frac{3}{2} C_{\pm}^{\phi} \tag{2.73}$$

The parameter A_{ϕ} is shown by the following equation:

$$A_{\phi} = \frac{1}{3}\left(\frac{e_0}{\varepsilon_r k_B T}\right)^{\frac{3}{2}} \sqrt{\frac{2\pi d_0 N_{AV}}{1000}} \tag{2.74}$$

ε_r is the dielectric constant or relative permittivity, which is dimensionless; d_0 is the solvent density, kg L^{-1}; the Pitzer constants of α and b are 2 $mol^{1/2}kg^{1/2}$ and 1.2 $mol^{1/2}kg^{1/2}$, respectively. Other numerical values of parameters in Pitzer equation are shown in Table 2.12 for some selected electrolytes.

Table 2.12 The numerical constants of Pitzer equation for some electrolytes (Pitzer, 1979).

	HCl	NaCl	CsCl	NaH_2PO_4
$\beta_0, \left[\frac{\text{kg}}{\text{mol}}\right]$	0.1775	0.0765	0.0300	–0.0533
$\beta_1, \left[\frac{\text{kg}}{\text{mol}}\right]$	0.2945	0.2664	0.0558	0.0396
$C_{\pm}^{\phi}, \left[\frac{\text{kg}}{\text{mol}}\right]^2$	0.00080	0.00127	0.00038	0.00795

Meissner's theory

Meissner and Kusik (1978) defined the reduced activity coefficient to be able to use a computational method for calculating the mean molal ion–pair activity coefficient of a pure electrolyte in a solution at 25 ˚C.

$$\Gamma^{\circ} = \gamma_{\pm}^{\frac{1}{z_+ z_-}} \tag{2.75}$$

Here $\Gamma^{\circ}$is the reduced activity coefficient:

$$\Gamma^{\circ} = \left[1 + B\left(1 + 0.1 I_{m,T}\right)^{q} - B\right]\Gamma^{*} \tag{2.76}$$

Γ^{*} and B can be obtained as follows:

$$\log_{10} \Gamma^{*} = -\frac{0.5107\sqrt{I_{m,T}}}{1 + C\sqrt{I_{m,T}}} \tag{2.77}$$

$$B = 0.75 - 0.065\, q \tag{2.78}$$

in which C has an exponential relation with the total molal ionic strength.

$$C = 1 + 0.055\, q \exp(-0.023\, I_{m,T}^{3}) \tag{2.79}$$

Numerical values of the Meissner parameter (q) are indicated in Table 2.13 for some selected electrolytes:

Table 2.13 The values of parameter q for some electrolytes at 25˚C (Meissner and Kusik, 1978).

	CsCl	HCl	NaCl	Na_2SO_4	$CaCl_2$	NaH_2PO_4
q	0.16	6.69	2.23	–0.19	2.40	–1.59

None of these ion–pair methods can be easily extended to multi–ion systems in which dissociation of the salts is not complete. Moreover, these models are approximations in the activity coefficient determination. However, much of the existing data for simple solution e.g. Zemaitis et al. (1986) is based on one or more of these mentioned equation, so they are useful for validation.

2.2.6.2 Free–ion activity coefficients models

According to Gao (2010), ion–pairs and free ions activity coefficients are also essential to account for the calculation of the ionic strength of the multicomponent solution. For example, $CaCl_2$ can exist in solution as Ca^{2+}, Cl^-, and ion–pair $CaCl^+$. Therefore, a free ion activity coefficient model will help to determine activity coefficient and hence activities of all ions in any multicomponent solution. Below are various theories for calculation of free ion activity coefficient that were proposed for different systems in different scales.

Debye–Hückel theory

The Limiting Law (Equation 2.80) and Extended Debye–Hückel (Equation 2.81) theories can be applied to both cations, anions, and ion–pairs of the multicomponent solution to obtain the molal activity coefficient of all species (Debye and Hückel, 1923):

$$\log_{10}\gamma_+ = -A_{DH}z_+^2\sqrt{I_{m,P}}; \quad \log_{10}\gamma_- = -A_{DH}z_-^2\sqrt{I_{m,P}} \tag{2.80}$$

$$\log_{10}\gamma_+ = \frac{-A_{DH}z_+^2\sqrt{I_{m,P}}}{1 + B_{DH}\sigma\sqrt{I_{m,P}}}; \quad \log_{10}\gamma_- = \frac{-A_{DH}z_-^2\sqrt{I_{m,P}}}{1 + B_{DH}\sigma\sqrt{I_{m,P}}} \tag{2.81}$$

Although the partial molal ionic strength formula ($I_{m,P}$) is apparently identical to the Equation (2.64), it involves the molal concentration and charge of free ions as well as ion–pairs. Therefore, the subscript *P* represents the partial dissociation of electrolyte.

Similarly, Debye–Hückel theories are applicable to the molarity scales.

The Limiting Law and Extended Debye–Hückel equations give good estimation of free ion activity coefficient of diluted solutions, e.g. $I_{C,P} < 10$ mM and $I_{C,P} < 100$ mM for Limiting Law and Extended Debye–Hückel theories, respectively (van Boekel, 2008).

Several authors used different numerical values for the constant parameters of Debye–Hückel, e.g. Holt et al. (1981) modified the Debye–Hückel Extended equation as follows:

$$\log_{10} y_i = \frac{-0.358\, z_i^2 \Gamma^{\frac{1}{2}}}{1 + 2.32 a \Gamma^{\frac{1}{2}}} \tag{2.82}$$

where *a* is the closest distance approach or in other words, effective size parameter, nm; Γ is the partial molar ionic strength and is defined as twice the previously defined molar ionic strength:

$$\Gamma = \sum_i C_i z_i^2 = 2I_{C,P} \tag{2.83}$$

Davies theory

The Davies theory (Davies, 1962) for the mean ion–pair activity coefficient can be similarly used for the determination of free ion activity coefficient with larger ionic strength ($I_{C,P} <$ 0.5 M) by adding a 'salting out' term to the Extended Debye–Hückel formula as:

$$\log_{10} \gamma_i = -A_{DH} \left(\frac{z_i^2 \sqrt{I_{m,P}}}{1 + \sqrt{I_{m,P}}} - 0.2\, I_{m,P} \right) \tag{2.84}$$

The Davies equation error was generally estimated to be less than 3% and 8% for the molar ionic strength less than 0.1 M and 0.5 M, respectively (Butler, 1998).

Mean Spherical Approximation theory (MSA)

The finite size of free ions is neglected in the Debye–Hückel theory resulting in the overestimation of the ion–ion interaction effects. The Mean Spherical Approximation theory (MSA) was first proposed by Lebowitz and Percus (1966) who assumed the electrolyte as a group of hard spheres constituting the corresponding anions and cations. The hard spheres are presumed to be submerged in a dielectric continuum of solvent. This theory is considered as 'primitive', because the discrete nature of the solvent molecules are neglected (Fawcett and Tikanen, 1996). The strength of MSA theory is to include the excluded volume of the ions, short and long–range interactions leading to the prediction of activity coefficient at higher concentrations (Taghikhani and Vera, 2000). Hence, MSA theory is of great interest for researchers to thermodynamically determine the properties of multicomponent electrolyte solutions that has been widely applied to ionic solutions and real solutions (Liu et al., 1998).

Waisman and Lebowitz (1972) applied the MSA theory to a symmetrical electrolyte with identical sizes of ions. A general solution of the MSA with unequal ion size was proposed and is called 'unrestricted MSA' (Blum, 1975; Blum and Høye, 1977; Sanchez-Castro and Blum, 1989). It was used to predict the mean activity coefficient of the electrolyte solutions (Triolo

et al., 1976; Triolo et al., 1977, 1978). The term 'restricted' is used when the ions size are assumed to be equal (Fawcett and Tikanen, 1996).

The calculations of the equations are based on the molarity scale; hence, in some stage, conversion of molarity to molality can be necessary. The free ion molar activity coefficient is made up of two contributions; the electrostatic contribution, '*es*', that correlates any thermodynamic property of an aqueous multicomponent solution containing hard spheres of charged ions in a dielectric continuum, and the excluded volume of free ions is incorporated into the hard sphere contribution, '*hs*' (Vilariño and Sastre de Vicente, 1999; van Boekel, 2008):

$$\ln y_i = \ln y_i^{es} + \ln y_i^{hs} \tag{2.85}$$

The ion effective diameter of the species (σ_i) is assumed unequal according to the unrestricted approach of the electrostatic contribution. The molar free ion activity coefficient of the electrostatic contribution is obtained as (van Boekel, 2008):

$$\ln y_i^{es} = -L_B \left(\frac{\Gamma z_i^2}{1 + \Gamma \sigma_i} + \varsigma \sigma_i \left(\frac{2z_i - \varsigma \sigma_i^2}{1 + \Gamma \sigma_i} + \frac{\varsigma \sigma_i^2}{3} \right)^2 \right) \tag{2.86}$$

The equation for the restricted approach for when the ions size is equal is:

$$\ln y_i^{es} = -L_B \frac{\Gamma z_i^2}{1 + \Gamma \sigma_i} \tag{2.87}$$

The parameters of this equation are listed in the Table 2.14.

Several variations are given in the literature for the electrostatic contribution of MSA theory as shown in Table 2.15. In early work, electrostatic system of units (ESU) was used. So, the quantity of $4\pi\varepsilon_0$ did not appear in the equations.

Table 2.14 The parameters of the electrostatic contribution of the MSA (van Boekel, 2008).

Parameter	The equation	Approach	SI units
Γ	$\frac{\kappa}{2}$	Unrestricted	m^{-1}
	$\frac{1}{2\sigma}\left(\sqrt{1+2\kappa\sigma}-1\right)$	Restricted	m^{-1}
σ	$\frac{\sigma_{cation}+\sigma_{anion}}{2}$	both	m
κ	$\sqrt{4\pi L_B \sum_i \rho_i z_i^2}$	both	m^{-1}
ρ_i	$10^3 c_i N_{AV}$	both	$\frac{\text{Number of particles}}{m^3}$
ς	$\frac{\pi}{2\Omega\Delta}\sum_i \frac{\rho_i \sigma_i z_i}{1+\Gamma\sigma_i}$	Unrestricted	m^{-2}
Ω	$1+\frac{\pi}{2\Delta}\sum_i \frac{\rho_i \sigma_i^3}{1+\Gamma\sigma_i}$	Unrestricted	[−]
Δ	$1-\frac{\pi}{6}\sum_i \rho_i \sigma_i^3$	Unrestricted	[−]

Table 2.15 Variations in the electrostatic contribution of MSA.

Free ion activity coefficient of the electrostatic contribution	Reference
$\ln y_i^{es} = -L_B\left(\frac{\Gamma z_i^2}{1+\Gamma\sigma_i}+\varsigma\sigma_i\left(\frac{2z_i-\varsigma\sigma_i^2}{1+\Gamma\sigma_i}+\frac{\varsigma\sigma_i^2}{3}\right)^2\right)$	(van Boekel, 2008)
$\ln y_i^{es} = -L_B\left[\frac{\Gamma z_i^2}{1+\Gamma\sigma_i}+\varsigma\sigma_i\left(\frac{2z_i-\varsigma\sigma_i^2}{1+\Gamma\sigma_i}+\frac{\varsigma\sigma_i^2}{3}\right)\right]-\frac{L_B}{4\pi\varepsilon_0\varepsilon_r}\sum_i \rho_i z_i N_i \frac{\partial\varepsilon_r}{\partial\rho_i}$; where $N_i=\frac{\Gamma z_i+\varsigma\sigma_i}{1+\Gamma\sigma_i}$	(Fawcett et al., 1977)
$\Delta\ln y_i^{es} = -\frac{\beta e_0^2}{\varepsilon_r}\left[\frac{\Gamma z_i^2}{1+\Gamma\sigma_i}+\varsigma\sigma_i\left(\frac{2z_i-\varsigma\sigma_i^2}{1+\Gamma\sigma_i}+\frac{\varsigma\sigma_i^2}{3}\right)\right]+\sum_j \rho_j q_j\left[\frac{\partial\sigma_j}{\partial\rho_j}\right]+\frac{e_0^2\sum_i \rho_i z_i N_i}{k_B T \varepsilon_r^2}\left[\frac{\partial\varepsilon_r}{\partial\rho_i}\right]$*, where $q_j=\frac{\beta e_0^2}{\varepsilon_r}\left[\frac{\Gamma^2 z_j^2}{(1+\Gamma\sigma_j)^2}+\varsigma\frac{\varsigma\sigma_j^2\left(2-\Gamma^2\sigma_j^2\right)-2z_j}{(1+\Gamma\sigma_j)^2}\right]$;	(Simonin et al., 1996)

* This equation is in ESU units.

Mansoori et al. (1971) presented an equation of state for a multicomponent mixture of hard spheres to determine molar free ion activity coefficient of hard sphere contribution so–called 'Boublik–Mansoori–Carnahan–Starling–Leyland (BMCSL)':

$$\ln y_i^{hs} = -\ln(1 - X_3) + \sigma_i F_1 + \sigma_i^2 F_2 + \sigma_i^3 F_3 \tag{2.88}$$

where

$$X_n = \frac{\pi}{6} \sum_i \rho_i \sigma_i^n \tag{2.89}$$

$$F_1 = \frac{3X_2}{1 - X_3} \tag{2.90}$$

$$F_2 = \frac{3X_1}{1 - X_3} + \frac{3X_2^2}{X_3(1 - X_3)^2} + \frac{3X_2^2}{X_3^2} \ln(1 - X_3) \tag{2.91}$$

$$F_3 = \left(X_0 - \frac{X_2^3}{X_3^2}\right) \frac{1}{1 - X_3} + \frac{3X_1X_2 - \frac{X_2^3}{X_3^2}}{(1 - X_3)^2} + \frac{2X_2^3}{X_3(1 - X_3)^3} - \frac{2X_2^3}{X_3^3} \ln(1 - X_3) \tag{2.92}$$

The Percus–Yevick equation was presented for the hard sphere contribution when the ions are equal in size (σ) (Fawcett and Tikanen, 1996):

$$\ln y_i^{hs} = \ln y_{\pm}^{hs} = \frac{6X_3}{1 - X_3} + \frac{3X_3^2}{(1 - X_3)^2} + \frac{2X_3}{(1 - X_3)^3} \tag{2.93}$$

When the ions size are not identical then:

$$\ln y_i^{hs} = -\ln \Delta + \frac{\sigma_i^3 X_0 + 3\sigma_i^2 X_1 + 3\sigma_i X_2}{\Delta} + \frac{3\sigma_i^3 X_1 X_2 + \frac{9}{2}\sigma_i^2 X_2^2}{\Delta^2} + \frac{3\sigma_i^3 X_2^3}{\Delta^3} \tag{2.94}$$

The hard sphere term allows the equations to be used for species with zero charge numbers such as lactose and sucrose (van Boekel, 2008).

Pitzer theory

Pitzer (1980) described the mole fraction free ion activity coefficient (f_i) of a multicomponent solution with charge number (z_i) and mole fraction of ions:

$$\ln f_i = -\left(\frac{1000}{M_1}\right)^{\frac{1}{2}} A_\phi \left[\left(\frac{2z_i^2}{r}\right)\ln\left(1 + rI_x^{\frac{1}{2}}\right) + \frac{\left(z_i^2 I_x^{\frac{1}{2}} - 2I_x^{\frac{3}{2}}\right)}{\left(1 + rI_x^{\frac{1}{2}}\right)}\right] \tag{2.95}$$

where r is the Pitzer parameter set to 8.94 representing the closest approach term; M_1 is the solvent (water) molecular weight, [kg mol^{-1}]; I_x is the mole fraction ionic strength:

$$I_x = \frac{1}{2}\sum_i x_i z_i^2 \tag{2.96}$$

Non-Primitive Mean Spherical Approximation theory (NPMSA)

Blum and Wei (1987) developed the non–primitive mean spherical approximation theory (NPMSA), based on which the features of an arbitrary size multicomponent mixture containing charged ionic hard spheres can be described by three explicit parameters; a screening or ion–ion interaction parameter ($\Gamma, [\mathrm{nm}^{-1}]$), an ion–dipole interaction parameter ($B^{10}, [\mathrm{nm}^{-2}]$), and a dipole–dipole interaction parameter ($b_2, [-]$). A numerical method was deduced to solve NPMSA equations by iteration method from a set of three algebraic and non–linear equations in SI scaled version (nm, Coulombs, s, g, K) to validate the accuracy of units (Blum and Wei, 1987; Blum et al., 1992):

$$\sum_i \rho_i \left(a_i^0\right)^2 + \rho_n (a_n^1)^2 = \alpha_0^2$$
$$\left[\frac{\text{Number of particle i}}{\text{nm}^3}\ (\text{nm}^2)^2\right] + \left[\frac{\text{Number of solvent (water)}}{\text{nm}^3}\ (\text{nm}^2)^2\right] = \text{nm} \tag{2.97}$$

$$-\sum_i \rho_i a_i^0 K_{ni}^{10} + a_n^1 (1 - \rho_n k_{nn}^{11}) = \alpha_0 \alpha_2$$
$$\left[\frac{\text{Number of particle i}}{\text{nm}^3}\ \text{nm}^2\text{nm}^3\right] + [\text{nm}^2\text{dimensionless}] = \text{nm}^2 \tag{2.98}$$

$$(1 - \rho_n K_{nn}^{11})^2 + \rho_n \sum_i \rho_i \left(K_{ni}^{10}\right)^2 = y_1^2 + \rho_n \alpha_2^2$$
$$[-] + \left[\left(\frac{\text{Number of solvent (water)}}{\text{nm}^3}\right)^2 (\text{nm}^3)^2\right] = [-] + \left[\frac{\text{Number of solvent (water)}}{\text{nm}^3}\,\text{nm}^3\right] \tag{2.99}$$

All of the NPMSA parameters are listed in Table 2.16 accurately along with their dimensions in SI units.

Table 2.16 Parameters of NPMSA theory (Wei and Blum, 1987; Liu et al., 1998).

Parameters available in NPMSA theory	Dimension in SI
Electron charge: $e = 4.803 \times 10^{-10}\text{StatC} = 15.189$	$\text{g}^{0.5}\text{nm}^{1.5}\text{s}^{-1}$
$\beta = \frac{1}{k_B T} = \frac{1}{1.38\times10^{-2}\times298.15} = 0.243$	$\text{g}^{-1}\text{nm}^{-2}\text{s}^{2}$
The permittivity of vacuum: $\varepsilon_0 = 8.854 \times 10^{-42}$	$\frac{\text{s}^2\text{C}^2}{\text{nm}^3\text{g}}[=]\frac{\text{F}}{\text{nm}}$
$\alpha_0^2 = 4\pi\beta e^2$	nm
Electric dipole moment of solvent: $\mu = 10^{-18}\text{StatC} = 0.699$	$\text{g}^{0.5}\text{nm}^{2.5}\text{s}^{-1}$
$\alpha_2^2 = \frac{4\pi\beta\mu^2}{3}$	nm^3
$\beta_6 = 1 - \frac{b_2}{6}$	$[-]$
$\lambda = \frac{1+\frac{b_2}{3}}{\beta_6}$	$[-]$
$y_1 = \frac{4}{[(1+\lambda)^2\beta_6]}$	$[-]$
$a_i^0 = \frac{\beta_6\Gamma_i^S D_i^F}{D_{ac}}$	nm^2
$a_n^1 = \frac{D\beta_6\left[\frac{\sigma_n B^{10}}{2}+\frac{\Omega^{10}\lambda}{D\beta_6}\right]}{2D_{ac}}$	nm^2
$-K_{ni}^{10} = \frac{\sigma_n^2 D_i^F\left[\frac{V_\eta}{(\sigma_n+\sigma_i\lambda)}+\frac{\Omega^{10}\Gamma_i^S}{D_{ac}}\right]}{2D\beta_6^2} + \frac{\sigma_n^3 B^{10} a_i^0}{12\beta_6}$	nm^3
$1-\rho_n K_{nn}^{11} = \frac{\left[\lambda+\frac{\rho_n\sigma_n^2\Omega^{10}a_n^1}{2\beta_6^2}\right]}{D\beta_6} + \frac{\rho_n\sigma_n^3 B^{10}a_n^1}{12\beta_6}$	$[-]$
$D_i^F = \frac{z_i\beta_6}{[2(1+\sigma_i\Gamma-\Delta\Gamma_i)]}$	$[-]$
$\Gamma_i^S = \frac{[1+\sigma_i\Gamma-\Delta\Gamma_\text{i}]D-1}{\sigma_i}$	nm^{-1}
$m_i = \frac{V_\eta D_i^F}{(\sigma_n+\sigma_i\lambda)}$	nm
$\Delta\Gamma_i = \frac{V_\eta\rho_n\sigma_n^2\sigma_i^2 B^{10}}{[8\beta_6(\sigma_n+\sigma_i\lambda)]}$	$[-]$
$V_\eta = \frac{\left[-\frac{W_1}{2}+\sqrt{\left(\frac{W_1}{2}\right)^2+\frac{2B^{10}W_2}{\beta_6^2}}\right]}{W_2}$	nm^2
$w_1 = \sum_i \frac{\rho_i z_i^2}{[\beta_6(\sigma_n+\sigma_i\lambda)(1+\sigma_i\Gamma)]}$	nm^{-4}
$w_2 = \frac{1}{2}\rho_n\sigma_n^2 B^{10}\sum_i \frac{\rho_i z_i^2\sigma_n^2}{[2\beta_6(\sigma_n+\sigma_i\lambda)(1+\sigma_i\Gamma)]^2}$	nm^{-6}
$D_i^G = \frac{D_i^F}{D}$	$[-]$
$D_{ac} = \sum_i \rho_i\left(D_i^F\right)^2$	nm^{-3}
$\Omega^{10} = V_\eta\sum_i \frac{\rho_i\sigma_i\left(D_i^F\right)^2}{(\sigma_n+\lambda\sigma_i)}$	nm^{-1}
$D = 1 + V_\eta^2\rho_n\sigma_n^2\sum_i \frac{\rho_i\sigma_i^2\left(D_i^F\right)^2}{[2\beta_6(\sigma_n+\lambda\sigma_i)]^2}$	$[-]$
$N_i = \frac{2D_i^F}{\beta_6\sigma_i}\left[1+\frac{\rho_n\sigma_n^3 B_{10}\nu_\eta\sigma_i}{24(\sigma_n+\lambda\sigma_i)}\right] - \frac{z_i}{\sigma_i}$	nm^{-1}

NPMSA theory is able to predict free ion activity coefficient based on the mole fraction by assuming the indefinite dilution as the reference state for ions (Liu et al., 1998):

$$\ln f_i = \beta[\mu_i(x_i) - \mu_i(x_i \to 0)] \tag{2.100}$$

Here f_i is free ion activity coefficient of species *i* in a solution in mole fraction scale; μ_i is the chemical potential of species *i*; x_i is the mole fraction of species *i*.

The chemical potential of species *i* consists of two contributions for calculation: MSA and hard sphere contributions (Liu et al., 1998):

$$\beta\mu_i = \beta\mu_i^{MSA} + \beta\mu_i^{hs} \tag{2.101}$$

An equation was proposed by Hoye and Stell (1977) to obtain chemical potential of species *i* based on the MSA contribution:

$$\beta\mu_i^{MSA} = \frac{z_i(\alpha_0^2 N_i - \alpha_0\alpha_2\rho_n m_i)}{4\pi} \tag{2.102}$$

Mansoori et al. (1971) proposed a set of equations for the determination of hard sphere contribution of chemical potential of species *i* in a mixed solution given by Equations (2.103) to (2.106).

$$\begin{aligned}\beta\mu_i^{hs} = &-\ln\Delta + \frac{\pi P^{hs}\sigma_i^3\beta}{6} + \frac{3\sigma_i(\xi_2 + \xi_1\sigma_i)}{\Delta} + \frac{9\xi_2^2\sigma_i^2}{2\Delta^2} \\ &+ 3\left(\frac{\xi_2\sigma_i}{\xi_3}\right)^2\left[\ln\Delta + \frac{\xi_3}{\Delta} - \frac{1}{2}\left(\frac{\xi_3}{\Delta}\right)^2\right] - \left(\frac{\xi_2\sigma_i}{\xi_3}\right)^3\left[2\ln\Delta + \frac{\xi_3(1+\Delta)}{\Delta}\right]\end{aligned} \tag{2.103}$$

where

$$\frac{\pi P^{hs}\beta}{6} = \frac{\xi_0}{\Delta} + \frac{3\xi_1\xi_2}{\Delta^2} + \frac{(3-\xi_3)\xi_2^3}{\Delta^3} \tag{2.104}$$

$$\xi^I = \frac{\pi}{6}\sum_{i=1}^{n}\rho_i\sigma_i^I \qquad (I = 0, 1, 2, 3) \tag{2.105}$$

$$\Delta = 1 - \xi_3 \tag{2.106}$$

Another method was suggested by Liu et al. (2002) to give an equation for calculation of free ion activity coefficient based on the mole fraction scale on indefinite dilution as reference state:

$$\ln f_i = \beta[\mu_i(x_i) - \mu_i(x_i \to 0)] + \ln\left(\frac{\rho(x_i)}{\rho(x_i \to 0)}\right) \tag{2.107}$$

Several inconsistencies and typographical errors were found in the formulas and units of NPMSA theory. The contradictions with the corresponding references are shown in Table 2.17. Hence, it was very difficult to obtain a consistent set of variable of NPMSA with any certainty to solve free ion activity coefficients of species in the multicomponent solutions in this thesis.

A best guess of the algebraic parameters was made to enable a comparison between the NPMSA parameters shown in Table 2.16 and values given by Wei and Blum (1987). The resulting variables for sodium chloride are shown in Figure 2.5. b_2 had the best fit, while Γ and B^{10} were significantly different.

Based on the incomplete dissociation of an electrolyte in a solvent, the NaCl solution in water contains free ions and ion pairs (Na^+, Cl^-, $NaCl^\circ$), which have ionic diameters of 0.19 and 0.365 nm (Wei and Blum, 1987) for free sodium and chloride, and 0.365 nm for $NaCl^\circ$. The electric dipole moment of water was assumed to be 2.21 Debye, which is equivalent to 0.699 $g^{0.5}nm^{2.5}s^{-1}$. It is clear from Figure 2.5 that this simulation was not successful. More details on the simulation are shown in Appendix 1.

Therefore, NPMSA was rejected and MSA theory was used to calculate the free ion activity coefficients of species in the multicomponent solutions studied in this thesis.

Table 2.17 The inconsistencies of the Non–Primitive Mean Spherical Approximation theory (NPMSA).

Parameter	Inconsistency	SI unit	Reference
α_0^2	$4\pi\beta e^2$	$\mathrm{g^{-1}nm^{-2}s^2Coulomb^2}$	(Wei and Blum, 1987)
	$\frac{4\pi e^2}{k_B T}\sigma_i^2\sum_i \rho_i z_i$	$\frac{\mathrm{s^2Coulomb^2}}{\mathrm{nm^3g}}[=]\frac{\mathrm{F}}{\mathrm{nm}}$	(Blum et al., 1992)
	$\frac{4\pi\beta e^2}{4\pi\varepsilon_0}$	nm	(Lotfikhan and Modarress, 2003)
α_2^2	$\frac{4\pi\beta\mu^2}{3}$	$\mathrm{nm^3}$	(Wei and Blum, 1987)
	$\frac{4\pi\beta\rho_n\mu^2}{3}$	$[-]$	(Blum et al., 1992)
	$\frac{4\pi\beta\mu^2}{12\pi\varepsilon_0}$	$\frac{\mathrm{nm^6g}}{\mathrm{s^2C^2}}$	(Lotfikhan and Modarress, 2003)
w_2	$\frac{1}{2}\rho_n\sigma_n^2 B^{10}\sum_i \frac{\rho_i Z_i^2\sigma_n^2}{[2\beta_6(\sigma_n+\sigma_i\lambda)(1+\sigma_i\Gamma)]^2}$	$\mathrm{nm^{-6}}$	(Wei and Blum, 1987)
	$\frac{1}{2}\rho_n\sigma_n^2 B^{10}\sum_i \frac{\rho_i Z_i^2\sigma_i^2}{[2\beta_6(\sigma_n+\sigma_i\lambda)(1+\sigma_i\Gamma)]^2}$	$\mathrm{nm^{-6}}$	(Li et al., 1996; Lotfikhan and Modarress, 2003)
Γ_i^s	$\frac{1}{\sigma_i}\left(\frac{[1+\sigma_i\Gamma-\Delta\Gamma_\mathrm{i}]}{D}-1\right)$	$\mathrm{nm^{-1}}$	(Wei and Blum, 1987)
	$1+\sigma_i\Gamma-\Delta\Gamma_i$	$[-]$	(Li et al., 1996)
	$\frac{1}{\sigma_i}[1+\sigma_i\Gamma-\Delta\Gamma_\mathrm{i}]D-1$	$\mathrm{nm^{-1}}$	(Liu et al., 1998)
a_i^0	$\frac{\beta_6\Gamma_i^s D_i^F}{D_{ac}}$	$\mathrm{nm^2}$	(Wei and Blum, 1987)
	$\frac{\beta_6}{\sigma_i D_a}\left[\frac{z_i\beta_6}{2}-D_i^G-\frac{\pi\sigma_i^2}{2\Delta}\sum_{i=1}^{n-1}\rho_i\sigma_i D_i^G\right]$	$\mathrm{nm^2}$	(Li et al., 1996)
D_i^F	$\frac{z_i\beta_6 D}{[(2(1+\sigma_i\Gamma_\mathrm{i}^s)]}$	$[-]$	(Wei and Blum, 1987)
	$\frac{z_i\beta_6}{[2(1+\sigma_i\Gamma-\Delta\Gamma_i)]}$	$[-]$	(Liu et al., 1998)
N_i	$z_i\left[\frac{1}{\sigma_i\Gamma_i^s}+\frac{\rho_n\sigma_n^3 B^{10}V_\eta}{24(\sigma_n+\lambda\sigma_i)\Gamma_i^s}\right]$	$[-]$	(Li et al., 1996)
	$\frac{2D_i^F}{\beta_6\sigma_i}\left[1+\frac{\rho_n\sigma_n^3 B_{10}\nu_\eta\sigma_i}{24(\sigma_n+\lambda\sigma_i)}\right]-\frac{z_i}{\sigma_i}$	$\mathrm{nm^{-1}}$	(Liu et al., 1998)

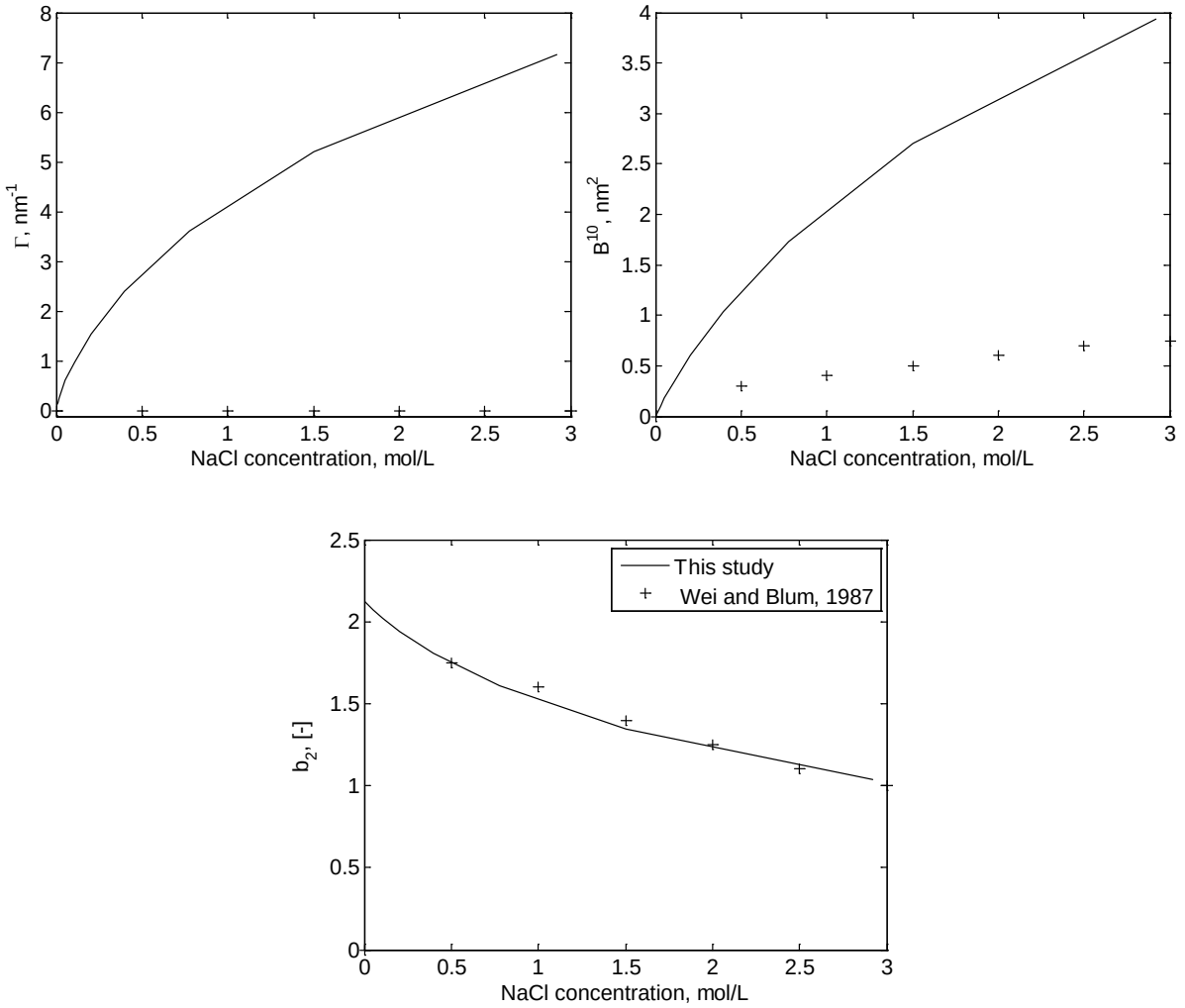

Figure 2.5 NPMSA explicit parameters for different molar concentrations of NaCl. The '+' symbol represents some spots of the simulated results by Wei and Blum (1987).

2.2.7 Ion speciation models

Ion speciation models that determine the ionic equilibria as well as the ions interaction of milk and milk–like solutions, have been extensively studied since the 1980s (Holt et al., 1981). Wood et al. (1981) proposed a computational model for the ion equilibria between the milk components by neglecting the presence of milk proteins, magnesium, and phosphate esters. The model was then extended by Lyster (1981) who assumed the supersaturation of calcium and magnesium phosphate salts at different temperature and pH ranges. The presence of magnesium ions was included in the model.

Holt et al. (1981) developed a comprehensive model, into which almost all of the milk serum components were incorporated except milk proteins. Additionally, they calculated free calcium and magnesium ions concentrations theoretically that were in good agreement with

the corresponding experiments. They solved conservation, dissociation equilibria, and activity coefficients by using the Debye–Hückel equation. They calculated the total molar concentration of serum milk phase, and later Holt (2004) determined the composition of milk components by including milk proteins. The intrinsic association constants were obtained from Smith and Martell (1976a) and were extrapolated for dilute solutions.

These effective models have been applied to various dairy and biological systems by several researchers for many years to ascertain the ion interactions between the salts and to understand the physicochemical features of casein micelles.

van Kemenade and de Bruyn (1987) investigated the formation of various calcium phosphate compounds in terms of different pH values and initial supersaturation. Then, they studied the effect of temperature on solubility isotherms of octacalcium phosphate and DCPD. The concentration of all ions and complexes were computed by the model of Holt et al. (1981).

Kent et al. (1998) examined the calcium partitioning in sows' milk and studied the relationships between the free and diffusible calcium and citrate ions by using the model proposed by Holt and Muir (1979).

Chhettry et al. (1999) attempted to solve the relevant equilibria of apatite dissolution systems by assuming a probe phase and find out a set of mathematical parameters for the evaluation of the apatite metastable equilibrium solubility. A probe phase was used to assess the equilibrium constants, which were essential to examine the solubility behaviour of the apatites. Therefore, dicalcium phosphate dihydrate was selected as it is equilibrated quickly, and the numerical value for its solubility product is well defined in phosphate solutions.

Le Graët and Gaucheron (1999) determined the molar concentration of calcium, magnesium, inorganic phosphate, citrate, and chloride during casein micelle acidification in the pH range of 1.5–6.7. They used the computation model of Holt et al. (1981) to calculate the mineral contents of the milk ultrafiltrates.

Lu and Leng (2005) analysed the free energy, nucleation rate, and driving force of calcium phosphate precipitation in simulated body fluid. They obtained the molar activities of species mathematically by solving a set of mass balances, ion equilibria, and supersaturation equilibria using the model of Holt et al. (1981).

Nonetheless, the main weakness of these models is that the micellar calcium phosphate as well as the ion–pairs bound to casein were not included as a part of the casein micelles. Hence, more developments were required to predict the ion equilibria in milk and milk–like systems.

Holt (2004) proposed an equilibrium thermodynamic model for determination of the ion interactions in milk by assuming the micellar calcium phosphate in the form of CPN, for which an empirical formula was generalised to obtain the molar ratios of calcium, magnesium, inorganic phosphate, and citrate in association with a casein phosphorylated sequence, or phosphate centre. This model was capable of predicting ion equilibria in both aqueous and colloidal phases of milk and the simulated results were in reasonable agreement with the experimental data of White and Davies (1963). However, more expansions are essential to confirm the accuracy of the model under various conditions (Gao, 2010).

Mekmene, Le Graet, et al. (2009) developed the model of Holt et al. (1981) to improve the understanding of salt equilibria in both milk serum and casein and mineral–enriched milk (with $CaCl_2$, NaCl, Na_3Citrate, and Na_2HPO_4) by taking into account the cations (calcium, magnesium, sodium, and potassium) and casein molecules in the colloidal phase as well as the inorganic calcium phosphate solubility. However, the simulated results were based on the constant pH value of 6.75, and other pH values were not considered in the model. Moreover, the different types of casein were not considered, and only the total casein was included in the model.

Mekmene et al. (2010) extended the model of Mekmene, Le Graet, et al. (2009) to predict the salt partitioning in milk for a wide range of pH values upon acidification. However, other components such as sulphate and carbonate were not integrated in the model. According to Gao (2010), the existence of magnesium citrate in the colloidal phase of milk was an incorrect assumption of the model.

Rice et al. (2010) presented a model to describe the calcium, phosphate, and citrate equilibria as a function of pH and temperature which was solved using ‘an iterative approach’. Saturation ratios of different calcium phosphate solids were assumed in the model such as hydroxyapatite and octacalcium phosphate, however, the kinetics effects and supersaturated solutions in a metastable state were neglected. The non–electrolyte species was assumed to have an activity of unity.

Gao, van Halsema, et al. (2010) developed an ion speciation model, by which the ion composition of SMUF was calculated at thermodynamic equilibrium. Supersaturation of some solids were included in the model such as different calcium phosphate phases, calcium citrate, calcium phosphate, and calcium carbonate, and magnesium phosphate. Experiments were performed under different conditions with SMUF as well as SMUF with $CaCl_2$ and Na_2HPO_4 in the 4.8–7.4 pH range. They also proposed another model, by which the salt equilibria of freshly prepared SMUF were described, i.e. in the presence of no solid. The AESolve program was used to compute the salt equilibria by incorporating the main components of milk, however, the limitation of this model is that the lactose and proteins were excluded in the calculations.

Gao, van Leeuwen, et al. (2010) applied the MSA theory to milk–like solutions containing calcium chloride, potassium chloride, and potassium citrate as well as to SMUF and skim milk to understand pH and activity of free calcium (Ca^{2+}) in presence of disaccharides. For this purpose, the experiments were carried out in a multicomponent solution comprising the corresponding species with various sucrose concentrations.

Mekmene and Gaucheron (2011) investigated the association of calcium to species such as phosphoserine, caseinophosphopeptide, β–casein, caseinate, citrate, and pyrophosphate using a non–linear least squares model that enables fitting with the experimental data.

More recently, Bijl et al. (2018) improved the models of Holt (2004) and Little and Holt (2004) by assuming a reaction between all individual or grouped phosphorylated residues of a casein molecule and a calcium phosphate nanocluster. In other words, either the phosphorylated residues bind to a calcium phosphate nanocluster or there is no affinity between them. There is no affinity between κ–casein and the calcium phosphate, because this protein has no strong binding site either to bind or to sequester the calcium phosphate.

Little information is currently available regarding the salt equilibria in concentrated milk solutions by assuming all proteins in both casein and serum, whether it is time–dependent or not. Lactose has not been assumed in the salt partitioning calculations due to applying activity coefficient models that only incorporate charged ions. Therefore, activity coefficient and activity of zero–charged ions could not be involved in the previous simulations.

3 The Mathematical Model and its Applications

3.1 Introduction

Despite all the models given in Chapter 2, a mathematical model is still necessary to predict ion partitioning in milk and dairy liquids under various conditions. The aim of this chapter is to mathematically propose a comprehensive model to be able to accurately describe association, activity, and solubility of ions in any dairy liquid up to high concentrations. The previous works had generally identified the ion equilibria of various systems only for a low to medium concentrations by using either the Debye–Hückel or Davies theories and by incorporating phosphoserine and carboxylic residues of casein molecules (Mekmene, Le Graet, et al., 2009; Mekmene et al., 2010). The Mean Spherical Approximation (MSA) method was used to calculate free ion activity coefficients as it contained terms that enhanced accuracy at higher concentrations for ionic strengths beyond 1 mol L^{-1} (Rice et al., 2010), e.g. when milk is concentrated by evaporation or reverse osmosis. Further, it allows the addition of non–electrolyte components such as lactose. Lactose is of great importance as a sidestream product in dairy industry, thus, better understanding of association, kinetic precipitation, and interaction with salts seems useful to avoid any precipitation with lactose and whey proteins (Garcia et al., 2018).

3.2 Gibbs–Duhem equation

The Gibbs–Duhem relationship is an appropriate approach to obtain a numerical method for the calculation of water activity from ion activities to validate the activity coefficient results given by the MSA with literature. This is then to be applied using both ion–pair, and free–ion approaches to determine water activity, which must be independent of the approach used to calculate it. Hence, it should be possible to numerically compare different equations for free–ion and ion–pair activity coefficients.

3.2.1 Theory

The Gibbs–Duhem relationship can be applied to a mixture of c-1 species, i, in solvent 1 (normally water) at constant temperature and pressure.

$$n_1 d\mu_1 + \sum_{i=2,c} n_i d\mu_i = 0 \tag{3.1}$$

Here n represents the number of moles of a substance and μ is the chemical potential which is a function of temperature, pressure and composition. From this, an expression is required for water activity, a_1, in terms of the molal concentration of dissociated ions with their activity coefficients. It is useful to use molality scale, which is defined earlier in Chapter 2. Therefore, from the definition of molality and Equation (3.1):

$$d\mu_1 + M_1 \sum_{i=2,c} m_i d\mu_i = 0 \tag{3.2}$$

From the corresponding equations of chemical potential in Chapter 2, Equation (2.2):

$$RTd\ln a_1 + M_1 RT \sum_{i=2,c} m_i d \ln \gamma_i m_i = 0 \tag{3.3}$$

removing RT:

$$d\ln a_1 + M_1 \sum_{i=2,c} m_i d \ln \gamma_i m_i = 0 \tag{3.4}$$

With an ion–pair approach in mind having ν_1 cations M and ν_2 anions X, m_i was considered as the molality of ion i when $M_{\nu_1}X_{\nu_2}$ is fully dissociated, so m_i in this section has a different meaning to that in the free–ion approach section.

$$d\ln a_1 + M_1(m_M d \ln \gamma_M m_M + m_X d \ln \gamma_X m_X) = 0 \tag{3.5}$$

by rearranging the Equation (3.5):

$$d\ln a_1 + M_1(m_M d \ln \gamma_M + m_M d \ln m_M + m_X d \ln \gamma_X + m_X d \ln m_X) = 0 \tag{3.6}$$

by substituting the molal concentration of the undissociated electrolyte, m, into Equation (3.6):

$$d\ln a_1 + M_1(\nu_1 m d \ln \gamma_M + \nu_1 m d \ln m_M + \nu_2 m d \ln \gamma_X + \nu_2 m d \ln m_X) = 0 \tag{3.7}$$

and using some of the rules below:

$$d\ln a_1 + M_1\left(md\ln\gamma_M^{\nu_1} + md\ln\gamma_X^{\nu_2} + md\ln m_M^{\nu_1} + md\ln m_X^{\nu_2}\right) = 0 \quad (3.8)$$

which can be rewritten as:

$$d\ln a_1 + M_1\left(md\ln(\gamma_M^{\nu_1}\gamma_X^{\nu_2}) + md\ln(m_M^{\nu_1}m_X^{\nu_2})\right) = 0 \quad (3.9)$$

By substituting mean molality and mean molal activity coefficient into the Equation (3.9), and by considering total moles of ions:

$$d\ln a_1 + \nu M_1(m\, d\ln(\gamma_\pm m_\pm)) = 0 \quad (3.10)$$

Equation (3.10) was integrated from zero concentration up to a solution concentration *C*. It might or might not be useful to separate the integral:

$$\ln a_1 = -\nu M_1 \int_{C=0}^{C} m\, d\ln(m_\pm) - \nu M_1 \int_{C=0}^{C} m\, d\ln(\gamma_\pm) \quad (3.11)$$

Hence, Equation (3.11) can be rearranged as follows:

$$\ln a_1 = -\nu M_1 \int_{C=0}^{C} m\, d\ln(m_\pm\gamma_\pm) \quad (3.12)$$

Thus, water activity of solution can be determined by having mean molality and mean molal ion–pair activity coefficient of an electrolyte, by accounting complete dissociation of an electrolyte in a solution for the ion–pair approach.

The Gibbs–Duhem equation can also be applied for a partially dissociated electrolyte in a solution for the purpose of free–ion approach. Equation (3.4) was integrated from zero concentration up to a solution concentration *C*, noting that the water activity at zero concentration is 1.0. Here *C* was intentionally used to avoid confusion between molal concentrations, m_i, on the integration path, with the integration limit. Following the earlier outline of conversions, *C* could have any units that could be converted as required.

$$\ln a_1 = -M_1 \int_{C=0}^{C} \sum_{i=2,c} m_i d\ln m_i - M_1 \int_{C=0}^{C} \sum_{i=2,c} m_i d\ln\gamma_i \quad (3.13)$$

At this point (or its equivalent), Guggenheim (1967), Stokes (1991) and others were forced to assume a form for the relationship between γ and m, so that an analytical integration could follow. In this work, it is useful to proceed without such restrictions by allowing a numerical

solution to be used. Hence, Equation (3.13) is a sufficient description of the calculation of water activity for the free–ion approach, either numerically or analytically.

Nevertheless, several other validations were used depending on the solutions and their conditions that will be discussed in detail for each particular system. These calculations were also done for dynamic conditions, i.e. for time dependent to see the changes of ion partitioning over time.

3.2.2 Implementation of algorithm

Equation (3.13) can be applied to different systems for calculation of water activity as a method of validation for activity coefficient quantities. Below are the required steps toward the water activity calculation:

- An array of concentration from zero to the concentration of interest was defined.
- The molar activity coefficients were calculated at each concentration by the MSA theory using molar concentration, size, and charge of each species. The MSA theory was described in detail in Chapter 2.
- The molar activity of each species including cations, anions, and ion–pairs was calculated by using their corresponding molar activity coefficient and concentration.
- Molar activity was converted to molal activity for all components using the formula given in Chapter 2, Table 2.8, from that the molal activity coefficient was obtained.
- Molal activity coefficient and molal concentration were substituted into Equation (3.13).
- The cumulative trapezoidal numerical integration (cumtrapz) in MATLAB was used to compute the approximate integral for water activity calculation.

Hence, water activity could be solved theoretically for either ion–pair or free–ion approach in a multicomponent solution. Figure 3.1 indicates the water activities of sodium chloride, calcium chloride, and sulphuric acid solutions as a function of molal electrolyte concentration that were solved for both the ion–pair (Equation (3.12) (Zemaitis et al., 1986)) and the free–ion approach (Equation (3.13)). The simulated results for both approaches were in a good agreement with experimental data used from Robinson and Stokes (1959). The Gibbs–Duhem equation with the MSA theory was likely able to predict water activity for even high concentrations, e.g. 6 M of the electrolyte solution. Less experimental data are available for

water activity of binary and multicomponent solutions in literature. Therefore, these systems were used as the examples for water activity calculation.

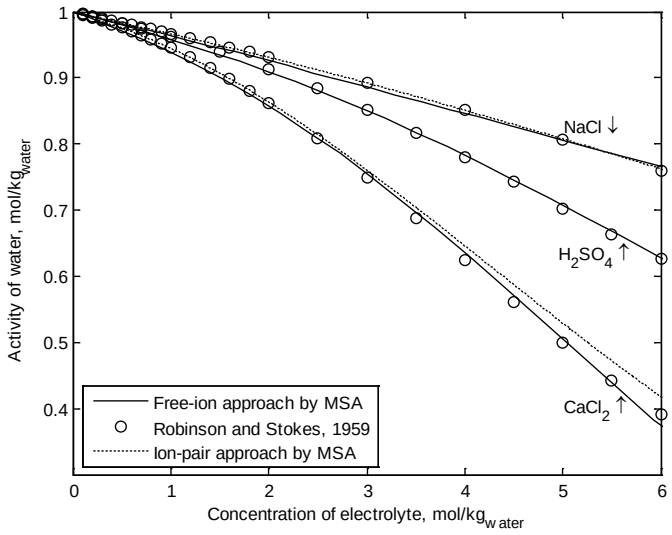

Figure 3.1 Water activity of sodium chloride, calcium chloride, and sulphuric acid solutions at 25 ˚C by both the ion–pair and free–ion approaches.

Water activity of both approaches yielded similar results representing the consistency of them. Stokes (1991) used Equation (3.14) to calculate water activity as a function of osmotic coefficient, values of which were experimentally obtained by Robinson and Stokes (1959) to validate the model that are shown in Figure 3.1.

$$\ln a_1 = -\frac{\phi}{M_1 \sum_i \nu_i m_i} \tag{3.14}$$

Here a_1 is water activity, mol kg^{-1}_{water}; ϕ is osmotic coefficient, [–]; M_1 is molar mass of water, kg mol^{-1}; ν_i is the number of ions in solution from each molecule of solute (assuming complete dissociation), [–]; m_i is the molal concentration of the electrolyte, mol kg^{-1}_{water}.

3.3 Ion speciation model

The model was based on the simultaneous calculations of equilibrium, conservation, and electroneutrality equations. Generally, the components, which can include cations, anions, lactose, and proteins available in milk, were clearly incorporated into each system mostly based on their molar activity.

3.3.1 Set of equations

The components are assumed to be in a thermodynamic equilibrium with each other through intrinsic association constants that lead to the formation of species such as free ions and ion–pairs. An example of thermodynamic equilibrium was given in Chapter 2, Equation (2.37). A full list of available cations, anions, and ion–pairs is shown in Table 3.1 along with the corresponding intrinsic association constants, which are only for the temperature range between 20–25 ˚C. The set of equations were assembled first for the steady state condition.

Duplicate components were dropped from the set of components to ensure the number of equations and variables are equal, e.g. H_2Cit^- acts both as anion and as ion–pair in a system containing citrate, therefore, it is only considered as an anion in the set of calculations, and was not included in the set of ion–pairs.

In Table 3.1 for milk serum, there are 5 cations, 15 anions, and 75 ion–pairs, and of these 7 ion–pairs are already in the list of anions, and the concentration of H_2O is determined independently. Thus, there are 5+15+75–7–1=87 concentration variables. Table 3.1 provides 74 equilibria in the form of Equation (2.37).

The hydrogen ion and hydroxide ion equilibrium was constructed as another essential equation in the conservation calculation, for which water activity (a_{water}, mol L^{-1}) is essential:

$$K_w = \frac{a_{water}}{a_{H^+} a_{OH^-}} \tag{3.15}$$

where K_w is water association constant which can be used from Table 3.1. Molar water activity was ascertained as follows;

$$a_{water} = \frac{\rho_{soln} - \sum_i C_i MW_i}{MW_{water}} \tag{3.16}$$

Here ρ_{soln} is the density of solution, [kg L^{-1}], which was set as the density of a NaCl solution for the simulations in this thesis due to insufficient data for density of multicomponent systems that was calculated according to the Appendix 2; C_i is the total molar concentration of the species, [mol L^{-1}]; MW_i and MW_{water} are the molecular weight of species and water [kg mol^{-1}], respectively.

Table 3.1 Intrinsic association constant between the principal ions of milk serum at 25 ˚C (Holt et al., 1981; Mekmene, Le Graet, et al., 2009; Mekmene et al., 2010).

	Ca^{2+}		Mg^{2+}		Na^{+}		K^{+}		H^{+}	
	Ion–pair	K_a, mol^{-1} L	Ion–pair	K_a, mol^{-1} L	Ion–pair	K_a, mol^{-1} L	Ion–pair	K_a, mol^{-1} L	Ion–pair	K_a, mol^{-1} L
H_2Cit^-	CaH_2Cit^+	28	MgH_2Cit^+	15	NaH_2Cit	1	KH_2Cit	1	H_3Cit	1380
$HCit^{2-}$	CaHCit	876	MgHCit	402	$NaHCit^-$	10	$KHCit^-$	10	H_2Cit^-	6×10^4
Cit^{3-}	$CaCit^-$	1.65×10^5	$MgCit^-$	1.11×10^5	$NaCit^{2-}$	20	$KCit^{2-}$	16	$HCit^{2-}$	2.57×10^6
$H_2PO_4^-$	$CaH_2PO_4^+$	11	$MgH_2PO_4^+$	12	NaH_2PO_4	1	KH_2PO_4	1	H_3PO_4	200
HPO_4^{2-}	$CaHPO_4$	642	$MgHPO_4$	838	$NaHPO_4^-$	17	$KHPO_4^-$	13	$H_2PO_4^-$	2.87×10^7
PO_4^{3-}	$CaPO_4^-$	2.88×10^6	$MgPO_4^-$	8.35×10^4	$NaPO_4^{2-}$	100	KPO_4^{2-}	100	HPO_4^{2-}	2.47×10^{12}
HCO_3^-	$CaHCO_3^+$	23	$MgHCO_3^+$	19	$NaHCO_3$	1	$KHCO_3$	1	H_2CO_3	2.25×10^6
CO_3^{2-}	$CaCO_3$	1.4×10^3	$MgCO_3$	758	$NaCO_3^-$	10	KCO_3^-	10	HCO_3^-	2.13×10^{10}
HSO_4^-	$CaHSO_4^+$	10	$MgHSO_4^+$	10	$NaHSO_4$	1	$KHSO_4$	1	H_2SO_4	1×10^{-8}[d]
SO_4^{2-}	$CaSO_4$	204	$MgSO_4$	170	$NaSO_4^-$	5	KSO_4^-	7	HSO_4^-	98
Cl^-	$CaCl^+$	9.4	$MgCl^+$	5.6	NaCl	0.9	KCl	1	HCl	$1\times10^{-9.3}$
Glc–1–PH^-	CaGlc–1–PH^+	10	MgGlc–1–PH^+	10	NaGlc–1–PH	1	KGlc–1–PH	1	Glc–1–PH_2	1×10^{-10}
Glc–1–P^{2-}	CaGlc–1–P	316	MgGlc–1–P	295	NaGlc–1–P^-	7	KGlc–1–P^-	5	Glc–1–PH^-	3.19×10^6
$RCOO^-$	$CaRCOO^+$	15	$MgRCOO^+$	19	NaRCOO	0.7	KRCOO	0.7	RCOOH	5.71×10^4
OH^-	$CaOH^+$	25.11[a]	$MgOH^+$	162.18[a]	NaOH	0.2[b]	KOH	0.2[b]	H_2O	K_w[c]

[a] (Clark, 2015), [b] (van Boekel, 2008), [c] The intrinsic association constant of water for one kilogram of molecule: 5.507×10^{15} mol^{-1}L, [d] Assumed to be very low.

Electroneutrality provides another equation to describe the need for the identical numbers of equations and species:

$$\sum_i C_i z_i = 0 \tag{3.17}$$

The total concentration of each group of species was required to equal the specified total. It was constructed as a sum of all corresponding free ions and ion–pairs for each species providing the mass balance equations for Ca, Mg, Na, K, citrate, phosphate, carbonate, sulphate, chloride, phosphate esters, and carboxylate giving 11 equations.

Hence, there were 74+1+1+11=87 equations, which matched the number of variables.

Steady state calculations of ion–equilibria were implemented by the total amount of each species as an initial guess to enable covering a wide range of concentration and subsequently pH values. A concentration ratio was defined to mathematically make up various initial concentrations of cations, anions, and ion–pairs from dilute to concentrated ones. Mathematical addition of NaOH/HCl to the multicomponent solution enabled the pH to be indirectly adjusted.

3.3.2 Activity coefficient and dielectric constant

The molar activity of each species was calculated by the multiplication of molar concentration and molar–based activity coefficient calculated by the MSA theory that was described in detail in Chapter 2.

The relative permittivity of water was another variable for calculation of Bjerrum distance in the set of MSA equations.

Equation (3.18), which was given by Tikanen and Fawcett (1996) and Buchner et al. (1999), was used to determine the relative permittivity of water for sodium chloride solution and was compared with the experimental data presented by Mollerup and Breil (2015) that was shown in Figure 3.2.

$$\varepsilon_{r_{NaCl}} = 78.65 - 15.45C + 3.76C^{1.5}$$
$$\varepsilon_{r_{NaCl}} = 78.65 - AC + BC^{D} \tag{3.18}$$

Here $\varepsilon_{r_{NaCl}}$ is the relative permittivity of water for the NaCl solution; [–]; *A*, *B*, and *D* represent the coefficients for the equation; C is molar concentration of electrolyte.

Figure 3.2a shows that the parameter values given by the literature were not provided a match with the experimental data for the NaCl solution, but a much better fit was obtained with the numerical values of 15.8, 2.0, and 1.7 for *A*, *B*, and *D* coefficients, respectively.

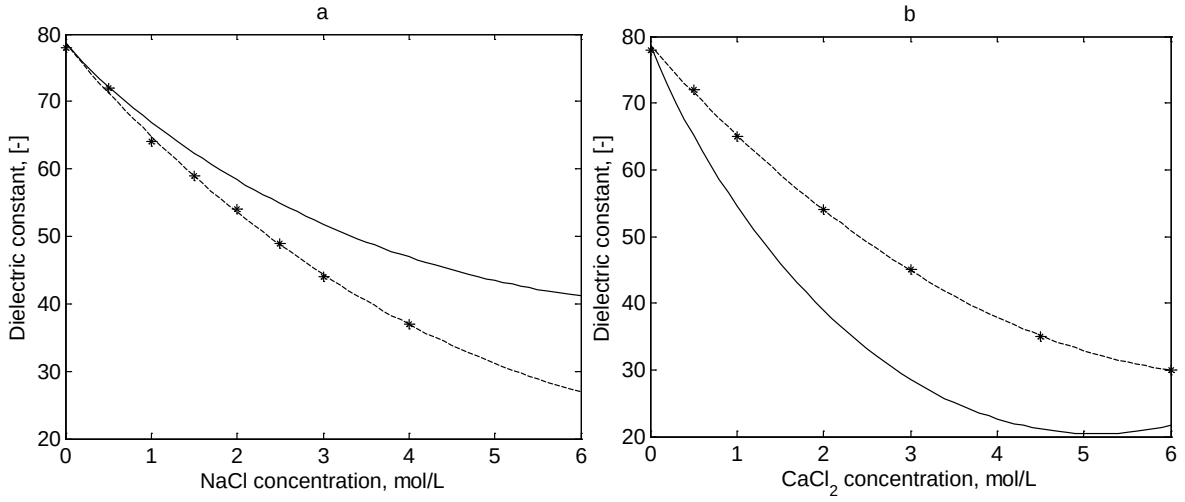

Figure 3.2 The dielectric constant as a function of a) sodium chloride and b) calcium chloride molar concentration for various coefficients of the Equations (3.18) and (3.19). The solid curves are from the Equations (3.18) and (3.19) given by Tikanen and Fawcett (1996) using *A*=15.45, *B*=3.76, and *D*=1.5 for sodium chloride solution, and *A*=34, *B*=10, *D*=1.5 for calcium chloride solution. The symbol '∗' represents the experimental data from and Mollerup and Breil (2015). The dash lines represent the best fit with the experimental data.

Similarly, Tikanen and Fawcett (1996) and Buchner et al. (1999) proposed an equation for the dielectric constant of water in a calcium chloride solution as a function of molar concentration of electrolyte:

$$\varepsilon_{r_{CaCl_2}} = 78.65 - 34C + 10C^{1.5}$$
$$\varepsilon_{r_{CaCl_2}} = 78.65 - AC + BC^{D} \quad (3.19)$$

The $CaCl_2$ data were also fitted using the same equation giving the numerical values of *A*=14.7, *B*=1.2, *D*=1.9.

For simple binary solutions such as calcium chloride, the free calcium and chloride ion concentrations were substituted for the electrolyte concentration in the water dielectric constant formula, but for multicomponent solutions, the two main cation and anion of that

system were used for this purpose. Due to lack of sufficient equations for water dielectric constant in various solutions, Equation (3.18) was assumed for both binary and multicomponent solutions in this thesis with *A*=15.45, *B*=3.76, *D*=1.5 as found for NaCl.

3.3.3 $CaCl_2$ solution as an example

Calcium chloride solution is used as an example for the ion equilibria calculation. The solution contains 7 species: Ca^{2+}, Cl^{-}, hydrogen, and hydroxide ions as free ions, and ion–pairs $CaCl^{+}$, HCl, and $CaOH^{+}$. They are relaxed according to the Equations (3.20) to (3.23) with the corresponding intrinsic association constant (K_a, $[\mathrm{mol}^{-1}\mathrm{L}]$):

$$K_{a_1} = \frac{a_{CaCl^+}}{a_{Ca^{2+}} a_{Cl^-}} = \frac{[CaCl^+]\, y_{CaCl^+}}{[Ca^{2+}]\, y_{Ca^{2+}} [Cl^-]\, y_{Cl^-}} \tag{3.20}$$

$$K_{a_2} = \frac{a_{CaOH^+}}{a_{Ca^{2+}} a_{OH^-}} = \frac{[CaOH^+]\, y_{CaOH^+}}{[Ca^{2+}]\, y_{Ca^{2+}} [Cl^-]\, y_{Cl^-}} \tag{3.21}$$

$$K_{a_3} = \frac{a_{HCl}}{a_{H^+} a_{Cl^-}} = \frac{[HCl]\, y_{HCl}}{[H^+]\, y_{H^+} [Cl^-]\, y_{Cl^-}} \tag{3.22}$$

$$K_w = \frac{a_{water}}{a_{H^+} a_{OH^-}} = \frac{a_{water}}{[H^+]\, y_{H^+} [OH^-]\, y_{OH^-}} \tag{3.23}$$

The brackets represent the molar concentration of species; y is the molar free–ion activity coefficient, which was obtained by the MSA theory and was discussed in detail in Chapter 2. Charge number, size, and molar concentration of each component were required to substitute in the MSA theory enabling molar activity coefficient calculation. Table 3.2 shows the size of each species used in the MSA theory in nanometres. The component sizes for milk system are given in Appendix 3.

Table 3.2 Numerical values of size for each component in calcium chloride solution.

	Cl^-	OH^-	Ca^{2+}	H^+	$CaCl^+$	$CaOH^+$	HCl
Size, nm	0.365	0.28	0.8	0.226	0.5	0.5	0.4

Equation (3.19) was used as the water dielectric constant formula, for which the fitted coefficients *A*=14.7, *B*=1.2, *D*=1.9 were used.

The mass balance for total calcium, and total chloride were written as follows:

$$[Ca]_{total} = [Ca^{2+}] + [CaCl^{+}] + [CaOH^{+}] \quad (3.24)$$

$$[Cl]_{total} = [Cl^{-}] + [CaCl^{+}] + [HCl] \quad (3.25)$$

The electroneutrality was constructed according to the following equation:

$$2\,[Ca^{2+}] + [CaCl^{+}] + [CaOH^{+}] + [H^{+}] - [Cl^{-}] - [OH^{-}] = 0 \quad (3.26)$$

There are seven equations, (3.20) to (3.26), equally the number of species.

The proposed model is capable of predicting ion association in any aqueous solution regardless of any charge or size of the components. This means lactose can be incorporated into the ion partitioning calculation of solutions. In later sections, lactose was also treated as an individual species that can affect the solution.

3.3.4 Solving using Newton's method

The equations form a non–linear system, which can be solved using Newton's method. Newton's method uses the iteration scheme as follows:

$$\mathbf{x}_{k+1} = \mathbf{x}_k - \mathbf{J}^{-1}\mathbf{f}(\mathbf{x}_k), \quad k = 0, 1, \ldots \quad (3.27)$$

The vector $\mathbf{x}_0$ is the initial guess and **J** is the Jacobian matrix of the vector function **f**(**x**). The functions must be in the form of **f**(**x**)=0.

In this work, the Jacobian matrix was obtained numerically as given in Appendix 4. The variables in **x** and the functions varied greatly in scale. It was found that using units of μmol L^{-1} gave a satisfactory range for **x**. Each of the functions was scaled, by dividing the entire function by a power of 10, so that extreme function values were avoided. The solution obtained at any iteration was constrained by upper and lower bounds, which were set to maintain the solution in a physically feasible space.

The simulations were implemented in MATLAB R2013b and R2017a which unexpectedly returned slightly different results for the solution of **J** Δ**x**=–**f** using the syntax Δ**x** =–**J****f**.

The MATLAB language programming is a user–friendly software that enables using purpose–written programs, which could be controlled and manipulated by the user. The MATLAB programs for the Newton's and Jacobian functions are shown in Appendix 4.

The initial guess for each component was equal to the total concentration of the corresponding species in the solution. Then, the previous mathematical solution was used as the next initial guess when Newton's method was used again for a similar concentration, e.g. when producing a graph. For some systems, it was found necessary to refine the initial guesses to smaller values.

3.4 Extra equations for precipitation

Solid precipitates were incorporated into the calculation by considering the ion activity product (*IAP*) and solubility product (K_{sp}) of the solid phase, which were mostly available in literature. Concentration of potential solid phase was obtained using Euler's method, by which the level of precipitation was ascertained for each time step as follows:

$$C_{\text{precipitate}_{(s)(i+1)}} = C_{\text{precipitate}_{(s)(i)}} + \frac{dC_{(s)(i)}}{dt}.\Delta t \tag{3.28}$$

Here $C_{\text{precipitate}_{(s)(i+1)}}$ is molar concentration of potential solid phase at the time step $i+1$; $C_{\text{precipitate}_{(s)(i)}}$ is molar concentration of potential solid phase at the time step i; Δt is time step, [min]; $\frac{dC_{(s)(i)}}{dt}$ is the rate of solid phase concentration over time, [mol L^{-1} min^{-1}], which is the sum of precipitation and dissolution differential equations (Kazadi Mbamba, 2016):

$$\frac{dC_{(s)(i)}}{dt} = \frac{dC_{\text{precipitation}_{(s)(i)}}}{dt} + \frac{dC_{\text{dissolution}_{(s)(i)}}}{dt} \tag{3.29}$$

$$\frac{dC_{\text{precipitation}_{(s)(i)}}}{dt} = k_{prec}\, C_{\text{precipitate}_{(s)(i)}}\, \sigma^{n}; \quad \sigma = S\text{at}^{\frac{1}{\nu}} - 1 \tag{3.30}$$

$$\frac{dC_{\text{dissolution}_{(s)(i)}}}{dt} = k_{diss}\, C_{\text{precipitate}_{(s)(i)}}\, \sigma \tag{3.31}$$

Here *n* is the solid phase reaction order; k_{prec} and k_{diss} are precipitation and dissolution rate constants of solid phase that are unlikely available in literature. '*Sat*' represents saturation as defined in Section 2.2.5.

Precipitation and dissolution equations were constructed for each potential solid component and were recalculated for each time step. Small time steps gave accurate results. Initial concentration of each precipitate was normally assumed to be 0.02 μmol L^{-1} as nucleation kinetics were not included.

For instance, the precipitation of dicalcium phosphate dihydrate (DCPD, $CaHPO_4.2H_2O$) is a common phenomenon in the milk liquids that results from supersaturation of calcium and phosphate ions (Pouliot et al., 1991). The saturation equilibrium of dicalcium phosphate dihydrate can be written as:

$$CaHPO_4.2H_2O_{(s)} \leftrightarrow Ca^{2+}_{(aq)} + {HPO_4^{2-}}_{(aq)}$$
$$Sat = \frac{a_{Ca^{2+}} a_{HPO_4^{2-}}}{K_{sp}} = \frac{IAP}{K_{sp}} \quad (3.32)$$

The dynamic simulation of calcium phosphate solution was implemented for time incorporation by applying Euler's method, by which the level of precipitation was ascertained for each time step using the following equation:

$$C_{\mathrm{DCPD}_{(s)(i+1)}} = C_{\mathrm{DCPD}_{(s)(i)}} + \frac{dC_{\mathrm{DCPD}_{(s)(i)}}}{dt}.\Delta t \quad (3.33)$$

The precipitation and dissolution rate constants were chosen 0.25 and 0.0001 min^{-1}, respectively with the precipitation reaction order of 2.

3.5 Application of the model to sodium chloride and calcium chloride solutions

Sodium chloride and calcium chloride solutions were used to validate the model by assuming both ion–pair and free–ion approaches, because they are significant components of milk and a large amount of accurate experimental data is available in literature.

3.5.1 Ion–pair approach

Although the ion–pair approach ignores free complexes and interactions between free ions, several activity coefficient models were presented in literature to determine the mean activity coefficient. The base ten logarithms of the mean molar ion–pair activity coefficients of sodium chloride and calcium chloride solutions were plotted as a function of molar ionic strength at 25 ˚C (Figure 3.3).

The MSA theory performs better than the other theories to fit with the experimental data for the ion–pair approach for the both solutions. Many researchers have used Davies theory to calculate ion partitioning for obtaining mean and free ion activity coefficients in various systems, but the MSA theory shows better agreement with the experimental data particularly for higher concentrations of the electrolyte. Figure 3.3 also shows that the Debye–Hückel theory is only valid for lower sodium chloride concentrations when the total molar ionic strength is lower than 0.3 mol L^{-1}.

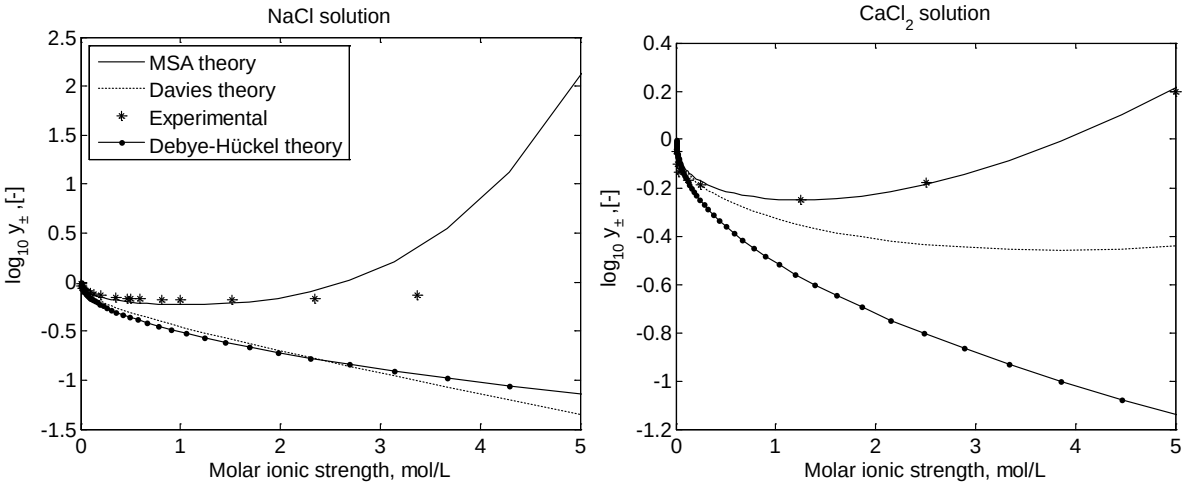

Figure 3.3 Mean molar ion–pair activity coefficient of NaCl and $CaCl_2$ solutions at 25 ˚C. The experimental data were taken from van Boekel (2008).

Figure 3.4 indicates a direct correlation between the effective ion size parameter (σ) and the mean ion–pair activity coefficient of sodium chloride solution ($y_{\pm}$). 0.5 nm was selected as the optimum size for the sodium and chloride ion for Figure 3.4 which is slightly larger than Kielland (1937) suggested. However, the effective size parameter for free calcium was assumed 0.6 nm according to Kielland (1937). The effect of size parameters of the free sodium (Na^+), free chloride (Cl^-), and free calcium (Ca^{2+}) ions were identical. The size of free hydrogen (H^+) and hydroxide (OH^-) ions seemed to have no effect on the mean ion–pair activity coefficient of both sodium chloride and calcium chloride solutions.

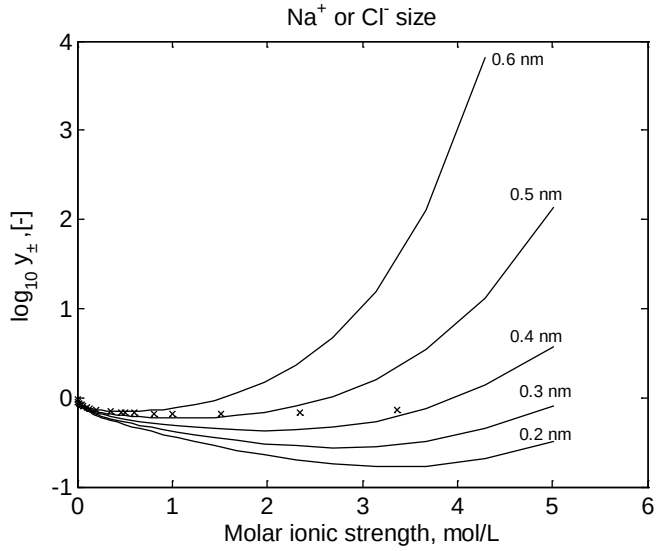

Figure 3.4 Mean ion–pair activity coefficient of NaCl solution for different ion size of Na^+ and Cl^- by the MSA theory; the '×' symbol refers to experimental data taken from van Boekel (2008).

3.5.2 Free–ion approach

The free–ion approach will be required when considering milk solutions with many different ions and ion–pairs. Therefore, it was also used for the simulation of both calcium chloride and sodium chloride solutions. Figure 3.5 shows the natural logarithm of free ion activity coefficient of sodium chloride solution and calcium chloride showing that the MSA theory fits best to predict free ion activity coefficients over the range of concentrations. To obtain these results, the size of following ions were adjusted: Na^+ to 0.51, Cl^- to 0.44 nm, Ca^{2+} to 0.8 nm.

The Davies theory is unable to individually predict the molar activity coefficient for the free ions due to lack of a parameter that can differentiate the cation from the anion activity coefficients, whereas the MSA theory can distinguish the free ion activity coefficients by adjusting the effective size parameter leading to the different numerical values for the free ion activity coefficient in a particular system.

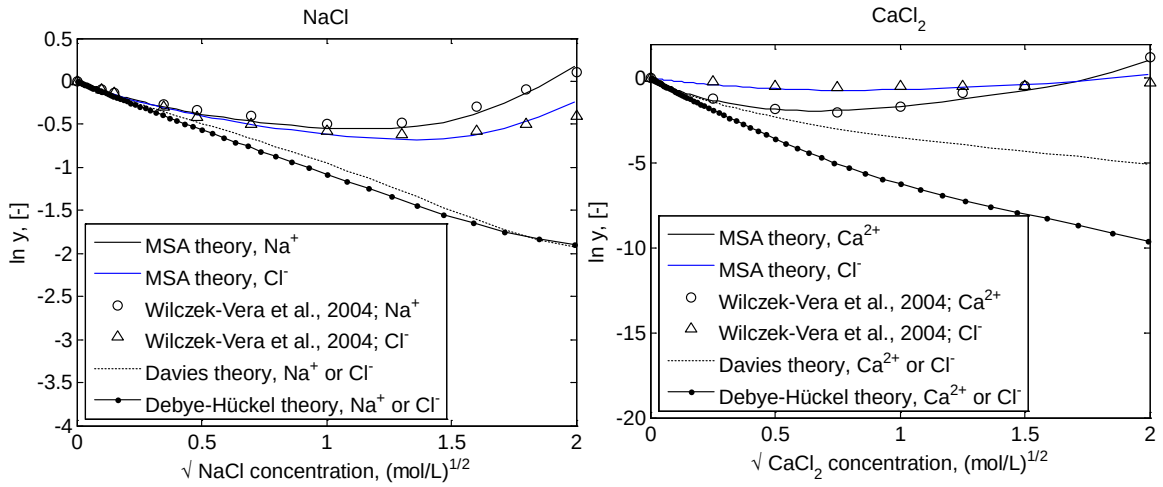

Figure 3.5 The natural logarithm of molar free–ion activity coefficient as a function of molar concentration of NaCl and $CaCl_2$.

Figure 3.5 was drawn up to the maximum solubility of the electrolytes where they remain soluble in this range. The MATLAB scripts for sodium chloride solution is detailed in Appendix 5.

From Sections 3.2–3.5, it can be concluded that:

1. The MSA theory could satisfactorily predict molar activity coefficient of any free ions of an assumed solution up to high concentration, and enabled better fitting with the experimental data in compared with the other theories.
2. Water activity of both approaches was in a good agreement with the corresponding experimental data as a means of validation.
3. As there is no similar relationship for the correlation between the dielectric constant and the molar concentration of various electrolytes and multicomponent solutions in literature, Equation (3.18) was applied to the simulation of all models in this study.

3.6 Application of the model to buffer systems

Buffer solutions are derived from weak acids and bases along with their conjugate bases and acids with the intrinsic association constants close to the neutral pH, i.e. the effective buffer solution should normally have pH=pK_a±1.5, and subsequently strong electrolytes with pK_a values either larger or smaller than the range that called '*non–buffer ions*' (Constable, 1997).

Buffer solutions such as citrate and phosphate were modelled, not only because of the containing significant ions in milk, but also they are appropriate examples with available

titration data in literature. Additionally, lactose was incorporated experimentally and mathematically into the citrate buffer, for which the MSA theory and not Davies theory was believed to predict the non–electrolyte activity coefficient.

3.6.1 Citrate and phosphate buffer solutions

Citrate buffer was prepared by mixing 0.1 mol L^{-1} citric acid monohydrate ($H_3Cit.H_2O$) and 0.1 mol L^{-1} trisodium citrate dihydrate ($Na_3Cit.2H_2O$) to get 0.1 L of 0.1 mol L^{-1} citrate buffer as shown by Table 3.3 (Promega, n.d).

The table did not cover the whole range of pH values, i.e. for pH lower than 3.0 and larger than 6.2. Therefore, more experiments were carried out to extend the range.

Table 3.3 The experimental recipe for preparing the citrate buffer (Promega, n.d).

pH of the buffer	Volume of the citric acid solution, [mL]	Volume of the sodium citrate solution, [mL]
3.0	82.0	18.0
3.2	77.5	22.5
3.4	73.0	27.0
3.6	68.5	31.5
3.8	63.5	36.5
4.0	59.0	41.0
4.2	54.0	46.0
4.4	49.5	50.5
4.6	44.5	55.5
4.8	40.0	60.0
5.0	35.0	65.0
5.2	30.5	69.5
5.4	25.5	74.5
5.6	21.0	79.0
5.8	16.0	84.0
6.0	11.5	88.5
6.2	8.0	92.0

3.6.1.1 Method of preparation

2.1014 g (equivalent to 0.1 mol L^{-1}) of citric acid monohydrate ($C_6H_8O_7.H_2O$ or $H_3Cit.\ H_2O$) (AnalaR, VWR International Ltd. Poole, England) with molecular weight of 210.14 g mol^{-1} was weighed in a 25 mL beaker. The dry citric acid was transferred to a 100 mL glass volumetric flask by slightly dissolving with ultrapure Milli–Q water (Merk Millipore, 18.2 MΩ cm at 25 ˚C). The flask was then filled with water to 100 mL.

2.9410 g (equivalent to 0.1 mol L^{-1}) of trisodium citrate dihydrate ($C_6H_5Na_3O_7.2H_2O$ or $Na_3Cit.2H_2O$) (Merck, Germany) with molecular weight of 294.10 g mol^{-1} was weighed by the balance and made up to 0.1 mol L^{-1} like the afore–mentioned procedure for the citric acid solution.

One mL of the citric acid solution was drawn up by a clean and dry 1±0.007 mL glass pipette and was thrown away to be able to have 99 mL of the citric acid solution. The same volume was drawn up from the sodium citrate solution and was then added to the citric acid solution to make up 0.1 mol L^{-1} citrate buffer. Other volumes of the solutions were made up similarly to for low and high pH values, i.e. 97, 92, and 85 mL of citric acid solutions with corresponding 3, 8, and 15 mL of sodium citrate solutions. The other experiments were based on the Table 3.3.

pH of solutions was measured by a CyberScan pH 310 pH/mV meter (Eutech, Germany) that was equipped with an automatic temperature control probe and an Eutech pH probe with a capability of measuring to two decimal places. Calibration was carried out every day before the measurements to avoid any experimental errors for the pH meter using three standard buffer solutions with pH values of 4, 7, and 10. The uncertainty was estimated to be ±0.02.

3.6.1.2 Results and analysis of data

The experimental data from literature and those carried out in this study were compared with the simulated ones in terms of ratio of total sodium to citric acid and pH value, as shown in Figure 3.6a. The intrinsic association constants of ions given by Holt et al. (1981) were used. However, small changes were made to the K_a of hydrogen citrate and citrate in equilibrium with free hydrogen ions. The pH values seem to be sensitive to the intrinsic association constants of hydrogen citrate and citrate with hydrogen ion leading to the formation of dihydrogen and hydrogen citrates. The constants, K_{a_1} and K_{a_2}, (as defined below) were changed from 6.00×10^4 to 7.9×10^4 and from 2.57×10^6 to 6.9×10^6 mol^{-1} L, respectively, to be able to get better fitting with the experimental data. The K_a values of other species remained unchanged in the simulation.

$$H_2Cit^- \overset{K_{a_1}}{\longleftrightarrow} HCit^{2-} + H^+ \qquad K_{a_1} = \frac{a_{H_2Cit^-}}{a_{HCit^{2-}} a_{H^+}} \tag{3.34}$$

$$HCit^{2-} \overset{K_{a_2}}{\longleftrightarrow} Cit^{3-} + H^{+} \qquad K_{a_2} = \frac{a_{HCit^{2-}}}{a_{Cit^{3-}} a_{H^{+}}} \tag{3.35}$$

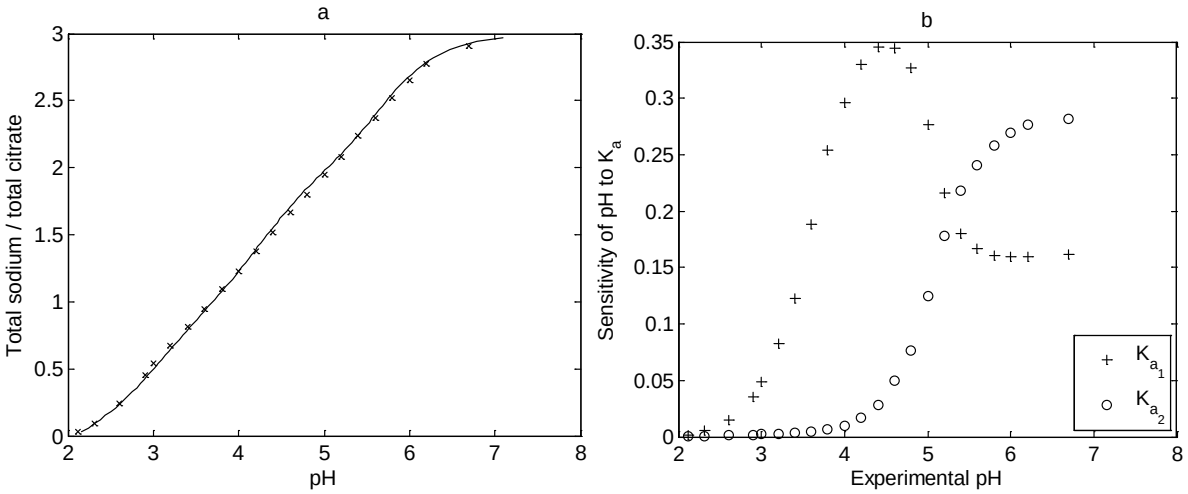

Figure 3.6 (a) The ratio of total sodium to total citrate for citrate buffer as a function of pH. The solid curve and '×' symbol respectively represent this study and experimental data from Promega (n.d). (b) The sensitivity of pH to K_{a_1} and K_{a_2} values with the experimental pH.

To test the sensitivity of the pH to K_{a_1} and K_{a_2}, the values of K_{a_1} and K_{a_2} were increased by 32% and 100%, respectively. Sensitivity was defined as change in pH over relative change in K_a, i.e. $\Delta\text{pH}/\frac{(K_{a\,\text{adjusted}} - K_a)}{K_a}$. pH was more sensitive to K_{a_1} in the pH range of 3–6, whereas it was sensitive to K_{a_2} at pH values greater than 4.5 as shown by Figure 3.7. The larger quantity of K_{a_2} caused less citrate (Cit^{3-}) and hydrogen ions in the solution and hence caused higher pH, whereas a lower value of K_{a_1} led to release of hydrogen citrate ($HCit^{2-}$) and more hydrogen ion according to Equations (3.34) and (3.35). The citrate ion was the dominant species in higher pH values, while dihydrogen citrate and hydrogen citrate ions were produced in more acidic environments. The intrinsic association constant for other species did not significantly influence the ion interactions due to their very small values compared with K_{a_1} and K_{a_2} values.

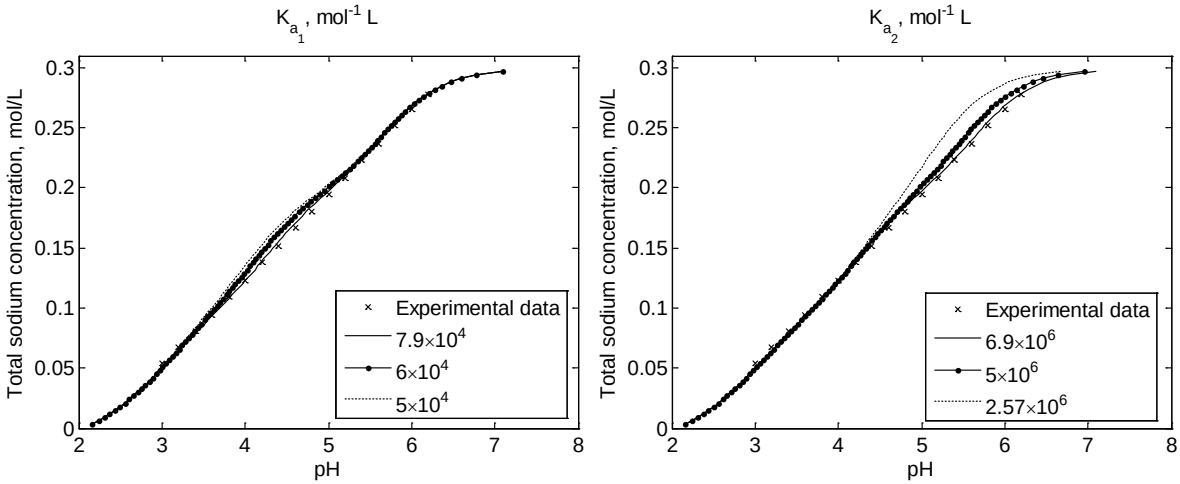

Figure 3.7 The effect of K_{a_1} and K_{a_2} on pH of citrate buffer solution and the comparison with the experimental data.

Similarly, the phosphate buffer system was mathematically simulated and was compared with the experimental data presented by Promega (n.d), in which various ratios of disodium hydrogen phosphate dihydrate ($Na_2HPO_4.2H_2O$) and sodium dihydrogen phosphate monohydrate ($NaH_2PO_4.H_2O$) were experimentally made up and mixed to prepare 0.1 mol L^{-1} phosphate buffer solution. Disodium hydrogen phosphate dihydrate produces only one hydrogen ion in the solution, whereas sodium dihydrogen phosphate monohydrate is able to release two hydrogen ions.

The pH of the phosphate buffer solution is shown as a function of total sodium to total phosphate ratio in Figure 3.8a. No adjustment was made to the intrinsic association constants of the phosphate buffer solution. Figure 3.8b indicates that the dihydrogen phosphate ion was the most abundant phosphate species across the pH range 4–6, where hydrogen phosphate ion started to form and then became the most plentiful species in the pH range of about 7–8. The simulated results were very similar to simulated data points from Rice et al. (2010).

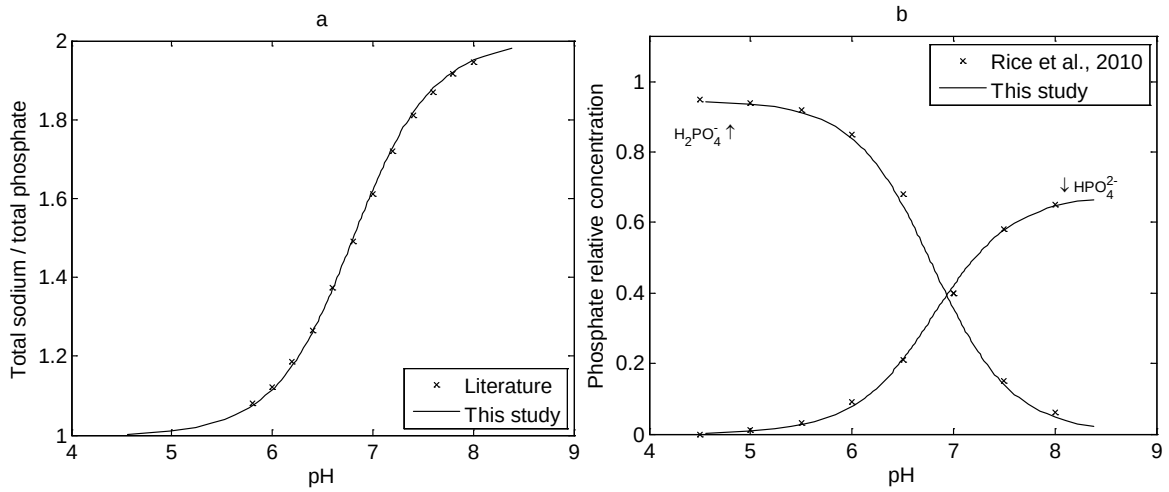

Figure 3.8 (a) Total sodium to phosphate ratio vs pH of phosphate buffer solution; (b) Relative concentration of dihydrogen phosphate and hydrogen phosphate ions.

3.6.2 Citrate buffer with lactose solution

The ion equilibria of citrate buffer were simulated and experimentally studied with two different concentrations of lactose to determine the effect of milk sugar on the ions interaction: 45 g L^{-1} and 250 g L^{-1}, that are roughly equal to, and five times, the lactose concentration in milk, respectively.

Citric acid and sodium citrate solutions were made up of 0.1 mol L^{-1} in a 100 mL glass volumetric flask, each of which was prepared similarly to the recipe for the preparation of citrate buffer without lactose solution that was described in the previous section. Solutions were made up with citric acid, sodium citrate, and monohydrate lactose ($C_{12}H_{22}O_{11}.H_2O$) (BDH Chemicals Ltd., Poole, England) with molecular weight of 360.312 g mol^{-1}. The final concentrations of lactose were 0, 45, and 250 g L^{-1}. A range of pH values were obtained by varying the volumes of 0.1 mol L^{-1} citric acid and sodium citrate added.

Lactose was assumed theoretically as a non–electrolyte in the simulation with zero charge number and effective size parameter of 0.455 nm (Isaad and Perwuelz, 2010). pH was mathematically calculated for 45 g L^{-1} and 250 g L^{-1} as shown in Figure 3.9a.

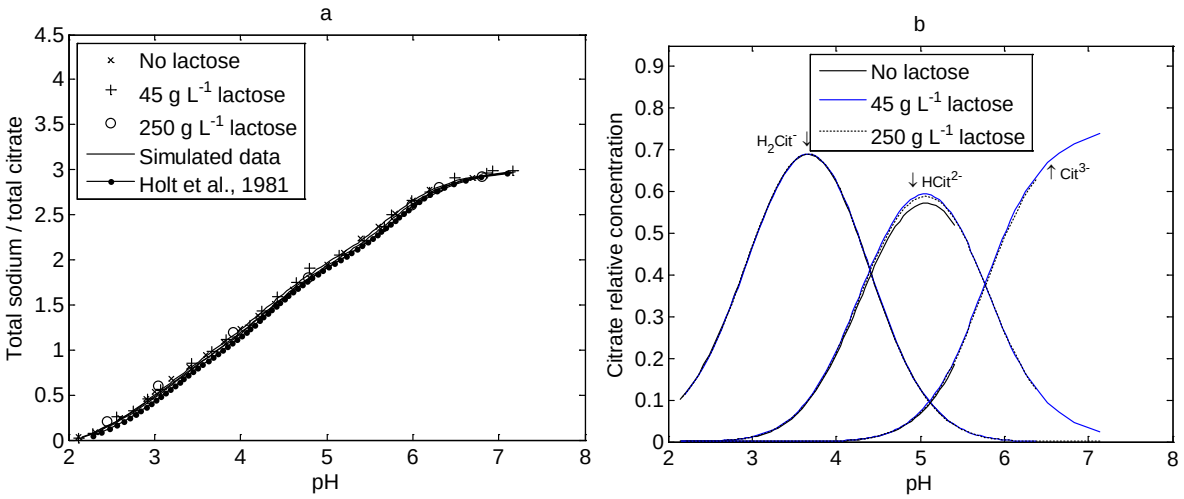

Figure 3.9 (a) The total sodium concentration versus pH of citrate buffer solution with and without lactose; (b) The relative concentration of citrate ions using MSA theory.

The model was fitted with the experimental data for no lactose, 45 g L^{-1} lactose, and 250 g L^{-1} lactose solutions as shown in Figure 3.9a indicating no significant change between the pH of the buffer solution with and without lactose. Figure 3.9b shows that there is a little change in the concentrations of different ions. The activity coefficients of the species were obtained by the Extended Debye–Hückel theory, in which the effective size parameter was assumed 0.9 nm for H^+, 0.5 nm for Cit^{3-}, and 0.4 nm for the monovalent ions (Holt et al., 1981), and then compared with the corresponding data calculated by the MSA theory for the citrate buffer solution with 250 g L^{-1} lactose.

H_2Cit^- was the most abundant citrate species across the pH range 2–4. Following this, $HCit^{2-}$ was the most plentiful species in the pH range of about 4–6, after which Cit^{3-} became the most prevalent species when citric acid had the lowest concentration in the buffer solution. The arrows in Figure 3.9b represent the corresponding pK_a values of citrate ions.

Since lactose did not show notable influence on the equilibria of the buffer solution, the molar activity coefficients of citrate species were obtained for the solution containing no lactose and 250 g L^{-1} lactose and are shown in Figure 3.10a and b. This confirms that the molar activity coefficients of citrate species in the 250 g L^{-1} lactose solution are higher than in solutions without lactose, demonstrating the strength of MSA theory to predict activity coefficient of solutions containing the non–electrolyte. In contrast, Davies theory shows similar results for the buffer solution with and without lactose. The differences predicted by the MSA theory are

because of the hard sphere term enabling determination of molar activity coefficient of species containing both electrolyte and non–electrolyte for any concentration.

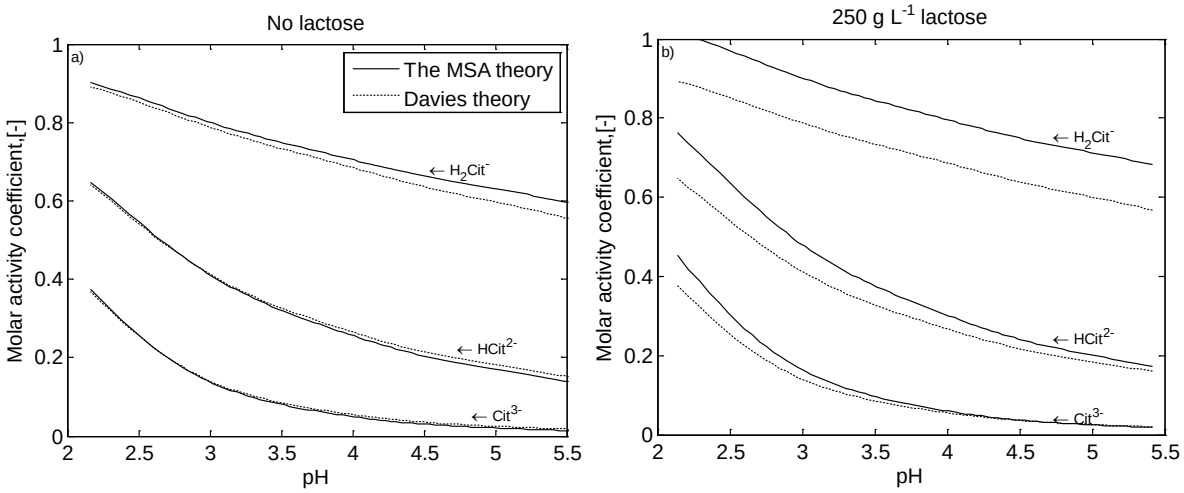

Figure 3.10 (a) Molar activity coefficient of citrate ions in the buffer solutions with no lactose; (b) Molar activity coefficient of citrate ions in the citrate buffer solution with 250 g L^{-1} lactose by the MSA and Davies theories.

Figure 3.11 shows that the hard sphere contribution of the MSA theory for the citrate buffer solution containing 250 g L^{-1} lactose is approximately 20% larger than that without lactose. Davies theory was unable to predict activity coefficient of lactose due to terms that only incorporate ionic strength.

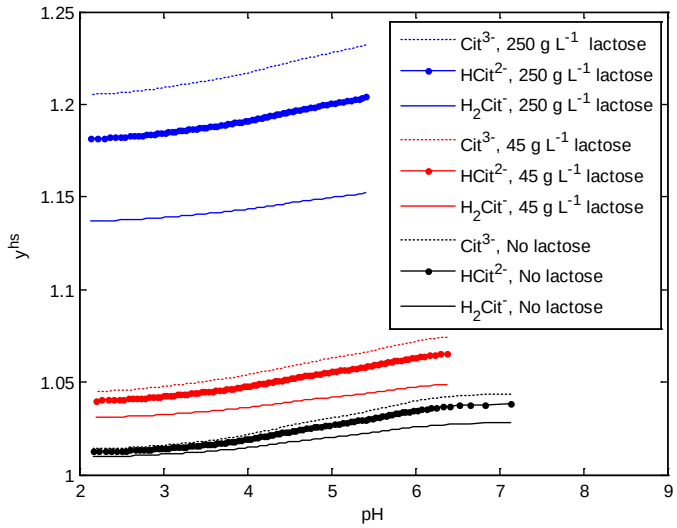

Figure 3.11 Hard sphere contribution of the MSA theory for citrate buffer solutions with and without lactose.

From this section, it can be concluded that:

1. The proposed model using MSA theory could satisfactorily predict ion equilibria of citrate buffer with and without lactose, as well as the phosphate buffer lactose.
2. The interactions between hydrogen citrate, citrate ions, and hydrogen were more likely to affect the ion equilibria rather than other species in the citrate buffer solution, the intrinsic association constants of which were adjusted to get better fitting with the corresponding experimental data.
3. The results showed that lactose had a marginal effect on the ion equilibria of citrate buffer solution, but significantly affected the activity coefficients through its effect on the hard sphere contribution of all ions.

3.7 Application of the model to solid phase systems

Supersaturated solutions can exist as metastable and unstable phases. They occur in many scientific fields such as biology, industrial processes, and material sciences (Brečević and Füredi-Milhofer, 1972; Söhnel and Mullin, 1982; Brečević et al., 1986; Brečević and Nielsen, 1989).

During evaporation or reverse osmosis of milk, the concentration of ions can easily exceed the solubility limits. This leads to heterogeneous precipitation of milk minerals on evaporator surfaces or reverse osmosis membranes, which reduces the operating time of the equipment before cleaning is required (Kezia et al., 2017).

Several investigations have been done on the ion equilibria in dairy liquids by incorporating solid phases, which are mainly calcium phosphate ($CaHPO_4$), calcium carbonate ($CaCO_3$), calcium citrate (Ca_3Cit_2) (Mekmene, Quillard, et al., 2009; Gao, van Halsema, et al., 2010; Kazadi Mbamba, 2016; Kezia et al., 2017; Garcia et al., 2018). However, most of these studies focused on the solubility of solid phase and did not provide investigation of high concentration of electrolytes by either considering steady state condition or dynamically. In this thesis, the proposed model was applied individually to calcium carbonate, calcium phosphate, and calcium citrate solutions along with lactose. The MSA theory was used to determine activity coefficients of species by both assuming time dependent and equilibrium conditions, because it is believed that, the MSA theory is better able to predict activity coefficients at high concentrations of species.

3.7.1 Calcium carbonate solution

Calcium carbonate is one of the most significant minerals, which can be found in nature abundantly (Njegić-Džakula et al., 2010). Various metastable phases of calcium carbonate can be formed during a spontaneous precipitation such as calcite, aragonite, and vaterite, among which calcite is the most stable type at ordinary conditions with low solubility (Brečević and Nielsen, 1989). Calcium carbonate can exist as hexahydrate, monohydrate, or amorphous (Brooks et al., 1950). In milk, apart from calcium phosphate as the main precipitating component with low solubility, calcium carbonate is another potential insoluble salt in the serum phase of skimmed milk with an approximate concentration of 0.014 mM (Walstra and Jenness, 1984).

3.7.1.1 Steady state study

The ion equilibria of calcium carbonate solution were determined mathematically and experimentally when hydrochloric acid (HCl) was incorporated into the system to maintain the pH values of the solutions without disturbing the equilibria. The available data in literature was not sufficient, so several experiments were implemented to measure pH values of calcium carbonate and hydrochloric acid mixtures.

0.01 g (equivalent to 1 mmol L^{-1}) of anhydrous calcium carbonate ($CaCO_3$) (AnalaR Normapur, VWR PROLABO, Belgium) with molecular weight of 100.09 g mol^{-1} was weighed and transferred to a clean and dry 100 mL glass volumetric flask.

One mL of 1.0 mol L^{-1} hydrochloric acid solution was drawn up by a clean and dry 1±0.007 mL glass pipette and was then added to the volumetric flask containing calcium carbonate. The flask was filled up with fresh and ultrapure Milli–Q water to be able to prepare a solution with 1.0 mmol L^{-1} calcium carbonate and 10 mmol L^{-1} hydrochloric acid. Similarly, several calcium carbonate solutions were made up with 10 mmol L^{-1} hydrochloric acid, and pH was measured.

The results were then compared with other experimental data available in literature that are shown in Figure 3.12. The experimental data of this study were closest to the data presented by Reardon and Langmuir (1974); however, more deviation was observed for higher concentration of calcium carbonate solution when the system became complicated with more

ion interaction. The solutions were supersaturated in respect to calcium carbonate, and no sign of precipitation was observed by either eye or shining a laser pointer through the solution.

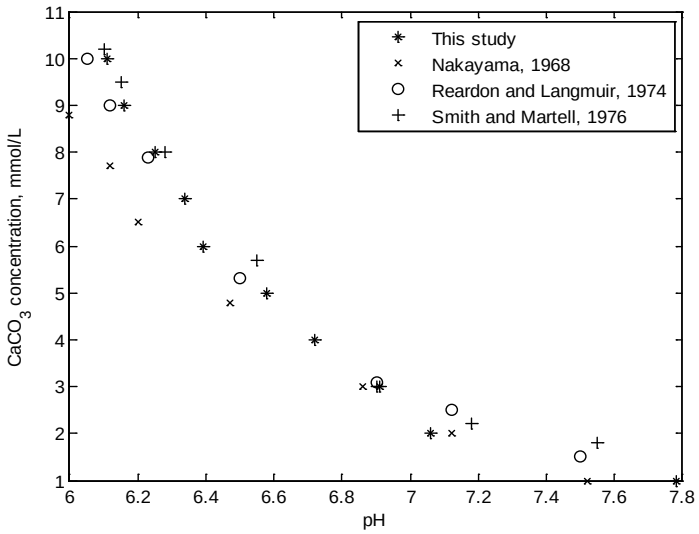

Figure 3.12 Experimental pH values investigated in this study and compared with Nakayama (1968), Reardon and Langmuir (1974), and Smith and Martell (1976b).

Calcium carbonate solution was simulated by the proposed model. Figure 3.13 shows the pH of different concentrations of calcium carbonate for various numerical values of the intrinsic association constant, which was adjusted to 9×10^{9} from 2.13×10^{10} mol^{-1} L given by Holt et al. (1981). This adjustment was made according to the Equation (3.36) for the equilibrium between hydrogen and carbonate ions (CO_3^{2-}) to get better fitting with the corresponding experimental data. Intrinsic association constants of other species remained unchanged in the simulation and were used from Table 3.1.

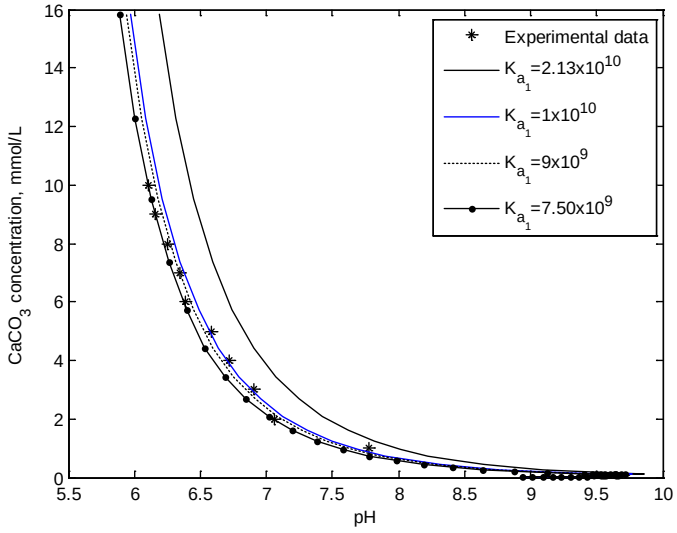

Figure 3.13 Adjustment of the intrinsic association constant to the corresponding experimental data.

$$HCO_3^- \leftrightarrow H^+ + CO_3^{2-} \qquad K_a = \frac{a_{HCO_3^-}}{a_{H^+} a_{CO_3^{2-}}} \tag{3.36}$$

A lower intrinsic association constant than the original value represents high dissociation and thus higher concentration of hydrogen and carbonate ions. Therefore, a lower pH was obtained lower for a particular total concentration of calcium carbonate solution. Figure 3.14 shows the relative concentration of each individual calcium or carbonate ion.

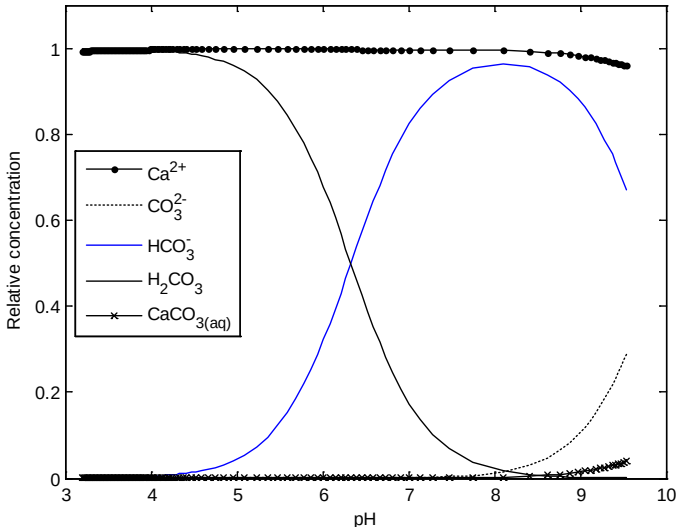

Figure 3.14 Simulated distribution of calcium and carbonate species in supersaturated aqueous calcium carbonate solution.

Free calcium remained at a relative concentration above 99% below pH 8.5, after which it started to drop corresponding to the formation of free carbonate ions, and the calcium carbonate ion–pair. This simulation did not calculate precipitation dynamics so the predicted concentration of $CaCO_{3(aq)}$ is likely to exceed the solubility limit.

Molar activity coefficients of the free carbonate and calcium were calculated by both the MSA and Davies methods as shown in Figure 3.15. The hydrogen carbonate activity coefficient obtained from the MSA is much higher than that calculated by Davies theory. This difference is more likely to be observed at concentrations above 100 mmol L^{-1} of calcium carbonate solution where the MSA theory is more likely capable for prediction of activity coefficients than Davies theory.

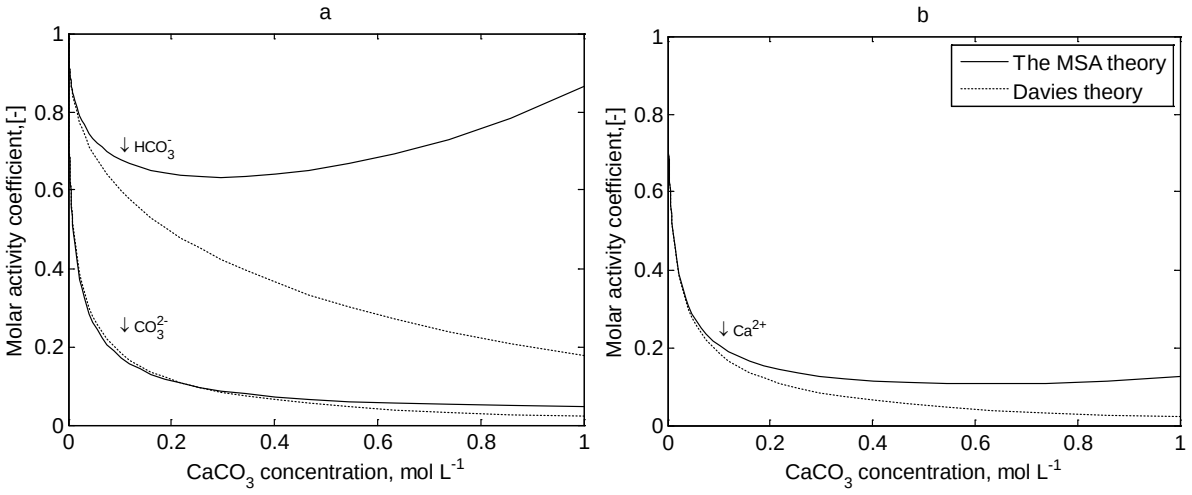

Figure 3.15 Molar activity coefficient of free a) carbonate and b) calcium species in the calcium carbonate solution.

3.7.1.2 Dynamic study

The proposed model in this study was applied dynamically to the calcium carbonate system to determine ion equilibria and parameters changing over time. Precipitation of calcium carbonate was investigated mathematically and experimentally by Kazadi Mbamba (2016) to develop an approach for wastewater applications, and data from this work were used as a validation for the current study.

The dynamic simulation of calcium carbonate solution was implemented over time by applying Euler's method as outlined in Section 3.4.

The rate of calcium carbonate precipitation, [mol L^{-1} min^{-1}] was given by the following equation:

$$\frac{dC_{CaCO_{3(s)(i)}}}{dt} = k_{prec}\, C_{CaCO_{3(s)(i)}}\, \sigma^{n}; \quad \sigma = Sat^{\frac{1}{\nu}} - 1 \tag{3.37}$$

where the solid phase reaction order (n) and precipitation rate constant (k_{prec}) were chosen to be 2 and 0.0025 min^{-1}, respectively (Kazadi Mbamba, 2016). σ is the relative supersaturation which was calculated according to the saturation parameter that was considered as an individual species in the set of ions and obtained as follows:

$$Sat = \frac{IAP}{K_{sp}} = \frac{a_{Ca^{2+}}\, a_{HCO_3^{2-}}}{K_{sp}} \tag{3.38}$$

The solubility product was obtained $10^{-8.48}$ mol^2 L^{-2}.

Kazadi Mbamba (2016) prepared the carbonate solution by mixing 1.96 mM $CaCl_2$, 4.95 mM $NaHCO_3$, and then added 2.6 mM NaOH with flowrate of 2.5 mL min^{-1}. The calculated data were fitted to the titration experiment results by Kazadi Mbamba (2016). Figure 3.16 shows that when the solid phase of calcium carbonate starts to form, there is a slight drop in pH and a drastic decrease in the total soluble calcium concentration that indicates the precipitation of calcium carbonate after about 80 minutes, clearly not as pH continues to change.

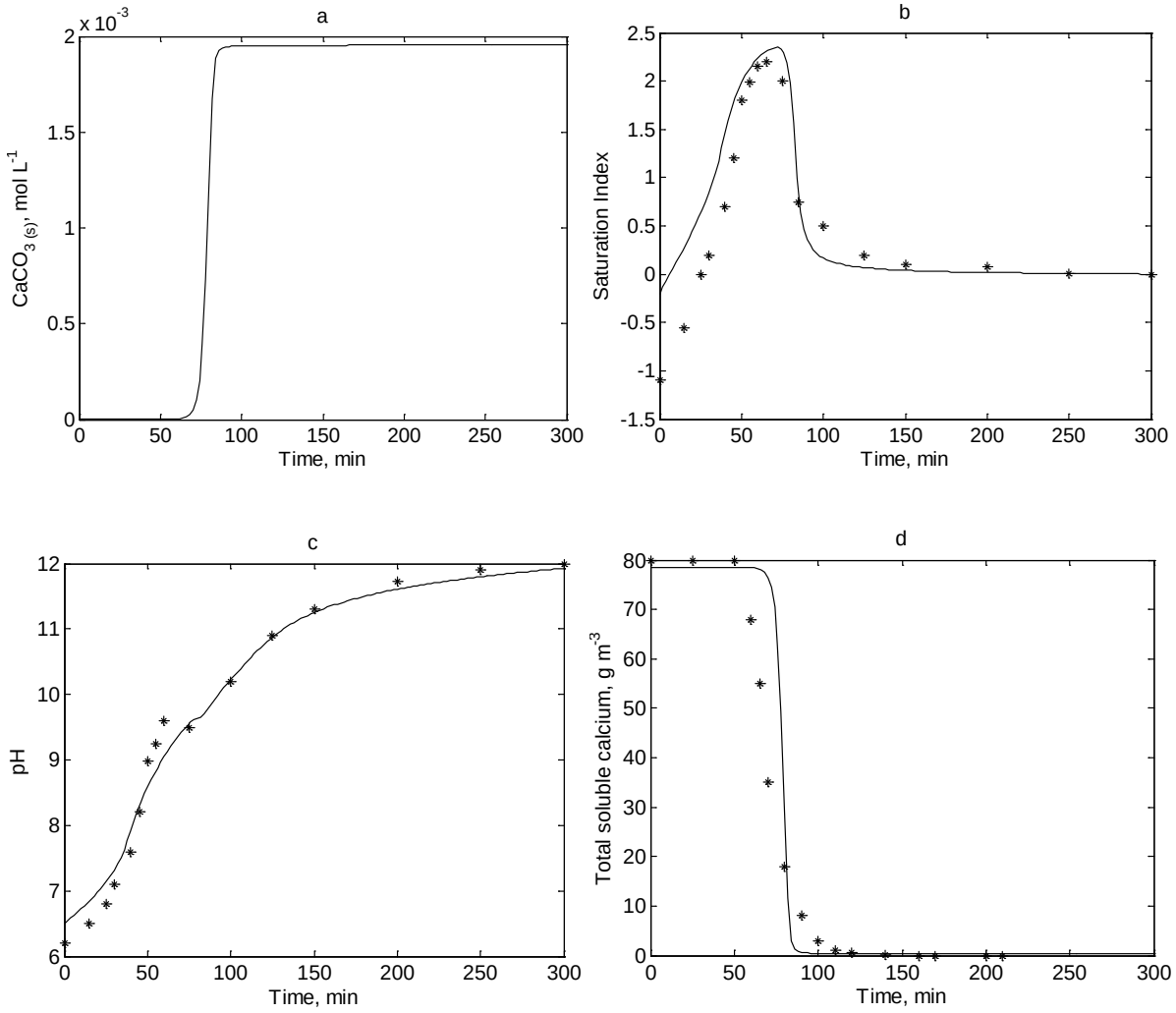

Figure 3.16 Dynamic simulation of calcium carbonate solution fitted with the corresponding experimental data of Kazadi Mbamba (2016) that is shown by the '*' symbol.

Figure 3.16 was plotted after adjusting the numerical values of the solubility product and intrinsic association constant for better fitting to the experimental data. The solubility product was altered from $10^{-8.48}$ to $10^{-9.2}$ mol^2 L^{-2} signifying higher saturation and saturation index, and thus bringing forward the precipitation. Similarly, an increase in the association constant

between free calcium and hydrogen carbonate (K_{a_1}) from 1.4×10^3 to 9.0×10^3 mol^{-1} L leads to lower level of free ions, thus higher quantities of saturation according to the Equation (3.39).

$$CaHCO_{3(aq)} \leftrightarrow Ca^{2+} + HCO_3^- \qquad K_{a_1} = \frac{a_{CaHCO_{3(aq)}}}{a_{Ca^{2+}}\, a_{HCO_3^-}} \tag{3.39}$$

The intrinsic association constant between hydrogen and carbonate ions (K_{a_2}) (Equation (3.40)) was roughly doubled from 2.13×10^{10} to 4.5×10^{10} mol^{-1} L, resulting in lower pH values in the very early stage of reaction for the purpose of better fitting.

$$HCO_3^- \leftrightarrow H^+ + CO_3^{2-} \qquad K_{a_2} = \frac{a_{HCO_3^-}}{a_{H^+}\, a_{CO_3^{2-}}} \tag{3.40}$$

The Runge–Kutta fourth–order method was also employed in the dynamic simulation of calcium carbonate, as this method has higher accuracy than Euler's method. K_{a_1} and K_{a_2} were kept the same with the Runge–Kutta method. The solubility product of calcium carbonate was the only parameter that was altered from $10^{-8.48}$ to $10^{-8.722}$ mol L^{-1} showing less saturation in the very early stage of the dissolution as shown in Figure 3.17b compared to Figure 3.16b. In addition, the decrease in pH was matched better with the experimental data when the precipitation started to occur at about 80 minutes. However, this method did not influence on the kinetics of formed precipitates and could only bring forward the total calcium concentration.

3.7.2 Calcium phosphate solution

Calcium phosphate precipitation has been studied extensively in various research areas such as medical, biological, and environmental sciences for analysing kidney stones, accumulation of calcium salts in the body, mechanically stabilising bone and teeth, and extraction of phosphate components from wastewater (Joko, 1984; Nicollas et al., 1989; Raynaud et al., 2002; Bleek and Taubert, 2013). In milk, calcium is bound with inorganic phosphate forming a sparingly soluble calcium phosphate that is stabilised by the micellar organic phosphate so–called phosphoseryl residues of casein (Holt, 1992; Little and Holt, 2004).

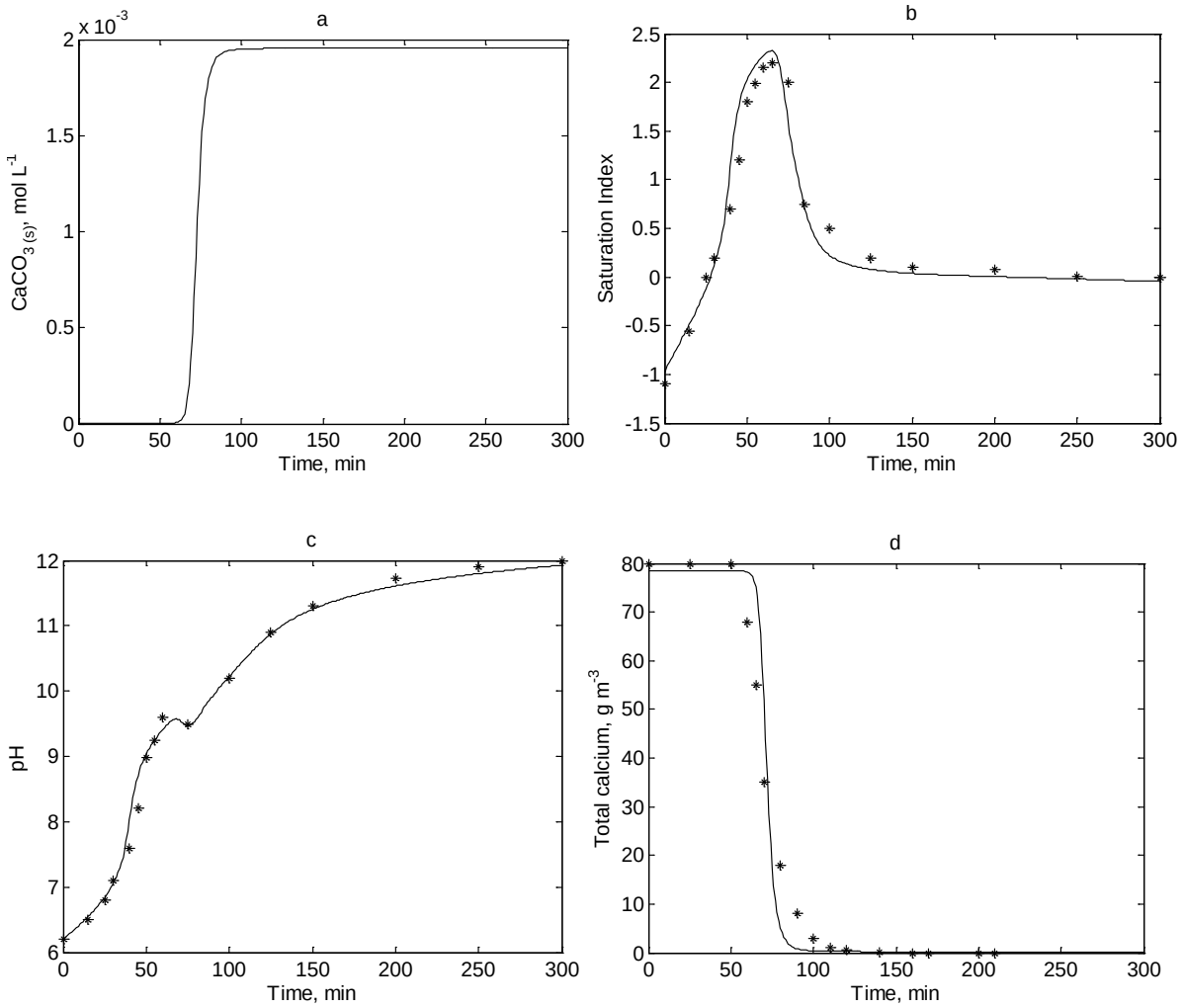

Figure 3.17 Dynamic simulation of calcium carbonate using Runge–Kutta method fitted with the corresponding experimental data of Kazadi Mbamba (2016) that is shown by the '*' symbol.

Investigations of calcium phosphate solubility are complicated and continuing due to incongruent mechanisms throughout the equilibria (Miyazaki et al., 2009; Pan and Darvell, 2009a, 2009b). A large number of investigations has been done on the solubility of calcium phosphate, but less data are available for the speciation of ions in a wide range of pH and for high concentration of the solution either at equilibrium or dynamically. The aim of this section is to evaluate how changes in pH and ions activity can affect the speciation and the precipitation of the solution.

3.7.2.1 Controlling pH by NaOH in steady state study

The speciation of calcium phosphate system was determined by the model, to which the MSA theory was applied for calculation of activity coefficient of ions. The saturation of dicalcium phosphate dihydrate was calculated using the solubility product of 2.07×10^{-7} mol^2 L^{-2}, which

was taken from Mekmene, Quillard, et al. (2009). The simulation was implemented for calcium and phosphate speciation in which pH was controlled mathematically by adding sodium hydroxide to the solution. Typical results for phosphate and calcium relative concentrations are shown in Figure 3.18 with 2 mM concentrations for calcium and phosphate compounds. These calculations were done with the assumption that all products remain as stable ion–pairs in solution and do not precipitate.

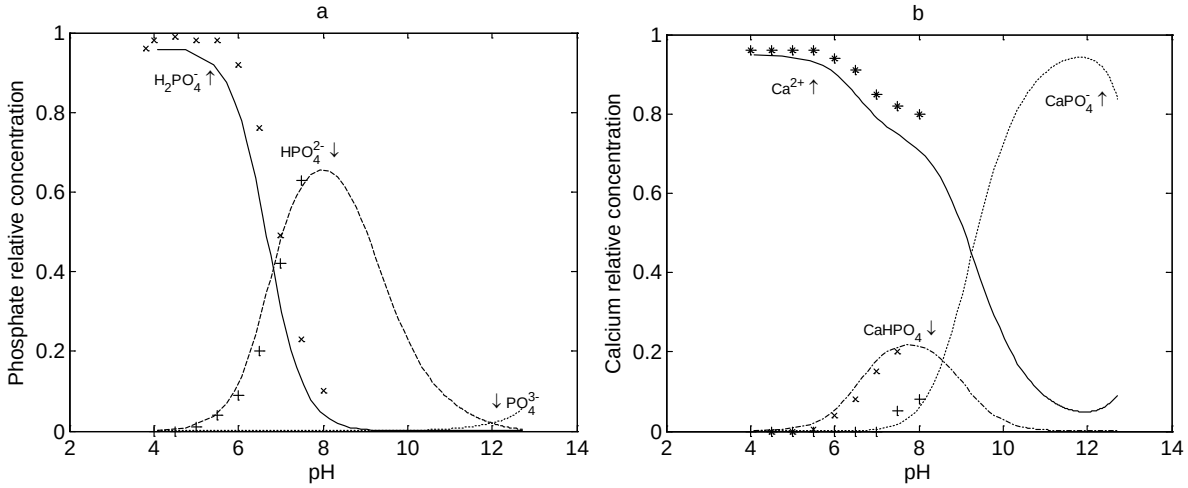

Figure 3.18 Simulated relative concentrations of 2 mM; a) phosphate ions and b) calcium ions and other components in water with pH adjustment by NaOH. The symbols '×', '+', and '*' represent some points of simulated data from Rice et al. (2010).

Figure 3.18 shows the simulated phosphate and calcium species in a calcium phosphate system that was compared with the predicted data from Rice et al. (2010). They used the Davies model to calculate activity coefficients and hence it was not expected that identical results would be obtained. Dihydrogen phosphate ion ($H_2PO_4^-$) was the most plentiful species in the pH range of 4–7, while hydrogen phosphate ion started to increase from pH of 5. The contribution of other species was low to be incorporated into Figure 3.18.

The graphs of dihydrogen phosphate and hydrogen phosphate ions intersected each other at pH about 7 representing the pK_a numerical value between those species approximately. The intrinsic association constants were from Table 3.1 without altering any values.

From the calculation of ion speciation and activities, one can obtain the ion activity product and hence the saturation as shown in Figure 3.19. The concentration of both Ca^{2+} and PO_4^{3-} in milk serum are about 10 mM (Walstra et al., 2006). If no other ions were present, which would reduce the ion activities, then 10 mM Ca^{2+} and PO_4^{3-} would be about 25 times the saturation limit at a typical pH of 6.7.

Figure 3.19 indicates the saturation for lower concentrations of Ca and PO_4 started from the pH about 4 where no NaOH had been added. Precipitation was predicted to start occurring from pH about 5 for the 10 mM Ca and PO_4 concentrations, but the 5 mM and 3 mM solutions might start to precipitate at pH higher than 5. The highest saturations are predicted to occur at pH about 7.5 for all three solutions, where hydrogen phosphate are likely at its maximum in the solution.

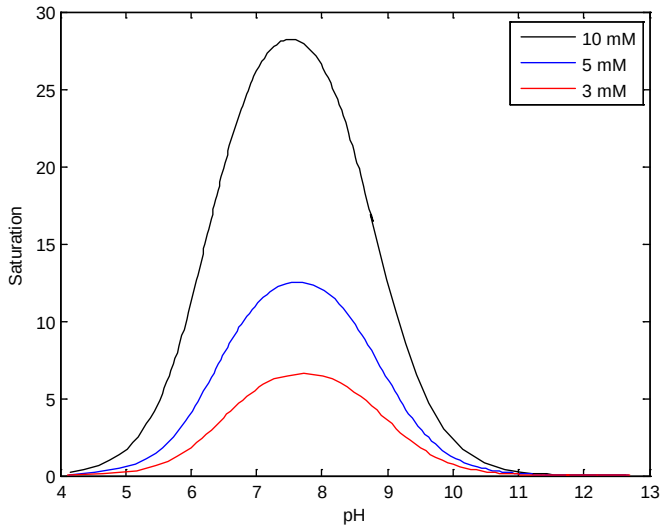

Figure 3.19 Saturation of $CaHPO_4$ at different molar concentration of Ca^{2+} and PO_4^{3-}.

The MSA and Davies theories were employed to calculate free calcium activity coefficient for 3 and 20 mM concentrations of Ca^{2+} and PO_4^{3-} as shown in Figure 3.20. The ionic strength values of marked points are provided in Table 3.4 to explicitly indicate the distinction between the two different points. The ionic strength, which appears directly in the Davies equation, but indirectly through ς in the MSA equation, was defined earlier in Chapter 2.

Table 3.4 Numerical values of ionic strength at four marked points shown in Figure 3.20 at 3 and 20 mM concentrations of Ca^{2+} and PO_4^{3-}.

	Ca^{2+} and PO_4^{3-} concentrations, mM			
	3		20	
NaOH, mM	3.2	6.2	20	40
Ionic strength term for MSA, ς	6.05×10^{14}	-3.57×10^{14}	2.85×10^{15}	-2.22×10^{15}
Ionic strength, I	0.014	0.010	0.08	0.06

Generally, addition of NaOH increases the total concentration of added ions, but it changes the speciation and hence can reduce the ionic strength, and increase activity coefficients.

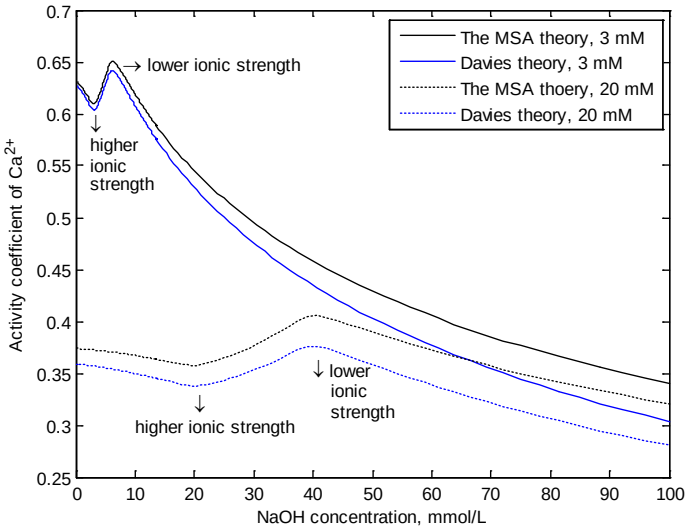

Figure 3.20 Activity coefficient of Ca^{2+} by the MSA and Davies theories in a Ca^{2+}, PO_4^{3-}, and Na^+ solution.

Figure 3.20 shows that the activity coefficients hit a low point at 20 mM NaOH for 20 mM Ca^{2+} and PO_4^{3-} concentration corresponding to a high concentration of free calcium and sodium ions. This causes a strong positive contributions to the ionic strength term 'ς' which causes the electrostatic contribution to activity coefficient 'y^{es}' in the MSA theory to have a lower value. In contrast, chloride and aqueous ion–pair calcium phosphate ($CaPO_{4(aq)}^{-}$) made strong negative contributions at 40 mM NaOH concentration but with a lower ionic strength, because the ions exist as an ion–pair with lower charge. The ionic strength term represents the effect of either positive or negative contributions of ion–pairs for the Davies theory. Similarly, the ionic strength values was higher for the 3 mM Ca^{2+} and PO_4^{3-} concentration at 3.2 mM NaOH for both approaches leading to lower y^{es} and hence lower activity coefficient.

The term 'ς' for the MSA theory and ionic strength for Davies theory was calculated for the four minimum and maximum points indicated in Figure 3.20 and Table 3.4. There is a stronger positive contribution to ς and ionic strength for 20 mM Ca^{2+} and PO_4^{3-} concentration at 20 mM NaOH than that of 3 mM Ca^{2+} and PO_4^{3-} concentration at 3.2 mM NaOH. Hence, the low point of 20 mM of Ca^{2+} and PO_4^{3-} concentration had lower value of Ca^{2+} activity coefficient.

Similarly, stronger negative contributions of chloride ion for 3 mM Ca^{2+} and PO_4^{3-} concentration at 6.2 mM NaOH than that of 20 mM Ca^{2+} and PO_4^{3-} concentration at 40 mM NaOH represent higher Ca^{2+} activity coefficient value. Generally, lower concentrations of

Ca^{2+} and PO_4^{3-} need less NaOH to get to the low point where there has strong positive contribution to ς. This example shows some of the complexity in this system.

3.7.2.2 Dynamic study by continuously adding NaOH

Dynamic simulations of calcium phosphate solution were also performed to monitor the change over time. To obtain more data for validation, an experiment was also carried out in which the pH was monitored after a solution of 6 mM $CaCl_2$ and NaH_2PO_4 was created.

Arifuzzaman and Rohani (2004) tested a set of experiments to obtain pH of calcium phosphate over time. 6 mM $CaCl_2$ and 6 mM NaH_2PO_4 were assumed as initial concentrations with continuous addition of NaOH at a flowrate of 6.4 mL min^{-1}. Due to their short time scale, similar experiments were needed to a cover wider time scale.

0.882 g calcium chloride dihydrate ($CaCl_2.2H_2O$) (99.0 –105.0% UNIVAR, Thermo Fisher Scientific, Australia) with molecular weight of 147.008 g mol^{-1} was transferred to a clean and dry 500 mL volumetric flask and then filled up with Milli–Q water until to the limit line of the flask. Similarly, 0.828 g sodium dihydrogen phosphate monohydrate ($NaH_2PO_4.H_2O$) (99.0 –102.0 % AnalaR Normapur, VWR Chemicals, Poole, England) with molecular weight of 137.99 g mol^{-1} was made up in a 500 mL volumetric flask. The prepared solutions were mixed up together to get 6 mM concentration of $CaCl_2$ and NaH_2PO_4 in a 2L beaker that was then covered by a cling wrap to avoid any carbon dioxide dissolution from air. In the meantime, 2 L of 0.01 mol L^{-1} NaOH (97.0% Proanalys AR ACS LabServ, Thermo Fisher Scientific, Australia) with molecular weight of 39.997 g mol^{-1} solution was prepared. The sodium hydroxide solution was added gradually to the mixed solution to increase pH using a peristaltic pump at a flowrate of 6.4 mL min^{-1}.

The proposed model in this study was applied dynamically to the calcium phosphate system to determine ion equilibria and parameters changing over time. Precipitation of calcium phosphate was investigated experimentally to ascertain the effect of initial calcium and phosphate concentration on the formation of precipitate phase. The dynamic modelling of calcium phosphate solution was simulated similarly to that of calcium carbonate system that was described in Section 3.7.1.2.

The progression of the simulated precipitation over time is shown for 6 mM concentrations of Ca and PO_4 in Figure 3.21a. The K_a value given by Holt et al. (1981) was used for the equilibrium between H^+ and HPO_4^{2-} according to Equation (3.41):

$$H_2PO_4^- \leftrightarrow H^+ + HPO_4^{2-} \qquad K_{a_1} = \frac{a_{H_2PO_4^-}}{a_{H^+}\, a_{HPO_4^{2-}}} \tag{3.41}$$

However, that was altered from 2.84×10^7 suggested by Holt et al. (1981) to 2.29×10^7 mol^{-1} L to get better fitting particularly in the area where pH is increasing in the time range between 20 to 40 minutes, after which the solution pH started to drop signifying the formation of precipitate as shown in Figure 3.21b. This was also observed experimentally by observation of turbidity after 10 minutes. Interestingly, Mekmene et al. (2010) used a K_a value of 1.0×10^7 mol^{-1} L which is even lower. The decrease in K_a leads to higher activity of H^+ and hence lower pH for a specific time that was desired to get better agreement with the corresponding experimental data. Arifuzzaman and Rohani (2004) analysed the crystal in the precipitate phase using XRD, FTIR, and SEM revealing the presence of brushite (DCPD, $CaHPO_4.2H_2O$) as the most possible type of calcium phosphate in the solid phase solution.

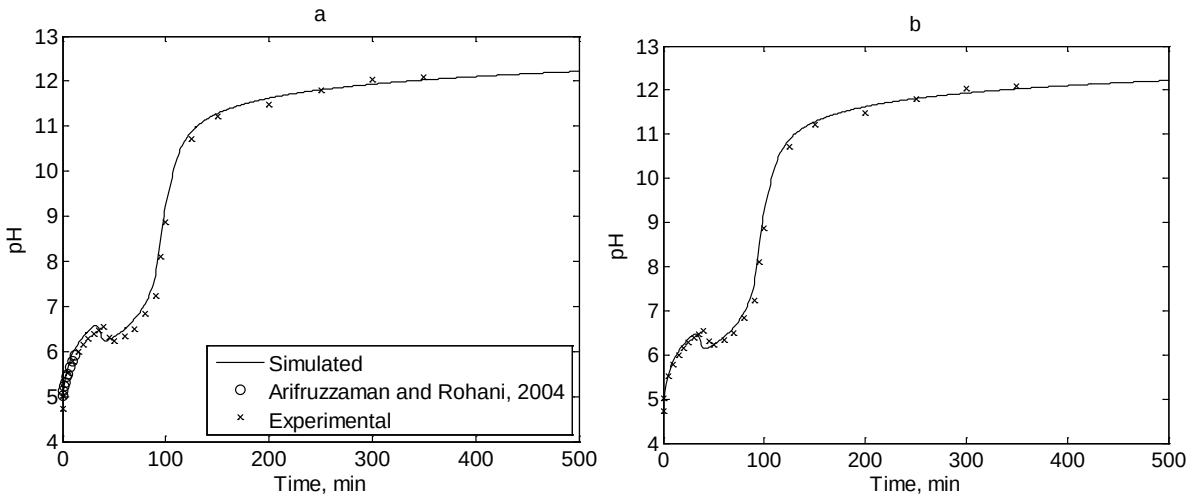

Figure 3.21 Dynamic pH changes for a 6 mM $CaCl_2$ and NaH_2PO_4 solution; a) No adjustment was made on K_a b) K_a between H^+ and HPO_4^{2-} was adjusted to 2.29×10^7 mol^{-1} L.

At pH less than about 6.7, $H_2PO_4^-$ is the most abundant form of phosphate in solution. When it reaches the saturation level with Ca^{2+} it forms $CaHPO_4$ releasing a proton and lowering the pH. One could also state this as when an HPO_4^{2-} ion precipitates with Ca^{2+}, an $H_2PO_4^-$ ion dissociates to HPO_4^{2-} releasing a proton.

3.7.2.3 Effect of pH and Ca/P ratio in the dynamic study

Another investigation was done by Mekmene, Quillard, et al. (2009) on the time response of calcium phosphate solutions to determine the effect of pH and calcium to phosphate ratio on the calcium phosphate precipitates. A model of this study was compared with their results and is shown in Figure 3.22. They used NaH_2PO_4 and $CaCl_2$ to combine 20 mM PO_4^{3-} with Ca^{2+} at Ca/P ratios of 1.0, 1.5, and 2.0. Mekmene, Quillard, et al. (2009) described the irregularity of slow decrease due to the formation of an intermediate phase. DCPD was found to be the most possible crystalline in the precipitates according to the characterisation analyses such as XRD, FTIR, and SEM. Therefore, DCPD was assumed as the solid phase in the mathematical solution, but another solid phase was needed to justify the first decrease of pH over time, which might be dicalcium phosphate anhydrous (DCPA) in this thesis.

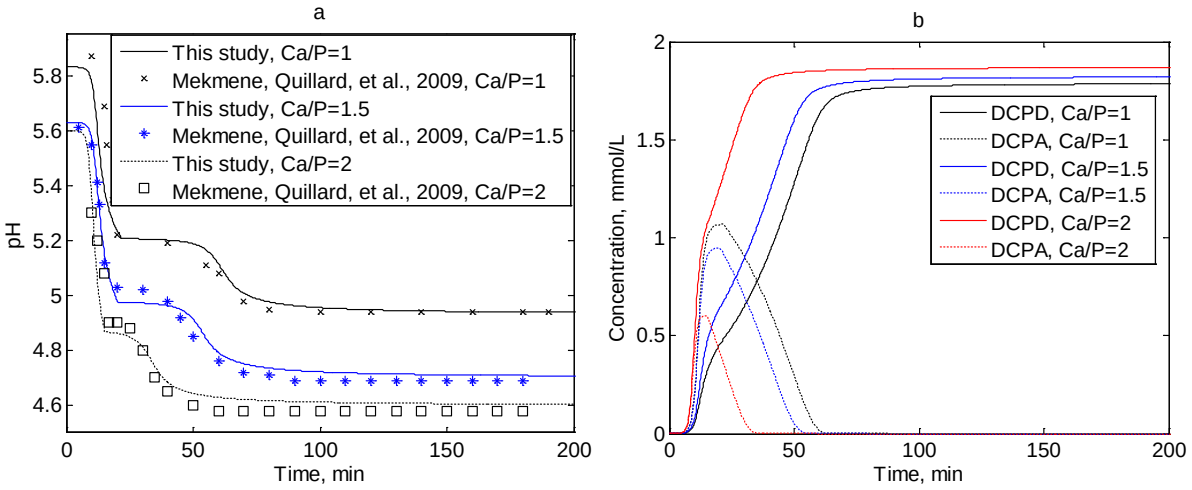

Figure 3.22 A comparison of simulations with experimental data from Mekmene, Quillard, et al. (2009) a) pH development of calcium phosphate; b) DCPD and DCPA concentrations over time for 1.0, 1.5, and 2.0 calcium to phosphate molar ratios with initial 20 mM phosphate.

Mekmene, Quillard, et al. (2009) proposed that both DCPD and DCPA were formed. The model was modified to allow precipitation of both and the subsequent dissolution of either. DCPA is more soluble than DCPD and both were assumed to have the same *IAP* ($a_{Ca^{2+}}a_{HPO_4^{2-}}$). However, by setting the precipitation rate constant for DCPA higher than DCPD, it was possible to simulate precipitate of DCPA.

The K_{sp} of DCPD was set to 2.09×10^{-7} mol^2 L^{-2} from Mekmene, Quillard, et al. (2009) and the K_{sp} of DCPA was adjusted to 4.0×10^{-7} mol^2 L^{-2}. The precipitation rate constants were set at 0.255 and 0.9 min^{-1} for DCPA and DCPD respectively, with n=2 for both. The

dissolution rate constant was set to 5 min^{-1} for DCPA. Figure 3.22a shows that these parameters enabled the data of Mekmene, Quillard, et al. (2009) to be fitted well. Figure 3.22b shows the simulated concentrations of the precipitates. These results were obtained by assuming that DCPA can form less soluble DCPD, but the results neither disprove nor prove a mechanism. Consequently, DCPA seemed to have a higher solubility but faster precipitation than DCPD.

pH was considered as the main variable that indicated the precipitation of calcium phosphate leading to the release of H^+ and removal of HPO_4^{2-}, and thus decrease in pH. The pH reduced very quickly after an initial lag signifying the calcium phosphate precipitation in a supersaturated solution. After that, an irregular slow decrease occurred for all three ratios followed by another decrease in pH values at about 40 to 60 minutes, after which the solution reached equilibrium.

3.7.2.4 Effect of lactose in the dynamic study

Lactose was incorporated into the mathematical simulation to dynamically identify its influence on the pH and activity coefficient for the calcium phosphate system. In this section, lactose was individually added to the mathematical solution with 0.147 and 0.817 mol L^{-1} (Walstra et al., 2006), which are respectively one–fold and 5.5 times bovine milk lactose concentration (4.5%w/w, 25%w/w) in a solution with 20 mM PO_4 concentration and Ca/P of 1 (Figure 3.23a). Other calcium to phosphate ratios indicated similar results and thus only one ratio has been shown in this thesis.

Lactose caused a slight decrease in pH over time for all ratios of calcium phosphate solution. This is because lactose altered the solution speciation by changes in activity coefficient of species predicted by the MSA theory. For instance, when lactose is added to a solution containing many species, it will increase the activity coefficient of species such as H^+, and subsequently this will increase activity and hence solubility leading to decrease in pH that is also confirmed by Figure 3.23b. Consequently, the activities of Ca^{2+} and HPO_4^{2-} ions increase when lactose is added, causing a higher ion activity product and hence a lower solubility of $CaHPO_4$.

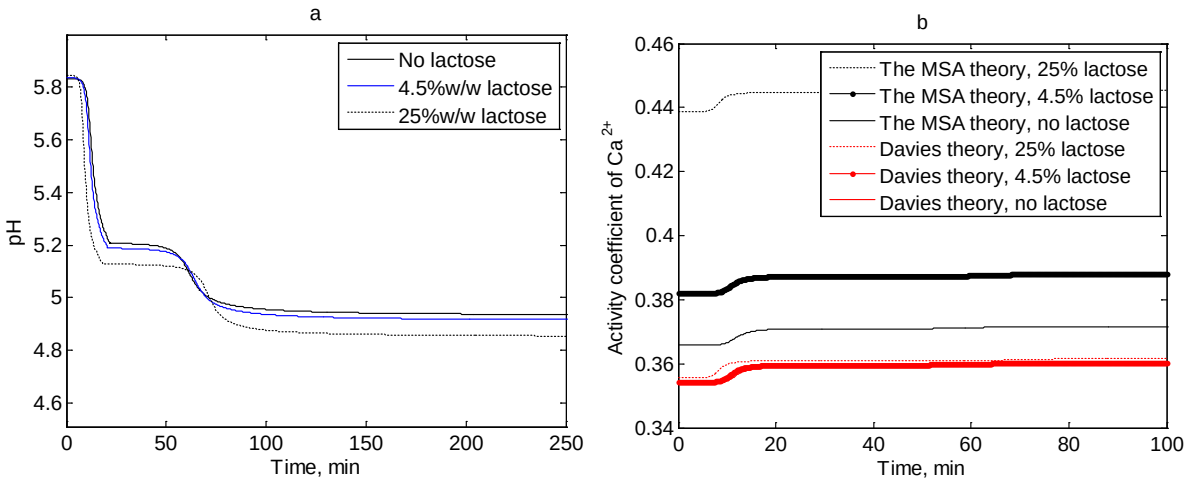

Figure 3.23 a) pH development and b) activity coefficient of Ca^{2+} of calcium phosphate solution over the time with no, 4.5% w/w, and 25% w/w lactose for Ca/P=1.

In Chapter 4, full details of the role of lactose in the calcium phosphate solubility will be investigated experimentally with varied and controlled pH and at different concentration.

The MSA and Davies theories were both used to dynamically monitor activity coefficient alterations shown in Figure 3.23b. Ca^{2+} was used as an example although other species had similar results. The time range for Figure 3.23b was shorter to be able to see the slight increase of Ca^{2+} activity coefficient at about 10 minutes.

Figure 3.23b indicates that the activity coefficients of higher concentration lactose solutions obtained using the MSA theory were higher than those with less or no lactose. This is because zero–charge species are incorporated into the hard sphere contribution leading to give different results for different lactose concentrations. Conversely, Davies theory ignores the contribution of zero–charge species automatically as it calculates the activity coefficient based on the ionic strength of solution, and hence it is not capable of predicting the effect of sugars on activity coefficients.

There is a similar logic for the decrease and increase in the activity coefficient value to those of Figure 3.20 as shown in Figure 3.23b, i.e. strong positive contribution to the ionic strength causes lower electrostatic contribution and vice versa.

3.7.3 Calcium citrate solution

Citrate has a significant content in milk and dairy products (Garnsworthy et al., 2006). The affinity between citrate and calcium is relatively high in milk serum (Holt et al., 1981; Holt,

1992; Little and Holt, 2004), in which about 65% of calcium and 28% of magnesium are bound to citrate as aqueous calcium citrate ($CaCit^-$) and aqueous magnesium citrate ($MgCit^-$). Free citrate ions including $HCit^{2-}$ and Cit^{3-} constitute the rest of this fraction (Mekmene et al., 2010). 10% of the citrate is associated with the casein micelles at natural pH as calcium citrate (Ca_3Cit_2) and magnesium citrate (Mg_3Cit_2) (Davies and White, 1960; Gaucheron et al., 1996), or as CPN (see Section 2.1.4.3).

Addition of phosphate to calcium citrate solutions may cause precipitation as sparingly soluble calcium salts (Kubantseva et al., 2004; Vavrusova et al., 2013; Vavrusova and Skibsted, 2016). Precipitation of calcium citrate and phosphate salts leads to fouling increasing the need for cleaning (Jeurnink and Brinkman, 1994; Jeurnink et al., 1996). The solubility of sparingly soluble calcium citrate salt has been extensively studied by several researchers for various systems (Vavrusova and Skibsted, 2016; Vavrusova et al., 2017; Garcia et al., 2018; Vavrusova et al., 2018). Less study has been done on the speciation of ions in a wide range of pH and for high solution concentrations either at equilibrium or dynamically, or on the solubility of calcium citrate in milk–like systems. The aim of this section is to evaluate how changes in pH and ions activity can affect the speciation and the precipitation of the solution.

3.7.3.1 Controlling pH by NaOH at equilibrium

The speciation of calcium and citrate in solution was calculated at equilibrium using the MSA theory to determine activity coefficients. Moreover, the saturation of tricalcium citrate tetrahydrate ($Ca_3Cit_2.4H_2O$, TCCT) and tricalcium citrate hexahydrate ($Ca_3Cit_2.6H_2O$, TCCH) were calculated with the solubility products of 2.29×10^{-18} and 2.10×10^{-17} $mol^5\ L^{-5}$ (Gao, van Halsema, et al., 2010; Vavrusova and Skibsted, 2016).

Vavrusova and Skibsted (2016) defined two types of solubility product, one of which was the so–called '*thermodynamic solubility product*' (K_{sp}) based on the activity of species and is generally valid at room temperature, whereas the other definition was according to the molar concentrations of species:

$$K_{sp} = a^3_{Ca^{2+}}\, a^2_{Cit^{3-}} \tag{3.42}$$

$$K_{sp} = [Ca^{2+}]^3[Cit^{3-}]^2 \tag{3.43}$$

The Equation (3.42) was used in this thesis. Typical results for citrate and calcium are shown in Figure 3.24 in a system of 2 mM $CaCl_2$, 2 mM KH_2Cit, and 10 mM KCl. These calculations were done with the assumption that all products remained as single ion–pairs in solution. The contribution of species with less than 1% was not included. pH was controlled by adding NaOH from zero to about 15 mM concentration, or 10 mM hydrochloric acid for the lower range of pH.

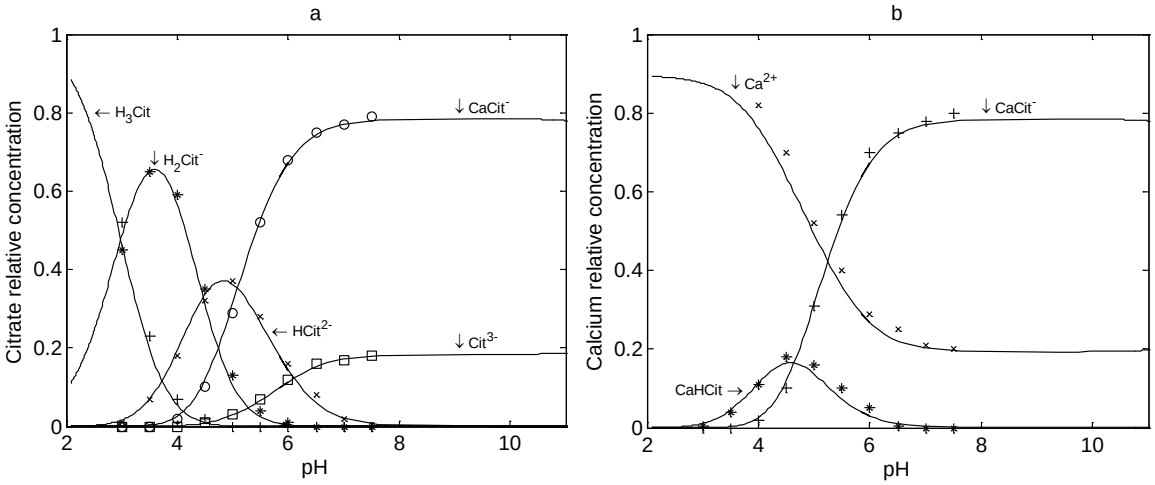

Figure 3.24 a) Citrate and b) calcium simulated distributions at 10 mM KCl, 2 mM $CaCl_2$ and KH_2Cit in water; symbols show some of the simulated points calculated by Rice et al. (2010).

As seen in Figure 3.24a, there is an expected change in speciation from H_3Cit to H_2Cit^- then $HCit^{2-}$, but above pH 5.1, the ion–pair $CaCit^-$ becomes the most abundant species. Similarly, $CaCit^-$ is the most plentiful of the Ca ions at pH values above 5.1. This is because of high affinity between free calcium and citrate ions according to Table 3.1.

An adjustment was made on the intrinsic association constant between the Ca^{2+} and $HCit^{2-}$ from 876 to 1500 mol^{-1} L signifying higher concentration of CaHCit that enables a better fitting with other simulations. Moreover, the K_a value (8.0×10^4 mol^{-1} L) between Ca^{2+} and Cit^{3-} suggested by Mekmene et al. (2010) was used instead of 1.65×10^5 mol^{-1} L (Table 3.1) leading to a lower concentration of $CaCit^-$ and hence improved the fitting.

Figure 3.25a and b show that the saturation of tricalcium citrate tetrahydrate and tricalcium citrate hexahydrate remained below 1 for the 2 and 5 mM $CaCl_2$ and KH_2Cit solutions. But the saturations start to grow gently from pH about 4 because of Cit^{3-} release in the solution, and then reached a peak at about pH 6 due to high association between free calcium and citrate

leading to high concentration of ion–pair calcium citrate, and then slightly drop due to decrease in free calcium and citrate ions.

These simulated results were in good agreement with the simulated results presented by Rice et al. (2010). The concentration of both Ca^{2+} and Cit^{3-} in milk serum are about 10 mM (Holt, 1997). If no other ions were present, which would reduce the ions activities, then 10 mM Ca^{2+} and Cit^{3-} would be about 1.6 and 0.17 times the saturation limit in presence of TCCT and TCCH at a typical pH of 6.7, respectively. Consequently, the system was predicted to be supersaturated in respect to calcium citrate tetrahydrate.

As shown by Figure 3.25, the saturation of TCCT is always higher than that of TCCH. This is because of the larger solubility product of TCCH than that of TCCT signifying higher solubility and hence less saturation of TCCH.

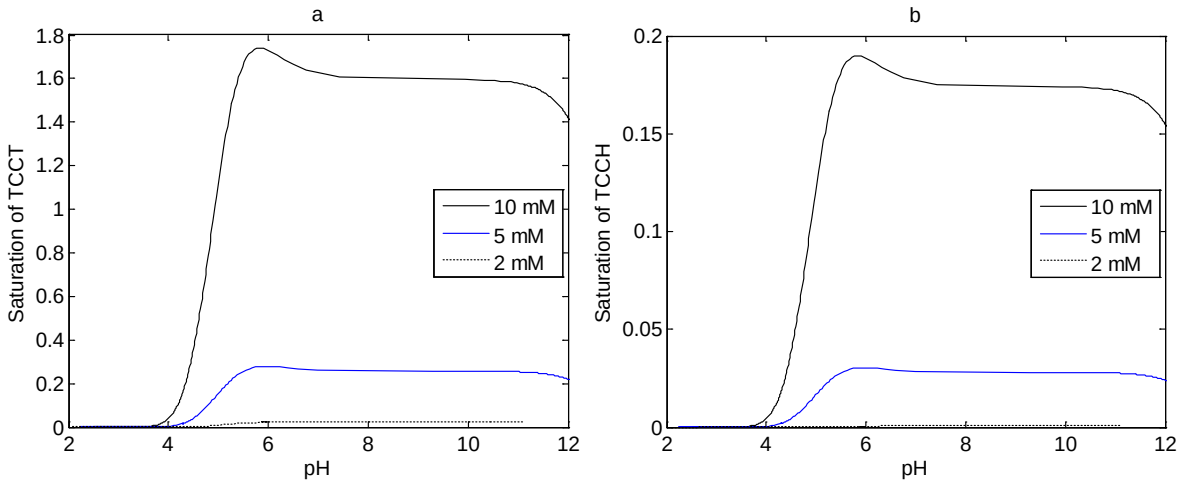

Figure 3.25 a) Saturation of tricalcium citrate tetrahydrate and b) tricalcium citrate hexahydrate at different molar concentrations of $CaCl_2$ and KH_2Cit, with 10 mM KCl. The y–axes scales of graphs are different.

3.7.3.2 Addition of phosphate to steady state study of calcium citrate

In another study, 2 mM potassium hydrogen phosphate (KH_2PO_4) was incorporated into the simulation of calcium citrate based on Rice et al. (2010). Figure 3.26a shows the predicted distribution of free ions in the phosphate–citrate system in which the solubility product of DCPD was assumed to be 2.07×10^{-7} mol^2 L^{-2}. Generally, the calcium citrate system with phosphate was similar to the system without phosphate. Small quantities of calcium phosphate species were formed at pH above 6 where the concentrations of hydrogen phosphate and citrate started to increase.

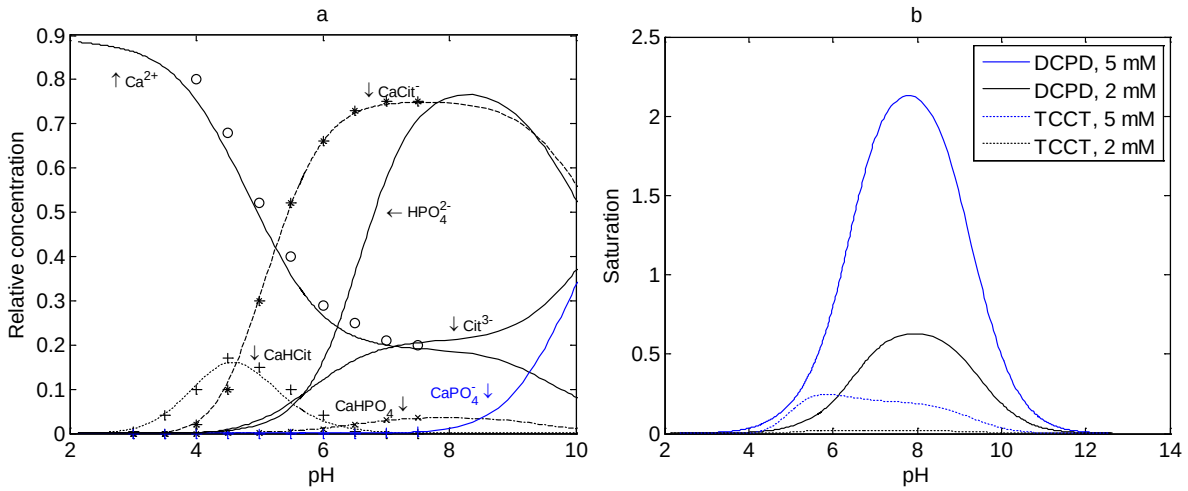

Figure 3.26 a) Simulated distribution of calcium in 10 mM KCl, 2 mM $CaCl_2$, 2 mM KH_2Cit, and 2 mM KH_2PO_4; b) Saturation of DCPD and TCCT for both 10 mM KCl, 5 mM $CaCl_2$, 5 mM KH_2Cit, 5 mM KH_2PO4 and 10 mM KCl, 2 mM $CaCl_2$, 2 mM KH_2Cit, 2 mM KH_2PO4. The symbols express some of simulated points calculated by Rice et al. (2010).

Saturations of DCPD and TCCT were compared for 2 and 5 mM concentrations as shown in Figure 3.26b according to the Equations (3.44) and (3.45). Although the K_{sp} of DCPD is larger than that of TCCT, it does not necessarily mean less saturation of DCPD as the ion activity product equations are different. It can be seen that the hydrogen phosphate concentration is higher than the citrate ion for almost the entire pH range in Figure 3.26a.

$$K_{sp_{DCPD}} = \frac{a_{Ca^{2+}}\, a_{HPO_4^{2-}}}{Sat_{DCPD}} = 2.07 \times 10^{-7}\ \text{mol}^2\text{L}^{-2} \tag{3.44}$$

$$K_{sp\,TCCT} = \frac{a_{Ca^{2+}}^3\, a_{Cit^{3-}}^2}{Sat_{TCCT}} = 2.29 \times 10^{-18}\ \text{mol}^5\text{L}^{-5} \tag{3.45}$$

Generally, the presence of citrate decreases the saturation of DCPD in a solution containing calcium phosphate (Hignett and Brabson, 1961). This can be seen clearly by comparing Figure 3.19 and 3.26b, in both of which the saturation of DCPD is plotted as a function of pH for 5 mM calcium and phosphate solutions. The one containing citrate (Figure 3.26b) had a maximum of about 2, whereas the peak point of saturation reached 12 in Figure 3.19. Mekmene et al. (2012) investigated the effect of some additives such as citrate in a milk–like solutions containing calcium phosphate. They claimed that the saturation of solutions were reduced by addition of citrate due to sequestration of free calcium. Similarly, Vavrusova et al. (2017) claimed that excess sodium citrate drops the Ca^{2+} ion concentration because of strong affinity between Ca^{2+} and Cit^{3-} leading to higher calcium citrate solubility, and hence,

Ca^{2+} concentration is controlled by Cit^{3-} concentration. Both figures confirm that the level of free calcium was lower when citrate was present.

3.7.3.3 Addition of lactate to equilibrium of calcium citrate and phosphate

Calcium lactate ($CaLact_2$) is another salt available in dairy products such as Cheddar cheese that may precipitate under certain conditions (Dybing et al., 1988). For instance, sodium gluconate was used as an additive to Cheddar cheese to prevent calcium lactate precipitation (Ramachandan et al., 2006; Phadungath and Metzger, 2011). Several works have been done on the solubility of solutions composed of calcium lactate with other salts at different temperatures (Vavrusova et al., 2013; Vavrusova et al., 2014; Vavrusova and Skibsted, 2014).

Despite these, no study has been done on the speciation of lactate in a solution constituting of citrate and phosphate. Therefore, the MSA theory was employed to simulate a solution containing 10 mM KCl, 2 mM $CaCl_2$, 2 mM KH_2Cit, 2 mM KH_2PO_4, and 2 mM lactic acid, the pH of which was controlled continuously by NaOH addition. Apart from DCPD, TCCT, and TCCH saturations, calcium lactate saturation was incorporated into the simulation as an individual species with solubility product of 5.8×10^{-3} mol^3 L^{-3} according to Vavrusova et al. (2013) based on the Equation (3.46):

$$\text{Saturation}_{\text{CaLact}_2} = \frac{a_{Ca^{2+}}\, a_{Lact^-}^2}{K_{sp}} \tag{3.46}$$

The intrinsic association constants of lactate ($Lact^-$) and other cations in the system were used according to Table 3.5, but other K_a values remained the same as in previous systems.

Table 3.5 Intrinsic association constants (mol^{-1} L) between lactate ($Lact^-$) and principal cations in the simulation.

	Ca^{2+}		Na^+		K^+		H^+	
	Ion–pair	K_a	Ion–pair	K_a	Ion–pair	K_a	Ion–pair	K_a
$Lact^-$	$CaLact^+$	15[a]	NaLact	2[b]	KLact	2[b]	HLact	7.14×10^{3}[c]

[a] (Jackson, 2004), [b] assumed values according to the other components ratios, [c] (Kubantseva and Hartel, 2002).

Typical results for calcium are shown in Figure 3.27a and for lactate in Figure 3.27b. Similar to previous equilibrium systems, calculations were done with the assumption that all products remained as single ion–pairs in solution without precipitation. The species with a contribution of less than 1% are $CaH_2PO_4^+$, $CaHPO_4$, CaH_2Cit^+, $CaLact^+$, and KLact. Among the ion–pairs in the solution, $Lact^-$ is higher than the others for almost the entire pH range, following by the

ion–pairs $CaCit^-$ and $CaPO_4^-$. The high concentration of lactic acid (HLact) in the acidic part of graph is due to high affinity between $Lact^-$ and H^+.

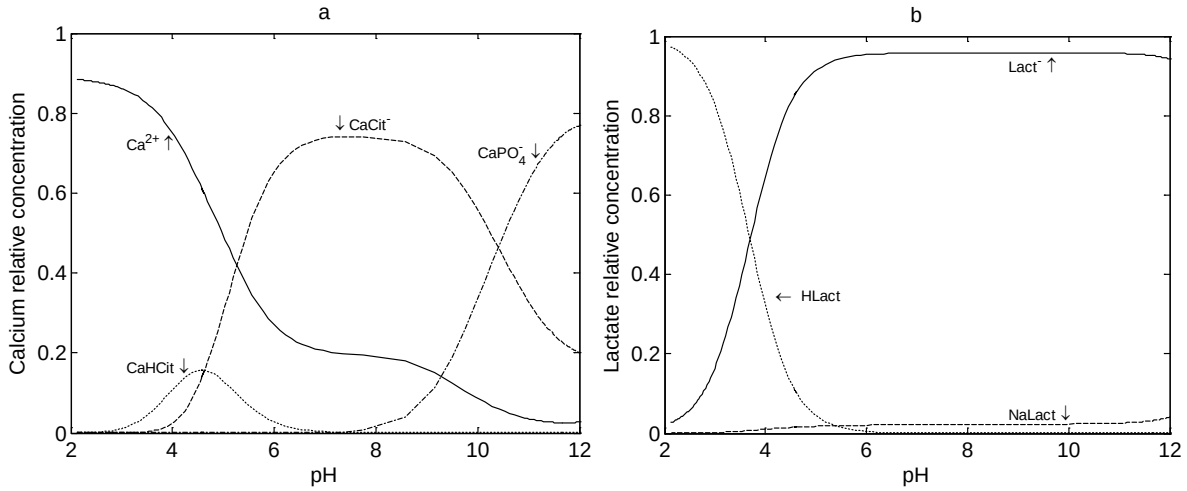

Figure 3.27 Predicted distribution of a) calcium and b) lactate and compounds in a solution containing 10 mM KCl, 2 mM $CaCl_2$, 2 mM KH_2Cit, 2 mM KH_2PO_4, and 2 mM lactic acid.

The addition of lactate does not lower considerably the concentration of calcium species. This is because of the low value of association constant between free calcium and lactate leading to release of Ca^{2+} and $Lact^-$ ions. The association constants between free calcium and Cit^{3-} and PO_4^{3-} are quite large, hence, calcium complexes are not affected greatly by the presence of lactate.

Similar to previous citrate and citrate–phosphate systems, addition of lactate decreased the DCPD saturation in a solution of calcium citrate–phosphate due to the sequestration of free calcium. Hence, DCPD seems to precipitate first among the other salts, e.g., calcium citrate and calcium lactate, according to the saturation graphs. However, this cannot be generalised as the mechanism of precipitation determines the order of solid phase formation and the subsequent rate of growth (Nancollas, 1992).

The simulation can be used to estimate the amount of lactic acid required to acidify milk from its natural pH of 6.7 to the lowest possible pH of milk where the *isoelectric point* (IEP) of casein is 4.6 according to Walstra et al. (2006) (Figure 3.28). The pH value at which the average net charge of protein is equivalent to zero, is termed as isoelectric point at which the protein has the least solubility (Southward, 1998; Salis et al., 2011). Casein proteins precipitates around the pH of 4.6 at which casein proteins have no net charge leading to milk coagulation. In bovine milk, the casein micelles are stable at pH of about 6.7 because of negative net charge (Walstra et al., 2006).

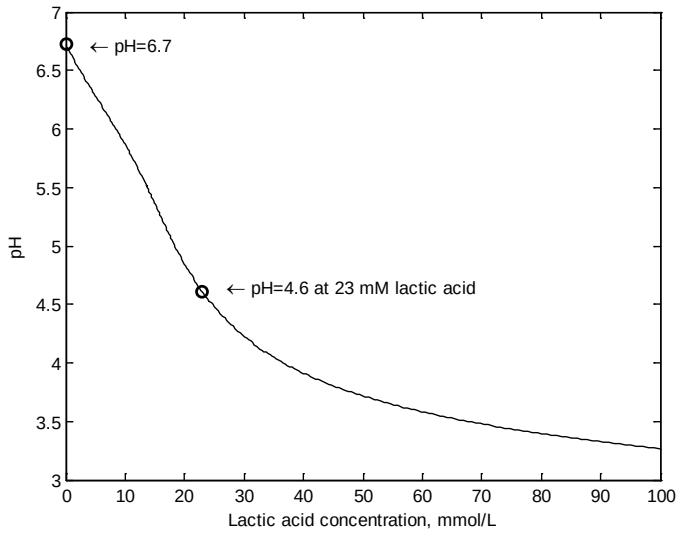

Figure 3.28 The required amounts of lactic acid needed to change the pH of a solution of milk electrolytes from pH 6.7.

Hence, in this study, calcium and potassium as cations, and chloride, citrate, and phosphate as anions were incorporated into the simulations with the same salt concentrations of milk: Ca (29 mM) (Mekmene, Le Graet, et al., 2009), K (38.3 mM), Cl (30.4 mM), Cit (9.5 mM) , PO_4 (20.6 mM) (Holt, 2004). Figure 3.28 shows that no lactic acid was required to reach to natural pH, and 23 mM was the amount of lactic acid required to get a pH of 4.6. Therefore, an addition of 23 mM of lactic acid would cause this pH change. However, only the main electrolyte constituents of milk were included in the model and the role of other components such as sodium, sulphate, carbonate, lactose, and proteins were neglected.

3.7.3.4 Effect of lactose on calcium, potassium, chloride, and citrate solution

Another simulation, in which the MSA theory was used to calculate activity coefficient and subsequently Ca^{2+} molar activity and pH, was implemented with various lactose contents in a multicomponent solution comprising $CaCl_2$, KCl, and K_3Cit. The reason for choosing this mixture is that similar work has been done on this system theoretically and experimentally with sucrose rather than lactose. Therefore, results of Gao, van Leeuwen, et al. (2010) were reproduced as an appropriate validation for this study with 5 mM $CaCl_2$, 55 mM KCl, and 4 mM K_3Cit throughout the range of sucrose.

In this study, the association between calcium, potassium, and the sugars were considered despite of their tiny values, although Gao, van Leeuwen, et al. (2010) presumed only the affinity between sugars and hydrogen ion. Another adjustment was the ionic size which was

used from the data of Gao, van Leeuwen, et al. (2010) and Isaad and Perwuelz (2010), for sucrose (0.7 nm) and lactose (0.454 nm), respectively, although no value was found for the size of corresponding ion–pairs, therefore, they were estimated relatively close to those sugar sizes, i.e. 0.6 nm for sucrose and 0.4 nm for lactose ion–pairs.

Figures 3.29a, b, and d show that pH, Ca^{2+} activity, and molar activity coefficients calculated by the MSA theory were in good agreement with the literature results for sucrose solutions. However, sucrose was allowed to dissociate in the solution as an anion (*Sucrose*$^{-}$) that interacted with the cations such as calcium, potassium (K^{+}), and hydrogen by their corresponding association constants. Stearn (1931) proposed intrinsic association constants between H^{+} and sugars including sucrose and lactose which are 5.00×10^{12} and 1.31×10^{12} mol^{-1} L, respectively according to Equations (3.47) and (3.48). $HSucrose$ represents undissociated sucrose. In addition, the saturation of TCCT was included in the calculation and was shown in Figure 3.29c.

$$HSucrose \leftrightarrow H^{+} + Sucrose^{-} \quad K_a = \frac{a_{HSucrose}}{a_{H^{+}} a_{Sucrose^{-}}} \tag{3.47}$$

$$HLactose \leftrightarrow H^{+} + Lactose^{-} \quad K_a = \frac{a_{HLactose}}{a_{H^{+}} a_{Lactose^{-}}} \tag{3.48}$$

Since the association constant of sucrose is larger than that of lactose, less *HSucrose* dissociated to the H^{+} and *sucrose*$^{-}$ than *HLactose* to its corresponding free ions. Hence, the pH of sucrose solutions was higher than that of lactose. On the other hand, the association constant for *sucrose*$^{-}$ and *lactose*$^{-}$ were adjusted to 500 and 2000 for Ca^{2+}, 100, and 2200 mol^{-1} L for K^{+}, respectively to be able to get better fitting in pH graph leading to higher Ca^{2+} activity in sucrose solution that than of lactose (Equations (3.49) and (3.50)). Hence, the saturation of TCCT in sucrose solutions was higher than that of lactose solutions because higher activity of Ca^{2+}.

$$CaLactose \leftrightarrow Ca^{2+} + Lactose^{-} \quad K_a = \frac{a_{CaLactose}}{a_{Ca^{2+}} a_{Lactose^{-}}} = 2000 \tag{3.49}$$

$$KLactose \leftrightarrow K^{+} + Lactose^{-} \quad K_a = \frac{a_{KLactose}}{a_{K^{+}} a_{Lactose^{-}}} = 2200 \tag{3.50}$$

The variation in Ca^{2+} activity and pH became larger between simulated and experimental data at higher concentrations of sugars. This is probably because of the non–ideality of highly concentrated solutions for which the MSA theory still has some uncertainty. Nonetheless, the MSA theory is likely capable of activity coefficient prediction for high concentrations of sugars in a multicomponent solution.

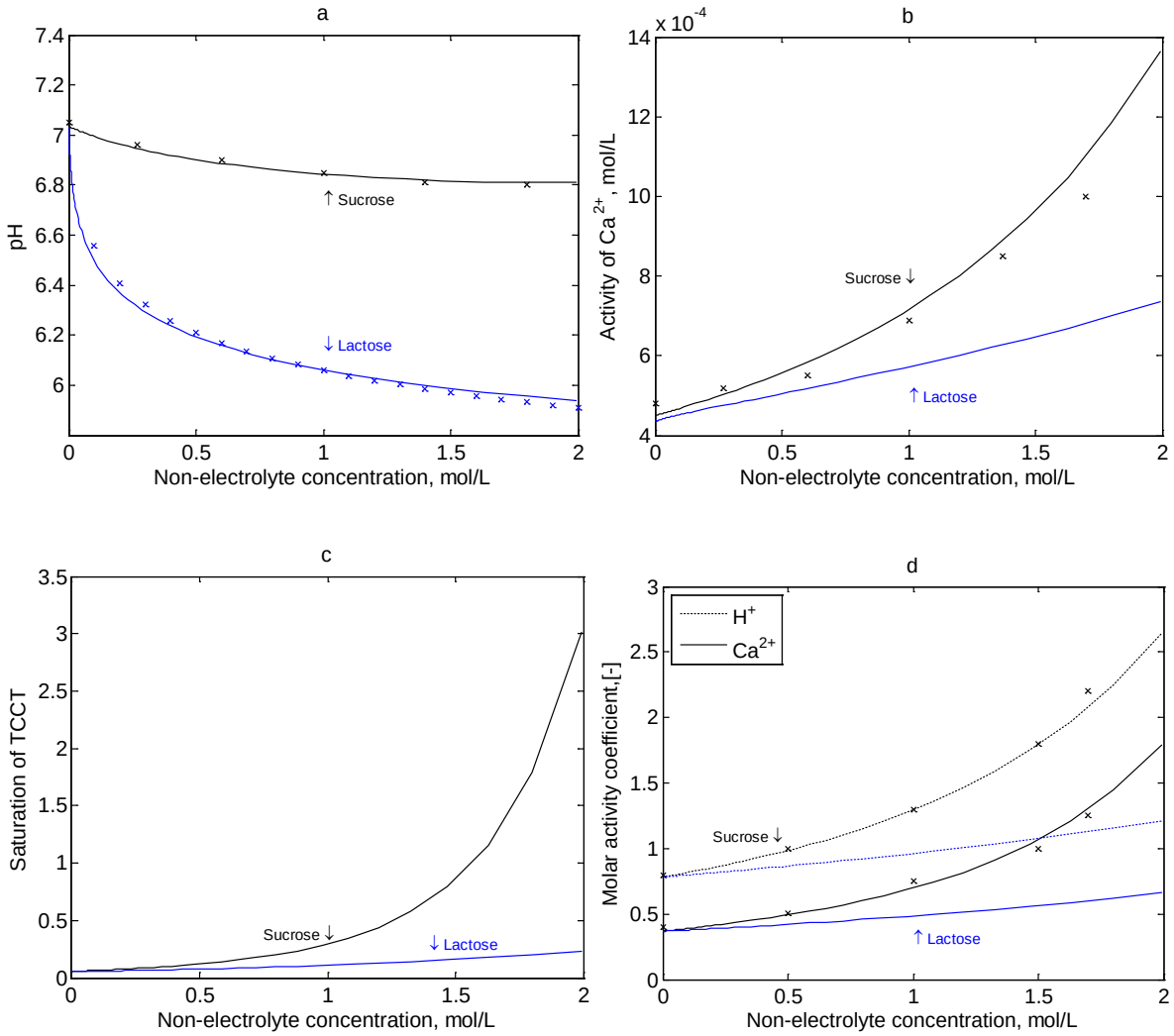

Figure 3.29 Effect of sucrose on a) pH, b) Ca^{2+} molar activity, c) TCCT saturation and d) predicted molar activity coefficient of Ca^{2+} and H^+ by the MSA theory in a multicomponent system containing 5 mM $CaCl_2$, 55 mM KCl, and 4 mM K_3Cit. The solid and dash curves represent this study based on the simulation. × and × symbols indicate experimental data from Gao, van Leeuwen, et al. (2010) and data based on the calculation, respectively.

3.7.3.5 Dynamic study of calcium citrate system

In a study, Garcia et al. (2018) measured pH over time to dynamically investigate precipitation of amorphous calcium citrate (ACP) for 0.1 mol L^{-1} equimolar binary solutions of aqueous calcium chloride with sodium dihydrogen phosphate (NaH_2PO_4), trisodium citrate (Na_3Cit),

or disodium hydrogen citrate (Na_2HCit). This system was simulated using the MSA theory with the precipitation and dissolution rate constants set to 0.01 and 4×10^{-4} min^{-1} for TCCT and to 0.2 and 0.5 min^{-1} for TCCH, respectively to reasonably match the experimental data. Figure 3.30 shows the pH of binary solutions over time for three aforementioned species, in all of which precipitation was recognisable from the change in pH trend, although it initiated differently for each solution depending on the ions interaction.

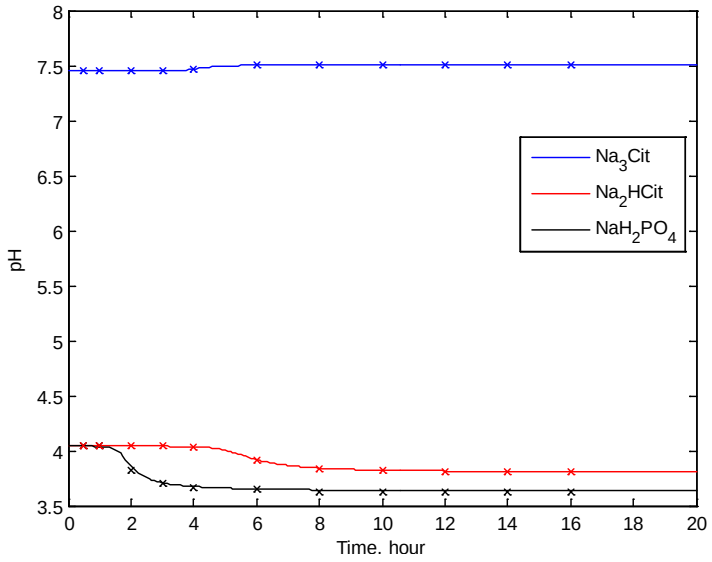

Figure 3.30 pH of solutions of 0.1 mol L^{-1} $CaCl_2$ with Na_3Cit, Na_2HCit, or NaH_2PO_4. The curves and × symbols represent simulation from this study and experimental data from Garcia et al. (2018).

Dynamic simulation of calcium citrate solutions were performed to determine the solubility and precipitates over time in multicomponent solutions containing 30 mM $CaCl_2$, 20 mM NaH_2PO_4, and 9.5 mM KH_2Cit with 0, 4.5, and 25%w/w lactose contents. The reason for choosing this composition is that no similar work has been done dynamically on the calcium citrate and phosphate system by assuming potential precipitate phases. Therefore, concentrations close to milk were selected with various levels of lactose. The pH of solution was controlled by continuous addition of sodium hydroxide for each time step. Similar to the previous simulations, Euler's method was employed together with the equilibrium calculations for each presumed solid phase species (DCPD, DCPA, TCCT, and TCCH) along with their solubility products. Lactose was also incorporated into the system and was allowed to dissociate to form an anion with a single negative charge ($lactose^-$) that is in association with the other cations in the system.

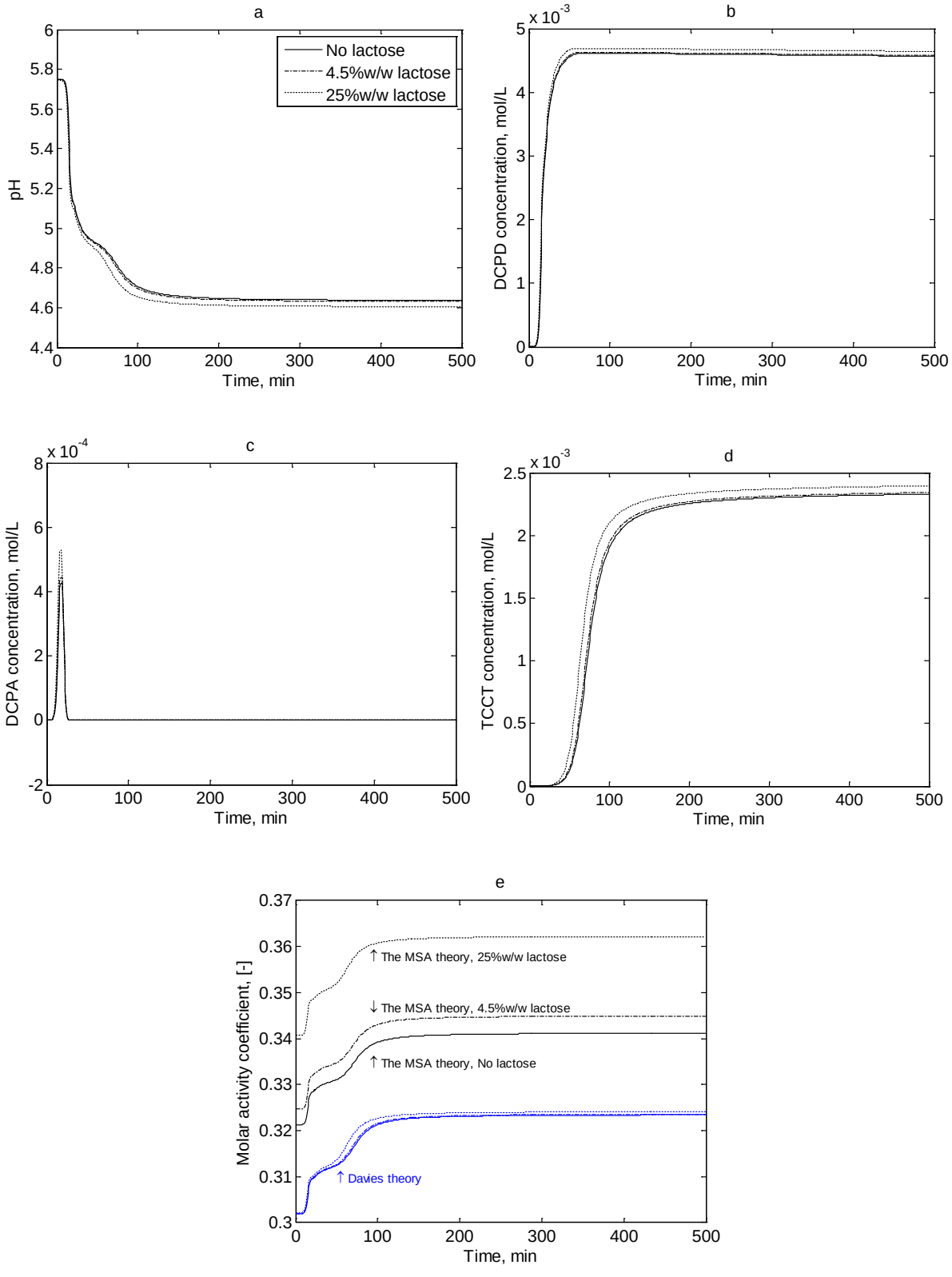

Figure 3.31 Dynamic simulation of precipitation in a multicomponent solution comprising $CaCl_2$, NaH_2PO_4, and KH_2Cit with 0, 4.5, and 25%w/w lactose. a) pH changes; b) DCPD; c) DCPA; d) TCCT; and e) molar activity coefficient of Ca^{2+} over the time.

Figure 3.31 shows the changes in pH, DCPD, DCPA, TCCT, and molar activity coefficient over time for the solution containing no lactose, 4.5, and 25%w/w lactose. Figure 3.31a, b, c, and d indicate that the parameters were unlikely affected by the addition of lactose. However, a slight difference between highest content of lactose (25%w/w) with the two other fractions (0 and 4.5%w/w) is observed from the graphs. The principal change is evident in Figure 3.31e, for which molar activity coefficient of Ca^{2+} was calculated by the MSA and Davies theories. The MSA theory could satisfactorily distinguish the distinct between various lactose contents because of the hard sphere contribution in the formula.

The initial pH drop in Figure 3.31a indicates the formation of the first solid phase in the first 5 minutes of the reaction followed by a second pH drop representing TCCT formation at about 50 minutes. DCPD and TCCT were predicted to remain insoluble in the solution, while DCPA dissolved as seen in Figure 3.31c. TCCH and all other solids were given a low initial concentration to avoid modelling primary nucleation. The trends of precipitate concentrations, pH, and activity coefficient are highly dependent on the precipitation and dissolution rates, for which no reliable source could be found. Therefore, they were adjusted to a set of values, for which results of Garcia et al. (2018) were reproduced (Figure 3.30).

From this section, it can be concluded that:

1. The proposed model is adequately able to predict salt partitioning and speciation of ion–pairs in a solution containing solid phase by calculating the saturation of calcium salts as an individual species in the set of ions.
2. Kinetics of precipitation calcium salts including calcium carbonate, phosphate, and citrate were predicted satisfactorily by the proposed model. However, more experimental data is required to determine the precipitation and dissolution mechanisms and their rates as well as crystallisation of various forms of calcium salts by taking account of lactose.
3. Calcium phosphate is thermodynamically the most stable solid phase (Elliot, 1994) that is formed in the mixed solutions under certain concentrations, following by the calcium citrate but with lower stability possibly due to the smaller value of solubility product and subsequently lower solubility. During sudden precipitation, some intermediate solid phases may be formed but dissolution may occur later.

3.8 Application of the model to milk serum

The electrolytes in milk are essential as nutrients and for osmotic balance and have been well characterised at normal milk concentrations. When milk, whey, whey permeate or milk protein concentrates are concentrated by evaporation or reverse osmosis, the concentration of ions particularly calcium phosphate can easily exceed solubility limits. This leads to heterogeneous fouling of salts on the evaporators' surfaces or reverse osmosis membranes, causing a serious reduction in performance and thus gradual depreciation of equipment in dairy industry (Kezia et al., 2017).

Several investigations have been carried out on the ion equilibria and interactions of milk serum under various conditions by assuming different solid phases in milk that were discussed earlier in this chapter. However, less study has been done on ion association, activity, and solubility in concentrated bovine milk. The aim in this section is to develop a robust method for predicting the state of minerals in any dairy serum (without proteins) up to high concentrations. The MSA method was used to calculate free–ion activity coefficients as it contained terms that enhanced accuracy at higher concentrations. The role of proteins in milk will be thoroughly investigated in Chapter 5.

3.8.1 Equilibrium study of milk serum

The proposed model was used in order to calculate the ion partitioning of milk serum, in which lactose and saturations of potential solid phase species such as brushite, monetite (DCPA), octacalcium phosphate (OCP), whitlockite (WH), hydroxyapatite (HAP), calcium–deficient apatite (CDA), calcium carbonate (calcite), tricalcium citrate tetrahydrate, and magnesium phosphate ($Mg_3(PO_4)_2$) were calculated. The following species were included in the model: calcium, magnesium, sodium, and potassium as cations; citrate, phosphate, carbonate, sulphate, chloride, phosphate esters, and carboxylate as anions. Lactose was included in the system as an individual species but the presence of milk proteins was ignored here and is dealt with separately in Chapter 5. The components were presumed to be equilibrated by their corresponding intrinsic association constants for ion–pairs and by solubility products for solid phase species. Table 3.1 shows the intrinsic association constants for the serum milk ions and Table 3.6 shows the solubility products of solid phases. These were presented first by Holt et al. (1981) and then modified by Mekmene, Le Graet, et al. (2009) and Mekmene et al. (2010).

Table 3.6 Solubility products of solid phase components (Driessens and Verbeeck, 1990; Mekmene, Quillard, et al., 2009; Gao, van Halsema, et al., 2010).

Chemicals	Chemical formula	Solubility product	*IAP*
DCPD	$CaHPO_4.2H_2O$	2.09×10^{-7} mol^2 L^{-2}	$a_{Ca^{2+}} \times a_{HPO_4^{2-}}$
DCPA	$CaHPO_4$	4.00×10^{-7} mol^2 L^{-2}	$a_{Ca^{2+}} \times a_{HPO_4^{2-}}$
OCP	$Ca_8(HPO_4)_2(PO_4)_4.5H_2O$	3.16×10^{-73} mol^{14} L^{-14}	$a^8_{Ca^{2+}} \times a^2_{HPO_4^{2-}} \times a^4_{PO_4^{3-}}$
HAP	$Ca_{10}(PO_4)_6(OH)_2$	1.58×10^{-117} mol^{18} L^{-18}	$a^{10}_{Ca^{2+}} \times a^6_{PO_4^{3-}} \times a^2_{OH^-}$
CDA	$Ca_9(HPO_4)(PO_4)_5(OH)$	7.94×10^{-86} mol^{16} L^{-16}	$a^9_{Ca^{2+}} \times a_{HPO_4^{2-}} \times a^5_{PO_4^{3-}} \times a_{OH^-}$
WH	$Ca_{10}(HPO_4)(PO_4)_6$	1.99×10^{-82} mol^{17} L^{-17}	$a^{10}_{Ca^{2+}} \times a_{HPO_4^{2-}} \times a^6_{PO_4^{3-}}$
Calcite	$CaCO_3$	4.8×10^{-9} mol^2 L^{-2}	$a_{Ca^{2+}} \times a_{CO_3^{2-}}$
Magnesium phosphate	$Mg_3(PO_4)_2$	1.0×10^{-24} mol^5 L^{-5}	$a^3_{Mg^{2+}} \times a^2_{PO_4^{3-}}$
TCCT	Ca_3Cit_2	2.29×10^{-18} mol^5 L^{-5}	$a^3_{Ca^{2+}} \times a^2_{Cit^{2-}}$

The total concentration of each component in milk serum (Table 3.7) was used to determine initial guesses of ion equilibria in milk serum.

Table 3.7 The total concentration of each principal constituent in milk serum (Holt, 1997).

Anions	Total concentration, mM
Citrate	9.368
Inorganic phosphate	12.394
Carbonate	0.448
Sulphate	1.205
Chloride	32.300
Carboxylate	3.110
Phosphate esters	2.592
Cations	
Calcium	10.184
Magnesium	3.407
Sodium	22.006
Potassium	38.006

Figure 3.32 shows the saturation of potential precipitates in a milk–like solution, for which a wide range of concentration was assumed without precipitation. Figure 3.32a and b indicate the role of lactose on the saturation of calcium salts. Magnesium salts were not significantly affected by the addition of lactose, and thus they were not included in these graphs. Lactose has a significant effect on saturation of calcium phosphate particularly DCPD and DCPA and less effect on the other solid phases, when milk serum is concentrated up to 50% solids. This was also confirmed by Herrington (1934) who stated that lactose associates with calcium and increase supersaturation of solution with respect to calcium salt compounds.

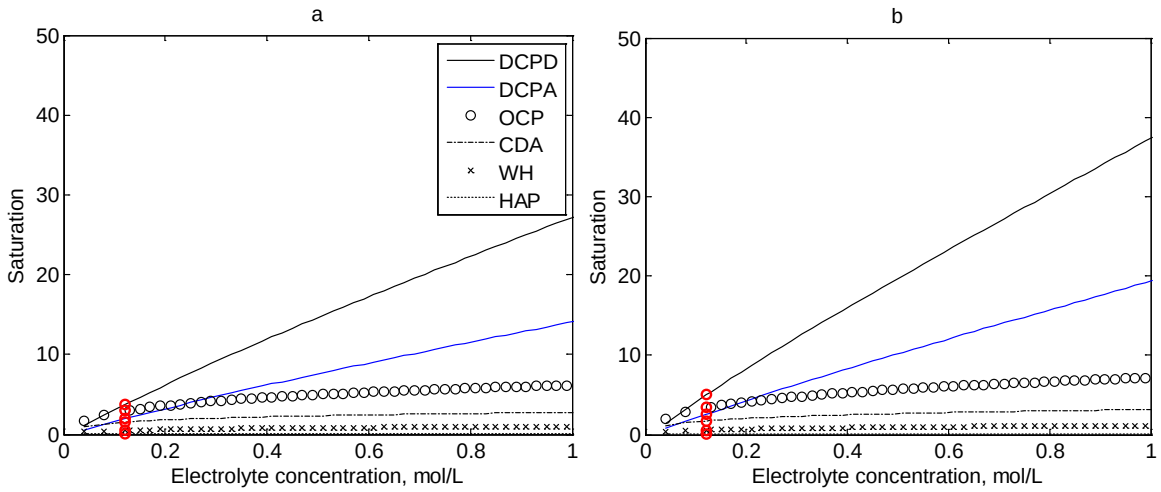

Figure 3.32 Saturation of solid phase calcium salts with a) no lactose; b) 25% lactose. The '○' indicates points corresponding to the normal electrolyte concentrations of serum (121.4 mM). See Table 3.6 for calcium phosphate abbreviations.

3.8.2 Dynamic study of milk serum

The kinetics of change in salt equilibria in milk and milk–like systems have been less investigated. More recently, Gao, van Halsema, et al. (2010) proposed a theoretical model for the ion partitioning prediction of freshly prepared SMUF, for which a kinetics study was investigated to ascertain the change of solubility product over time using the AESolve program.

Despite this study and those that were previously described in Chapter 2, further research is required to clarify the change in ion equilibria as well as the formation of potential precipitates over time. Milk ions and solid phase salts were incorporated into the dynamic system. The intrinsic association constants and solubility products were used from Tables 3.1 and 3.6.

Figure 3.33 illustrates the simulated dynamic change on salt equilibria of milk serum when the solution has 0, 4.5%w/w, and 25%w/w lactose, showing that higher contents of lactose cause formation of higher concentrations of DCPD and DCPA (Figure 3.33c), and an earlier drop in pH (Figure 3.33a). DCPD is known to be the dominant precipitate formed in the solution, whose saturation and concentration was higher than other solid salts as confirmed by van Kemenade and de Bruyn (1987). Gao, van Halsema, et al. (2010) claimed that DCPD precipitate was the main reason for the pH drop in SMUF over time.

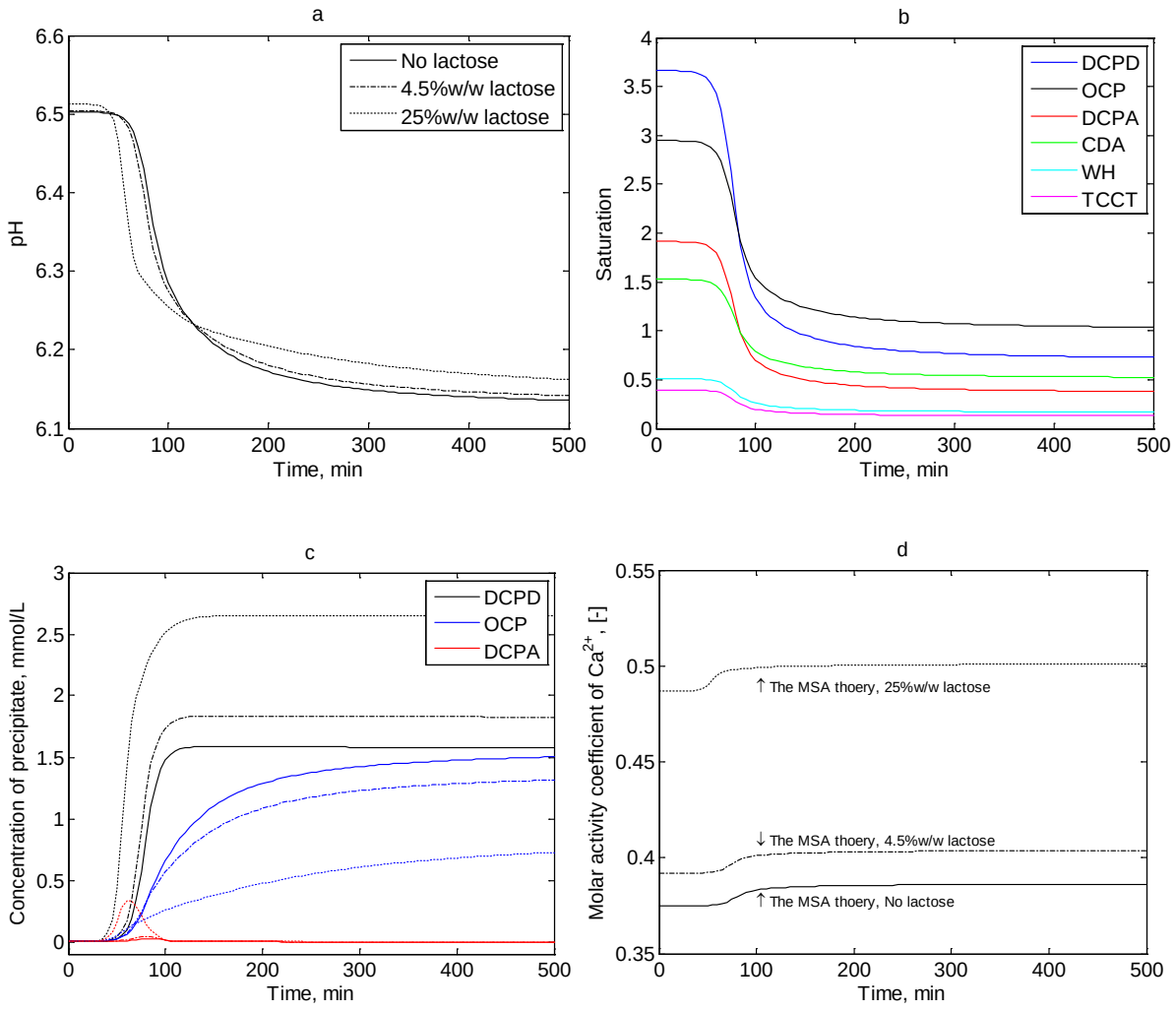

Figure 3.33 Influence of lactose addition on a) pH; b) saturation of potential solid phase species with no lactose in the solution; c) dominant solid phase concentrations; and d) molar activity coefficient of Ca^{2+} over time in a simulation containing milk serum components. The legend from Figure 3.33a corresponds also to Figure 3.33c.

Gao, van Halsema, et al. (2010) predicted the precipitation of calcium salts such as DCPD, OCP, and DCPA to a higher degree, and less quantities of CDA from milk serum. $Mg_3(PO_4)_2$,

$CaCO_3$, and WH remained soluble in the solution and the saturation of hydroxyapatite (HAP) was close to zero (Gao, van Halsema, et al., 2010).

In milk serum, the ions are either free or in association as ion–pairs according to their association constants. As shown in Figure 3.34, about 70% of total soluble calcium was associated with the calcium citrate, and 20% was present as free calcium, which were in a good agreement with the mineral distribution calculated by Mekmene, Le Graet, et al. (2009) for a milk serum solution. The reason for low concentration of calcium phosphate was its low solubility. Other calcium salts constituted the remaining 10% of total soluble calcium. Nonetheless, these values dropped over time due to formation of calcium solid phase salts that are mainly DCPD, OCP, and DCPA with a total concentration of about 3 mM. However, the milk serum is supersaturated in respect to calcium phosphate salts, and hence no precipitation should be predicted. The time scale here is quite fast, but in a study by Howell (1998), fouling in the whey permeate occurred over days showing that fouling content did not change much over few days.

The soluble calcium phosphates had lower concentration than soluble calcium citrates, remaining mainly as ion–pairs with total concentration of 5.70 mM as indicated in Table 3.8, while calcium phosphates appeared mostly as calcium solid phases.

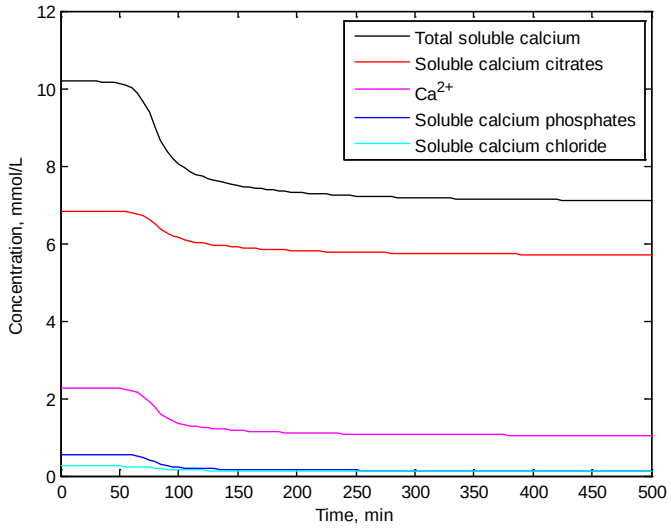

Figure 3.34 The simulated dynamic change of total calcium species over time in the milk serum solution.

Table 3.8 shows the simulated soluble and insoluble calcium species in the milk serum solution after 500 minutes.

The precipitation and dissolution rate constants of the solid phase salts were estimated to get results as discussed in the earlier sections on precipitation in previously reported systems. The rate constant values are provided in Appendix 6. The DCPD rate constants were used to guess for other rate constants of potential salts. E.g. DCPA might have higher solubility and hence precipitation than DCPD leading to have large precipitation rate constants. Further, DCPA dissolves in the solution implying higher dissolution rate constant than DCPD.

Table 3.8 The calcium ion–pairs and precipitates at 500 minutes.

Soluble ions	Concentration, mM	Total, mM		Precipitate	
				Chemical formula	mM
CaH_2Cit^+	4.75×10^{-5}	5.70		TCCT	5.64×10^{-5}
CaHCit	0.03				
$CaCit^-$	5.67			DCPD	1.57
$CaH_2PO_4^+$	0.03	0.13			
$CaHPO_4$	0.01			OCP	1.50
$CaPO_4^-$	3.96×10^{-4}				
$CaHCO_3^+$	0.002	0.002		DCPA	10^{-82}
$CaCO_3$	7.91×10^{-6}				
$CaHSO_4^+$	1.01×10^{-7}	0.03		HAP	1.24×10^{-6}
$CaSO_4$	0.03				
$CaCl^+$	0.11	0.11		CDA	2.28×10^{-4}
$CaGlc–1–PH^+$	0.004	0.06			
CaGlc–1–P	0.06			WH	2.58×10^{-6}
$CaRCOO^+$	0.02	0.02			
$CaOH^+$	2.26×10^{-7}	2.3×10^{-7}		$CaCO_3$	10^{-33}
Ca^{2+}	1.04	1.04			
Total soluble calcium		7.10		Total insoluble calcium	3.08

In another similar dynamic simulation of milk serum, initial concentrations were doubled to check the effect on the ion equilibria of milk serum. Other parameters remained unchanged as it is desirable to see only the effect of concentrations. The higher concentration of species caused a higher initial pH and subsequently higher pH after 500 minutes, leading to double the saturation over time for all potential salts. The DCPD concentration was seen to be

relatively high among the other solid phase species with about 8 mM, followed by the DCPA formation in the first 100 minutes. The OCP concentration was too small to include in Figure 3.35c.

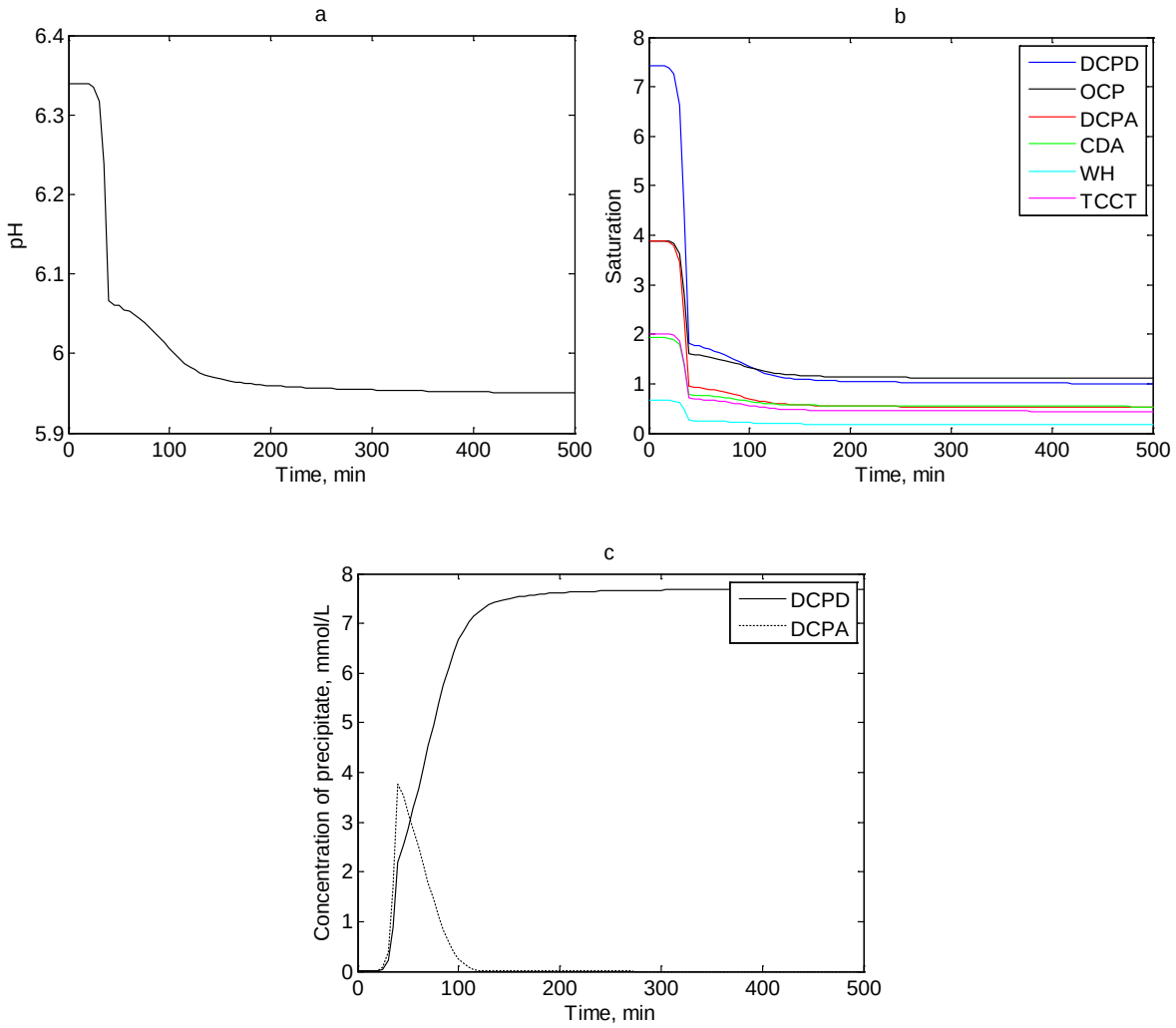

Figure 3.35 Effect of double the normal concentration of milk serum on a) pH; b) saturation; and c) concentrations of potential solid phase salts.

3.9 Conclusions

The simulation method was able to predict speciation and precipitation in a range of solutions, some of which were validated using experimental data. The model gave satisfactory results for various aqueous solution, in the sense that there was a good match of the shape and values of the graphs between the results of this study and other works either experimentally or by simulation.

Adjustments of association constants were sometimes necessary to get better fitting with corresponding experimental and simulated data in literature because there are many different values for each association constant.

The Mean Spherical Approximation (MSA) method was used to calculate free–ion activity coefficients as it contained terms that enhanced accuracy at higher concentrations. Further, it allows the addition of zero–charge component such as lactose, whereas the other models like Davies theory or Extended Debye–Hückel contain the charge term in their formula leading to activity coefficient of unity for zero–charge species. The MSA theory is capable of making distinction between activity coefficient of a solution comprising sugar by incorporating size and concentrations related terms as the main strength of this method.

The results were in reasonable agreement with those presented by the literature from either experiments or other simulations. This shows that the assumptions made are quite accurate for calculations of salt partitioning in various systems, and can be applied to various milk–like systems as long as the initial concentrations are well defined and determined. However, more validation with complex milk solutions is desirable. The intrinsic association constants and solubility products were assumed in the temperature range of 20–25 ˚C. More research is required to identify the constants for other temperatures to be able to expand this model for other milk–like solutions and possibly in cheese making process where heat treatment and other temperature–related factors are inevitable (Mekmene, Le Graet, et al., 2009).

No sufficient data are available for the precipitation and dissolution rate constants of precipitates in milk, and hence investigations seem necessary for the calculations of those values under different conditions.

4 Experimental Aspects of Calcium Phosphate Precipitation

4.1 Introduction

The aim of this chapter was to investigate the effect of lactose on the solubility of calcium phosphate with varied and controlled pH and at different concentrations. Different concentrations of calcium chloride, sodium phosphate, sodium hydroxide with and without lactose were mixed, and pH and conductivity were measured to follow the precipitation of calcium phosphate over the time. This system was used because it is one the simplest to mimic milk. Moreover, calcium phosphate can precipitate as the principal salt available in milk. The outcomes of this study will show a possible role of lactose in stabilising calcium phosphate solutions possibly by formation of calcium phosphate nanoparticles.

Doherty and Wright (2004) studied the effect of sugars on various calcium salts in a calcium oxalate (CaC_2O_4) solution in presence of sucrose. In other research, Besic (1985) speculated that sucrose influences calcium and phosphate solubility in teeth.

The experiment work was begun with research into the effect of milk minerals on "fouling" of reverse osmosis membranes used for concentration of milk (Tew, 2015) and then the effect of ion activities on solubility of calcium phosphate in milk in Chapter 3. Preliminary experiments of the model solutions containing $CaCl_2$, NaH_2PO_4, and NaOH showed an unexpected absence of precipitation when lactose was added. Although similar results have been obtained using simulated body fluids (Oyane et al., 2002), no work with lactose in the calcium phosphate system has been found. Little data are available from literature for validation in this thesis. Therefore, a few experiments were carried out to gain more data for comparison.

4.2 Materials and methods

4.2.1 Chemicals and reagents

Fresh stock solution of 1 mol L^{-1} calcium chloride dihydrate ($CaCl_2.2H_2O$, Thermo Fischer Scientific, Australia), 1 mol L^{-1} sodium dihydrogen phosphate monohydrate ($NaH_2PO_4.H_2O$, AnalaR, VWR International Ltd., Poole, England), and 1 mol L^{-1} sodium hydroxide (NaOH, LabServ, Australia) were prepared.

14.7 g (equivalent to 1 mol L^{-1}) $CaCl_2.2H_2O$ was weighed into a 100 mL volumetric flask and was made up to 100 mL with Milli–Q water.

Likewise, stock solutions of sodium phosphate and sodium hydroxide were prepared individually in 100 mL volumetric flasks. Dilute stock solutions of sodium hydroxide with 0.5 and 0.02 mol L^{-1} were also prepared.

Stock solutions were made up a day before the experiments to ensure that their temperatures were fully equilibrated to the laboratory temperature.

Generally, solutions of lactose monohydrate ($C_{12}H_{22}O_{11}.H_2O$, AnalaR, Poole, England) with a concentration of 9.5%w/w lactose were made up in 100 mL volumetric flasks a day before for experiments containing lactose. However, due to three different recipes for mixing solutions containing lactose, full descriptions on the preparation will be given at each related section.

All of the experiments were carried out at room temperature, which was about 23 ˚C, but the temperature was recorded throughout the runs over time to ensure no heat was produced that might affect the results.

4.2.2 Analytical instruments

4.2.2.1 pH meter

The pH of solutions was measured by a CyberScan pH 510 pH/mV meter (Eutech, Germany) with an Eutech pH probe that was equipped with an automatic temperature compensation. Another CyberScan pH 310 pH/mV meter (Eutech, Germany) was also used when the pH of two solutions needed to be adjusted simultaneously before mixing. The pH meters were calibrated to ±0.02 of standard buffer pH values.

4.2.2.2 Conductivity meter

The electrical conductivity meter of solutions were measured with a Lab 960 conductivity meter that was equipped with a Lab LF413T standard conductivity cell (Schott, Germany) with a resolution of ±1 μS cm^{-1}. The conductivity meter was set to a linear temperature compensation with an accuracy of ±0.5% and a temperature coefficient of 1.754% K^{-1}. The probe was rinsed with Milli–Q water before and after each measurement.

4.2.2.3 Dynamic Light Scattering

Dynamic light scattering (DLS, Zetasizer, Model Nano Series, Malvern Instruments, Worcestershire, United Kingdom) was used to determine size distribution of particles in the mixed solutions. Three runs were defined in the software, in which water was chosen as a dispersant with the refractive index of 1.333 and absorption of zero. Temperature and equilibration time were set to 23 ˚C and 90 minutes, respectively. Standard operating procedures were followed.

4.2.3 Solution preparations

In this section, binary solutions of $CaCl_2$, NaH_2PO_4, and lactose were individually tested, because in initial experiments (without argon), it was found that the pH of ingredient solutions, especially $CaCl_2$, fluctuated rapidly within minutes when magnetically stirred and exposed to air. Hence, ternary solutions of $CaCl_2$, NaH_2PO_4, and lactose with NaOH were also prepared to improve pH and conductivity stabilisation over time. This enabled the estimation of the right concentration of each solution before mixing to obtain the desirable initial and stable pH values after mixing.

4.2.3.1 Preparation of binary solutions of $CaCl_2$ and NaH_2PO_4

Six mL (equivalent to 0.06 mol L^{-1}) of the calcium chloride stock solution was drawn up by a clean and dry 5±0.015 mL glass pipette and 1 mL by a 1±0.007 mL glass pipette. They were transferred to a clean and dry 100 mL volumetric flask, which was filled up with milli–Q water to 100 mL. The calcium chloride solution was shaken gently and was transferred to a 250 mL glass beaker, into which probes of analytical instruments were placed to measure pH, conductivity, and temperature over time. 60 mM NaH_2PO_4 solution was made up similar to the preparation of 60 mM $CaCl_2$ solution.

4.2.3.2 Preparation of binary solution of lactose

A solution of 9.5%w/w lactose was prepared by adding 10%w/w lactose monohydrate to water.

The lactose solution was incubated at 40 ˚C with orbital shaking at 140 rpm for approximately 4 hours to ensure complete dissolution of lactose. It was then stored at laboratory temperature (23 ˚C) to equilibrate.

4.2.3.3 Preparation of ternary solutions of $CaCl_2$ or NaH_2PO_4 or lactose with NaOH

Ternary solutions of $CaCl_2$ or NaH_2PO_4 or lactose with NaOH were made up very similar to the preparation of corresponding binary solutions, but a certain amount of NaOH was added to 100 mL of flask. For example, identically, 6 mL (equivalent to 0.06 mol L^{-1}) of the $CaCl_2$ stock solution was drawn up and transferred to a 100 mL volumetric flask, to which 2 mL (equivalent to 1 mM) of the 0.05 M NaOH stock solution was added. The solution was then filled up with Milli–Q water and was poured to a container for pH and conductivity measurements.

Smaller quantities of NaOH were drawn up by micropipettes in the range of 20–100, or 200–1000 μL, both of which were calibrated before each set of experiment to ensure the accuracy of taken volume by weighting Milli–Q water on the balance.

Similarly, ternary solutions of lactose and NaOH solutions were made up in the same way but a different amount of NaOH was added.

4.2.3.4 Preparation of mixed solutions

For each mixed solution, solutions of both $CaCl_2$ and NaH_2PO_4 (unmixed) were prepared in a 100 mL volumetric flask with various concentrations, and sodium hydroxide was added to achieve a desired pH value in a similar way of ternary solution preparations. Once both solutions reached to a stable and same pH values, they were mixed.

For mixed solutions containing lactose, two 9.5%w/w lactose solutions with NaOH were prepared in an identical method to the preparation of ternary solutions. One lactose solution was used for preparation of calcium chloride solution and the other one for sodium phosphate solution.

4.2.3.5 Experimental operation conditions

Five modes of operation were tested to determine how the experimental conditions would affect the pH and conductivity of the solutions:

1. The solution was poured to a beaker which is exposed to open air;
2. The container was sealed by a lid to avoid CO_2 absorption from air;
3. The container was open to air placed on magnetic stirrer while bubbling air in;
4. The container was placed on a magnetic stirrer while flowing argon into the headspace;
5. The container was placed on a magnetic stirrer while bubbling argon into the solution as shown in Figure 4.1.

Holes were drilled in the lid of container for gas and probes as shown in Figure 4.1. Instruments grade argon gas was bubbled at 40 cm^3 min^{-1} to the bottom of each solution to strip and prevent absorption of any carbon dioxide which strongly influenced pH. pH, conductivity, and temperature were measured and recorded over time while argon was bubbling in. Samples were taken from time to time for the particle size analysis using the DLS instrument to identify the possible formation of nanoparticles.

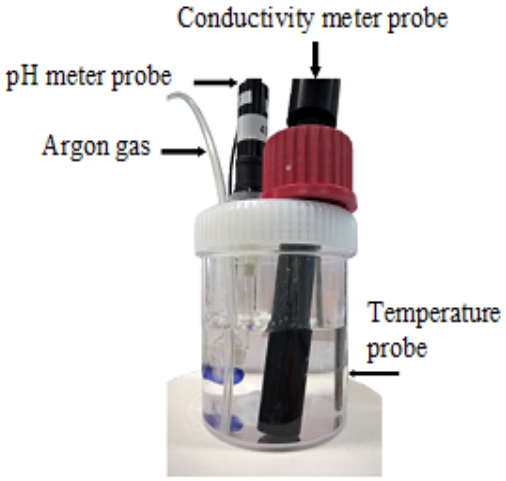

Figure 4.1 The experimental set–up for the majority of experiments.

4.3 Results and discussion

4.3.1 $CaCl_2$ solution

A binary solution of $CaCl_2$ was exposed to air to monitor how pH and conductivity are affected dynamically. Figure 4.2a shows the values of pH and conductivity of 60 mM $CaCl_2$ solution which was exposed to air. The drop in pH and conductivity clearly implies absorption of carbon dioxide from air.

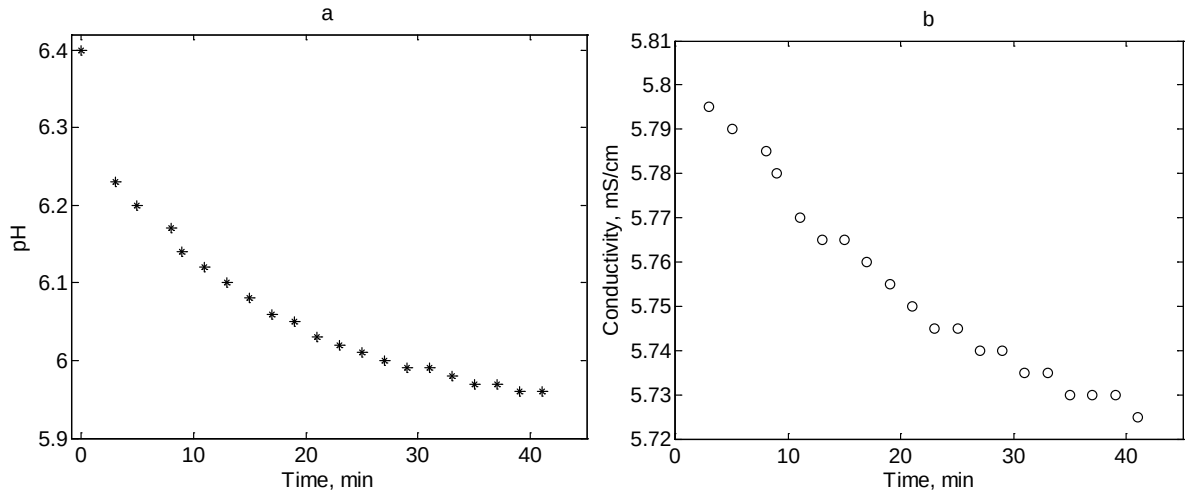

Figure 4.2 pH and conductivity changes of 60 mM $CaCl_2$ solution over the time while open to air.

It was believed that gaseous CO_2 enters the aqueous phase of a solution to achieve thermodynamic equilibrium with atmosphere:

$$CO_{2(g)} \overset{K_{CO_2}}{\longleftrightarrow} CO_{2(aq)} \tag{4.1}$$

where K_{CO_2} is the solubility coefficient of CO_2 in the aqueous phase of solution, dissolution of which is about 0.038 mol L^{-1} bar^{-1}.

$$\left[CO_{2(aq)}\right] = K_{CO_2} P_{CO_2} \tag{4.2}$$

Here $[CO_{2(aq)}]$ is the molar concentration of CO_2 in the aqueous phase; P_{CO_2} is the partial pressure of CO_2 on the surface solution, [bar].

The dissolved carbon dioxide thermodynamically interacts with water forming carbonic acid, which may lose up two protons according to the following equilibria with three different intrinsic association constants (Zeebe and Wolf-Gladrow, 2001; Wikipedia, n.d):

$$CO_{2(aq)} + H_2O_{(l)} \leftrightarrow H_2CO_{3(aq)} \qquad K_{a_1} = \frac{a_{H_2CO_3}}{a_{CO_2}} = 1.7 \times 10^{-3}[-] \tag{4.3}$$

$$H_2CO_3 \leftrightarrow HCO_3^- + H^+ \qquad K_{a_2} = \frac{a_{H_2CO_3}}{a_{HCO_3^-} a_{H^+}} = 4 \times 10^3 \ [\text{mol}^{-1}\ \text{L}] \tag{4.4}$$

$$HCO_3^- \leftrightarrow CO_3^{2-} + H^+ \qquad K_{a_3} = \frac{a_{HCO_3^-}}{a_{CO_3^{2-}} a_{H^+}} = 2.13 \times 10^{10}\ [\text{mol}^{-1}\ \text{L}] \tag{4.5}$$

The K_{a_2} value is inconsistent and far lower than that of the 2.25×10^6 mol^{-1} L presented by Holt et al. (1981). Zeebe and Wolf-Gladrow (2001) used the ratio $\frac{K_{a_2}}{K_{a_1}}$ representing:

$$\frac{K_{a_2}}{K_{a_1}} = \frac{a_{CO_{2(aq)}}}{a_{HCO_3^-} a_{H^+}} = 2.35 \times 10^6 \tag{4.6}$$

The transmission of gaseous to aqueous CO_2 then to carbonic acid leads the solution to release up to two hydrogen ions and subsequently drop in pH.

These equilibria were used to simulate influence of CO_2 absorption on pH values of $CaCl_2$ solution. Calcium, bicarbonate (HCO_3^-), carbonate (CO_3^{2-}), hydrogen, hydroxide ions were incorporated into the model with identical corresponding intrinsic associations given in Chapter 3 (Zeebe and Wolf-Gladrow, 2001).

Figure 4.3 illustrates the pH drop in 60 mM $CaCl_2$ solution as a function of CO_2 concentration as the result of simulation. This clearly shows that pH reduces rapidly at very low CO_2 concentrations and then drops slowly for higher concentration. According to Figure 4.2, the initial pH value was 6.4 for the experimental measurement of $CaCl_2$ solution that is equivalent to absorption of about 4 ppm CO_2 from air into the solution. This is possibly because there was a little delay in pH measurement due to pouring the solution and adjusting analytical probes in the beaker.

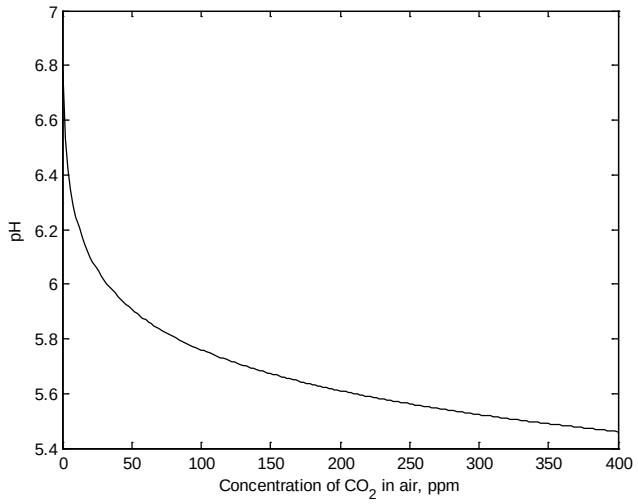

Figure 4.3 pH of 60 mM $CaCl_2$ solution when it was assumed to be exposed to air.

4.3.1.1 Ternary solution of $CaCl_2$ with NaOH

Since it was noticed that measuring pH of $CaCl_2$ in a beaker exposed to air was not a reliable operational method, titration of the solution with NaOH was tested to see how it could help to stabilise the solution. Titration results with NaOH were inconsistent as shown in Figure 4.4, and clearly showed absorption of CO_2 during a lunch break. The equilibrium pH of $CaCl_2$ before the addition of NaOH was less than 5.5. Hence, NaOH alone is not sufficient to stabilise the pH. Therefore, other operational conditions needed to be carried out on $CaCl_2$ solution to minimise pH fluctuations over time, one of which would probably be covering the beaker solution to avoid entering carbon dioxide into the solution. The other conditions were described separately in Section 4.2.3.5.

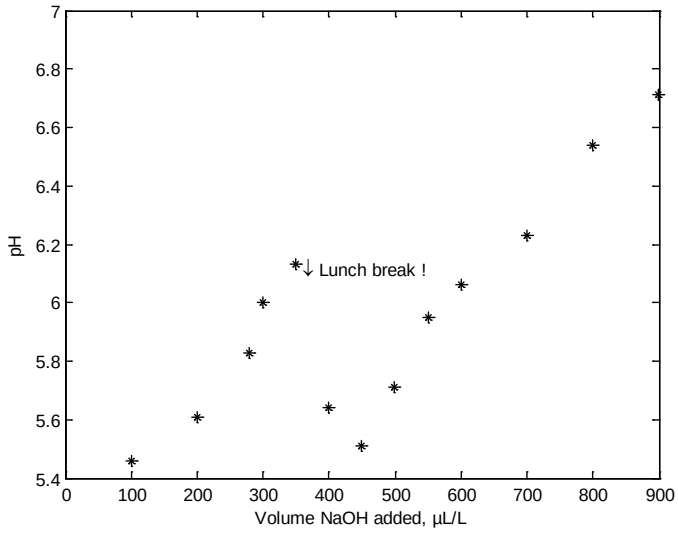

Figure 4.4 Titration of 60 mM $CaCl_2$ solution with NaOH while stirred and open to air.

The experiment was carried out by the first four modes of operation, in which the $CaCl_2$ solution was exposed to air in an open beaker, was sealed with a lid, was open to air while air bubbling in, and was treated with argon gas bubbling in the headspace as shown in Figure 4.5. The solution was more stable when it was sealed with a lid on indicating less absorption of carbon dioxide. It was expected that bubbling air in the solution could obtain a consistent equilibrium with atmosphere carbon dioxide, but the data for pH and conductivity could not prove that. However, the solution became consistent after about 20 minutes by purging argon in the headspace while it was sealed with a lid.

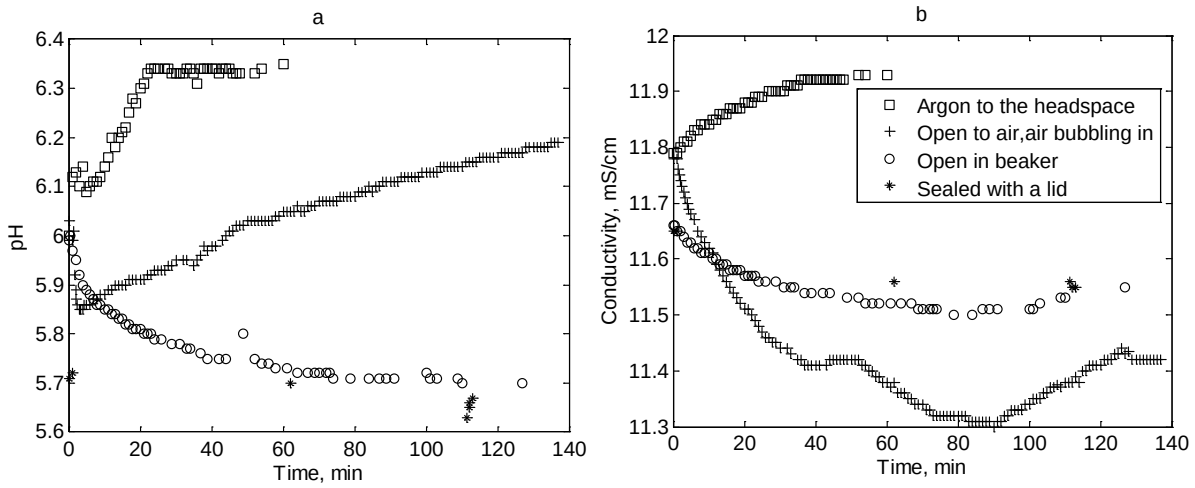

Figure 4.5 pH and conductivity of 60 mM $CaCl_2$ solutions under four different experimental operations.

Subsequently, bubbling argon in the aqueous phase along with the addition of NaOH was found the most effective operational condition in comparison with the others. Figure 4.6a shows the pH of $CaCl_2$ solutions with different concentrations of NaOH operating under bubbling argon. When argon was bubbled through the solution, the pH values were about 1.5 units higher and more repeatable between experiments than those exposed to air. It clearly shows that NaOH and bubbling argon could effectively improve pH stabilisation over time especially for higher amounts of NaOH. Thus, it seems that $CaCl_2$ solution with lower quantities of NaOH could be harder to control due to potential absorption of carbon dioxide into the solution as the pH gets closer to natural milk pH.

Figure 4.6b indicates the titration results of $CaCl_2$ solution with NaOH, which is more consistent than those exposed to air. Figure 4.6 helped to determine the required amount of NaOH to get the desired initial pH value before mixing solutions.

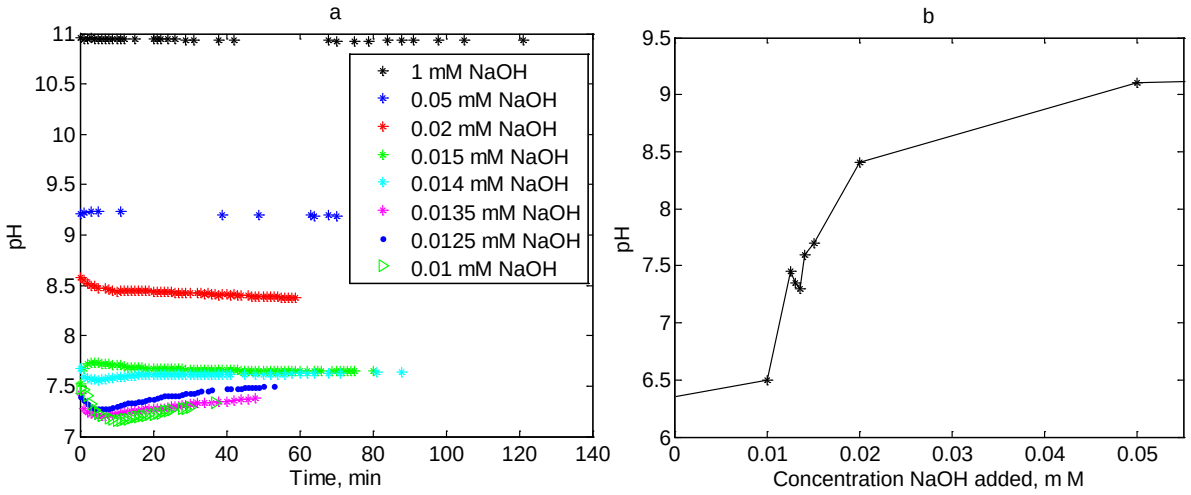

Figure 4.6 pH of 60 mM $CaCl_2$ solution with bubbled argon a) over time; and b) as a function of various NaOH added in mM.

4.3.2 NaH_2PO_4 solution

Solutions of sodium phosphate were much more stable even without NaOH addition or bubbling argon. This is because the solution has naturally low pH hence addition of carbonic acid is not able to reduce pH anymore.

Similarly, pH and conductivity of NaH_2PO_4 solutions were measured by addition of NaOH and argon gas bubbling in to avoid any CO_2 absorption. Figure 4.7a shows the pH and conductivity of 60 mM NaH_2PO_4 solution when pH was adjusted to 7.5 by adding NaOH in the middle of the experiment. First, 10 mM NaOH was added to the solution giving pH of about 6.1, then about 47.1 mM was added to reach to adjusted pH but it was a bit higher than expected. 45 mM NaOH gave closer stable pH values but a bit lower than the adjusted one. Therefore, 9 mM more was added to the solution giving pH about 7.5. Figure 4.7b indicates the measured conductivity, which corresponds to the pH change data for the three sodium phosphate solutions. This shows that solutions containing more NaOH are likely more conductive, this is because the solution contains more charged species.

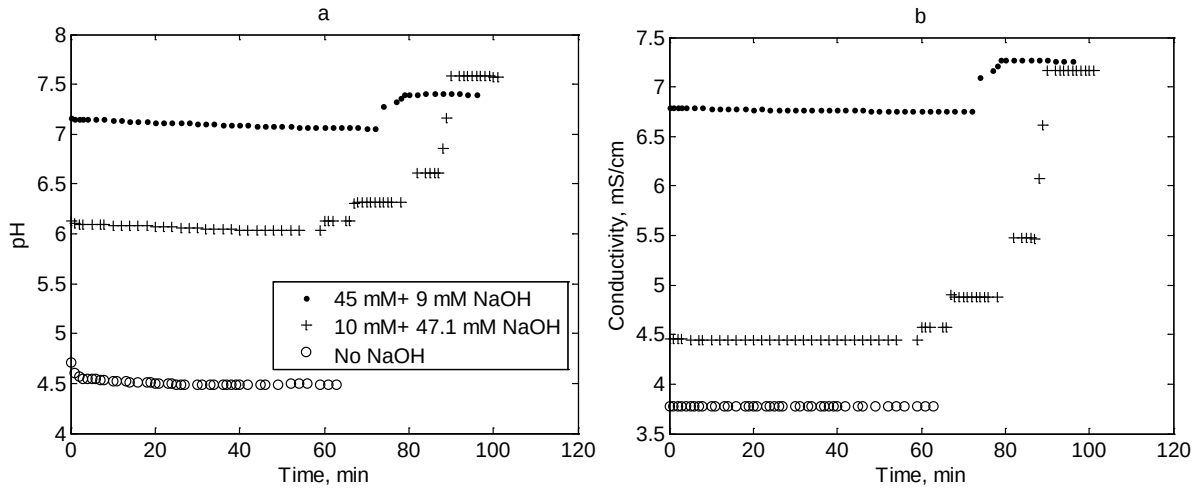

Figure 4.7 a) pH and b) conductivity of 60 mM NaH_2PO_4 solution titrated with NaOH while argon gas bubbled in the aqueous phase.

4.3.3 Lactose solution

Binary solutions of lactose in water with 2.5, 5, and 7.5%w/w lactose were tested in open beakers exposed to air and a 9.5%w/w solution was tested with argon bubbling into the solution. The resulting pH and conductivity are shown in Figure 4.8. During the experiments, conductivity, and especially pH values were unstable for those solutions exposed to air, so the mean value of each measurement was recorded each minute. However, more improvement was observed once the solution was sealed with a lid with argon bubbling. This is probably because of less carbon dioxide absorbed in the solution. The 9.5%w/w solution will have been more stable because of its lower pH.

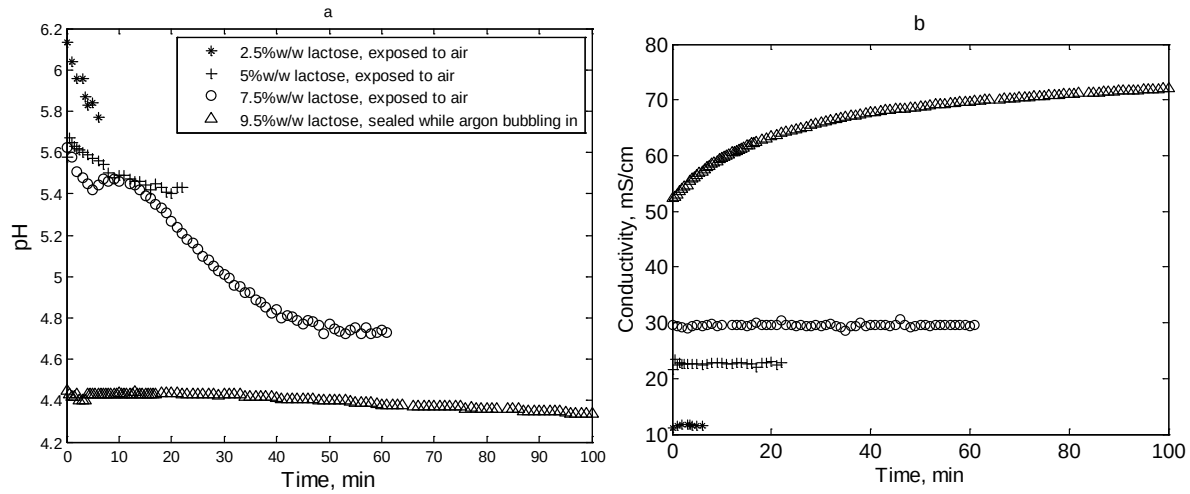

Figure 4.8 a) pH and b) conductivity of lactose solutions with 2.5, 5, 7.5, and 9.5%w/w contents when they are either exposed to air or sealed while argon gas purging in.

Hence, the titration of lactose with NaOH seemed necessary with bubbling argon gas to stabilise pH values. Figure 4.9a shows the titration of 9.5%w/w lactose with different concentrations of NaOH to see how much base is needed to obtain the adjusted pH. Moreover, consistent and stable results were observed for each solution of lactose with NaOH over time.

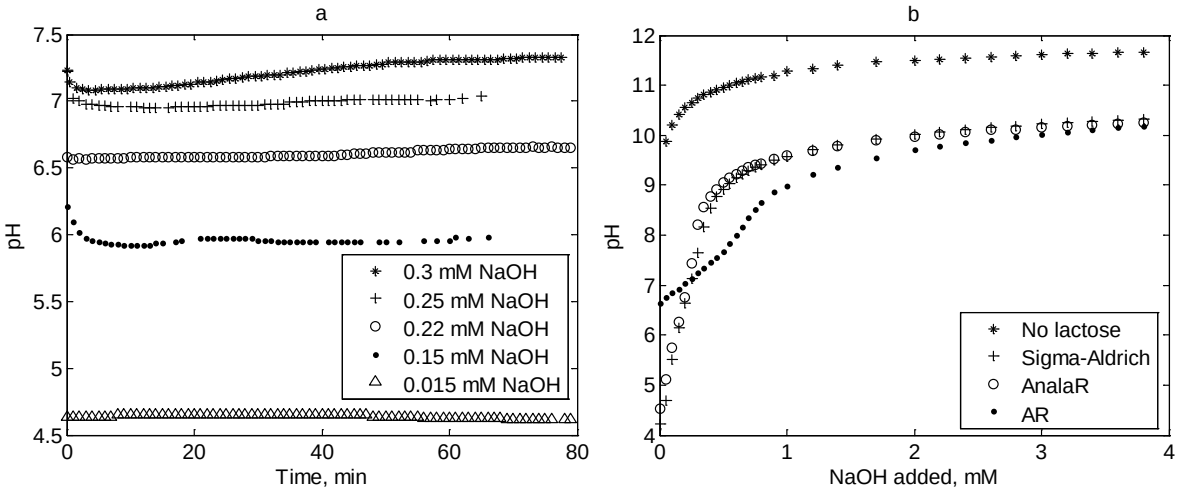

Figure 4.9 Titration of 9.5%w/w lactose solutions with argon bubbling a) with various NaOH concentrations, and b) by different lactose sources.

During pH adjustment, it was noticed that adjustment of lactose solutions required more NaOH than expected. Lactose can dissociate a very small amount in solution with a K_{ac} given by Stearn (1931) of 7.6×10^{-13} mol^{-1} L. Using this acidity constant one can calculate that a 9.5% solution has an expected pH of 6.33. Once 3 mmol/L of NaOH has been added the pH is expected to tend to about 11.5 but the pH reached only 10.2 in the experiments as shown in Figure 4.9b. The test was repeated using three different samples of lactose from Sigma–Aldrich, AR, and AnalaR, though is possible that all samples had the same origin. The possibility of the presence of lactose phosphate was considered as this would have the effect of lowering the pH and would interact with NaOH more than lactose (Lifran, 2007).

4.3.4 Mixed solutions

Solutions of $CaCl_2$ and NaH_2PO_4 with a 1:1 ratio of Ca/P were prepared individually for the mixed solutions either with or without lactose but with NaOH based on the preparation method given in Section 4.2.3.4.

Concentrations after mixing of 3.5, 5, and 10 mM Ca and PO_4 with the adjusted initial pH of about 6.5 were tested and shown in Figure 4.10 along with their corresponding DLS analysis

results as a function of particle size. Samples were taken for analysis as soon as the previous run of Zetasizer was completed to ensure each part of the graph was analysed by the Zetasizer.

Differences were seen for 5 mM solutions with and without lactose at pH about 6.5 (Figure 4.10c). In this figure, it can be seen that precipitation, as indicated by the pH drop, is not instantaneous. This is explained by the rate of precipitation being proportional to the area of precipitated particles already in the system. The solution with lactose delayed precipitation even though it was at a slightly higher pH and hence less stable. Similarly, for 3.5 mM (Figure 5a) with almost identical pH in both solutions, the presence of lactose increased the stability of the solution. No precipitation was observed even after 200 minutes. Figure 4.10e illustrates the pH change over time for 10 mM solution, in which both solutions with 9.5 and 19.95%w/w lactose had a slightly lower initial pH, even though the ternary solution pH values were stabilised at about 6.5, but it immediately dropped. This is probably because of higher saturation of the solution so the stabilisation by lactose was insufficient.

By comparing Figures 4.10a, c, and e, it can be concluded that lower contents of $CaCl_2$ and NaH_2PO_4 are more stable and thus the precipitation occurs at a later time with a small drop in pH.

The most striking difference between solutions with and without lactose was shown by the Zetasizer response as seen in Figure 4.10b, d, and f. Mixtures with 9.5% w/w lactose at a pH about 6.5 showed a peak at a particle diameter close to 1 nm. Mixtures without lactose did not show this peak. The same peak was observed in a sample with lactose that had been kept for 3 days before particle size measurement, indicating that the particles were stable. Samples of lactose only did not show any peaks so it was concluded that the peak is from a reaction product and not an artefact.

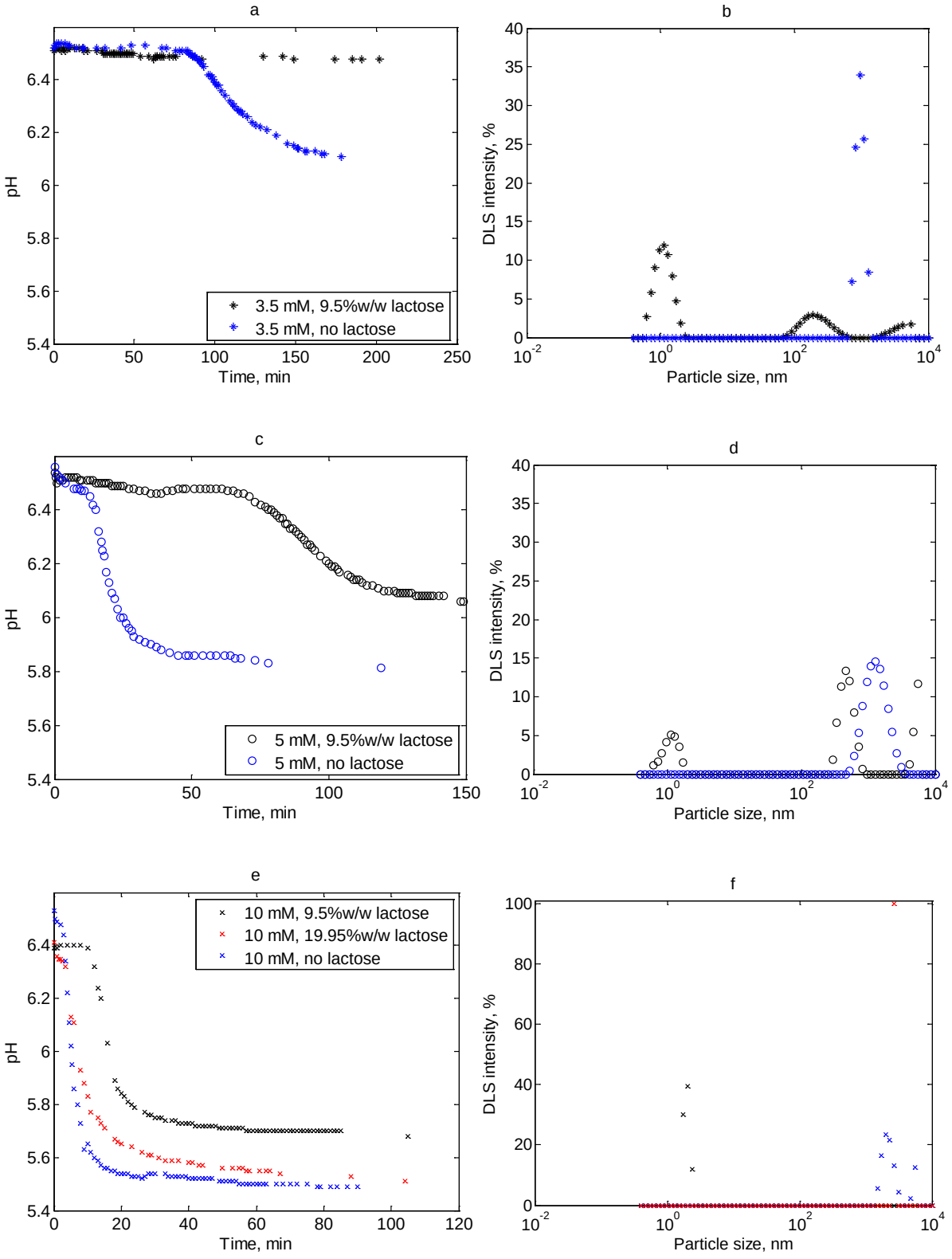

Figure 4.10 pH changes and DLS analysis, indicating precipitation, for a, b) 3.5 mM; c, d) 5 mM; and e, f) 10 mM $CaCl_2$ and NaH_2PO_4 with 9.5%w/w and without lactose with adjusted initial pH of about 6.5.

In another experiment with 2.5 mM of $CaCl_2$ and NaH_2PO_4 without lactose, no precipitation was detected either by eye, by shining a laser pointer through the solution, even though a

small peak is seen at about 10^3 nm in Figure 4.11b. pH remained relatively constant for about 1 hour indicating the absence of precipitation.

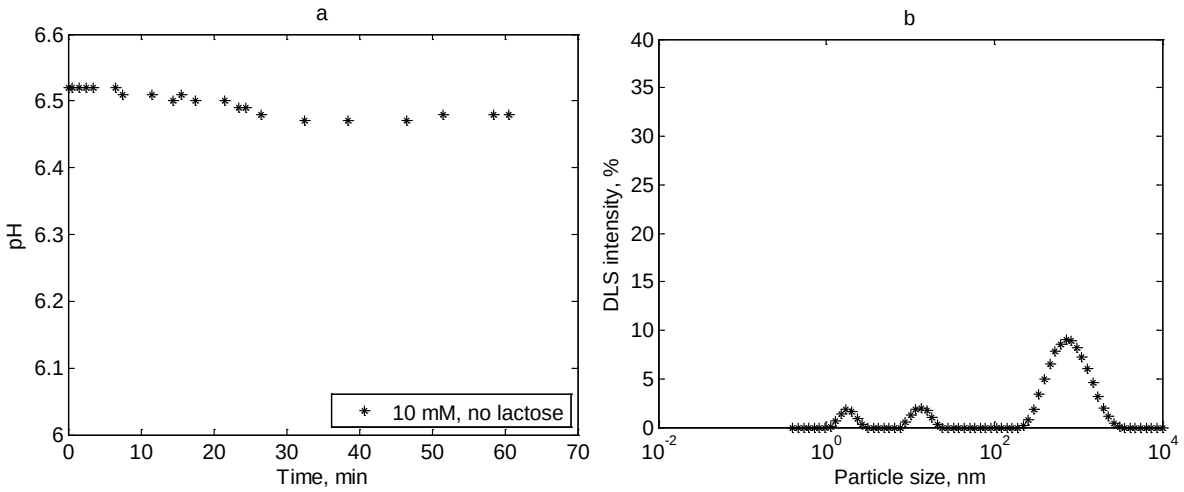

Figure 4.11 a) pH changes, and b) DLS analysis of 2.5 mM $CaCl_2$ and NaH_2PO_4 without lactose.

The initial pH of solutions was adjusted to about 5.5 by adding less NaOH for the solution with 10 mM concentration to see if any precipitation occurred in the solution. At lower pH values, solutions with 10 mM no sign of precipitation was seen either with or without lactose at pH 5.2 as shown in Figure 4.12a and b. These results are consistent with the lower saturation at lower pH that was simulated previously in Figure 3.19 in Chapter 3. Hence, the amount of NaOH or the pH is a factor affecting the formation of nanoparticles in the mixed solutions. Figure 4.12c indicates that precipitation started immediately for the 20 mM solution without lactose and within 3 minutes for the solution with lactose.

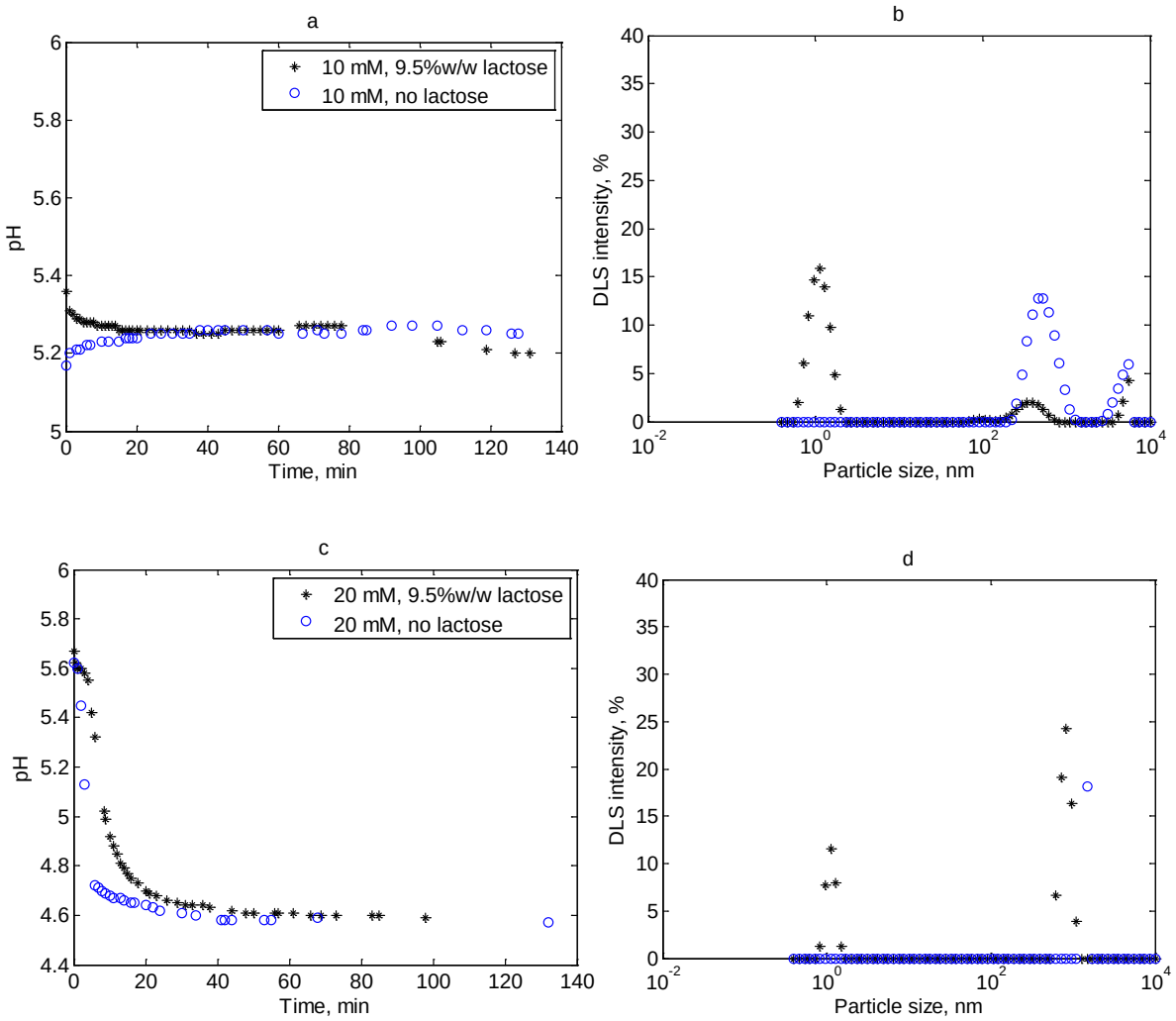

Figure 4.12 pH changes and DLS analysis, for a, b) 10 mM; c, d) 20 mM; $CaCl_2$ and NaH_2PO_4 with 9.5%w/w and without lactose with adjusted initial pH of about 5.5.

Similar nm size particles have been found in simulated body fluids by Oyane et al. (2002) using 2.5 mM Ca^{2+} and 1.0 mM HPO_4^{2-} at pH 7.4 and by Onuma and Ito (1998). Kellermeier et al. (2012) found stable clusters in a calcium carbonate silica system. A number of structures have been proposed. A popular one has been the Posner cluster (Posner and Betts, 1975), $Ca_9(PO_4)_6$, which has a theoretical diameter of 0.95 nm. Lin and Chiu (2017) simulated possible structures for calcium phosphate clusters with sizes of about 1 nm and obtained some alternative structures with lower energies than the Posner cluster.

Without a known composition, it was not possible to include the nanoparticles into the model. Hence, simulation of the pH change was not possible.

The results shown in Figure 4.10 are the key results of this chapter. When lactose is added to the calcium phosphate system with concentrations similar to those found in bovine milk,

nanoparticles are formed. The formation of these seems to prevent or reduce the precipitation of calcium phosphate and hence will add to the stability of calcium phosphate in milk. This effect will be in addition to the role of casein in stabilising calcium phosphate in milk as discussed by Holt (2004). Lactose will act in the milk serum (outside of the casein micelles) so might have a role in stabilising the fraction in the serum.

There are many uncertainties in these experiments and the mechanism for the increased stabilisation is unclear. It is reasonably certain that when lactose is present, nanoparticles of about 1 nm are formed, while solutions containing no lactose formed precipitates with larger particles size.

There is no evidence at this stage of the composition or structure of these particles. Given the unexpected titration curve of lactose, it is possible that there is a significant amount of lactose phosphate or other substance in the lactose, and that this forms part of the nanoparticle. If lactose does not make up part of the nanoparticle, there are other mechanisms for interactions. The presence of lactose will increase the solution viscosity and possibly reduce the rate of normal precipitation. Disaccharides like sucrose, maltose, and lactose typically are hydrated by about five water molecules in solution, which reduces the water activity, hence affecting calcium and phosphate ion interaction. Little and Holt (2004) showed that β–casein phosphopeptide in milk will stabilise casein phosphate nanoparticles, but did not speculate on a structure. Likewise Oyane et al. (2002) who measured 1 nm calcium phosphate particles did not discuss their structure. Lin and Chiu (2017) showed that the structures have not yet been confirmed.

In this preliminary work, the Ca/P ratio used as 1:1, but the Posner cluster has a ratio of 1.5:1. Little and Holt (2004) suggested a lower limit of 1.15 for Ca/P in a CPN solution containing 5 mg β–casein in a buffer solution of 30 mM $Ca(NO_3)_2$, 5 mM $Mg(NO_3)_2$, 20 mM KH_2PO_4, 26 mM KNO_3, and 1.5 mM NaN_3. It is expected that a ratio closer to 1.5 will increase stability so some future experiments are recommended with this ratio.

The nanoparticles have been found to be stable for at least 3 days, but this duration needs to be extended and tested for a range of conditions. Oyane et al. (2002) showed stability for 7 days in simulated body fluids.

Lactose is the first sugar found to form nanoparticles with calcium phosphate, but the effect of other sugars like disaccharides and monosaccharides are unknown monosaccharides are

unknown which are useful to be tested to see how they can influence the solubility of calcium phosphate solution.

4.4 Conclusions

Binary solutions of calcium chloride and sodium phosphate as well as corresponding ternary solutions with lactose were stabilised by designing an effective experimental set–up to reach the desired initial pH value before mixing them together and to prevent any carbon dioxide absorption from the air which strongly affected the pH of ingredient solutions especially calcium chloride. Given the experimental results, it was found that purging argon in the solution and sealing the container could satisfactorily minimise carbon dioxide absorption from air into the solutions.

The experimental results clearly showed the formation of a 1 nm nanoparticle in solutions of lactose and calcium and phosphate ions. Lactose was found to prevent or slow down the precipitation of calcium phosphate, probably as calcium dihydrogen phosphate. The structure of the nanoparticle is not known and, based on current research in this area, might be difficult to determine. The effects of many of the conditions such as concentration, ion ratios, pH, lactose concentration, and time need to be tested. The effects of lactose in this ideal system indicate that it might have a role for the stabilisation of calcium phosphate in milk that might add to the stabilisation produced by the casein micelles.

5 Development of the Model to Bovine Milk

5.1 Introduction

Fundamental research has been conducted on the calculations of salt equilibria in milk serum and simulated milk ultrafiltrate (SMUF) without proteins (Holt et al., 1981; Lyster, 1981; Wood et al., 1981; Gao, van Halsema, et al., 2010) and fewer studies have been done on salt partitioning of milk by incorporating phosphoserine residues of casein molecule (Holt, 2004; Little and Holt, 2004; Mekmene, Le Graet, et al., 2009; Mekmene et al., 2010). More recently, Bijl et al. (2018) developed a comprehensive model, in which magnesium ions were assumed to bind to caseins with identical association constants as calcium and by incorporating dissociable side groups of amino acids in casein proteins. In this thesis, the proposed model described in Chapter 3 was applied to milk to calculate ion equilibria between the aqueous and micellar phases of milk by including dissociable amino acids of both phases. Further, the model was used to predict dynamic changes due to supersaturation in milk.

5.2 Description of the model

The proposed model, which was fully described in Chapter 3, was used to determine ion speciation in milk. The model was applied to various systems and gave reasonable results under various conditions. The major constituents of aqueous and micellar phases of milk that were included in the model are calcium, magnesium, sodium, potassium, hydrogen, citrate, inorganic phosphate, carbonate, sulphate, phosphate esters, chloride, carboxylate, and hydroxide. In this chapter, the model is extended to include the amino acids of α_{s1}–, α_{s2}–, β–, κ–casein and β–lactoglobulin, α–lactalbumin, and bovine serum albumin.

Some of the amino acids in proteins have a dissociable side chain in their structures that is either basic or acidic depending on their dissociation constants. Only dissociable side groups of particular amino acid were used in the model. E.g., alanine is a non–polar and uncharged side chain, which is unlikely to affect pH of the solution, whereas aspartic acid with one dissociable side group acts as an acid (Belitz and Grosch, 1999). The chemical structure of all amino acids with either charged or uncharged side groups are listed in Appendix 7. Table 5.1 gives the dissociable side groups of amino acids with their dissociation constants.

Table 5.1 The dissociation of the amino acids side groups of the milk proteins (Belitz and Grosch, 1999; Mercadé-Prieto et al., 2007).

Amino acid	Side group	The equilibrium	K_d of the side group
Arginine	–$CH_2CH_2CH_2NHCNHNH_2$ (–RNH_2)	$\mathrm{Arg} + \mathrm{H^+} \leftrightarrow \mathrm{ArgH^+}$	$K_{d_{Arg}} = \frac{[-\mathrm{RNH_2}][\mathrm{H^+}]}{[-\mathrm{RNH_3^+}]} = \frac{[\mathrm{Arg}][\mathrm{H^+}]}{[\mathrm{ArgH^+}]} = 10^{-12.52}$
Aspartic acid	–CH_2COOH (–RCOOH)	$\mathrm{Asp^-} + \mathrm{H^+} \leftrightarrow \mathrm{AspH}$	$K_{d_{Asp}} = \frac{[-\mathrm{RCOO^-}][\mathrm{H^+}]}{[-\mathrm{RCOOH}]} = \frac{[\mathrm{Asp^-}][\mathrm{H^+}]}{[\mathrm{AspH}]} = 10^{-4.0}$
Cysteine	–CH_2SH (–RSH)	$\mathrm{Cys^-} + \mathrm{H^+} \leftrightarrow \mathrm{CysH}$	$K_{d_{Cys}} = \frac{[-\mathrm{RS^-}][\mathrm{H^+}]}{[-\mathrm{RSH}]} = \frac{[\mathrm{Cys^-}][\mathrm{H^+}]}{[\mathrm{CysH}]} = 10^{-8.5}$
Glutamic acid	–CH_2CH_2COOH (–RCOOH)	$\mathrm{Glu^-} + \mathrm{H^+} \leftrightarrow \mathrm{GluH}$	$K_{d_{Glu}} = \frac{[-\mathrm{RCOO^-}][\mathrm{H^+}]}{[-\mathrm{RCOOH}]} = \frac{[\mathrm{Glu^-}][\mathrm{H^+}]}{[\mathrm{GluH}]} = 10^{-4.0}$
Histidine	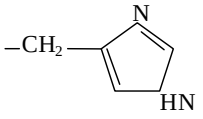 (–RNH, imidazole)	$\mathrm{His} + \mathrm{H^+} \leftrightarrow -\mathrm{HisH^+}$	$K_{d_{His}} = \frac{[-\mathrm{Imidazole}][\mathrm{H^+}]}{[-\mathrm{ImidazoleH^+}]} = \frac{[\mathrm{His}][\mathrm{H^+}]}{[\mathrm{HisH^+}]} = 10^{-6.0}$
Lysine	–$CH_2CH_2CH_2CH_2NH_2$ (–RNH_2)	$\mathrm{Lys} + \mathrm{H^+} \leftrightarrow \mathrm{LysH^+}$	$K_{d_{Lys}} = \frac{[-\mathrm{RNH_2}][\mathrm{H^+}]}{[-\mathrm{RNH_3^+}]} = \frac{[\mathrm{Lys}][\mathrm{H^+}]}{[\mathrm{LysH^+}]} = 10^{-10.95}$
Serine	–CH_2OH (–RCOH)	$\mathrm{Ser^-} + \mathrm{H^+} \leftrightarrow \mathrm{SerH}$	$K_{d_{Ser}} = \frac{[-\mathrm{RCO^-}][\mathrm{H^+}]}{[-\mathrm{RCOH}]} = \frac{[\mathrm{Ser^-}][\mathrm{H^+}]}{[\mathrm{SerH}]} = 10^{-13.22}$
Threonine	–$CHOHCH_3$ (–RCOH)	$\mathrm{Thr^-} + \mathrm{H^+} \leftrightarrow \mathrm{ThrH}$	$K_{d_{Thr}} = \frac{[-\mathrm{RCO^-}][\mathrm{H^+}]}{[-\mathrm{RCOH}]} = \frac{[\mathrm{Thr^-}][\mathrm{H^+}]}{[\mathrm{ThrH}]} = 10^{-13.22}$
Tyrosine	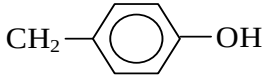 (–RCOH)	$\mathrm{Tyr^-} + \mathrm{H^+} \leftrightarrow \mathrm{TyrH}$	$K_{d_{Tyr}} = \frac{[-\mathrm{RCO^-}][\mathrm{H^+}]}{[-\mathrm{RCOH}]} = \frac{[\mathrm{Tyr^-}][\mathrm{H^+}]}{[\mathrm{TyrH}]} = 10^{-9.60}$

Note: the formula written in the parentheses represent the abbreviated form of the side groups.

Each protein molecule has many different residues with potential hydrogen ion equilibria. Dissociable acidic and basic side groups are bound covalently to a higher degree to hydrogen ions and to a lesser degree to other cations (Kuehner et al., 1999). The affinity between other cations and amino acids was not ignored despite being small. At any pH given, these residues will be in various protonation states depending on their individual ion dissociation constant, i.e. K_d often expressed as pK_d. Thus, the protein will have a net charge, which varies with pH. With knowledge of all the individual pK_d values of all the possible hydrogen ion and other cations ion–pairs found in a protein, it is possible to calculate the absolute net electric charge of a protein as a function of pH.

Each amino acid was treated as an anion with either negative or neutral charge depending on their acidic or basic side groups. Consider arginine in a protein. The $H_2N–CH–COOH$ head has been condensed as a part of the protein group $–CH_2CH_2CH_2NHCNHNH_2$ abbreviated here as $–RNH_2$. In acid conditions leaving the side, this will carry an extra proton and be $–RNH_3^+$, dissociation constant of which was shown in Table 5.1. The forms will be designated as Arg and $ArgH^+$ ($–RNH_3^+$). The other side groups in milk proteins with the same behaviour are lysine and histidine, and the NH_2 terminal group. –RCOOH is the side group for aspartic acid, which dissociates to $–RCOO^–$. The forms will be designated as $Asp^–$ and AspH. Dissociation of other acidic amino acids will be the same as aspartic acid such as cysteine, glutamic acid, serine, threonine, and tyrosine.

5.2.1 Net charge of a protein

Physico–chemical properties of a protein are highly affected by the parameter ‘net electric charge’ of the medium that implies the solution but the charge is of the protein. The pH at which the electric repulsion between proteins is minimised and near to zero, is called ‘isoelectric point (IEP)’ (Ninham and Lo Nostro, 2010). Hence, the net electric charge of the molecule is zero at the IEP, i.e. positive and negative charge numbers of a zwitterion become equal (Sørensen et al., 1927).

Net electric charge was calculated by three different methods, all of which should give consistent results for any protein. In this thesis, all three methods were used as a means of mathematical validation.

5.2.1.1 Approach 1 for net charge calculation

Cameselle et al. (1986) defined the net electric charge as the total number of charges (z) divided by the total number of molecules (n, see Equation (5.6)). The degree of ionisation (α) determines instant charge of a particular group due to the continuous fluctuating values. Therefore, the net electric charge is obtained as the total charge number of a molecule:

$$\text{Net charge} = \frac{\sum z}{n} \tag{5.1}$$

The degree of ionisation is identical to the time fraction of an acid–base molecule for dissociated groups, while the degree of non–dissociation $(1 - \alpha)$ is attributed to the time fraction for undissociated ones. The net charge should be equal to the sum over all the side groups in a protein:

$$\text{Net charge} = \sum z_d \alpha + z_u (1 - \alpha) \tag{5.2}$$

where z_d and z_u are charge numbers of dissociated and undissociated groups, respectively.

The Henderson–Hasselbach (Equation (5.3)) can be rearranged as a function of degree of ionisation (Fennema, 1996):

$$\frac{[\text{dissociated form}]}{[\text{undissociated form}]} = 10^{\text{pH}-pK_a} = \frac{\alpha}{1 - \alpha} \tag{5.3}$$

Therefore:

$$\alpha = \frac{1}{10^{pK_a - \text{pH}} + 1} \tag{5.4}$$

Substituting in Equation (5.2) gives:

$$\text{Net charge} = \frac{z_d}{10^{pK_a - \text{pH}} + 1} + \frac{z_u}{10^{\text{pH} - pK_a} + 1} \tag{5.5}$$

Hence, the overall net electric charge can be obtained for a molecule:

$$\text{Net charge} = \sum_{i=1}^{n} \left(\frac{z_{i_d}}{10^{pK_i - \text{pH}} + 1} + \frac{z_{i_u}}{10^{\text{pH} - pK_i} + 1} \right) \tag{5.6}$$

Here n is the number of amino acid side groups.

5.2.1.2 Approach 2 for net charge calculation

Salis et al. (2011) proposed a formula for calculation of bovine serum albumin surface charge at various pH values based on the potentiometric titrations, but Equation (5.7) can be also applicable to other proteins:

$$\text{Net charge} = \frac{C_{\text{HCl}} - C_{\text{NaOH}}}{m_{\text{protein}}/MW_{\text{protein}}} \tag{5.7}$$

C_{HCl} and C_{NaOH} are molar concentrations of HCl and NaOH, [mol L^{-1}] that are required to achieve a net zero surface charge; m_{protein} is mass of protein, [g L^{-1}]; MW_{protein} is the molar mass of protein, [g mol^{-1}].

5.2.1.3 Approach 3 for net charge calculation

Another method was used to calculate the net charge of a protein molecule as a function of the molar concentration and charge number of each amino acid and their corresponding ion–pairs per protein as follows:

$$\text{Net charge} = \frac{\sum_i C_i z_i}{m_{\text{protein}}/MW_{\text{protein}}} \tag{5.8}$$

The subscript i represents the species. This approach is originated from the net charge definition, which is used as the main method for this study.

However, all these methods assume no interaction between amino acid residues. Li et al. (2005) outlined a more rigorous method that takes into account these interactions.

5.2.2 Initial concentration of each amino acid

The molar concentration of each protein in milk should be determined to be able to obtain the concentration of each amino acid that was required for the simulation. The concentration of each dissociable amino acid was calculated from concentration of each protein in milk and the number of each dissociable amino acid per protein as shown in Table 5.2.

Table 5.2 Dissociable amino acid concentration in bovine milk and per protein of milk (Walstra and Jenness, 1984; Walstra et al., 2006).

	β–lg		α–la		BSA		α_{s1}–casein		α_{s2}–casein		β–casein		κ–casein	
	$\frac{\text{mol}_{AA^*}}{\text{mol}_{\beta\text{-lg}}}$	$\frac{\mu\text{mol}_{AA}}{L_{milk}}$	$\frac{\text{mol}_{AA}}{\text{mol}_{\alpha\text{-la}}}$	$\frac{\mu\text{mol}_{AA}}{L_{milk}}$	$\frac{\text{mol}_{AA}}{\text{mol}_{BSA}}$	$\frac{\mu\text{mol}_{AA}}{L_{milk}}$	$\frac{\text{mol}_{AA}}{\text{mol}_{\alpha s1}}$	$\frac{\mu\text{mol}_{AA}}{L_{milk}}$	$\frac{\text{mol}_{AA}}{\text{mol}_{\alpha s2}}$	$\frac{\mu\text{mol}_{AA}}{L_{milk}}$	$\frac{\text{mol}_{AA}}{\text{mol}_{\beta\text{-}}}$	$\frac{\mu\text{mol}_{AA}}{L_{milk}}$	$\frac{\text{mol}_{AA}}{\text{mol}_{\kappa\text{-}}}$	$\frac{\mu\text{mol}_{AA}}{L_{milk}}$
Arg	3	540	1	88	23	144	6	2813	6	640	4	1605	5	898
Asp	10	1800	9	789	42	262	7	3282	4	427	4	1605	4	718
Cys	5	900	8	701	35	219	0	0	2	213	0	0	2	359
Glu	16	2880	8	701	62	387	25	11723	25	2666	18	7224	13	2334
His	2	360	3	263	17	106	5	2345	3	320	5	2007	3	539
Lys	15	2700	12	1051	60	375	14	6565	24	2560	11	4415	9	1616
Ser	7	1260	7	613	28	175	16	7502	17	1813	16	6422	13	2334
Thr	8	1440	7	613	34	212	5	2345	15	1600	9	3612	14	2513
Tyr	4	720	4	350	19	119	10	4689	12	1280	4	1605	9	1616

*AA abbreviated for amino acid.

Table 5.3 gives the molar concentrations of β–lactoglobulin, α–lactalbumin, bovine serum albumin, α_{s1}–, α_{s2}–, β–, and κ–casein in bovine milk.

Table 5.3 Concentration of micellar and serum proteins of milk (Walstra and Jenness, 1984; Walstra et al., 2006).

Protein	Concentration, kg kg^{-1}_{milk}	MW, kg mol^{-1}	Concentration, μmol L^{-1}_{milk}
β–lg	0.0032	18.40	180
α–la	0.0012	14.18	88
BSA	0.0004	66.27	6
α_{s1}–casein	0.0107	23.62	469
α_{s2}–casein	0.0026	25.23	107
β–casein	0.0093	23.99	401
κ–casein	0.0033	19.02	180

5.3 Results and discussion

5.3.1 Individual aqueous proteins

Individual simulations were implemented by the proposed model for casein and serum proteins, among which more data are available for β–lactoglobulin net charge as a means of validation. Figure 5.1a shows the net electric charge of β–lactoglobulin in solution, for which neither NaOH nor HCl was added mathematically to see, what range of pH is covered with only dissociable side groups of the amino acids. pH was changed by changing the concentration of β–lactoglobulin in water. The pH values between about 5 to 7 were obtained showing negative net charge values. The curves from this study and Cameselle et al. (1986) were overlapped, so that they might be seen as one solid curve in Figure 5.1. The calculations of Figures 5.1 and 5.2 were based on the adjusted pK_d values of amino acids to get IEP of about 5.2 for β–lactoglobulin solution.

Figure 5.1b shows the net charge of solution when both HCl and NaOH were added to cover the acidic and basic parts with a predicted IEP of about 5.2 which is in good agreement with 5.2 given by Walstra et al. (2006). The titration curve of this study was fitted effectively with those theoretically predicted by Cameselle et al. (1986) and Burrington (2017); however, the net charge values estimated by Meissner et al. (2015). Approach 2 (Section 5.2.1.2) did not match with the current study calculations. Cornell and Patterson (1989) claimed that the net charge of β–lactoglobulin is between 8 to 10 electron volts per molecule at pH 4.4. The current study predicted a net charge of 9.9, which is within the range.

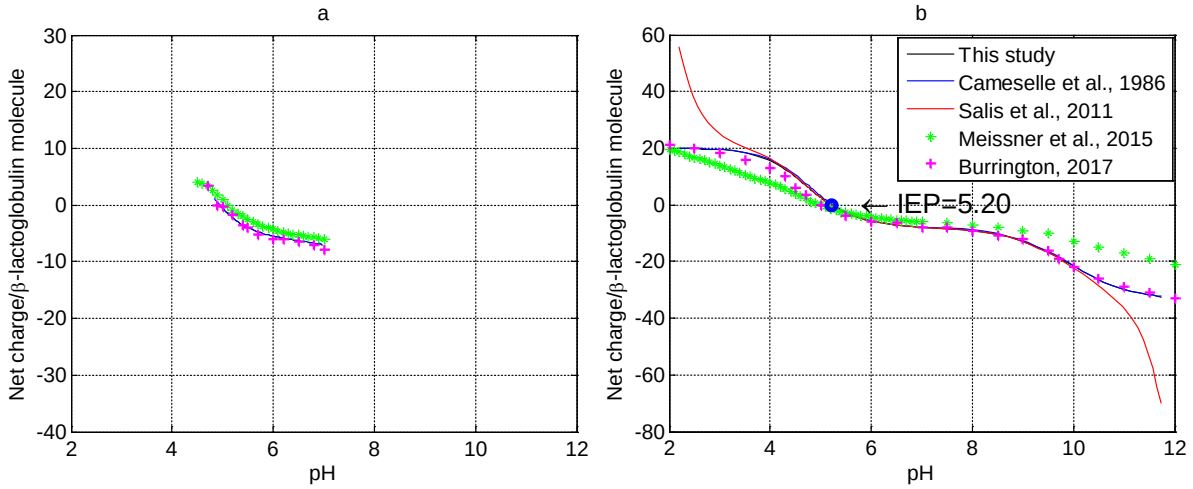

Figure 5.1 The net electric charge of β–lactoglobulin as a function of pH when a) neither NaOH nor HCl was used; b) both NaOH and HCl were used for the of β–lactoglobulin solution. IEP=5.20. The '*' symbol shows some of the simulated data from Meissner et al. (2015).

At low pH, the overall net charge of protein is positive, leading to increasing repulsive forces in the solution (Ye, 2008) and hence the prevention of interaction between proteins even if they are heated (Burrington, 2017). Figure 5.2 depicts the contribution of each residue over the whole range of pH. At low values of pH the basic amino acids, such as arginine with 3 residues per molecule, histidine to a lower extent with 2 residues and lysine to a higher degree with 15 side groups, contribute to the positive net charge.

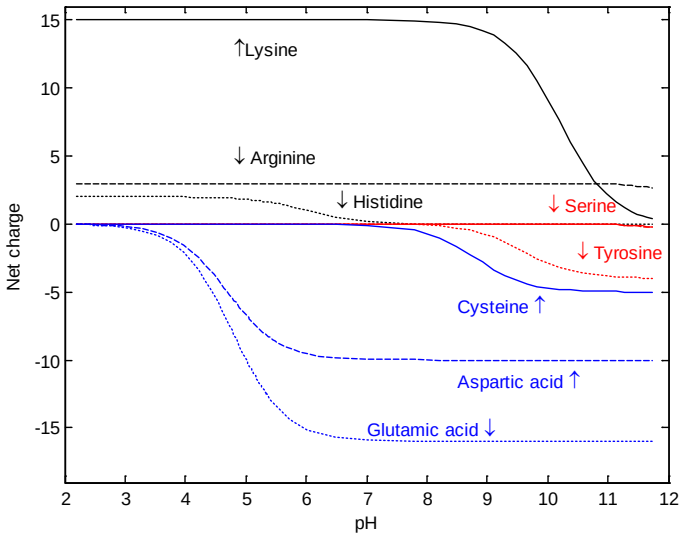

Figure 5.2 Contribution of each residue as a function of pH for a solution of β–lactoglobulin. Threonine residue is overlapped with serine.

As the pH increases, the role of basic amino acids becomes insignificant and then the net charge is affected by the acidic residues mainly through the 16 glutamic acid and 10 aspartic

acid residues. As the charges of glutamic acid and aspartic acid become negative from pH above about 4, the net charge of protein starts to drop until about pH 6, from which glutamic acid and lysine partly neutralise the charge of each other up to pH 8. Hence, less drop in net charge as seen in Figure 5.1b in this range of pH that is mainly caused by aspartic acid. The influence of cysteine residues starts to grow and lysine residues begin to drop from pH 8, leading to a large decrease in the overall net charge.

Consequently, lysine, aspartic acid, and glutamic acid are the major amino acids that control the β–lactoglobulin net charge. The net charge was also calculated using various dissociation constants given by literature as shown in Table 5.4. Dissociation constants of other residues remained unchanged from Table 5.1 for this comparison.

Table 5.4 IEPs of β–lactoglobulin solution examined with different pK_d values.

Reference	pK_d			IEP
	Asp	Glu	Lys	
(Belitz and Grosch, 1999)	3.65	4.25	10.28	4.538
(Fennema, 1996)	3.65	4.25	10.53	4.538
(Walstra and Jenness, 1984)	3.90	4.30	10.60	4.634
(Mercadé-Prieto et al., 2007)	4.0	4.0	10.95	4.467
Adjustments in this study	4.70	4.79	10.20	5.203

The IEP of solution is altered even by a slight change in dissociation constants between the amino acids and hydrogen. The pK_d values of aspartic acid and glutamic acid should be slightly increased to increase the net charge to obtain a higher IEP, i.e. low dissociation constants will produce less hydrogen and hence will give higher pH and IEP.

Aspartic acid and glutamic acid pK_d values are effective for determination of IEP because their values are near the range of IEP of β–lactoglobulin protein. However, glutamic acid contains more residues than aspartic acid and hence influences the IEP greatly with a small change of dissociation constant as shown in Figure 5.3. Lysine pK_d is only able to alter net charge over the basic ranges.

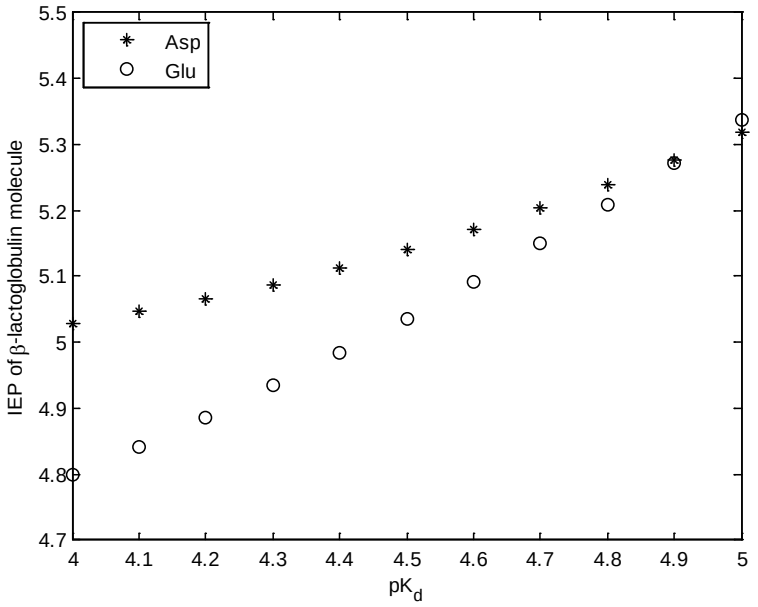

Figure 5.3 IEP change of β–lactoglobulin solution as a function of pK_d when one was kept constant and the other one was changed.

Similarly, α–lactalbumin solution was simulated as a function of pH with the residues, and side group numbers given in Table 5.2. Figure 5.4a shows the net charge per molecule of α–lactalbumin, which was also calculated by Approaches 1 and 2. An effective matching was seen between the data calculated by this study and the Approach 1 (Cameselle et al., 1986), but the Approach 2 (Salis et al., 2011) did not fit well for low and high pH values. Similar to β–lactoglobulin, glutamic acid, aspartic acid, and lysine are key amino acids to determine net charge of the solution as shown in Figure 5.4b. The effect of aspartic and glutamic acids are less in α–lactalbumin than in β–lactoglobulin, due to smaller numbers of aspartic acid and glutamic residues (8 and 9) in α–lactalbumin than those in β–lactoglobulin (10 and 16).

The IEP calculated by this study was about 4.35 which is in a good agreement with the 4.3 value given by Walstra and Jenness (1984). The IEP of α–lactalbumin is lower than that of β–lactoglobulin, reflecting that α–lactalbumin carries less positive and more negative charges than β–lactoglobulin. This leads to weaker repulsive forces in β–lactoglobulin, and hence, α–lactalbumin molecule is less likely to aggregate or precipitate at natural pH (Anandharamakrishnan et al., 2008). The calculated net charge of the protein was about –3 at pH of 6.7 which is in a reasonable agreement with the –3 IEP value presented by Al-Makhlafi et al. (1994).

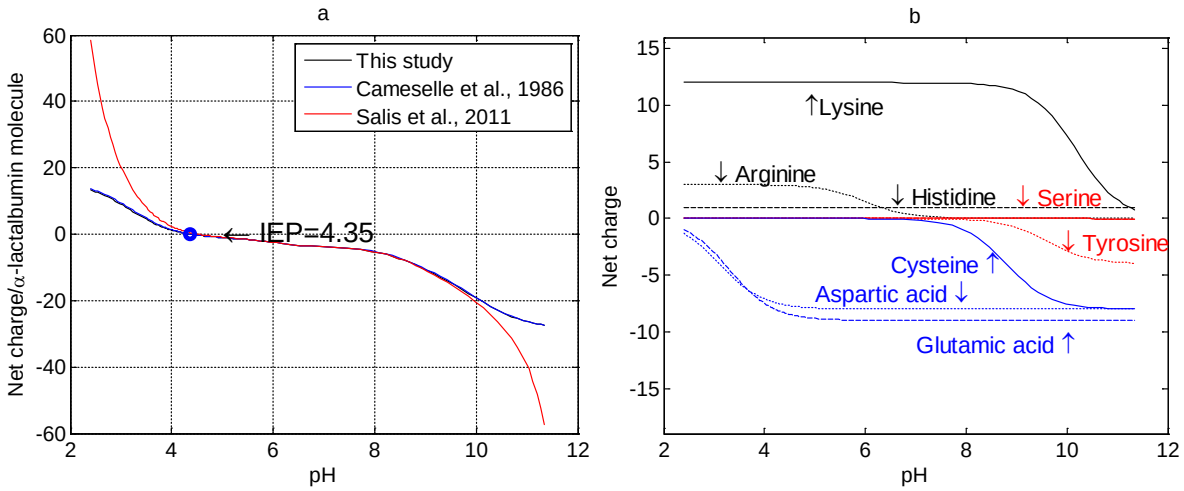

Figure 5.4 a) Net charge per molecule of α–lactalbumin calculated by the approaches 1 (Cameselle et al., 1986) and 2 (Salis et al., 2011) with IEP of about 4.35; b) Net charge contributions of amino acids as a function of pH. The black and blue solid curves overlap in Figure 5.4a.

5.3.2 Individual micellar proteins

The casein proteins were simulated individually also in the same manner as the serum proteins of milk. These are α_{s1}–, α_{s2}–, β–, and κ–casein shown in Figure 5.5 with added NaOH and HCl to simulate the acidic and basic ranges. The predicted IEPs were in good agreements with those claimed by Walstra et al. (2006) that are reported 4.5 for α_{s1}–casein, 5.0 for α_{s2}–casein, 4.8 for β–casein, and 5.6 for κ–casein. Similarly, the net charge calculation method proposed by Cameselle et al. (1986) was a good match with this study but the calculation approach claimed by Salis et al. (2011) did not fit well for pH below 4 and above 10 for α_{s1}–casein as shown in Figure 5.5a. The net charge was also calculated by the Approaches 1 and 2 for other casein proteins giving similar results as for α_{s1}–casein but these are not included in this document.

α_{s1}–casein variant B 8P (i.e., with 8 phosphorylated serine residues, SerP) is the more predominant isoform with relatively high negative charges over the natural pH range (Spuergin et al., 1996), than the less common isoform with 9 phosphate groups. The high negative charge at high pH and low charge at low pH are due to large quantities of glutamic acid and lysine residues as shown in Figure 5.5b. α_{s1}–casein has a lower charge than α_{s2}–casein because α_{s1}–casein contains 5 threonine residues and no cysteine while α_{s2}–casein has 15 threonine residues, although the numbers of aspartic acid residues in α_{s1}–casein is higher than that of α_{s2}–casein.

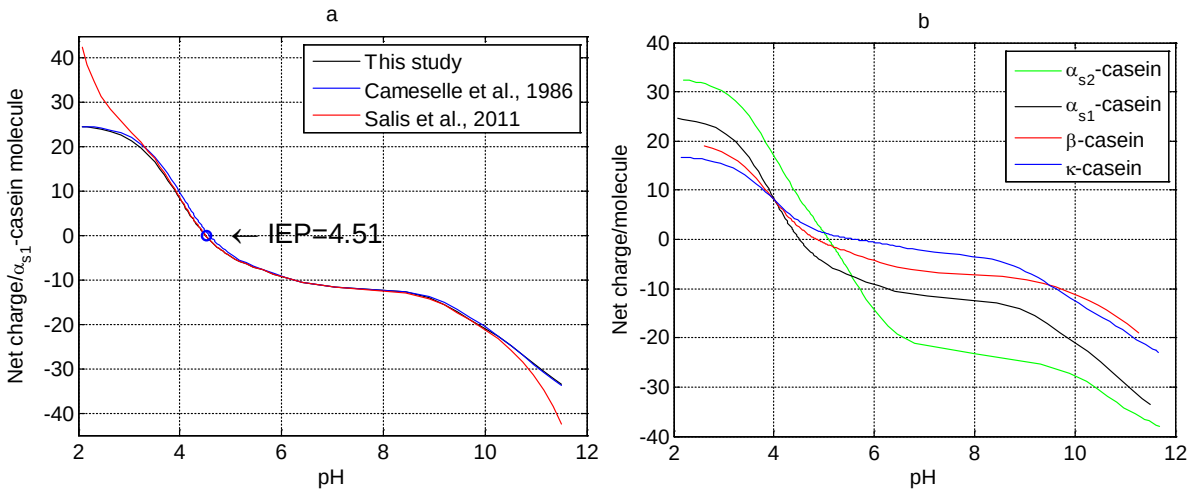

Figure 5.5 Net charge distribution of a) α_{s1}–casein, b) α_{s1}–, α_{s2}–, β–, and κ–casein per molecule as a function of pH. $IEP_{\alpha_{s1}-casein}$=4.51, $IEP_{\alpha_{s2}-casein}$=5.09, $IEP_{\beta-casein}$=4.85, $IEP_{\kappa-casein}$=5.62.

α_{s2}–casein is known to have 10 to 14 phosphorylated amino acids but the form with 11 phosphorylated amino acids is the most common (Fang et al., 2017). Six of these are considered as the strong binding sites with a large and positive net charge due to 24 moles of lysine per molecule of protein. The overall net charge at the neutral pH of milk was estimated to be about –21 by Farrell et al. (2004) caused mainly by the 2 strong anionic clusters of phosphoserine residues that corresponds well to the same value at pH 6.7 in Figure 5.5b. α_{s2}–casein has the highest positive and negative charges over the pH because of large numbers of glutamic acid and lysine residues.

β–casein has five phosphoserine residues (3 strong and 2 weak bonds) that occur more near the N–terminus head. These mostly determine the net charge of molecule which was calculated to be about –11 at milk pH by Farrell et al. (2004). That is more negative than that calculated in this study. The remaining 80% carries no charge and is quite hydrophobic (Cosman et al., 2005). κ–casein has no strong phosphorylated serine residues in its structure with a net charge of about –3.0 which is close to –3.6 as given by Bijl et al. (2018) at the natural pH of milk.

Marchessau et al. (1997) measured higher IEPs for casein proteins and reported then as 5.1 for α_{s1}–casein, 5.3 for β–casein, and 5.4 for κ–casein. These are contradictory with those calculated in this study, although the values can be achieved by slightly altering dissociation constants between amino acids and hydrogen leading to a change in pH and hence net charge per each protein molecule.

Apart from pH, the protein net charge is dependent on the ionic strength of the solution (Kuehner et al., 1999), which is 0.08 M in this simulation; however, less data are available in literature to examine the net charge of protein solution at different ionic strengths. According to Kuehner et al. (1999), net charges increase for higher ionic strengths at low pH.

Kuehner et al. (1999) simulated the net charge of hen–egg–white lysozyme over a range of pH values, for which the residues at the N– and C–terminuses were incorporated into their model. Similarly, arginine and tryptophan residues were assumed to attach to hydrogen and hydroxide ions at the head and tail of α_{s1}–casein, the pK_d values of which were 9.04 for arginine and 2.38 for tryptophan (Fennema, 1996).

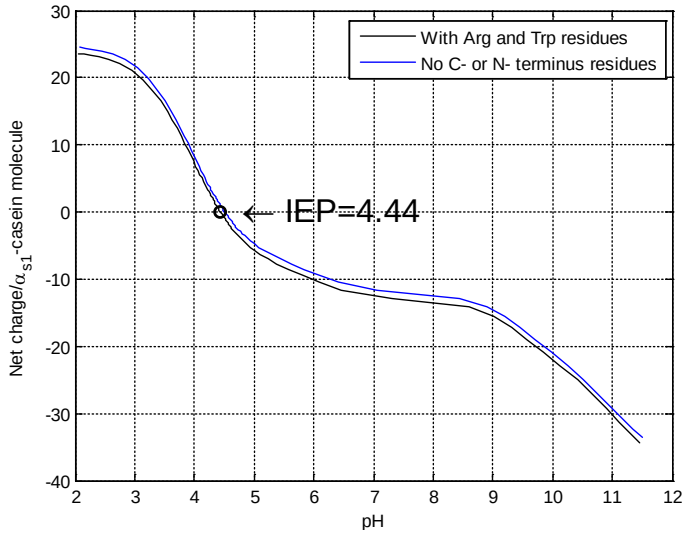

Figure 5.6 Net charge distribution of α_{s1}–casein with arginine and tryptophan residues at the N– and C– terminuses of the molecule.

Figure 5.6 indicates the net charge of α_{s1}–casein protein, for which 1 residue of each C– and N– terminuses amino acids were used. This gives more negative net charge compared with the simulation without C– or N– terminuses, and hence lowered the IEP of the protein. Despite of potential accuracy of the calculations, the lower IEP would match with the IEP reported by literature with a slight difference. It is likely that greater accuracy could be obtained using more advanced methods such as the method by Li et al. (2005).

5.3.3 Milk solutions

In this section, milk proteins such as β–lactoglobulin, α–lactalbumin, blood serum albumin, α_{s1}–casein, α_{s2}–casein, β–casein, and κ–casein were included in the mathematical model with

their amino acid side groups. Concentration of each amino acid was assumed as the sum of each amino acid concentration in each protein. Additionally, milk salts were included in the mathematical model with total concentrations similar to milk i.e., citrate (9.5 mM), phosphate (20.6 mM), carbonate (0.4 mM), sulphate (1.2 mM), chloride (30.4 mM), phosphate esters (2.6 mM), and carboxylate (2.58 mM) as potential anions, and calcium (29 mM), magnesium (4.9 mM), sodium (22 mM), and potassium (38.3) as potential cations. 0.147 mol L^{-1} lactose (equivalent to 4.5%w/w) was included in the model. Intrinsic association constants between amino acids, anions, and cations were used from the previous sections and were remained unchanged. The calculation was implemented by the addition of HCl and NaOH enabling to cover almost all ranges of pH. Results of net protein charge are shown in Figure 5.7 with only proteins, and with proteins, salts, and 0.147 mol L^{-1} lactose.

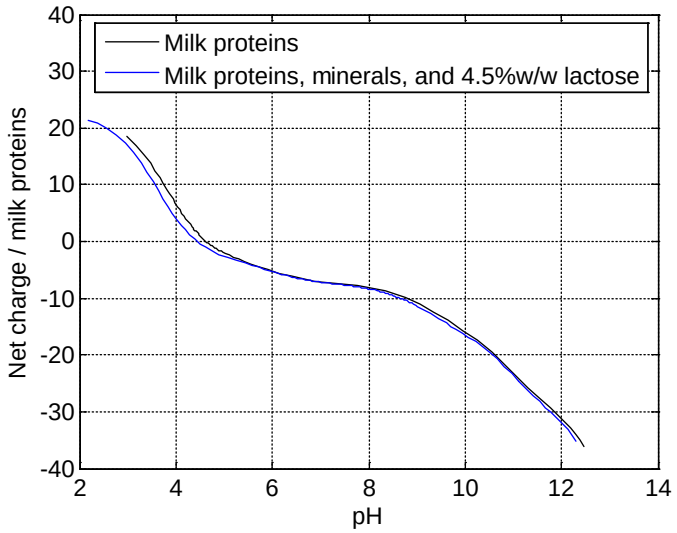

Figure 5.7 Net charge distribution as a function of pH for the solution containing only milk proteins in terms of dissociable amino acid side groups with IEP=4.63, and the solution containing both milk proteins, salts, and 0.147 mol L^{-1} lactose with IEP=4.49.

The predicted net charge distribution for both solutions shows similar trends, however, a slight deviation was seen for low pH values indicating higher net charge for the solution containing only milk proteins than that of the solution with both proteins, minerals, and lactose. This is possibly because the small associations between calcium, magnesium, potassium, and amino acids were not included in the solution containing only proteins. Hence, the simulations did not result in the same IEP value for both solutions.

At lower pH approaching the IEP, the charge reduces to zero and hence casein micelles aggregate and precipitate (Broyard and Gaucheron, 2015). The casein micelles are negatively

charged at natural pH and quite stable (Southward, 1998). It is not common to perform milk alkalinisation in dairy industry, but it has been studied to predict and understand salt partitioning of casein micelles at high pH values. The net charge of casein micelles becomes more negative leading to decrease opaqueness and whiteness of milk especially at pH higher than 9 (Broyard and Gaucheron, 2015). It seemed necessary to theoretically predict ion speciation over the pH range for the milk solution.

Figure 5.8 shows the simulated prediction of the main component speciation over the pH range for the milk solution with dissociable amino acid side groups of casein and serum proteins. Negative–charged glutamic acid has a higher contribution than other residues with about 28 mM concentration at pH higher than 4, followed by aspartic acid with about 8 mM that are shown in Figure 5.8a. Glutamic and aspartic acids followed by the cysteine and serine residues mainly determine the net charge at high pH values as shown by Figure 5.8b. But, hydrogen lysine ($LysH^+$), hydrogen histidine ($HisH^+$), and hydrogen arginine ($ArgH^+$), which are all positive charged species determine the net charge for pH lower than 4 as shown in Figure 5.8c. The other amino acid side groups are neutral at low pH and do not contribute to the net charge. The ion–pairs formed by the amino acids and other cations are likely to be at low concentrations, so the net charge are unlikely be affected by them. This assumption was ignored in the study by Bijl et al. (2018).

H_2Cit^- was the most abundant citrate species across the pH range 2–4, after which $CaCit^-$ became the most plentiful because of large association between free calcium and citrate ions that was shown in Figure 5.8d. The Cit^{3-} concentration started to increase when hydrogen citrate deprotonated and release one hydrogen and citrate ion above pH about 6. Figure 5.8e depicts the calcium relative concentrations, among which free calcium remained at the level of about 75% until pH 8.5, after which it started to drop, coinciding with $CaPO_4^-$ formation as the most plentiful species at pH about 9 because of high affinity between free calcium and phosphate ions.

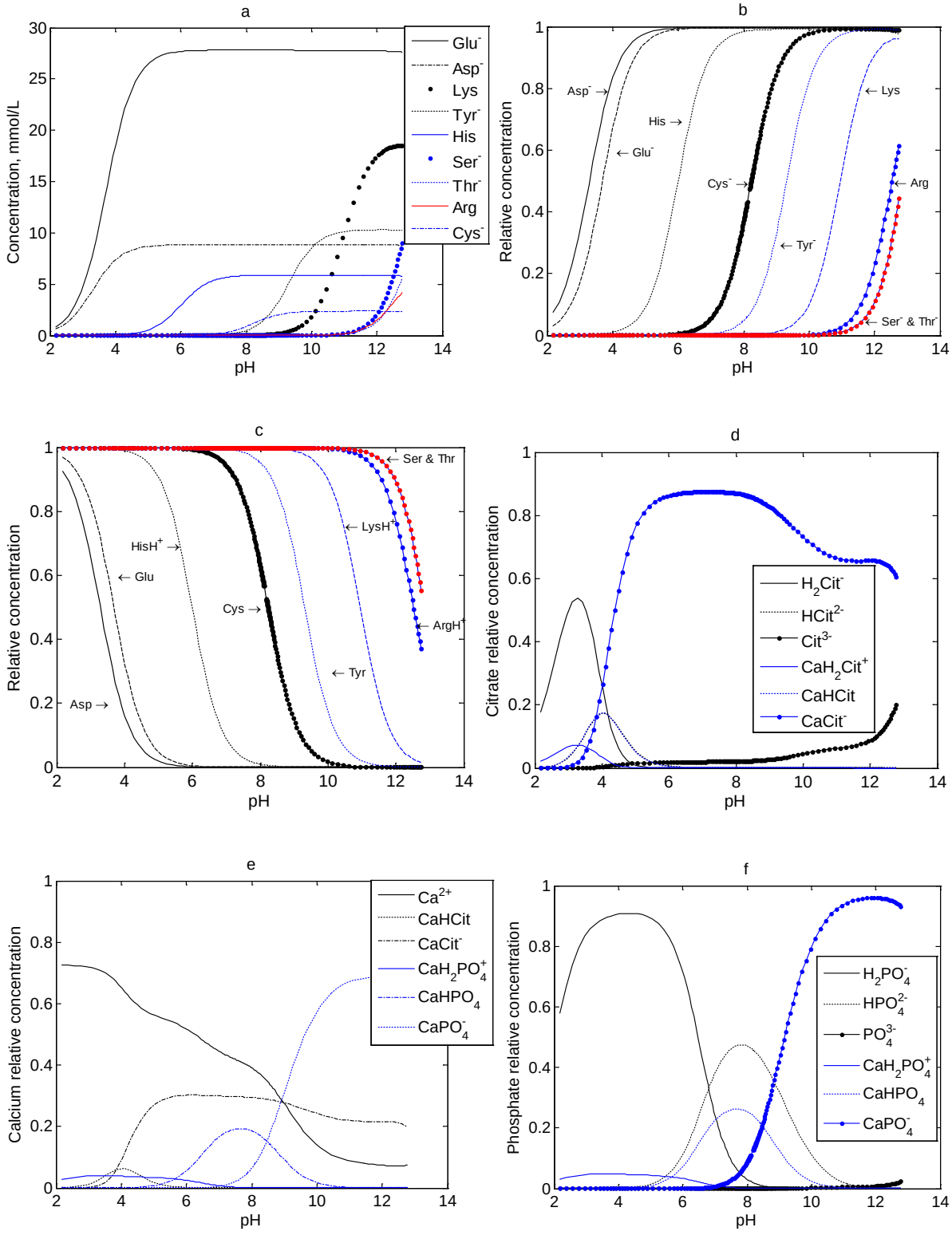

Figure 5.8 a) Simulated concentration and b) relative concentration of dissociable amino acids side groups as anion; c) as ion–pairs. Simulated distribution of d) citrate; e) calcium; and f) phosphate; species as a function of pH in a milk solution containing 29 mM calcium, 4.9 mM magnesium, 22 mM sodium, 38.3 mM potassium, 20.6 mM phosphate, 9.5 mM citrate, 4 mM carbonate, 1.2 mM sulphate, 30.4 mM chloride, 2.6 mM phosphate esters, and 2.58 mM carboxylate.

Similarly, dihydrogen phosphate is at the highest level at low pH value among the other phosphates, following by the hydrogen phosphate at pH between 6 to 8 that was shown in Figure 5.8f. $CaH_2PO_4^+$ had the lowest content due to its low intrinsic association constant between free calcium and dihydrogen phosphate.

5.3.4 Calcium phosphate nanoclusters in the milk simulation

The interaction between the caseins and amorphous calcium phosphate mainly occurs through a few phosphorylated residues known as 'phosphate centres'. The sequestration of amorphous calcium phosphate forms CPN with the phosphate centres (Holt et al., 1986; Follows et al., 2011). In other words, the phosphate centres are a group of at least two phosphorylated amino acids, especially phosphoserine (SerP) that act together as the core of a calcium phosphate nanocluster (Holt, 2004). A bovine casein micelle has about 800 calcium phosphate nanoclusters, each of which has a 60 kDa molecular weight and a radius of 2.4 nm (Bijl et al., 2018).

Holt (2011) determined that the structure of CPN is:

$$[\mathrm{Ca}_{13.2}(\mathrm{HPO}_4)_{6.5}\mathrm{Mg}_{1.0}\mathrm{Cit}_{1.3}\mathrm{Casein}_{1.0}(\mathrm{SerP})_4]_{49} \quad (5.9)$$

but this seems to require 49 casein molecules to be involved, each with 4 SerP. Bijl et al. (2018) seemed to have refined this to $(SerP)_4$ and $(SerP)_3$. They proposed that at least one strong divalent cation should present in the sequestering caseins. Given that $(SerP)_3$ was considered in each casein protein for the milk simulation, $Casein_{1.0}$ can be ignored. Therefore, another representation could be:

$$\left[\mathrm{Ca}_{13.2}(\mathrm{HPO}_4)_{6.5}\mathrm{Mg}_{1.0}\mathrm{Cit}_{1.3}(\mathrm{SerP})_{\mathrm{group}}\right]_{49} \quad (5.10)$$

Here $SerP_{group}$ means a group of three phosphorylated serines. For the model, there is no need to consider 49 repeats. Hence the *IAP* might be:

$$IAP = [\mathrm{Ca}^{2+}]^{13.2}[\mathrm{HPO}_4^{2-}]^{6.5}[\mathrm{Mg}^{2+}][\mathrm{Cit}^{3-}]^{1.3}[\mathrm{SerP}_3] \quad (5.11)$$

Without evidence, an arbitrary choice will be made to use the ions as shown and to obtain a K_a value that gives a suitable equilibrium with milk. Table 5.5 shows the estimation of CPN concentration in casein which was assumed to have a concentration of 0.026 kg kg_{milk}^{-1}. 0.9

was chosen for the fraction of SerP groups occupied at natural pH. By choosing a value less than 1.0 to determine the K_a, it is then possible for other conditions to increase the fraction.

Having these in mind, the K_a value for CPN could be guessed according to *IAP* and total of Ca in CPN. A reasonable value was found and adjusted to be 9.2×10^{-62} $\mu mol^{22}\ L^{-22}$. That gave a total concentration of Ca as CPN in the casein micelles of 18 mM which corresponds to the value of 18.8 mM given by Holt (2004).

Table 5.5 CPN estimation in each casein proteins (Walstra and Jenness, 1984; Bijl et al., 2018).

Casein proteins	Mole fraction	Concentration, mM	$(SerP)_3$ per molecule	Maximum CPN, mM	Ca in CPN, mM
α_{s1}–casein	0.37	0.43	2	0.86	10.23
α_{s2}–casein	0.103	0.12	2	0.24	2.85
β–casein	0.372	0.41	1	0.41	4.93
κ–casein	0.156	0.22	0	0.00	0.00
Total	1.00		–	1.52	18.00

5.3.4.1 Simulation of milk at equilibrium

The proposed model in Chapter 3 was applied to this system by considering all of the principal cations and anions in milk including calcium, magnesium, sodium, potassium, hydrogen, citrate, phosphate, carbonate, sulphate, phosphate esters, carboxylate, chloride as well as $(SerP)_3$ and phosphoserine (SerP). Bijl et al. (2018) determined an affinity between different types of $(SerP)_3$ and phosphoserine (SerP) as anions and cations with their association constants according to Table 5.6. The dissociable side groups of amino acids were incorporated into the simulation for the calculation of ion equilibria in milk including Arg, Asp, Cys, Glu, His, Lys, Ser, Thr, and Tyr in both casein and whey proteins. The saturations of potential calcium salts were calculated from their solubility products. 0.147 mol L^{-1} lactose (equivalent to 4.5%w/w) was included in the model as a non–electrolyte. The MATLAB scripts for the milk simulation is given in Appendix 8.

Table 5.6 Association constants between the $(SerP)_3$, SerP, and principal cations in milk (Bijl et al., 2018).

	Ca^{2+}		Mg^{2+}		Na^{+}		K^{+}		H^{+}	
	Ion–pair	K_a, mol^{-1} L	Ion–pair	K_a, mol^{-1} L	Ion–pair	K_a, mol^{-1} L	Ion–pair	K_a, mol^{-1} L	Ion–pair	K_a, mol^{-1} L
$((SerP)_3H_2)^{-4}$	$((SerP)_3H_2Ca)^{-2}$	380	$((SerP)_3H_2Mg)^{-2}$	100	$((SerP)_3H_2Na)^{-3}$	1	$((SerP)_3H_2K)^{-3}$	1	$((SerP)_3H_3)^{-3}$	7.94×10^{5}
$((SerP)_3H)^{-5}$	$((SerP)_3CaH)^{-3a}$	380	$((SerP)_3HMg)^{-3}$	100	$((SerP)_3HNa)^{-4}$	1	$((SerP)_3HK)^{-4}$	1	$((SerP)_3H_2)^{-4a}$	7.94×10^{5}
$((SerP)_3)^{-6}$	$((SerP)_3Ca)^{-4a}$	3000	$((SerP)_3Mg)^{-4}$	3000	$((SerP)_3Na)^{-5}$	1	$((SerP)_3K)^{-5}$	1	$((SerP)_3H)^{-5a}$	1.0×10^{7}
$((SerP)_3Ca_2)^{-2b}$	$((SerP)_3Ca_3)$	380	$((SerP)_3Ca_2Mg)$	100	$((SerP)_3Ca_2Na)^{-1}$	1	$((SerP)_3Ca_2K)^{-1}$	1	$((SerP)_3Ca_2H)^{-1a,b}$	7.85×10^{5}
$((SerP)_3CaH)^{-3b}$	$((SerP)_3Ca_2H)^{-1}$	380	$((SerP)_3CaHMg)^{-1}$	100	$((SerP)_3CaHNa)^{-2}$	1	$((SerP)_3CaHK)^{-2}$	1	$((SerP)_3H_2Ca)^{-2a,b}$	7.94×10^{5}
$((SerP)_3Ca)^{-4b}$	$((SerP)_3Ca_2)^{-2a}$	380	$((SerP)_3CaMg)^{-2}$	100	$((SerP)_3CaNa)^{-3}$	1	$((SerP)_3CaK)^{-3}$	1	$((SerP)_3CaH)^{-3a,b}$	7.94×10^{5}
$PSerH^{-}$	$PSerHCa^{+}$	10	$PSerHCa^{+}$	10	PSerHNa	1	PSerHK	1	$PSerH_2$	200
$PSer^{2-}$	PSerCa	10	PSerCa	10	$PSerNa^{-}$	1	$PSerK^{-}$	1	$PSerH^{-a}$	7.94×10^{5}

[a] Duplicate components. [b] Duplicate equilibria with H^{+}.

The association constants between magnesium, sodium, and potassium with hydrogen were estimated to be small, because of the low affinity between them.

It was also assumed that the activity coefficient of CPN and $(SerP)_3$ are independent of the conditions, so unity was used arbitrarily for both components. 1.52 and 0.1 mM were the initial values for $(SerP)_3$ and SerP concentrations corresponding to the total Ser in milk. The CPN charge was calculated from the Equation (5.11) to be –1 if there are no other amino acids involved. When there is one positive charge from another amino acid, the CPN will be neutral, but there is no need in the model for neutrality. The charge of CPN was set to –1 in the simulation.

Similar to previous simulations, the calculations were performed both at equilibrium and dynamically. No adjustments were made to the association constants of species. Duplicate components were dropped from the set of ions as shown in Table 5.6. Three duplicate equilibria were removed due to being equivalent to the product of two other equilibria. For example, Equation (5.12) gives similar products as the Equation (5.13), so only Equation (5.12) was incorporated into the model and Equation (5.13) was removed from the set of equations.

$$(\mathrm{SerP})_3\mathrm{Ca}_2\mathrm{H} \leftrightarrow \mathrm{Ca}^{2+} + (\mathrm{SerP})_3\mathrm{CaH} \tag{5.12}$$

$$(\mathrm{SerP})_3\mathrm{Ca}_2\mathrm{H} \leftrightarrow \mathrm{H}^{+} + (\mathrm{SerP})_3\mathrm{Ca}_2 \tag{5.13}$$

Figure 5.9a shows the concentration of CPN and the total of $(SerP)_3$ over the pH range for the milk solution at equilibrium. The CPN concentration starts to increase from pH about 4.3, reaching to 1.5 mM at pH between 6 and 9, then it drops to zero at pH 11. For pH values between 4 to 9, where the CPN has its highest value, $(SerP)_3$ reaches to almost zero, implying that CPN is produced by using up $(SerP)_3$ components.

The saturations of potential milk salts are shown in Figure 5.9b, in which DCPD is the most insoluble calcium phosphate salt formed in milk, following by the DCPA and OCP to a lower extent at pH about 6.7. But this does not necessarily mean that DCPD is the dominant calcium phosphate over the entire pH range. For example, the CDA and OCP seem to be the main calcium phosphate salt at high pH values, while TCCT is the dominant calcium citrate at low pH values. The HAP saturation remains closest to zero throughout the pH range.

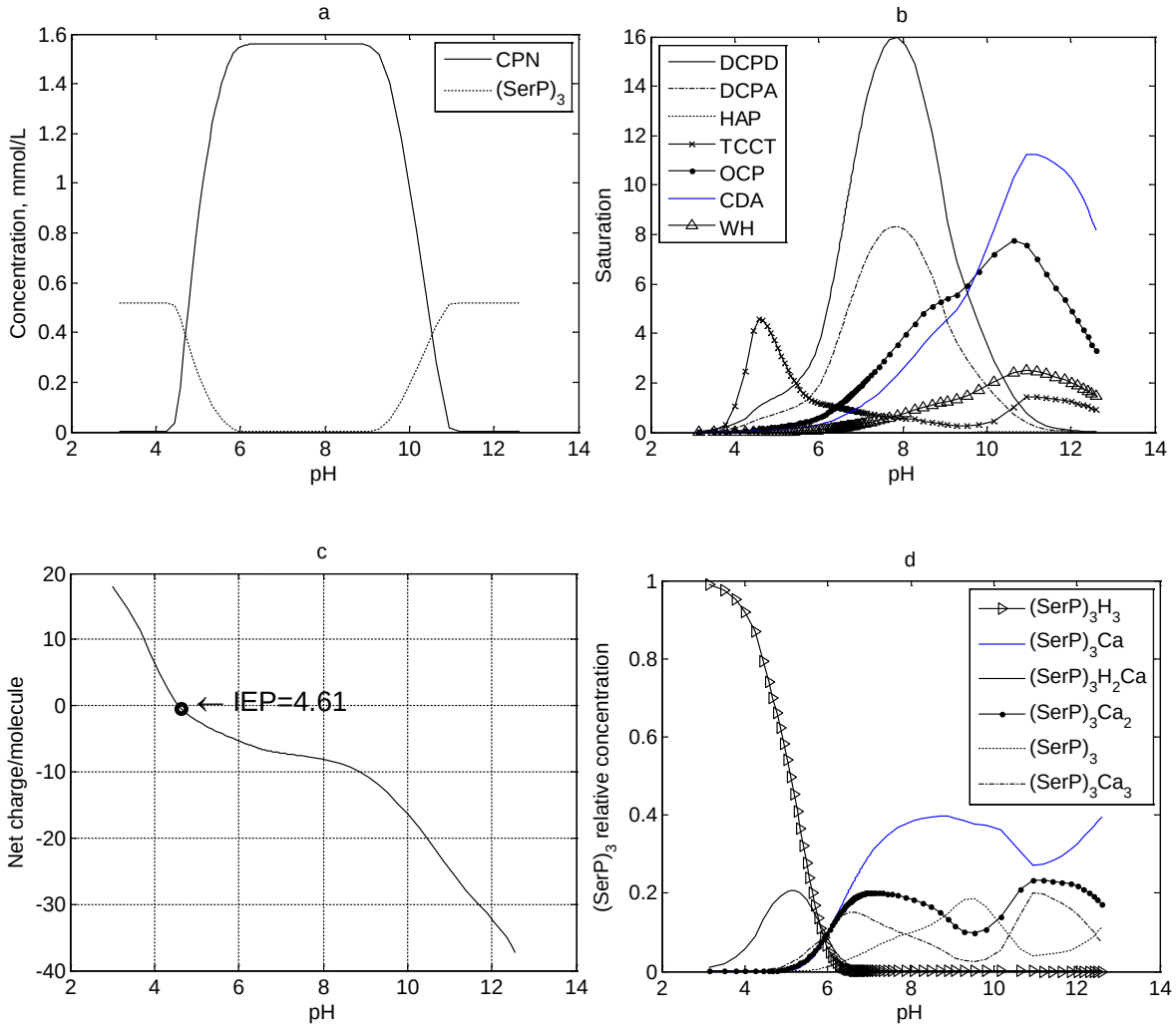

Figure 5.9 The simulated distribution of a) CPN concentration, b) saturation of potential solid phases, c) net charge, d) $(SerP)_3$ relative concentration over the pH in milk solution.

Figure 5.9c shows the trend of milk net charge over the pH estimating IEP of about 4.61 that is in a good agreement with the 4.60 value reported in Walstra et al. (2006). The precipitation of milk starts from below 5.0 because of instability of casein micelles. At pH of 6.7, about 10% of the $(SerP)_3$ is included in CPN. The relative concentration of the remaining $(SerP)_3$ species is shown in Figure 5.9d. $(SerP)_3H_3$ is the most abundant phosphoserine species up to pH 5. $(SerP)_3Ca$ becomes the most plentiful between pH 6 to 9, where CPN is formed and uses up $(SerP)_3Ca$. Therefore, $(SerP)_3Ca$ relative concentration is not very high.

Consequently, this model is capable of predicting the ion speciation, saturation, and net charge in the milk including all casein and whey proteins. The model is flexible enough to test a wide range of milk components under different concentrations, and in all cases, it could obtain feasible solution. This implies that there is no limitation for the number of components

included in the model, and thus it can simulate milk as a good and complex example constituting a large number of ions, sugar, and proteins. Hence, it seems very likely that other dairy liquids can be simulated accordingly.

5.3.4.2 Simulation of concentrated milk

Milk was concentrated up to 4 times by using the proposed model applied to all initial concentrations of milk components including proteins. Therefore, a concentration ratio was defined for concentrating from the range 1 to 4, at which no precipitation is yet expected to be seen in milk. Figure 5.10a and b show the pH changes and saturations of DCPD, DCPA, and OCP as the potential dominant calcium salts.

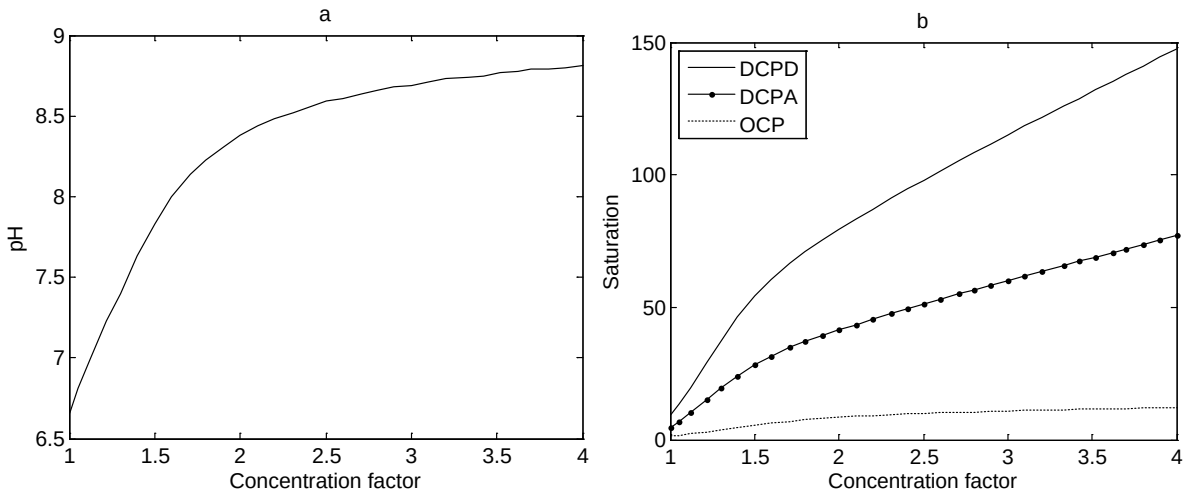

Figure 5.10 a) Simulated pH, and b) DCPD, DCPA, and OCP saturations when milk concentrated up to 4 times of its normal concentration.

The natural pH of milk solutions starts to increase significantly from 6.67 to about 8.4 as milk gets concentrated up to twice of its normal concentration. This is because, milk is getting more supersaturated with respect to the calcium phosphate leading to producing less hydrogen ions and increasing pH values. The trend becomes slow due to the releasing less hydrogen ions as the concentration factors increases compared to the less concentrated milk. Figure 5.10b confirms that DCPD is the main potential calcium salt with a relatively high saturation, following by the DCPA, and OCP to a lesser extent. Other potential solid phases were not included in the graphs as they remain at low saturation. The IEP point of each individual concentrated solution was estimated to be between 4.6 to 4.7 as long as there can be a positive net charge calculated. However, for concentrated solutions with concentration factor higher

than 2.5, no IEP could be calculated because the proteins have a negative charge throughout the pH range which is unexpected.

5.3.4.2 Dynamic simulation of milk

The dynamic simulation of milk was also carried out with a solution at normal concentration containing calcium (30 mM), magnesium (4.9 mM), sodium (22 mM), and potassium (38.7 mM) as cations, citrate (9 mM), phosphate (20.04 mM), carbonate (0.4 mM), sulphate (1.205 mM), chloride (30.4 mM), RCOO (3 mM), and phosphate esters (2.5 mM) as anions as well as $(SerP)_3$, phosphoserine, and amino acids of both serum and casein proteins. Similarly, CPN and lactose with 0.147 mol L^{-1} were included in the model. The precipitation and dissolution of potential solid phases were calculated using rate constants given in Appendix 6. The CPN association constant was adjusted to 7.0×10^{-50} μmol^{22} L^{-22} to get reasonable decreasing trend for pH.

Figure 5.11 indicates the dynamic simulated responses for the milk solution containing almost all components. The initial pH was predicted to be 6.67, which is very close to the natural pH. However, it is predicted to decrease to a pH value of about 6 after 1000 minutes. The initial CPN concentrations is predicted 1.55 mM, which is in the reasonable range, but it reaches to zero after about 750 minutes (Figure 5.11b). Here, t_0 represents the time when all the milk components was brought together in the simulation.

The saturations of potential solid phases of milk solution are shown in Figure 5.11c. As expected, DCPD following by OCP and DCPA are the dominant calcium salts that are formed in the solution as shown in Figure 5.11d. However, DCPA kinetics are predicted to be faster than OCP remaining longer in the solution and dissolves after 800 minutes. The DCPD concentration is predicted to remain about 3 mM roughly which is in a good agreement with the corresponding DCPD in milk serum that was already described in Chapter 3.

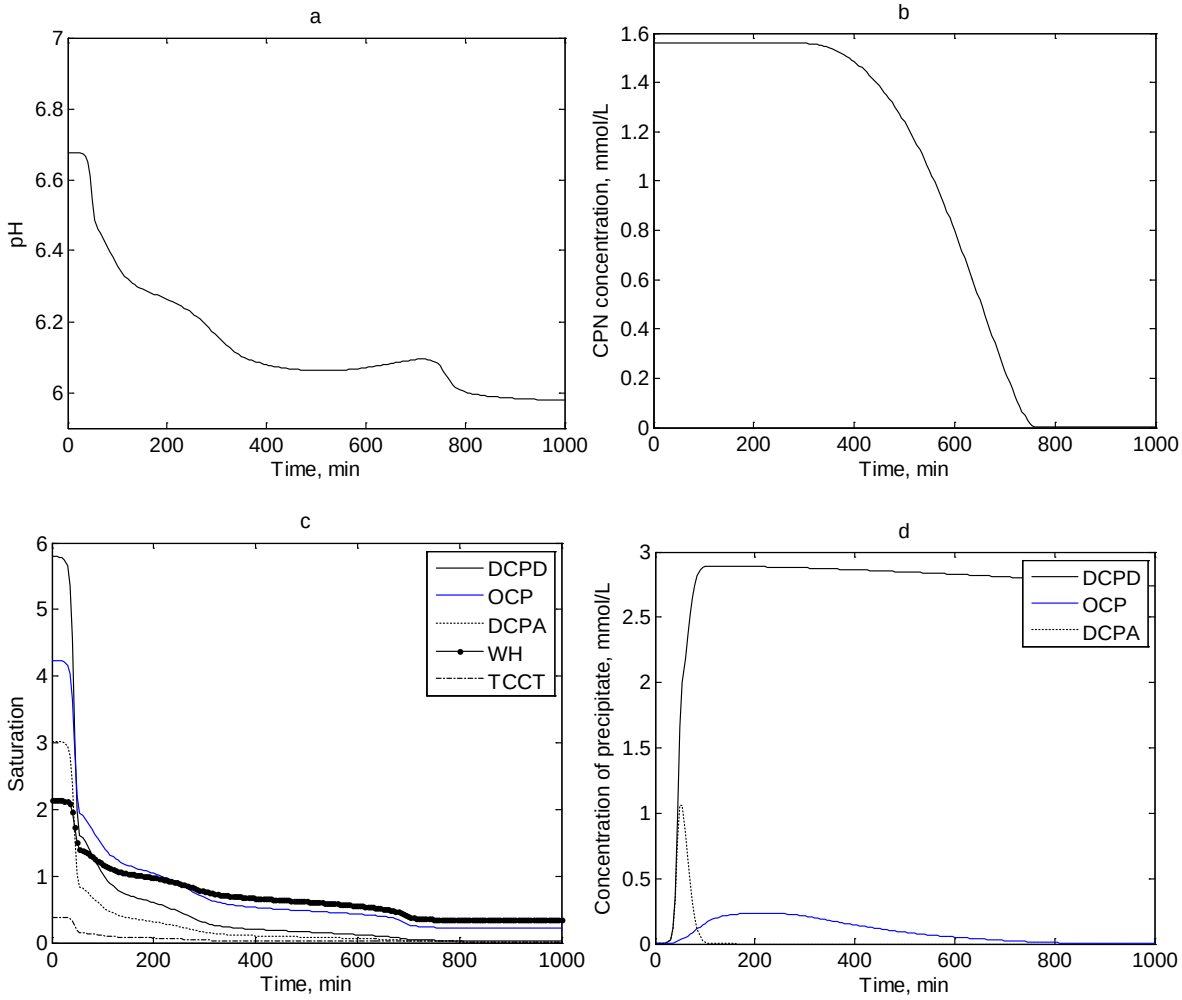

Figure 5.11 The simulated a) pH, b) CPN concentration, c) saturations of potential solid phases, and d) DCPD, OCP, and DCPA concentrations over time for milk solution with an adjustment of CPN K_a value from 9.0×10^{-62} to 7.0×10^{-50} μmol^{22} L^{-22}.

Nonetheless, no precipitation should be observed in skim milk despite the prediction of calcium phosphate precipitation over time. It is known that both milk serum and milk itself are supersaturated with respect to calcium phosphate salts (Lenton et al., 2015). If milk was not supersaturated, the saturations of calcium solid phases should have been calculated less than unity to represent lack of precipitation. Thus, the solution is in a metastable state or there are other components not included in the model, which lower the *IAP*s of possible precipitates. Hence, despite of robustness of model, it is not yet able to show all the mechanisms of stabilisation in milk.

5.4 Conclusions

The proposed model gave satisfactory results for different milk solutions by assuming dissociable side groups of amino acids either individually or in the mixed state. The net charge

of each protein was calculated as a means of validation due to lack of complex experimental data in literature. The IEP of each protein was used as another method of validation. Lysine, glutamic acid, and aspartic acid had the greatest contributions to charge among the amino acids in the simulated solutions.

For the milk solution containing all ions, proteins, and CPN, the model could predict the ions speciation, saturations, and potential solid phase concentrations. CPN concentrations were predicted within a reasonable range. However, more investigations seem required for considering a metastable phase to be able to show supersaturation of milk–like solutions in respect to calcium solid phases.

6 Overall Discussion

As mentioned in the previous chapters, several investigations have been extensively done on the ion equilibria of milk and milk–like solutions at different conditions. However, a comprehensive model seemed essential that could incorporate all the components of milk with their ions activities, activity coefficients, and solubilities of potential solid salts for a broad range of concentrations. The results of the proposed model in Chapter 3 show the effectiveness of the different aspects of a robust method for the salt partitioning prediction in various systems.

The first step of doing the research was to find an effective activity coefficient model enabling the distinction of electrolytes and non–electrolytes activity coefficients with sufficient complexity as well as the capability of activity coefficient calculation for high concentration systems. There are a vast number of models available in literature that can be used for activity coefficient prediction based on either the ion–pair or free–ion approach including ePC–SAFT (Held et al., 2014), which was applied to biochemical systems, but testing multiple models may have led to getting far from the scope of thesis. Although the ePC–SAFT model is quite strong for this purpose, it has its own drawbacks. For example, the model requires numerical determination of some parameters such as k_{ij} which is unlikely available for all ions in a complex solution like milk with about 180 free ions and ion–pairs. Hence, Debye–Hückel and Davies are the main models discussed in this thesis, which are most used models in literature for prediction of activity coefficient. Meanwhile, a model was required to be complex enough to be able to predict activity coefficient of ions in milk by incorporating the role of non–electrolytes with zero charge number. On the other hand, a suitable model required the most of its numerical parameters could be found in literature.

The non–primitive mean spherical approximation (NPMSA) theory, which was proposed by Blum and Wei (1987), was seen to offer rigorousness that is able to calculate activity coefficient species for solutions with the ionic strengths larger than 0.3 M (van Boekel, 1996). Unfortunately, it was very difficult to implement due to undefined units and several typographical errors (Section 2.2.6.2). Even with the best guess of a consistent set of equations, the resulting set of equations was ill–conditioned and they did not yield reliable values of activity coefficients.

Having this in mind, the MSA theory was used for the activity coefficient calculation of free–ions and ion–pairs in different systems. The hard sphere contribution allows the activity coefficient of individual electrolytes and non–electrolytes, such as lactose, to be determined by incorporating a size variable into the formula. Davies and other activity coefficient models are unable to calculate activity coefficient of non–electrolytes, and the electrolytes for concentrated solutions. The MSA formula for activity coefficient calculation requires the dielectric constant of the solution and the prediction was improved by using a concentration dependent value, and not the value for water (Valisko and Boda, 2015). It would be possible to further improve the calculation of the dielectric constant used in the simulation by obtaining more correlations for a range of electrolytes. Hence, the MSA theory stood up well by applying it to various milk solutions, and it seems suitable for any liquid dairy system.

Another feature of this work was the use of Newton's method as an appropriate mathematical approach used for conducting the ion equilibria in milk solutions. All of the past studies found seem to have used purpose-written iterative schemes. The mathematical calculation was not specified in the model developed by Holt et al. (1981), while Mekmene, Le Graet, et al. (2009) used a series of iterative loops as the computational method for calculation of ion equilibria in milk. Gao, van Halsema, et al. (2010) specified the 'AESolve' software package as the computational method used to calculate ion equilibria in SMUF.

Newton's method was effective and enabled extensions of the model to be made with ease. Solutions were obtained within about 30 seconds. It seemed to work well for a broad range of initial concentrations. Two key factors led to the success of this method. Firstly, equations and variables were scaled so that terms in the equations and the variables were closer to one and hence the Jacobian matrix was less likely to be singular. Hence the unit of concentration was set to μmol L^{-1}. The scaling of the equations was manual, but opportunities exit to find better systematic scaling procedures. Secondly, values at each iteration of Newton's method were bounded with upper and lower values. Attempted violation of the bounds were reported, enabling convergence problems to be identified easily. Normally the initial guesses of the system components were set to the maximum possible value based on the specified composition, though, in some cases, attempted violation of the bounds indicated the variables for which better initial guesses were required. To avoid divergence during the first few steps, a fractional step (relaxation) was used for a few initial steps.

The dynamic calculation of ion equilibria in milk solutions has not been studied so far, thus few experimental data were found for validation with the simulated results given by the proposed method in Chapter 3. To validate the method, the simulated data given by Kazadi Mbamba (2016) of calcium carbonate precipitation were used. Arifuzzaman and Rohani (2004) and Mekmene, Quillard, et al. (2009) investigated experimentally the dynamics of calcium phosphate solutions that were used as a means of validation for the simulation given in this study.

The proposed model in Chapter 3 was applied to several systems including the binary solutions of calcium chloride and sodium chloride, the buffer solutions of citrate and phosphate, solid phase systems such as calcium phosphate and calcium citrate, milk serum, milk with proteins, and CPN. They all gave reasonable and satisfactory results that were matched to the available experimental and simulated data in literature implying the success of the model. Hence, it is expected that this model can be applied to other liquid dairy solutions with a variety of components for any concentration.

Due to lack of sufficient data for the dynamics of calcium phosphate solution, precipitation of calcium phosphate was studied experimentally in Chapter 4. However, the simulation of the results was not possible, as the structure of precipitate was not known. The prediction of nanoparticles formed in the presence of lactose seems significant because it allows the understanding of solubility and kinetics of calcium phosphate solution. This area of research is quite fascinating and needs further investigations.

In Chapter 5, the model was extended to whey and casein proteins, for which the protein net charge was calculated and compared with the corresponding data in literature. Mekmene et al. (2010) specified the pH of milk for simulation and adjusted the concentration of a counter–ion (typically Cl^-) to achieve electroneutrality In the current study, the pH was one of the variables determined from the composition of the mixture.

The proposed model was successfully extended to include components of the casein micelles such as the addition of CPN, for which free calcium, free magnesium, hydrogen phosphate, aqueous citrate, and a group of three phosphoserine residues were incorporated into the ion association equation. The roles of casein carboxyl groups and citrate were ignored in the CPN ion activity product by Gao (2010). The casein carboxyl groups were automatically included in the current model by considering the dissociable side groups of amino acids in whey and

casein proteins. These side groups were free to associate with any counter-ion given the appropriate association constants.

The results of the dynamic solution of milk with proteins and CPN was clearly incorrect. This was either because the metastability of supersaturated components of milk was not included in the model, or because the model over-estimates the activity of these components. When milk was concentrated in the simulations the pH increased sharply for the double concentrated milk, and then slightly for higher concentration ratios. Despite this research, more investigations need to be carried out especially on the possible experiments that can determine the behaviour of supersaturated milk salts at various concentrations.

There are a large number of parameters in each simulation that vary significantly in each literature such as association constant for each equilibrium, solubility product for potential solid phase equilibrium, and initial concentration of each ingredient. Therefore, the uncertainty of variables were not involved in this thesis. However, the uncertainty of the association constants in citrate buffer solution was stated as the sensitivity of pH to K_a values in Chapter 3, Section 3.6.1.2. With reliable data, this approach could be extended to find the uncertainty of many other parameters used in the model, but without such data an analysis of uncertainties would be of limited value.

7 Conclusions and Future work

7.1 Conclusions

The objective of this study was to deeply understand the ion partitioning in milk and milk–like solutions at various concentration either time–dependently or at equilibrium. Therefore, an ion speciation model was proposed to comprehensively include milk components such as calcium, magnesium, sodium, potassium, and hydrogen as the principal cations, and citrate, phosphate, carbonate, sulphate, chloride, phosphate esters, carboxylate, and hydroxide as the main anions in aqueous phase of milk, as described in detail in Chapter 3. The model successfully determined the ion compositions in milk–like solutions and milk serum either at equilibrium over a wide range of pH values or dynamically over time.

Equilibrium calculation of the simulation required theoretical addition of HCl and NaOH to cover a wide range of pH values. The ion equilibria, conservation, and electroneutrality equations, which were applied to various systems, were scaled and then solved using Newton's method. The initial concentrations of species and scaling of equilibrium functions were significant parameters to lead convergence of the simulations.

Solid precipitates were incorporated into the simulation using the ion activity product (*IAP*) and solubility product (K_{sp}) of the solid phase, which were mostly available in literature. Differential equations were formulated for the precipitation equations and these were solved with Euler's method. The Euler's method was used in almost all dynamic simulations because it gives good results, which were in a good agreement with either the experimental or the simulated results available in literature. Dynamic calcium carbonate simulation was the only exception that did not give good matching with the experimental results. Therefore, the Euler's method was replaced with Runge–Kutta to get better fitting.

Ion–pair and free–ion approaches for activity coefficient calculations were defined based on the full and partial dissociation of electrolytes in solution, respectively. The ion–pair approach is thought to be an inaccurate description of dissociation, but it was used to obtain the mean activity coefficients and hence water activity of previous studied solutions. The Gibbs–Duhem relationship was applied to both approaches for the calculation of water activity as a means of validation. The results gave a satisfactory fitting between simulated and

experimental values given by Robinson and Stokes (1959) for water activity of $CaCl_2$, NaCl, and H_2SO_4 up to six molal electrolyte concentration.

The Mean Spherical Approximation (MSA) theory was used to accurately calculate free ion molar activity coefficients of any species regardless of its charge quantity in multicomponent solutions. This enabled incorporation of zero–charged species such as lactose in the calculation, while previous models such as Davies and Extended Debye–Hückel were not able to take into account the effects of zero–charged species. The size parameter is the factor that enables the calculation of unique activity coefficients for each ion, ion–pair, or non–electrolyte. This was shown by employing the MSA theory and afore–mentioned theories to citrate buffer solutions containing zero, 4.5%w/w, and 25%w/w lactose. Addition of lactose did not significantly influence the ion equilibria of citrate species, but notably affected the free–ion activity coefficients of citrate ions calculated by the MSA theory at different lactose contents.

Furthermore, the MSA allows the prediction of free–ion activity coefficient of species at high concentration of electrolyte. This was shown by comparing free–ion activity coefficient obtained by the Davies, Extended Debye–Hückel, and the MSA theories in calcium chloride and sodium chloride solutions individually by both ion–pair and free–ion approaches in Chapter 3. Hence, the effectiveness of MSA theory for free–ion activity coefficient calculation is because of the hard sphere contribution in the formula.

The model was applied to the citrate and phosphate buffer solutions individually, the results of which were in a good agreement with the literature data. However, the intrinsic association constants of citrate ions were slightly changed to get better fitting with experimental data. Phosphate association constants remained unchanged throughout the calculation.

The ion speciation of calcium carbonate system was also studied. The dynamic simulation of this gave close agreement to previous experimental data.

Calcium phosphate as the main insoluble milk component was investigated both steady state and dynamically. The simulated results showed reasonable pH at equilibrium and also over the time. $H_2PO_4^-$ was found to be the most abundant species at low pH values, following by the formations of HPO_4^{2-} and PO_4^{3-} at neutral and high pH. $CaPO_4^-$ was the most plentiful species among the calcium and phosphate component because of high association between

calcium and phosphate ion indicating potential formation of precipitate in the solution with respect to DCPD. A dynamic study of calcium phosphate either with or without addition of NaOH indicated that DCPA precipitated first but then dissolved while DCPD precipitated. Addition of lactose did not significantly influence pH over the time but affected the activity coefficient of species.

Calcium citrate as another potential solid phase system was studied using the proposed model. TCCT was found to have a higher saturation than TCCH. Additions of citrate and lactate to phosphate system altered the speciation of solution leading to a decrease in the saturation of calcium phosphate due to the formation of $CaCit^-$ ion–pairs.

Milk serum was investigated at equilibrium when lactose was added to the solution. The results showed that lactose significantly affected the saturation of solid phase salts particularly DCPD and DCPA. Dynamic simulation of milk serum indicated high saturation values of DCPD, OCP, and DCPA among the other assumed salts, although DCPA might dissolve in the solution. The calcium composition was calculated after 500 minutes predicting that 3 mM of the solid precipitates out of 10 mM total calcium in milk serum. This time scale is quite fast, but Howell (1998) investigated the effect of time on the fouling of whey permeate showing that the fouling changed with a time scale of days due to apparent precipitation within the whey.

In Chapter 4, calcium phosphate precipitation was studied experimentally at various concentrations under varied and controlled pH values. The experimental results clearly showed the formation of a 1 nm nanoparticle in solutions of lactose, calcium and phosphate ions. Lactose was found to prevent or slow down the precipitation of calcium phosphate, probably as calcium dihydrogen phosphate. The structure of the nanoparticle is not known and, based on current research in this area, might be difficult to determine. The effects of many of the conditions such as concentration, ion ratios, pH, lactose concentration, and time need to be tested.

The effects of lactose in this ideal system indicate that it might have a role for the stabilisation of calcium phosphate in milk that might add to the stabilisation produced by the casein micelles.

In Chapter 5, dissociable side groups of casein and serum proteins amino acids were incorporated as individual components in the simulation. Glutamic and aspartic acids

following by cysteine determined the negative contribution of net charge, while lysine and histidine were dominant amino acids contributing the positive net charge at low pH. The simulation of individual milk proteins gave satisfactory net charges over a pH range. A comparison was made between simulations with and without addition of minerals to milk proteins, resulting in relatively similar trend of net charge over pH but a slight difference in IEP possibly due to low affinity between principal cations and amino acids.

CPN was incorporated into the milk simulation and was estimated to be at about 1.5 mM concentration between the pH values 4–9, at which the $(SerP)_3$ concentration reached to 10%. Out of this range, the CPN concentration was predicted to be zero. DCPD, DCPA, and OCP were predicted to be the most dominant potential solid phases at natural pH, while TCCT was estimated to be the main calcium salt at low pH values.

The proposed model has strengths and limitations that need to be addressed:

- The matching between the simulated results obtained and experimental data in literature implies that the assumptions and adjustments were made accurately.
- The model can be applied to any dairy liquids up to high concentration even if one or more of species are zero–charged components.
- The distinction of different milk proteins are another feature of the model allowing addition of other proteins such as lactoferrin.
- Prediction of ion speciation was studied dynamically on different aqueous systems successfully.

However, the model was unable to determine the ion speciation at other temperatures other than 20–25 ˚C, e.g. during milk or cheese heat treatments. The model requires equations to describe the change of association and solubility constants with temperature. These might be difficult to obtain.

7.2 Future work

Some recommendations are suggested to enhance effectively the understanding of the milk partitioning at various conditions:

1. The proposed model in Chapter 3 could be made as a user–friendly software package for the prediction of ion speciation for any milk and milk–like solutions.

2. The model could be applied to different products such as milk protein concentrate (MPC) for prediction of solubility, as to be able to get acceptable appearance of product when it dissolves in water.
3. Further experimental studies could be performed on the different Ca/P ratios and pH with and without lactose in respect to calcium phosphate precipitation to find out at what condition nanoparticles form.
4. Other analytical tests could be implemented such as small angle x–ray scattering (SAXS) and synchrotron based extended x–ray absorption fine structure (EXAFS) to identify the structure in comparison with known crystalline compounds.
5. It would be interesting to test the calcium phosphate precipitation experimentation with other sugars such as sucrose and maltose to see if the nanoparticles are formed in presence of only lactose or not.
6. Experimental data is needed for validation of milk system simulation in the case of precipitation. It would be interesting to propose a comprehensive recipe for a model milk solution that could produce repeatable precipitation of minerals.
7. There are some relationships available for temperature effects of association constants in literature, but not much data is present. Hence, it might be a good idea to follow whey or whey permeate evaporation to be able to incorporate the effect of temperature on the simulation, especially for the changes of association constants with temperature.

References

Al-Makhlafi, H., McGuire, J., & Daeschel, M. (1994). Influence of preadsorbed milk proteins on adhesion of Listeria monocytogenes to hydrophobic and hydrophilic silica surfaces *Applied and Environmental Microbiology, 60,* 3560-3565.

Anandharamakrishnan, C., Rielly, C. D., & Stapley, A. G. F. (2008). Loss of solubility of α-lactalbumin and β-lactoglobulin during the spray drying of whey proteins. *LWT-Food Science and Technology, 41,* 270-277.

Andritsos, N., Yiantsios, S. G., & Karabelas, A. J. (2002). Calcium phosphate scale formation from simulated milk ultrafiltrate solutions. *Food and Bioproducts Processing, 80,* 223-230.

Arifuzzaman, S. M., & Rohani, S. (2004). Experimental study of brushite precipitation. *Journal of Crystal Growth, 267,* 624-634.

Atkins, P. W. (1990). *Physical chemistry*. Great Britain: Oxford University Press.

Auldist, M. J., Walsh, B. J., & Thomson, N. A. (1998). Seasonal and lactational influences on bovine milk composition in New Zealand. *Journal of Dairy Research, 65,* 401-411.

Babić-Ivančić, V., Kntrec, J., Brečević, L., & Kralj, D. (2006). Kinetics of struvite to newberyite transformation in the precipitation system $MgCl_2$–$NH_4H_2PO_4$–NaOH–H_2O. *Water Research, 40,* 3447-3455.

Belitz, H. D., & Grosch, W. (1999). *Food Chemistry*. Berlin: Springer.

Berg, J., Romijn, D., van Halbeek, H., Vlienenthart, J. F. G., & Visser, R. A. (1988). Characterisation of four lactose monophosphates by application of 31P-,13C-, and 1H-NMR spectroscopy. *Carbohydrate Research, 174,* 23-26.

Besic, F. C. (1985). Food materials for prevention of carious degradation of teeth, United States Patent No. 4515770A.

Bijl, E., Huppertz, T., van Valenberg, H. J., & Holt, C. (2018). A quantitative model of the bovine casein micelle: ion equilibria and calcium phosphate sequestration by individual caseins in bovine milk. *European Biophysics Journal*, 1-15.

Bleek, K., & Taubert, A. (2013). New developments in ploymer-controlled, bioinspired calcium phosphate mineralization from aqueous solution. *Acta Biomaterialia, 9,* 6283-6321.

Blum, L. (1975). Mean spherical model for asymmetric electrolytes. *Molecular Physics, 30,* 1529-1535.

Blum, L., & Høye, J. S. (1977). Mean spherical model for asymmetric electrolytes. 2. Thermodynamic properties and the pair correlation function. *The Journal of Physical Chemistry, 81*, 1311-1316.

Blum, L., Vericat, F., & Fawcett, W. R. (1992). Mean spherical approximation for hard ions and dipoles. *The Journal of Chemical Physics, 96*, 3039-3044.

Blum, L., & Wei, D. (1987). Analytical solution of the mean spherical approximation for an arbitrary mixture of ions in a dipolar solvent. *The Journal of Chemical Physics, 87*, 555-565.

Boskey, A. L., & Posner, A. S. (1976). Formation of hydroxyapatite at low supersaturation. *The Journal of Physical Chemistry, 80*, 40-45.

Brečević, L., & Füredi-Milhofer, H. (1972). Precipitation of calcium phosphates from electrolyte solutions. *Calcified Tissue Research, 10*, 82-90.

Brečević, L., & Nielsen, A. E. (1989). Solubility of Amorphous Calcium Carbonate. *Journal of Crystal Growth, 98*, 504-510.

Brečević, L., Škrtić, D., & Garside, J. (1986). Transformation of calcium oxalate hydrates. *Journal of Crystal Growth, 74*, 399-408.

Bressan, C., & Mathlouthi, M. (1994). Thermodynamic activity of water and sucrose and the stability of crystalline sugar. *Zuckerindustrie, 119*, 652-658.

Bromley, L. A. (1972). Approximate individual ion values of β (or B) in extended Debye-Hückel theory for uni-univalent aqueous solutions at 298.15 K. *The Journal of Chemical Thermodynamics, 4*, 669-673.

Brooks, R., Clark, L. M., & Thurston, E. F. (1950). Calcium carbonate and its hydrates. *Philosophical Transactions of the Royal Society of London, 243*, 145-167.

Broyard, C., & Gaucheron, F. (2015). Modifications of structures and functions of caseins: a scientific and technological challenge. *Dairy Science and Technology, 95*, 831-862.

Buchner, R., Hefter, G. T., & May, P. M. (1999). Dielectric relaxation of aqueous NaCl solutions. *The Journal of Physical Chemistry, 103*, 1-9.

Burrington, K. J. (2017). Whey protein heat stability: US Dairy, Dairy Research Institute.

Butler, J. N. (1998). *Activity coefficients and pH Ionic equilibrium-Solubility and pH calculations*. New York: John Wiley & Sons.

Cameselle, J. C., Ribeiro, J. M., & Sillero, A. (1986). Deviation and use of a formula to calculate the net charge of acid-base compounds. Its application to amino acids, proteins and nucleotides. *Biochemical Education, 14*, 131-136.

Cha, J., Lee, J. S., Yoon, S. J., Kim, Y. K., & Lee, J. K. (2013). Solid-state phase transformation mechanism for formation of magnetic multi-granule nanoclusters. *RSC Advances, 3*, 3631-3637.

Chhettry, A., Wang, Z., Fox, J. L., Baig, A. A., Zhuang, H., & Higuchi, W. I. (1999). Use of dicalcium phosphate dihydrate as a probe in an approach for accurate calculations of solution equilibria in buffered calcium phosphate systems. *Journal of Colloid and Interface Science, 218*, 47-56.

Clark, I. (2015). *Groundwater Geochemistry and Isotopes*. Boca Raton: CRC Press, Taylor & Francis Group.

Clegg, S. L., & Whitfield, M. (1991). Activity coefficients in natural waters. In K. S. Pitzer (Ed.), *Activity Coefficients in Electrolyte Solutions*. The USA: CRC Press, Inc.

Coico, R., & Geoffrey, S. (2009). *Immunology A short course*. The USA: John Wiley & Sons, Inc.

Combes, C., & Rey, C. (2010). Amorphous calcium phosphates: Synthesis, properties and uses in biomaterials. *Acta Biomaterialia, 6*, 3362-3378.

Constable, P. D. (1997). A simplified strong ion model for acid-base equilibria: application to horse plasma. *Journal of Applied Physiology, 83*, 297-311.

Cornell, D. G., & Patterson, D. L. (1989). Interaction of phospholipids in monolayers with β–lactoglobulin adsorbed from solution. *Journal of Agricultural and Food Chemistry, 37*, 1455-1459.

Corredig, M., & Dalgleish, D. G. (1996). Effect of different heat treatments on the strong binding interactions between whey proteins and milk fat globules in whole milk. *Journal of Dairy Research, 63*, 441-449.

Cosman, N. P., Faith, K., & Roscoe, S. G. (2005). Electrochemical impedance spectroscopy study of the adsorption behaviour of α-lactalbumin and β-casein at stainless steel. *Journal of Electroanalytical Chemistry, 574*, 261-271.

Creamer, L. K., & Sawyer, L. (2003). Beta-lactoglobulin. In H. Roginski, J. W. Fuquay & P. F. Fox (Eds.), *Encyclopedia of Dairy Sciences*. London: American Press.

Cruse, J. M., & Lewis, R. E. (2010). *Atlas of Immunology*. The USA: CRC Press.

Dalgleish, D. G. (2011). On the structural models of bovine casein micelles—review and possible improvements. *Soft Matter, 7*, 2265–2272.

Davies, C. W. (1962). *Ion Association* London: Butterworths Scientific Publications.

Davies, D. T., & White, J. C. D. (1960). The use of ultrafiltration and dialysis in isolating the aqueous phase of milk and in determining the partition of milk constituents between the aqueous and disperse phases. *Journal of Dairy Research, 27*, 171-190.

de Kruif, C. G. (1999). Casein micelle interactions. *International Dairy Journal, 9*, 183-188.

de Kruif, C. G., & Grinberg, V. Y. (2002). Micellisation of β-casein. *Colloids and Surfaces A: Physicochemical and Engineering Aspects, 210*, 183-190.

de Kruif, C. G., & Holt, C. (2003). Casein micelle structure, functions and interactions. In P. F. Fox & P. McSweeney (Eds.), *Advanced Dairy Chemistry. Proteins* (3 ed.). New York: Kluwer Academic/Plenum Publishers.

de Kruif, C. G., Tuinier, R., Holt, C., Timmins, P. A., & Rollema, H. S. (2002). Physicochemical study of κ- and β-casein dispersions and the effect of cross-linking by transglutaminase. *Langmuir, 18*, 4885-4891.

de La Fluente, M. A. (1998). Changes in the mineral balance of milk submitted to technological treatments. *Trends in Food Science and Technology, 9*, 281-288.

Debye, P., & Hückel, E. (1923). The theory of electrolytes, lowering of freezing point and related phenomena. *Physikalische Zeitschrift, 24*, 185-206.

Dey, A., Bomans, P. H., Muller, F. A., Will, J., Frederik, P. M., de With, G., & Sommerdijk, N. A. (2010). The role of prenucleation clusters in surface-induced calcium phosphate crystallization. *Nature Materials, 9*, 1010-1014.

Dickinson, E. (1999). Adsorbed protein layers at fluid interface: interactions, structure and surface rheology. *Colloids Surfaces B: Biointerfaces, 15*, 161-176.

Doherty, W. O. S., & Wright, P. G. (2004). A solubility model for calcium oxalate formation in a sugar mill. *Proceedings-Australian Society Of Sugar Cane Technologists, 26*, 519-526.

Dorozhkin, S. V. (2014). Calcium orthophosphates: Occurrence, properties and major applications. *Bioceramics Developments and Applications, 4*, 1-20.

Driessens, F. C. M., & Verbeeck, R. M. H. (1990). *Biominerals*. The USA: CRC Press.

Dybing, S. T., Wiegand, J. A., Brudvig, S. A., Huang, E. A., & Chandan, R. C. (1988). Effect of processing variables on the formation of calcium lactate crystals on Cheddar cheese. *Journal of Dairy Science, 71*, 1701-1710.

Eigel, W. N., Butlet, J. E., Ernstrom, C. A., Farrell, H. M., Harwalker, V. R., Jenness, R., & Whitney, R. M. (1984). Nomenclature of protein of cow's milk: fifth revision. *Journal of Dairy Science, 67*, 1599-1631.

El-Loly, M. M. (2011). Compostion, properties and nutritional aspects of milk fat globule membrane- A review. *Polish Journal of Food and Nutrition Sciences, 61*, 7-32.

Elliot, J. C. (1994). *Structure and chemistry of the apatite and other calcium orthophosphates.* Amsterdam: Elsevier Science B.V.

Fang, Z. H., Bovenhuis, H., Delacroix-Buchet, A., Miranda, G., Boichard, D., & Visker, M. H. P. W. (2017). Genetic and nongenetic factors contributing to differences in αs–casein phosphorylation isoforms and other major milk proteins. *Journal of Dairy Science, 100*, 5564-5577.

Farrell, J. H., Jimenez-Flores, R., Bleck, G. T., Butler, J. E., Brown, E. M., Creamer, L. K., . . . Swaisgood, H. E. (2004). Nomenclature of the proteins of cows' milk. *Journal of Dairy Science, 87*, 1641-1674.

Fawcett, W. R., & Tikanen, A. C. (1996). Role of solvent permittivity in estimation of electrolyte activity coefficients on the basis of the mean spherical approximation. *The Journal of Physical Chemistry, 100*, 4251-4255.

Fawcett, W. R., Tikanen, A. C., & Henderson, D. J. (1977). The mean spherical approximation and medium effects in the kinetics of solution reactions involving ions. *Canadian Journal of Chemistry, 75*, 1649-1655.

Fennema, O. R. (1996). *Food Chemistry*. New York: Marcel Dekker, Inc.

Ferguson, J. F., & McCarty, P. L. (1971). Effects of carbonate and magnesium on calcium phosphate precipitation *Environmental Science and Technology, 5*, 534-540.

Flynn, A., & Cashman, K. (1997). Nutritional aspects of minerals in bovine and human milks. In P. F. Fox (Ed.), *Advanced Dairy Chemistry: Lactose, Water, Salts and Vitamins* (2 ed., Vol. 3, pp. 257-302). London: Chapman & Hall.

Follows, D., Holt, C., Thomas, R. K., Tiberg, F., Fragneto, G., & Nylander, T. (2011). Co-adsorption of β–casein and calcium phosphate nanoclusters (CPN) at hydrophilic and hydrophobic solid-solution interfaces studied by neutron reflectometry. *Food Hydrocolloids, 25*, 724-733.

Fox, P. F. (2009). Milk: an overview. In A. Thompson, M. Boland & H. Singh (Eds.), *Milk Proteins: From Expression to Food*. Boston, US: Elsevier, Inc.

Fox, P. F., & McSweeney, P. (1998). *Dairy Chemistry and Biochemistry*. London, UK: Blackie Academic & Professional, an imprint of Chapman & Hall.

Fox, P. F., & McSweeney, P. L. H. (2003). Proteins *Advanced Dairy Chemistry* (3 ed., Vol. 1). New York, USA: Kluwer Academic-Plenum Publishers.

Freeley, R. M., Criner, P. E., & Slover, H. T. (1975). Major fatty acids and proximate composition of dairy products. *Journal of The American Dietetic Association, 66*, 140-146.

Gao, R. (2010). *Ion speciation in milk-like systems.* (Doctor of Philosophy), Wageningen University, Netherlands.

Gao, R., van Halsema, F. E. D., Temminghoff, E. J. M., van Leeuwen, H. P., van Valenberg, H. J. F., Eisner, M. D., . . . van Boekel, M. A. J. S. (2010). Modelling ion composition in simulated milk ultrafiltrate (SMUF). I: Influence of calcium phosphate precipitation. *Food Chemistry, 122*, 700-709.

Gao, R., van Leeuwen, H. P., Temminghoff, E. J. M., van Valenberg, H. J., Eisner, M. D., & van Boekel, M. A. J. S. (2010). Effect of disaccharides on ion properties in milk-based systems. *Journal of Agricultural and Food Chemistry, 58*, 6449-6457.

Garcia, A. C., Vavrusova, M., & Skibsted, L. F. (2018). Supersaturation of calcium citrate as a mechanism behind enhanced availability of calcium phosphates by presence of citrate. *Food Research International, 107*, 195-205.

Garnsworthy, P. C., Masson, L. L., Lock, A. L., & Mottaram, T. T. (2006). Variation of milk citrate with stage of lactation and de novo fatty acid synthesis in dairy cows. *Journal of Dairy Science, 89*, 1604-1612.

Gaucheron, F. (2005). The minerals of milk. *Reproduction Nutrition Development, 45*, 473-483.

Gaucheron, F., Le Graët, Y., Piot, M., & Boyaval, E. (1996). Determination of anions of milk by ion chromatography. *Lait, 76*, 433-443.

Ghishan, F. K., Stroop, S., & Meneely, R. (1982). The effect of lactose on the intestinal absorption of calcium and zinc in the rat during maturation. *Pediatric Research, 16*, 566-568.

Ginger, M. R., & Grigor, M. R. (1999). Comparative aspects of milk caseins. *Comparative Biochemistry and Physiology Part B, 124*, 133-145.

Goel, A. (2006). *Surface chemistry*. New Delhi: Discovery Publishing House.

Grandison, A. S., & Lewis, M. J. (1996). *Separation processes in the food and biotechnology industries: Principles and applications*. England: Woodhead Publishing Ltd.

Guéguen, L., & Pointillart, A. (2000). The bioavailability of dietary calcium. *The Journal of the American College of Nutrition, 19(sup2)*, 119S-136S.

Guggenheim, E. A. (1926). On the determination of the velocity constant of a unimoelcular reaction. *Philosophical Magazine, 2*, 538-543.

Guggenheim, E. A. (1967). *Thermodynamics, an advanced treatment for chemists and physics*. The Netherlands: North-Holland Publishing Company.

Haggarty, N. W. (2003). Minor proteins, bovine serum albumin and vitamin-binding proteins. In H. Roginski, J. W. Fuquay & P. F. Fox (Eds.), *Encyclopedia of Dairy Sciences*. London: Academic Press.

Hanze, M., Gujer, W., Mino, T., & Van Loosdrecht, M. (2000). *Activated sludge models ASM1, ASM2, ASM2d and ASM3*. London: IWA Publishing.

Harned, H., & Cook, M. A. (1937). The ionic activity coefficient product and ionization of water in uni-univalent halide solutions-A numerical summary. *Journal of The American Chemical Society, 59*, 2304-2305.

Heck, J. M., van Valenberg, H. J., Dijkstra, J., & van Hooijdonk, A. C. (2009). Seasonal variation in the Dutch bovine raw milk composition. *Journal of Dairy Science, 90*, 706-715.

Held, C., Reschke, T., Mohammad, S., Luza, A., & Sadowski, G. (2014). ePC-SAFT revised. *Chemical Engineering Research and Design, 92*, 2884-2897.

Herrington, B. L. (1934). Some physico-chemical properties of lactose. VI The solubility of lactose in salt solutions; the isolation of a compound of lactose and calcium chloride. *Journal of Dairy Science, 17*, 805-814.

Hignett, T. P., & Brabson, J. A. (1961). Evaluation of water-insoluble phosphorus in fertilizers by extraction with alkaline ammonium citrate solutions. *Journal of Agricultural and Food Chemistry, 9*, 272-276.

Hiraoka, Y., Segawa, T., Kuwajima, K., Sugai, S., & Murai, N. (1980). α–lactalbumin: a calcium metalloprotein. *Biochemical and Biophysical Research Communications, 95*, 1098-1104.

Holsinger, V. H. (1997). Physical and chemical properties of lactose. In P. F. Fox (Ed.), *Advanced Dairy Chemistry Volume 3: Lactose, water, salts and vitamins*. London: Chapman & Hall.

Holt, C. (1985). The milk salts: their secretion, concentration and physical chemistry. In P. F. Fox (Ed.), *Developments in Dairy Chemistry, Lactose and minor constituents* (Vol. 3, pp. 143-181). London: Elsevier Science

Holt, C. (1992). Structure and stability of bovine casein micelles. *Advances in Protein Chemistry, 43*, 63-151.

Holt, C. (1997). The milk salts and their interaction with casein. In P. F. Fox (Ed.), *Advanced Dairy Chemistry Volume 3: Lactose, Water, Salts and Vitamins* (2 ed., Vol. 3, pp. 233-254). London: Chapman & Hall.

Holt, C. (2004). An equilibrium thermodynamic model of the sequestration of calcium phosphate by casein micelles and its application to the calculation of the partition of salts in milk. *Eur Biophys J, 33*, 421-434.

Holt, C. (2011). Milk salts: interaction with caseins. In J. W. Fuquay, P. F. Fox & P. McSweeney (Eds.), *Encyclopedia of Dairy Sciences* (2 ed., Vol. 3, pp. 917-924). San Diego, CA: Academic Press.

Holt, C., Carver, J. A., Ecroyd, H., & Thorn, D. C. (2013). Invited review: Caseins and the casein micelle: Their biological functions, structures, and behavior in foods. *Journal of Dairy Science, 96*(10), 6127-6146.

Holt, C., Dalgleish, D. G., & Jenness, R. (1981). Calculation fo the ion equilibria in milk diffusate and comparison with experiment. *Analytical Biochemistry, 113*, 154-163.

Holt, C., Davies, D. T., & Law, A. J. R. (1986). Effects of colloidal calcium-phosphate content and free calcium-ion concentration in the milk serum on the dissociation of bovine casein micelles. *Journal of Dairy Research, 53*, 557-572.

Holt, C., Hasnain, S. S., & Hukins, D. W. L. (1982). Structure of bovine milk calcium phosphate determined by x-ray absorption spectroscopy. *Biochim Biophys Acta (BBA) - General Subjects, 719*, 299-303.

Holt, C., Lenton, S., Nylander, T., Sørensen, E. S., & Teixeira, S. C. M. (2014). Mineralisation of soft and hard tissues and the stability of biofluids. *Journal of Structural Biology, 185*, 383-396.

Holt, C., & Muir, D. D. (1979). Inorganic constituents of milk. I. Correlation of soluble calcium with citrate in bovine milk. *Journal of Dairy Research, 46*, 433-439.

Holt, C., Sørensen, E. S., & Clegg, S. L. (2009). Role of calcium phosphate nanoclusters in the control of calcification. *The FEBS Journal, 276*, 2308-2323.

Holt, C., Timmins, P., Errington, N., & Leaver, J. (1998). A core-shell model of calcium phosphate nanoclusters stabilized by β-casein phosphopeptides, derived from sedimentation equilibrium and small-angle X-ray and neutron-scattering measurements. *European Journal of Biochemistry, 252*, 73-78.

Holt, C., Wahlgren, N. M., & Drakenberg, T. (1996). Ability of a β-casein phosphopeptide to modulate the precipitation of calcium phosphate by forming amorphous dicalcium phosphate nanoclusters. *Biochemical Journal, 314*, 1035-1039.

Horne, D. S. (1998). Casein interactions: Casting light on the black boxes, the structure in dairy products. *International Dairy Journal, 8*, 171-177.

Horne, D. S. (2003). Casein micelles as hard spheres: limitations of the model in acidified gel formation. *Colloids and Surfaces A: Physicochemical and Engineering Aspects, 213*, 255-263.

Howell, J. M. (1998). *Whey permeate fouling of evaporators.* (Master of Engineering), University of Canterbury, Christchurch, New Zealand.

Hoye, J. S., & Stell, G. (1977). Thermodynamics of the MSA for simple fluids. *The Journal of Chemical Physics, 67*, 439-445.

Huppertz, T., & Fox, P. F. (2006). Effect of NaCl on some physico-chemical properties of concentrated bovine milk. *International Dairy Journal, 16*, 1142-1148.

Huppertz, T., Fox, P. F., de Kruif, K. G., & Kelly, A. L. (2006). High pressure-induced changes in bovine milk proteins: A review. *Biochimica et Biophysica Acta, 1764*, 593-598.

Illanes, A., Guerrero, C., Vera, C., Wilson, L., Conejeros, R., & Scott, F. (2016). *Lactose-Derived Prebiotics*. United Kingdom: Elsevier.

Isaad, J., & Perwuelz, A. (2010). New color chemosensors for cyanide based on water soluble azo dyes. *Tetrahedron Letters, 51*, 5810-5814.

Jackson, D. C. (2004). Surviving extreme lactic acidosis: the role of calcium lactate formation in the anoxic turtle. *Respiratory Physiology & Neurobiology, 144*, 173-178.

Jeurnink, T. J. M., & Brinkman, D. W. (1994). The cleaning of heat exchangers and evaporators after processing milk or whey. *International Dairy Journal, 4*, 347-368.

Jeurnink, T. J. M., Walstra, P., & de Kruif, C. G. (1996). Mechanisms of fouling in dairy processing. *Netherlands Milk and Dairy Journal, 50*, 407-426.

Johansson, A., Lugand, D., Rolet-Repecaud, O., Molle, D., Delage, M. M., Peltre, G., . . . Dupont, D. (2009). Epitope characterization of a supramolecular protein assembly with a collection of monoclonal antibodies: the case of casein micelle. *Molecular Immunology, 46*, 1058-1066.

Johnsson, M. S. A., & Nancollas, G. H. (1992). The role of brushite and octacalcium phosphate in apatite formation. *Critical Reviews in Oral Bilogy and Medicine, 3*, 61-82.

Joko, I. (1984). Phosphorus removal from wastewater by the crystallization method. *Water Science and Technology, 17*, 121-132.

Kazadi Mbamba, C. (2016). *Dynamic modelling of minerals precipitation in wasterwater treatment.* (Doctor of Philosophy), The University of Queensland, Australia.

Kell, G. S. (1975). Density, thermal expansivity, and compressibility of liquid water from 0˚ to 150˚C: Correlations and tables for atmospheric pressure and saturation reviewed and expressed on 1968 temperature scale. *Journal of Chemical and Engineering Data, 20*, 97-105.

Kellermeier, M., Gebauer, D., Melero-García, E., Drechsler, M., Talmon, Y., Kienle, L., . . . Kunz, W. (2012). Colloidal stabilization of calcium carbonate prenucleation clusters with silica. *Advanced Functional Materials, 22*, 4301-4311.

Kent, J. C., Arthur, P. G., & Hartmann, P. E. (1998). Citrate, calcium, phosphate and magnesium in sows' milk at initiation of lactation. *Journal of Dairy Research, 65*, 55-68.

Kezia, K., Lee, J., Zisu, B., Chen, G. Q., Gras, S. L., & Kentish, S. E. (2017). Solubility of calcium phosphate in concentrated dairy effluent brines. *J Agric Food Chem, 65*, 4027-4034.

Kielland, J. (1937). Individual activity coefficients of ions in aqueous solutions. *Journal of The Americal Chemical Society, 59*, 1675-1683.

Kinsella, J. E. (1984). Milk proteins: Physical and functional properties. *CRC Critical Reviews in Food Science and Nutrition, 21*, 197-262.

Kralj, D., Brečević, L., & Kontrec, J. (1997). Vaterite growth and dissolution in aqueous solution III. Kinetics of transformation. *Journal of Crystal Growth, 177*, 247-257.

Kubantseva, N., & Hartel, R. W. (2002). Solubility of calcium lactate in aqueous solution. *Food Reviews International, 18*, 135-149.

Kubantseva, N., Hartel, R. W., & Swearingen, P. A. (2004). Factors affecting solubility of calcium lactate in aqueous solutions. *Journal of Dairy Science, 87*, 863-867.

Kuehner, D. E., Engmann, J., Fergg, F., Wernick, M., Blanch, H. W., & Prausnitz, J. M. (1999). Lysozyme net charge and ion binding in concentrated aqueous electrolyte solutions. *Journal of Physical and Chemistry B, 103*, 1368-1374.

Kuhn, R., & Low, I. L. (1949). The occurrence of lactose in the plant kingdom. *Chemische Berichte, 82*, 479-481.

Lango, F., Rocha, S. D. F., Katsarou, L., & Demopoulos, G. P. (2012). Supersaturation-controlled synthesis of dicalcium phosphate dihydrate and nanocrystalline calcium-deficient hydroxyapatite. *Industrial & Engineering Chemistry Research, 51*, 6605-6612.

Le Graët, Y., & Gaucheron, F. (1999). pH-induced solubilization of minerals from casein micelles: influence of casein concentration and ionic strength. *Journal of Dairy Research, 66,* 215-224.

Lebowitz, J. L., & Percus, J. K. (1966). Mean spherical model for lattice gases with extended hard cores and continuum fluids. *Physical Review, 144*, 251-258.

Leclerc, E., & Calmettes, P. (1997). Interactions in micellar solution of β-casein *Physical Review Letters, 78*, 150-153.

Lenton, S., Nylander, T., Holt, C., Sawyer, L., Härtlein, M., Müller, H., & Teixeira, S. C. (2016). Structural studies of hydrated samples of amorphous calcium phosphate and phosphoprotein nanoclusters. *European Biophysics Journal, 45*, 405-412.

Lenton, S., Nylander, T., Teixeira, S. C., & Holt, C. (2015). A review of the biology of calcium phosphate sequestration with special reference to milk. *Dairy Science and Technology, 95*, 3-14.

Lewis, G. N., & Randall, M. (1921). The activity coefficient of strong electrolytes. *Journal of The American Chemical Society, 43*, 1112-1154.

Li, C., Li, Y., Lu, J., & Yang, L. (1996). Study of the ionic activity coefficients in aqueous electrolytes by the non-primitive mean spherical approximation equation. *Fluid Phase Equilibria, 124*, 99-110.

Li, H., Robertson, A. D., & Jensen, J. H. (2005). Very fast empirical prediction and rationalization of protein pK_a values. *Proteins: Structure, Function, and Bioinformatics, 61*, 704-721.

Lifran, E. V. (2007). *Role of lactose phosphate in lactose containing dairy products.* University of Western Sydney, Sydney, Australia.

Lin, T. J., & Chiu, C. C. (2017). Structures and infrared spectra of calcium phosphate clusters by ab initio methods with implicit solvation models. *Physical Chemistry Chemical Physics, 20*, 345-356.

Lindsay, R. C. (1996). Food additives. In O. Fennema (Ed.), *Food Chemistry* (pp. 767-823). New York: Marcel Dekker.

Little, E. M., & Holt, C. (2004). An equilibrium thermodynamic model of the sequestration of calcium phosphate by casein phosphopeptides. *European Biophysics Journal, 33*, 435-447.

Liu, W. B., Li, Y. G., & Lu, J. F. (1998). Nonprimitive model of mean spherical approximation applied to aqueous electrolyte solutions. *Industrial & Engineering Chemistry Research, 37,* 4183-4189.

Liu, Z. P., Li, Y. G., & Lu, J. F. (2002). Low-density xxpansion of the solution of mean spherical approximation for ion-dipole mixtures. *The Journal of Physical Chemistry, 106*, 5266-5274.

Lotfikhan, M., & Modarress, H. (2003). Modification and Application of a Non-Primitive Mean Spherical Approximation Model for Simple Aqueous Electrolyte Solutions. *Fluid Phase Equilibria, 209*, 13-27.

Lu, X., & Leng, Y. (2005). Theoretical analysis of calcium phosphate precipitation in simulated body fluid. *Biomaterials, 26*, 1097-1108.

Lyster, R. L. J. (1972). Review of the progress of dairy science, section C. Chemistry of milk proteins. *Journal of Dairy Science, 39*, 279-318.

Lyster, R. L. J. (1981). Calculation by computer of individual concentrations in a simulated milk salt solution. 2. an extension to the previous model. *Journal of Dairy Research, 48*, 85-89.

Lyster, R. L. J., Mann, S., Parker, S. B., & Williams, R. (1984). Nature of micellar calcium phosphate in cow's milk as studied by high resolution electron microscopy. *Biochimica et Biophysica Acta, 801*, 315-317.

Madsen, H. E. L., & Christensson, F. (1991). Precipitation of calcium phosphate at 40 ˚C from neutral solution. *Journal of Crystal Growth, 114*, 613-618.

Madsen, H. E. L., & Thorvardarson, G. (1984). Precipitation of calcium phosphate from moderately acid solution. *Journal of Crystal Growth, 66*, 369-376.

Mansoori, G. A., Carnahan, N. F., Starling, K. E., & Leland JR, T. W. (1971). Equilibrium thermodynamic properties of the mixture of hard spheres. *The Journal of Chemical Physics, 54*, 1523-1525.

Mansson, H. L. (2008). Fatty acids in bovine milk fat. *Food and Nutrition Research, 52*, 1-3.

Marchessau, S., Gastaldi, E., Lagaude, A., & Cuq, J. L. (1997). Influence of pH on protein interactions and microstructure of process cheese. *Journal of Dairy Science, 80*, 1483-1489.

Marti, N., Bouzas, A., Seco, A., & Ferrer, J. (2008). Struvite precipitation assessment in anaerobic digestion processes. *Chemical Engineering Journal, 141*, 67-74.

McDowell, H., Gregory, T. M., & Brown, W. E. (1977). Solubility of $Ca_5(PO_4)_3OH$ in the system $Ca(OH)_2$-H_3PO_4-H_2O at 5, 15, 25, and 37 °C. *Journal of Research of the Notional Bureau of Standards, 81A*, 273-281.

McGann, T., Buchheim, W., Kearney, R. D., & Richardson, T. (1983). Composition and ultrastructure of calcium phosphate-citrate complexes in bovine milk systems. *Biochimica et Biophysica Acta, 760,* 415-420.

Meissner, H. P., & Kusik, C. L. (1978). Electrolyte activity coefficients in inorganic processing. *AIChE Symposium Series 173*, *74*, 14-20.

Meissner, J., Prause, A., Bharti, B., & Findenegg, G. H. (2015). Characterization of protein adsorption onto silica nanoparticles: influence of pH and ionic strength. *Colloid and Polymer Science, 293*, 3381-3391.

Mekmene, O., & Gaucheron, F. (2011). Determination of calcium-binding constants of caseins, phosphoserine, citrate and pyrophosphate: A modelling approach using free calcium measurement. *Food Chemistry, 127*, 676-682.

Mekmene, O., Le Graet, Y., & Gaucheron, F. (2009). A model for predicting salt equilibria in milk and mineral-enriched milks. *Food Chemistry, 116*, 233-239.

Mekmene, O., Le Graët, Y., & Gaucheron, F. (2010). Theoretical model for calculating ionic Equilibria in milk as a function of pH: comparison to experiment. *Journal of Agricultural and Food Chemistry, 58*, 4440-4447.

Mekmene, O., Quillard, S., Rouillon, T., Bouler, J. M., Piot, M., & Gaucheron, F. (2009). Effect of pH and Ca/P molar ratio on the quantity and crystalline structure of calcium phosphates obtained from aqueous solutions. *Dairy Science Technology, 89*, 301-316.

Mekmene, O., Rouillon, T., Quillard, S., Pilet, P., Bouler, J. M., Pezennec, S., & Gaucheron, F. (2012). Effects of citrate and NaCl on size, morphology, crystallinity and microstructure of calcium phosphates obtained from aqueous solutions at acidic or near-neutral pH. *ournal of Dairy Research, 79*, 238-248.

Mercadé-Prieto, R., Falconer, R. J., Peterson, W. R., & Wilson, D. I. (2007). Swelling and dissolution of β-lactoglobulin gels in alkali. *Biomacromolecules, 8*, 469-476.

Mikheeva, L. M., Grinberg, N. V., Grinberg, V. Y., Khokhlov, A. R., & de Kruif, C. G. (2003). Thermodynamics of micellization of bovine ß-casein studied by high-sensitivity differential scanning calorimetry. *Langmuir, 19*, 2913–2921.

Miyazaki, T., Sivaprakasam, K., Tantry, J., & Suryanarayanan, R. (2009). Physical characterization of dibasic calcium phosphate dihydrate and anhydrate. *Journal of Pharmaceutical Sciences, 98*, 905-916.

Mollerup, J. M., & Breil, M. P. (2015). Modeling the permittivity of electrolyte solutions. *AlChe Journal, 61*, 2854-2860.

Mora-Gutierrez, A., & Farrell, H. M. (2000). Sugar-casein interaction in deuterated solutions of bovine and caprine casein as determined by oxygen-17 and carbon-13 nuclear magnetic resonance: A case of preferential interactions. *Journal of Agricultural and Food Chemistry, 48*, 3245-3255.

Mora-Gutierrez, A., Kumosinski, T. F., & Farrell, H. M. (1997). Oxygen-17 nuclear magnetic resonance studies of bovine and caprine casein hydration and actvity in deuterated sugar solutions. *Journal of Agricultural and Food Chemistry, 45*, 4545-4553.

Morrissey, P. A. (1985). Lactose: chemical and physiochemical properties. In P. F. Fox (Ed.), *Developments in dairy Chemistry 3: Lactose and Minor Constituents*. London: Elsevier Applied Science Publishers.

Mullin, J. W. (2001). *Crystallization*. Oxford: Elsevier Butterworth-Heinemann.

Nakayama, F. S. (1968). Calcium activity, complex and ion-pair in saturated $CaCO_3$. *Soil Science, 106*, 429-434.

Nancollas, G. H. (1992). The involvement of calcium phosphates in biological mineralization and demineralization processes. *Pure and Applied Chemistry, 64*, 1673-1678.

Ng-Kwai-Hang, K. F. (2003). Heterogeneity, fractionation and isolation. In H. Roginski, J. W. Fuquay & P. F. Fox (Eds.), *Encyclopedia of Dairy Sciences* (Vol. 3). London: Academic Press.

Nickerson, T. A. (1978). Why use lactose and its derivatives in food? *Food Technology, 32*, 40-46.

Nicollas, G. H., Lore, M., Perez, L., Richardson, C., & Zawacki, S. J. (1989). Mineral phases of calcium phosphate. *The Anatomical Record, 224*, 234-241.

Nielsen, A. E. (1984). Electrolyte crsytal growth mechanisms. *Journal of Crystal Growth, 67*, 289-310.

Nielsen, A. E., & Toft, J. M. (1984). Electrolyte crystal growth kinetics. *Journal of Crystal Growth, 67*, 278-288.

Ninham, B. W., & Lo Nostro, P. (2010). *Molecular forces and seld assembly in colloid, nano sciences and bilogy*. Cambridge: Cambridge University Press.

Njegić-Džakula, B., Falini, G., Brečević, L., Skoko, Ž., & Kralj, D. (2010). Effects of initial supersaturation on spontaneous precipitation of calcium carbonate in the presence of charged poly-L-amino acids. *Journal of Colloid and Interface Science, 343*, 553-563.

Onuma, K., & Ito, A. (1998). Cluster growth model for hydroxyapatite. *Chemistry of Materials (ACS Publications), 10*, 3346-3351.

Othman, K. I., Hassan, A. A., Abdelal, O. A. A., Elshazly, E. S., El-Sayed Ali, M., El-Raghy, S. M., & El-Houte, S. (2014). Formation mechanism of barium titanate by solid-state reactions. *International Journal of Scientific & Engineering Research, 5*, 1460-1465.

Oyane, A., Onuma, K., Ito, A., Kim, H. M., Kokubo, T., & Nakamura, T. (2002). Formation and growth of clusters in conventional and new kinds of simulated body fluids. *Journal of Biomedical Materials Research Part A, 64A*, 339-348.

Palmer, D. S., Sorensen, J., Schiott, B., & Fedorov, M. V. (2013). Solvent binding analysis and computational alanine scanning of the bovine chymosin−bovine κ-casein complex using molecular integral equation theory. *Journal of Chemical Theory and Computation, 9*, 5706-5717.

Pan, H. B., & Darvell, B. W. (2009a). Calcium phosphate solubility: The need for re-evaluation. *Crystal Growth and Design, 9*, 639-645.

Pan, H. B., & Darvell, B. W. (2009b). Solubility of dicalcium phosphate dihydrate by solid titration. *Caries Research, 43*, 254-260.

Park, K. H., Kim, S. J., Hwang, M. J., Song, H. J., & Park, Y. J. (2017). Biomimetic fabrication of calcium phosphate/chitosan nanohybrid composite in modified simulated body fluids. *Express Polym Lett, 11*, 14-20.

Phadungath, C., & Metzger, L. E. (2011). Effect of sodium glocunate on the solubility of calcium lactate. *Journal of Dairy Science, 94*, 4843-4849.

Pigman, W., & Horton, D. (1972). *The carbohydrates chemistry and biochemistry*. New York and London: Academic Press.

Pitzer, K. S. (1973). Thermodynamics of electrolytes. I. Theoretical basis and general equations. *The Journal of Physical Chemistry, 77*, 268-277.

Pitzer, K. S. (1979). Ion interaction approach: Theory and data correlation *Activity Coefficients in Electrolyte Solutions*. Boca Raton: CRC Press, Inc.

Pitzer, K. S. (1980). Electrolytes. From dilute solutions to fused salts *Journal of The American Chemical Society, 102*, 2902–2906.

Pollard, T. D. (2010). A guide to simple and informative binding assays. *Molecular Biology of the Cell, 21*, 4061-4067.

Posner, A. S., & Betts, F. (1975). Synthetic amorphous calcium phosphate and its relation to bone mineral structure. *Accounts of Chemical Research, 8*, 273-281.

Potter II, R. W., & Brown, D. L. (1977). *The volumetric properties of aqueous sodium chloride solutions from 0˚ to 500˚C at pressure up to 2000 bars based on a regression*

of available data in the literature. Washington: United States Goverment Printing Office.

Pouliot, Y., Landry, J., & Giasson, J. (1991). Induction of calcium phosphate precipitation in sweet whey permeate. *Lait, 71*, 313-320.

Promega. (n.d). Buffers for Biochemical Reactions. from https://worldwide.promega.com/resources/product-guides-and-selectors/protocols-and-applications-guide/buffers-for-biochemical-reactions/. www.promega.com

Ramachandan, S., Fontanille, P., Pandey, A., & Larroche, C. (2006). Gluconic acid: Properties, applications and microbial production. *Food Technology and Biotechnology, 44*, 185-195.

Raynaud, S., Champion, E., Bernache-Assollant, D., & Thomas, P. (2002). Calcium phosphate apatites with variable Ca/P atomic ratio. I. Synthesis, characterisation and thermal stability of powders. *Biomaterials, 23*, 1065-1072.

Reardon, E. J., & Langmuir, D. (1974). Thermodynamic properties of the ion pairs $MgCO_3^\circ$ and $CaCO_3^\circ$ from 10 to 50° C. *American Journal of Science, 274*, 599-612.

Reddy, M. M., & Wang, K. K. (1980). Crystallization of calcium carbonate in the presence of metal ions: I. Inhibitation by magnesium ion at pH 8.8 and 25°C. *Journal of Crystal Growth, 50*, 470-480.

Reimerdes, E. H. (1990). Lactose as a food ingredient *Association of Lactose Manufacturers*. Maarsse, The Netherlands: Expoconsult Publishers.

Reithel, F. J., & Venkataraman, R. (1956). Lactose in the sapotaceae. *American Association for the Advancement of Science, 123*, 1083-1084.

Renner, E. (1983). *Milk and dairy products in human nutrition*. Munich: Volkswirtschaftlicher Verlag.

Rice, G., Barber, A., O'Connor, A., Stevens, G., & Kentish, S. (2010). A theoretical and experimental analysis of calcium speciation and precipitation in dairy ultrafiltration permeate. *International Dairy Journal, 20*, 694-706.

Robinson, R. A., & Stokes, R. H. (1959). *Electrolyte solutions*. London: Butterworths Scientific Publications.

Rosmaninho, R., Rizzo, G., Müller-Steinhagen, H., & Melo, L. F. (2008). Deposition from a milk mineral solution on novel heat transfer surfaces under turbulent flow conditions. *Journal of Food Engineering, 85*, 29-41.

Salis, A., Boström, M., Medda, L., Cugia, F., Barse, B., Parsons, D. F., . . . Monduzzi, M. (2011). Measurements and theoetical interpretation of points of zero charge/potential of BSA protein. *Langmuir, 27*, 11597-11604.

Sanchez-Castro, C., & Blum, L. (1989). Explicit approximation for the unrestricted mean spherical approximation for ionic solutions. *The Journal of Physical Chemistry, 93*, 7478–7482.

Schmidt, D. G. (1982). Association of caseins and casein micelle structure. In P. F. Fox (Ed.), *Developments in Dairy Chemistry* (pp. 61-86). Barking, UK: Applied Science Publishers.

Schmidt, D. G., & Both, P. (1987). Studies on the precipitation of calcium phosphate. I. Experiments in the pH range 5.3 to 6.8 at 25 ˚C and 50 ˚C in the absence on additives. *Netherlands Milk and Dairy Journal, 41*, 105-120.

Shannon, R. D., & Prewitt, C. T. (1969). Effective ionic radii in oxides and flurides. *Acta Crystallographica Section, B25*, 925-946.

Shen, Y., Søndergaard, M., Christensen, M., Birgisson, S., & Iversen, B. B. (2014). Solid state formation mechanism of $Li_4Ti_5O_{12}$ from an anatase TiO_2 source. *Chemistry of Materials (ACS Publications), 26*, 3679-3686.

Shilov, I. Y., & Lyashchenko, A. K. (2015). The role of concentration dependent static permittivity of electrolyte solutions in the Debye-Hückel theory. *The Journal of Physical Chemistry, 119*, 10087-10095.

Simonin, J. P., Blum, L., & Turq, P. (1996). Real ionic solutions in the mean spherical approximation. 1. Simple salts in the primitive model. *The Journal of Physical Chemistry, 100*, 7704-7709.

Smith, R. M., & Martell, A. E. (1976a). *Critical Stability Constants* (Vol. 1-4). New York: Plenum.

Smith, R. M., & Martell, A. E. (1976b). *Critical statbility constants* (Vol. 4: Inorganic Complexes). New York: Plenum Press.

Söhnel, O., & Mullin, J. W. (1982). Precipitation of calcium carbonate. *Journal of Crystal Growth, 60*, 239-250.

Sørensen, S. P. L., Linderstrøm-Lang, K., & Lund, E. (1927). The influence of salts upon the ionisation of egg albumin. *Journal of General Physiology, 8*, 543-599.

Southward, C. R. (1986). Utilisation of milk components: Casein *Modern dairy Technology*. New York, USA: Elsevier Applied Science Publishers.

Southward, C. R. (1998). Casein products (Vol. III-Dairy-E-Casein-12, pp. Consumer and Applications Science Section, New Zealand Dairy Research Institute). New Zealand: The New Zealand Dairy Research Institute.

Spanos, N., Patis, A., Kanellopoulou, D., Andritsos, N., & Koutsoukos, P. G. (2007). Precipitation of calcium phosphate from simulated milk ultrafiltrate solutions. *Crystal Growth and Design, 7*, 25-29.

Spreer, E. (1998). *Milk and Dairy Product Technology*. New York: Marcel Dekker, Inc.

Spuergin, P., Mueller, H., Walter, M., Schiltz, E., & Forster, J. (1996). Allergenic epitopes of bovine αs1–casein recognized by human IgE and IgG. *Allergy, 51*, 306-312.

Stearn, A. E. (1931). The polybasicity of several common sugars. *The Journal of Physical Chemistry, 35*, 2226-2236.

Stokes, R. H. (1991). Thermodynamics of solutions. In K. S. Pitzer (Ed.), *Activity coefficients in electrolyte solutions* (2 ed.). Boca Raton, USA: CRC Press.

Stumm, W., & Morgan, J. J. (1996). *Aquatic chemistry: chemical equilibria and rates in natural waters*. New York: WIley.

Swaisgood, H. E. (2003). Chemistry of the caseins. In P. F. Fox & P. L. H. McSweeney (Eds.), *Advanced Dairy Chemistry-1 Proteins*. Boston, USA: Springer.

Taghikhani, V., & Vera, J. H. (2000). Correlation of activity coefficients in electrolyte solutions using a kelvin hard sphere-mean spherical approximation (K-MSA) model. *Industrial & Engineering Chemistry Research (ACS Publications), 39*, 759-766.

Tew, X. W. (2015). *Fouling and cleaning of reverse osmosis membranes in the dairy industry.* (PhD), University of Canterbury, Christchurch.

Tikanen, A. C., & Fawcett, W. R. (1996). Role of solvent permittivity in estimation of electrolyte activity coefficients for systems with ion pairing on the basis of the Mean Spherical Approximation. *Berichte der Bunsengesellschaft für physikalische Chemie, 100*, 634-640.

Triolo, R., Blum, L., & Floriano, M. A. (1977). Simple electrolytes in the mean spherical approximation. III. A workable model for aqueous solutions. *The Journal of Chemical Physics, 67*, 5956-5959.

Triolo, R., Blum, L., & Floriano, M. A. (1978). Simple electrolytes in the mean spherical approximation. 2. Study of a refined model *The Journal of Physical Chemistry, 82*, 1368-1370.

Triolo, R., Grigera, J. R., & Blum, L. (1976). Simple electrolytes in the mean spherical approximation. *The Journal of Physical Chemistry, 80*, 1858-1861.

Trucco, R. E., Verdier, P., & Rega, A. (1954). New carbohydrate compunds from cow milk. *Biochimica et Biophysica Acta, 15*, 852-853.

Valisko, M., & Boda, D. (2015). Comment on 'The role of concentration dependent static permittivity of electrolyte solutions in the Debye-Hückel theory'. *The Journal of Physical Chemistry B, 119*, 10087-10095.

van Boekel, M. A. J. S. (1996). Kinetic modelling of sugar reactions in heated milk-like systems. *Netherlands Milk and Dairy Journal, 50*, 245-266.

van Boekel, M. A. J. S. (2008). *Kinetic Modeling of Reactions in Foods*. Boca Raton: CRC Press, Taylor & Francis Group.

van Dijk, H. (1990). The properties of casein micelles. 1. The nature of the micellar calcium phosphate. *Netherlands Milk and Dairy Journal, 44*, 65-81.

van Kemenade, M. J. J. M., & de Bruyn, P. L. (1987). A kinetic study of precipitation from supersaturated calcium phosphate solutions. *Journal of Colloid and Interface Science, 118*, 564-585.

Vavrusova, M., Danielsen, B. P., Garcia, A. C., & Skibsted, L. F. (2018). Codissolution of calcium hydrogenphosphate and sodium hydrogencitrate in water. Spontaneous supersaturation of calcium citrate increasing calcium bioavailability. *Journal of Food and Drug Analysis, 26*, 330-336.

Vavrusova, M., Garcia, A. C., Danielsen, B. P., & Skibsted, L. F. (2017). Spontaneous supersaturation of calcium citrate from simultaneous isothermal dissolution of sodium citrate and sparingly soluble calcium hydroxycarboxylates in water. *RSC Advances, 7*, 3078-3088.

Vavrusova, M., Liang, R., & Skibsted, L. F. (2014). Thermodynamics of dissolution of calcium hydroxycarboxylates in water. *Journal of Agricultural and Food Chemistry, 62*, 5675-5681.

Vavrusova, M., Munk, M. B., & Skibsted, L. F. (2013). Aqueous solubility of calcium L-lactate, calcium D-gluconate, and calcium D-lactobionate: Importance of complex formation for solubility increase by hydroxycarboxylate mixtures. *Journal of Agricultural and Food Chemistry, 61*, 8207-8214.

Vavrusova, M., & Skibsted, L. F. (2014). Spontaneous supersaturation of calcium D-gluconate during isothermal dissolution of calcium L-lactate in aqueous sodium D-gluconate. *Food and Function, 5*, 85-91.

Vavrusova, M., & Skibsted, L. F. (2016). Aqueous solubility of calcium citrate and interconversion between the tetrahydrate and the hexahydrate as a balance between

endothermic dissolution and exothermic complex formation. *International Dairy Journal, 57*, 20-28.

Vilariño, T., & Sastre de Vicente, M. E. (1999). The mean spherical approximation methodology applied to the acid–base equilibria of glycine in artifcial seawater. *Physical Chemistry Chemical Physics, 1*, 2453-2456.

Visser, R. A. (1980). A natural crystal growth retarder in lactose. *Netherlands Milk and Dairy Journal, 34*, 255-275.

Visser, R. A. (1984). Experiments for tracing growth retarders in lactose. *Netherlands Milk and Dairy Journal, 38*, 107-133.

Visser, R. A. (1988). Crystal growth retarding of alpha-lactose hydrate by sugar phosphates, a continued study. *Netherlands Milk and Dairy Journal, 42*, 449-468.

Volkov, A. G. (2001). *Liquid interfaces in chemical, biological, and pharmaceutical applications*. New York, The USA: Marcel Dekker, Inc.

Waisman, E., & Lebowitz, J. L. (1972). Mean spherical model integral equation for charged hard spheres I . Method of solution. *The Journal of Chemical Physics, 56*, 3086-3093.

Walstra, P. (1990). On the stability of casein micelles. *Journal of Dairy Science, 73*, 1965-1979.

Walstra, P., & Jenness, R. (1984). *Dairy chemistry and physics*. New York: John Wiley and Sons , Inc.

Walstra, P., Wouters, J., & Geurts, T. J. (2006). *Dairy Science and Technology* (2 ed.). The United States of America: Taylor & Francis Group.

Wasserman, R. H. (1964). Lactose-stimulated intestinal absorption of calcium: a thoery. *Nature, 201*, 997-999.

Waugh, D. F. (1958). The interaction of αs, β- and κ-caseins in micelle formation. *Faraday Society Discuss, 25*, 186-192.

Webb, E. K., Pearman, G. I., & Leuning, R. (1980). Correction of flux measurements for density effects due to heat and water vapour transfer. *Quarterly Journal of the Royal Meteorological Society, 106*, 85-100.

Wei, D., & Blum, L. (1987). The mean spherical approximation for an arbitrary mixture of ions in a dipolar solvent: Approximate solution, pair correlation functions, and thermodynamics. *The Journal of Chemical Physics, 87*, 2999-3007.

White, J. C. D., & Davies, D. T. (1963). Determination of citric acid in milk and milk sera. *Journal of Dairy Research, 30*, 171-189.

Wiechers, H. N. S., Sturrock, P., & Marais, G. V. R. (1975). Calcium carbonate crystallization kinetics. *Water Research, 9*, 835-845.

Wikipedia. (n.d). Carbonic acid.

Williamson, A. G. (1967). *An introduction to non-electrolyte solutions*. Edinburgh, London: Oliver & Boyd.

Wong, D. W. S., Camirand, W. M., & Pavlath, A. E. (1996). Structures and functionalities of milk proteins. *Critical Reviews in Food Science and Nutrition, 36*, 807-844.

Wood, G. B., Reid, D. S., & Elvin, R. (1981). Calculation by computer of individual concentrations in a simulated milk salt solution. I. *Journal of Dairy Research, 48*, 77-83.

Ye, A. (2008). Complexation between milk proteins and polysaccharides via electrostatic interaction: principles and applications – a review. *International Journal of Food Science and Technology, 43*, 406-415.

Zadow, J. G. (1991). Lactose utilization *CSIRO Food Research Quarterly, 51*, 99-106.

Zadow, J. G. (2005). Review and report on whey utilization. Mardialloc, Victoria, Australia: Report for the Dairy Reserach and Development Corporation.

Zeebe, R. E., & Wolf-Gladrow, D. (2001). *CO_2 in seawater: Equilibrium, kinetics, isotopes*. Amsterdam, The Netherlands: Elsevier Oceanography Series.

Zemaitis, J. F., Clark, D. M., Rafal, M., & Scrivner, N. C. (1986). *Handbook of Aqueous Electrolyte Thermodynamics*. New York: American Institute of Chemical Engineers, INC.

Zhang, Y., & Brew, K. (2003). Alpha-lactalbumin. In H. Roginski, J. W. Fuquay & P. F. Fox (Eds.), *Encyclopedia of Dairy Sciences* (Vol. 3). London: Academic Press.

Appendix 1: MATLAB scripts for the NPMSA parameters

The following is a comparison between the NPMSA parameters (Γ, B^{10}, and b_2) calculated based on the variables and units given in Table 2.16 and the literature data from Wei and Blum (1987).

```
function RunFreeIonActCoeffNonPrimitiveLiuWeiBlumScaledNaCl
%============================================================
% The aim of writing this code is to see if the NPMSA parameters are fitted with
% the data from Wei and Blum, 1987.
% Written by Pariya Noeparvar on 12/08/2016 and updated on 30/08/2016.
% Last updated on 04/10/2018.
% The values started with upper case symbols represent Greek capital letters.
% References: Liu, 1998; Wei and Blum, 1987.
%============================================================
% Initial guess of three variable to solve for validation with the
% literature data
close all
% Initial guesses for the NPMSA parameters
Gamma=0.45;   %  1/nm
B10=0.02;  % nm²
b2=2;  % dimensionless
x0=[Gamma; B10; b2];  % Newton initial guess
niter=8000;   % Number of iterations
tolerance=1e-6;   % Tolerance
i=1;
param(1)=[i];
NaCl=logspace(-5, 0.465, 20); %Concentrations of NaCl solution, mol/L
param(2)=1e-3;
    for j=1: length(NaCl)
            if j>1
            x0=[Gamma(j-1); B10(j-1); b2(j-1)];
            end
    param(2)=NaCl(j);
    results=Newton(@NewtonEquns, x0,niter,tolerance, param);
    Gamma(j)=results(end,2);
    B10(j)=results(end,3);
    b2(j)=results(end,4);
    fprintf('NaCl = %5.3g, Gamma = %5.10g, B10 = %5.10g, b2 = %5.10g \n', NaCl(j), Gamma(j),
    B10(j), b2(j))
    % calc act coeff
    % call function
    lnf_x=CalcActCoeff(Gamma(j), B10(j), b2(j), param);   % return a vector of activity
    coefficients for all ions.
    fprintf('ln(f_i) %10.4f  %10.4f  %10.4f \n', lnf_x)
    end
% Literature values from Wei and Blum, 1987.
WeinBlum_conc=[ 0   0.5    1    1.5    2     2.5     3];
Gamma_Wei=zeros(1,7);
```

```
B10_Wei=[  0  0.3   0.4    0.5    0.6    0.7    0.75];
b2_Wei=[ 0 1.75  1.6 1.4  1.25  1.1  1.0];
figure
plot(NaCl, Gamma,'k')
ylim([-0.1 8])
hold on
plot(WeinBlum_conc, Gamma_Wei,'k+')
xlabel('NaCl concentration, mol/L', 'fontsize',13)
ylabel('\Gamma, nm^-^1', 'fontsize',13)
set(gca,'fontsize',13)
figure
plot(NaCl, B10,'k-')
hold on
plot(WeinBlum_conc, B10_Wei,'k+')
xlabel('NaCl concentration, mol/L','fontsize',13)
ylabel('B^1^0, nm^2','fontsize',13)
set(gca,'fontsize',13)
figure
plot(NaCl, b2,'k-')
hold on
plot(WeinBlum_conc, b2_Wei,'k+')
xlabel('NaCl concentration, mol/L','fontsize',13)
ylabel('b_2, [-]','fontsize',13)
legend('This study',' Wei and Blum, 1987')
set(gca,'fontsize',13)
end

function f=NewtonEquns(x, param, flag)
% Call Newton's method
[f, lnf_x]=FreeIonActCoeffNonPrimitive(x, param, flag);
End

function lnf_x=CalcActCoeff(Gamma, B10, b2, param)
% Activity coefficient calculation
flag='Act';
x=[Gamma; B10;b2];
[f, lnf_x]=FreeIonActCoeffNonPrimitive(x, param, flag);
End

function [f, lnf_x]= FreeIonActCoeffNonPrimitive(x, param, flag)
%=================================================================
% This function will solve free–ion activity coefficient by the NPMSA method.
%=================================================================
Scale=1e7;     % scale to convert cm to nm
i=param(1);
NaCl=param(2);
sigma=Scale*[0.19e-7; 0.365e-7; 0.52e-7];   % Wei and Blum 1987
sigma_d=Scale*0.265e-7;   %  Ion size parameter of water,nm  % Wei and Blum 1987
z=[1; -1; 0];       % charge numbers of Na+, Cl- and NaCl°
N_AV=6.022e23;    % Avogadro's number, mol^-1
Na=NaCl;     % Concentrations of Na+ solution, mol/L
```

```
Cl=NaCl;    % Concentrations of Cl- solution, mol/L
NaCl_0=1e-16;  %Concentrations of NaCl° solution, mol/L
rho=(1/Scale^3)*(N_AV*1e-3).*[Na(i); Cl(i); NaCl_0(i)];  % Number of particle per cm³ or nm³
rho_water=(1/Scale^3)*WaterConc(NaCl(i),25).*N_AV.*1e-3;    % Number of particle per cm³
or nm³
density=NaClDensityMolar(NaCl(i), 25)/1000;   % Density of the solution, kg/L
M=[0.0229898;  0.035453;  0.0229898+0.035453];   % Molar mass, kg/mol
% Molality of each species
m_NaCl=convertCtoM(NaCl(i),M(3,:),density);  %molality, mol/kg_water
m_Na=convertCtoM(Na(i),M(1,:),density);  %molality, mol/kg_water
m_Cl=convertCtoM(Cl(i),M(2,:),density);  %molality, mol/kg_water
m_NaCl_0=convertCtoM(NaCl_0(i),M(3,:),density);  %molality, mol/kg_water
%Mole fraction of each species
x_NaCl=molalitytomolefraction(m_NaCl(i));
x_Na=molalitytomolefraction(m_Na(i));
x_Cl=molalitytomolefraction(m_Cl(i));
x_NaCl_0=molalitytomolefraction(m_NaCl_0(i));
x_solv=1-(x_Na(i)+x_Cl(i)+x_NaCl_0(i));
k_B=Scale^2*1.38064852e-23*1e7;   % Boltzmann constant, nm².g.s^-2,K^-1
T=25+273.15;    % Absolute temperature, K
e=Scale^1.5*4.80320427e-10;    % electron charge, statC=g^0.5 cm^1.5.s^-1
% All variables are first defined to be able to solve three non-linear equations by Newton's
method.
beta=1/(k_B*T);
d_0=sqrt(4*pi*beta*e^2);   % nm
mu=Scale^2.5*2.21e-18;    %Dipole moment of water,1Debye=1e-18 StatCoulomb.cm
d_2=sqrt((4*pi*beta*mu.^2)/3);  % nm³
% initial guess of three variables of NPMSA
Gamma=x(1);
B10=x(2);
b2=x(3);
% NPMSA variables
beta_3=1+(b2/3);
beta_6=1-(b2/6);
lambda=beta_3/beta_6;
xi_0=pi./6*(sum(rho.*sigma.^0)+(rho_water.*sigma_d^0));
xi_1=pi./6*(sum(rho.*sigma.^1)+(rho_water.*sigma_d^1));
xi_2=pi./6*(sum(rho.*sigma.^2)+(rho_water.*sigma_d^2));
xi_3=pi./6*(sum(rho.*sigma.^3)+(rho_water.*sigma_d^3));
Delta=1-xi_3;
P_hs_term=(xi_0./Delta)+((3*xi_1.*xi_2)./Delta.^2)+(((3-xi_3).*xi_2.^3)./Delta.^3);
w1=sum((rho.*z.^2) ./(beta_6.*(sigma_d+lambda*sigma).*(1+Gamma*sigma)));
y1=4/(beta_6*(1+lambda)^2);
w2=0.5*rho_water*sigma_d^2*B10* ...
sum((rho.*z.^2.*sigma_d.^2)./(2*beta_6.*(sigma_d+(lambda.*sigma)).*(1+Gamma.*sigma)).^
2);
nu_eta=((-w1/2)+sqrt(((w1/2).^2)+((2*B10*w2)/beta_6^2)))./w2;
Delta_Gamma=(nu_eta*rho_water*sigma_d^2*sigma.^2*B10)./(8*beta_6*(sigma_d+(lambda
*sigma)));
D_F=(z*beta_6)./(2*(1+(sigma*Gamma)-Delta_Gamma));
```

```
D=1+(nu_eta^2*rho_water*sigma_d^2)*sum(rho.*sigma.^2.*D_F.^2./(2*beta_6*(sigma_d+la
mbda*sigma)).^2);
Gamma_s=((1+(sigma*Gamma)-Delta_Gamma).*D-1)./sigma;
m=(nu_eta*D_F)./(sigma_d+(lambda*sigma));
D_ac=sum(rho.*(D_F.^2));
Omega_10=nu_eta*sum(rho.*sigma.*D_F.^2./(sigma_d+lambda*sigma));
N=(2.*D_F./beta_6.*sigma).*(1+((rho_water.*sigma_d.^3.*B10.*nu_eta.*sigma)./24.*(sigma_
d+lambda.*sigma)))-(z./sigma);
a_0=beta_6*Gamma_s.*D_F./D_ac;
a_nI=(beta_6*D/(2*D_ac))*(sigma_d*B10*0.5+Omega_10*lambda/(D*beta_6));
k_n10=-(sigma_d^2*D_F/(2*D*beta_6^2).*(nu_eta./(sigma_d+lambda*sigma)+ ...
Omega_10.*Gamma_s/D_ac)+sigma_d^3*B10*a_0/(12*beta_6)); % vector
one_rho_k_nm11=1/(D*beta_6)*(lambda+rho_water*sigma_d^2*Omega_10*a_nI/(2*beta_6
^2))+ ...
rho_water*sigma_d^3*B10*a_nI/(12*beta_6);
% 1 - rho_n k_nm11
% Three equations which should be solved by Newton's method, are presented here.
f=zeros(3,1);
f(1)=  (sum(rho.*a_0.^2)+rho_water*a_nI^2-d_0^2);
f(2) =(-sum(rho.*a_0.*k_n10)+a_nI*one_rho_k_nm11-d_0*d_2);
f(3)=one_rho_k_nm11^2+rho_water*sum(rho.*k_n10.^2)-(y1^2+rho_water*d_2^2);
    if strcmp(flag, 'converged')
    dummy=1;
    end
    if strcmp(flag, 'maxiterations')
        dummy=1;
    end
        if  strcmp(flag, 'Act')
        Beta_Mu_hs=-
        log(Delta)+P_hs_term*sigma.^3+(3*sigma.*(xi_2+xi_1*sigma))./Delta+((9*xi_2^2*sigm
        a.^2)./(2*Delta^2))+ ...
        ((3*(xi_2*sigma/xi_3).^2).*(log(Delta)+(xi_3/Delta)-(xi_3/Delta)^2/2))- ...
        (((xi_2*sigma./xi_3).^3)*(2*log(Delta)+xi_3*(1+Delta)/Delta));  % dimensionless
        Beta_Mu_MSA=(z.*(d_0^2.*N-d_0*d_2*rho_water*m))/(4*pi);  %dimensionless
        Beta_Mu_ex=Beta_Mu_MSA+Beta_Mu_hs;
        % The actual equation is Ln f_x=exp(beta[μ(xi)-μ(xi to 0)], in which
        % f_x is free ion activity coeffcient based on mole fraction scale.
        lnf_x=Beta_Mu_ex;   %-exp(Beta_Mu_ex_x_0);
        else
        lnf_x=zeros(3,1);
        end
end

function water=WaterConc(MolarConc, T_C)
% Concentration of water in the solution.
MW_NaCl=58.44;   % g/mol
MW_water=18.01528;   % g/mol
water=(1000-((MolarConc.*MW_NaCl)./(NaClDensityMolar(MolarConc,T_C)/1000))) ...
.*(NaClDensityMolar(MolarConc,T_C)./(1000.*MW_water));    %mol/L
End
```

```
function density=NaClDensityMolar(MolarConc, T_C)
% Calculation of density (kg/m3) of a NaCl solution given molar concentration
% T_C is temperature in ˚C  based on 25 ˚C
% mole conc in mol/L of NaCl
density = waterdensity(T_C) *((-6.44E-4.*MolarConc.^2 + 4.04E-02.*MolarConc) + 1.00E+00);
% kg/m3
end

function density=waterdensity(T_C)
% From Kell JCED 1975 p97
density = (999.83952 + 16.945176 * T_C - 0.0079870401 * T_C ^ 2 - 0.000046170461 * T_C ^ 3
+ 0.00000010556302 * T_C ^ 4 - 2.8054253E-10 * T_C ^ 5) / (1 + 0.01687985 * T_C);
End

function m=convertCtoM(C,M, density)
% convert concentrations from molar to molal
% C is a vector of all the species (could be ions) in the solution in mol/L
% M is a vector of the corresponding molecular masses of the species kg/mol
% density input is kg/L
% output m is vector of molal concentrations mol/kgwater
m=C./(density.*(1- (sum(C.*M))./density));
end

function x=molalitytomolefraction(m)
% convert concentrations from molal to mole fraction
% m is a vector of all the species (could be ions) in the solution in mol/kgwater
% MWwater is molecular masses of the water kg/mol
% output x is vector of mole fraction concentration concentrations.
x=m./(1/0.018528+sum(m));
end
```

Appendix 2: Density of sodium chloride solution

The following is the density calculation of sodium chloride solution as a function of molar concentration of sodium chloride.

Generally, density of a solution is calculated from the weighted mass fraction ($w_i, [-]$) and density ($\rho_i, \left[\frac{\text{kg}}{\text{m}^3}\right]$) of all corresponding species including solvent (water) in a multicomponent solution:

$$\frac{1}{\rho_{soln}} = \sum_{i=1} \left(\frac{w_i}{\rho_i}\right) \tag{A.2.1}$$

Kell (1975) explored an equation for the water density ($\rho, \left[\frac{\text{kg}}{\text{m}^3}\right]$) depending on the temperature ($T, [°\text{C}]$) as:

$$\rho_{water} = \frac{999.83+16.94\,T-7.98\times10^{-3}T^2-4.61\times10^{-5}\times T^3+1.05\times10^{-7}\times T^4-2.80\times10^{-10}T^5}{1000\times(1+1.68\times10^{-2}\times T)} \tag{A.2.2}$$

Potter II and Brown (1977) complied the density of sodium chloride solution as a function of various weighted mass fraction at different temperature as indicated by Table A.2.1.

Then, relative density ($[-]$) was obtained for different mass fraction values for a particular temperature (Webb et al., 1980) as:

$$\text{Relative density} = \frac{\rho_i}{\rho_{water}} \tag{A.2.3}$$

The corresponding molar concentration ($C_i, [\text{mol L}^{-1}]$) of each relative density was then calculated as:

$$C_i = \frac{w_i\,\rho_i}{M_w} \tag{A.2.4}$$

Here M_w is the molecular weight (kg mol^{-1}) of the salt which is sodium chloride in this case.

Figure A.2.1 shows the relative density in terms of the molar concentration of NaCl at 25 ˚C that gives an equation for calculation of the density of solution as a function of molar concentration as:

$$\text{Density of NaCl solution} = -6.44 \times 10^{-4} C_{NaCl} + 4.04 \times 10^{-2} C_{NaCl} + 1.00 \quad \text{(A.2.5)}$$

Table A.2.1 Density of NaCl solution in terms of different mass fraction and temperature (Potter II and Brown, 1977).

Mass fraction, (w/w%)	$\rho_{NaCl_{soln}}, \left[\frac{\text{kg}}{\text{L}}\right]$				
	0, [°C]	25, [°C]	50, [°C]	75, [°C]	100, [°C]
0	0.99984	0.99704	0.98803	0.97485	0.95836
0.01	1.00755	1.00411	0.99480	0.98160	0.96300
0.03	1.02283	1.01823	1.00850	0.99520	0.97900
0.05	1.03814	1.03247	1.02220	1.00900	0.99300
0.07	1.05354	1.04688	1.03620	1.02290	1.00700
0.09	1.06908	1.06146	1.05030	1.03720	1.02100
0.11	1.08476	1.07624	1.06470	1.05160	1.03500
0.13	1.10060	1.09122	1.07930	1.06630	1.04900
0.15	1.11660	1.10639	1.09420	1.08130	1.06300
0.17	1.13276	1.12176	1.10930	1.09650	1.07800
0.19	1.14906	1.13732	1.12470	1.11190	1.09300
0.21	1.16551	1.15307	1.14030	1.12770	1.10900
0.23	1.18210	1.16900	1.15610	1.14360	1.12500
0.25	1.19880	1.18509	1.17220	1.15980	1.14200

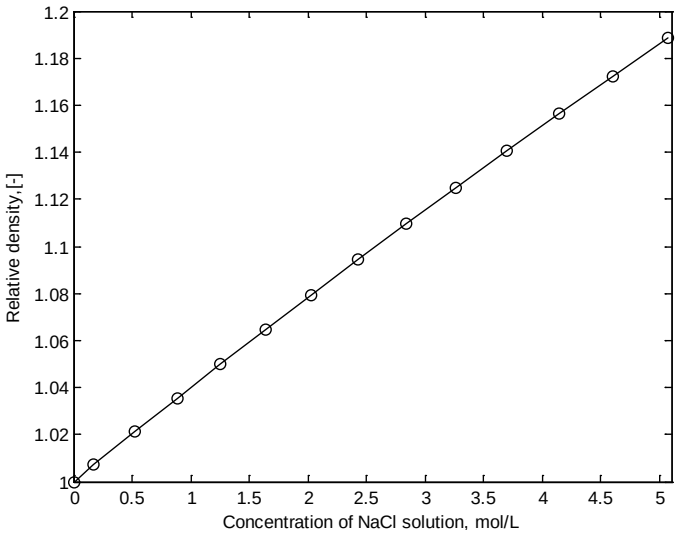

Figure A.2.1 Relative density of NaCl solution vs NaCl molar concentration.

Appendix 3: Milk components sizes

The following section shows the estimated sizes of milk components used in the MSA theory. The anions and ion–pairs formed by the H^+ interactions sizes were assumed larger than other ion–pairs.

Table A.3 Numerical values of size for each component in milk.

		Ca^{2+}, 0.8 nm		Mg^{2+}, 0.4 nm		Na^+, 0.365 nm		K^+, 0.45 nm		H^+, 0.226 nm	
Anions	Size, nm	Ion–pair	Size, nm	Ion–pair	Size, nm	Ion–pair	Size, nm	Ion–pair	Size, nm	Ion–pair	Size, nm
H_2Cit^-	0.65	CaH_2Cit^+	0.4	MgH_2Cit^+	0.5	NaH_2Cit	0.25	KH_2Cit	0.3	H_3Cit	0.55
$HCit^{2-}$	0.75	CaHCit	0.4	MgHCit	0.5	$NaHCit^-$	0.25	$KHCit^-$	0.3	H_2Cit^-	0.55
Cit^{3-}	0.65	$CaCit^-$	0.4	$MgCit^-$	0.5	$NaCit^{2-}$	0.25	$KCit^{2-}$	0.3	$HCit^{2-}$	0.55
$H_2PO_4^-$	0.69	$CaH_2PO_4^+$	0.4	$MgH_2PO_4^+$	0.5	NaH_2PO_4	0.25	KH_2PO_4	0.3	H_3PO_4	0.55
HPO_4^{2-}	0.35	$CaHPO_4$	0.4	$MgHPO_4$	0.5	$NaHPO_4^-$	0.25	$KHPO_4^-$	0.3	$H_2PO_4^-$	0.55
PO_4^{3-}	0.65	$CaPO_4^-$	0.4	$MgPO_4^-$	0.5	$NaPO_4^{2-}$	0.25	KPO_4^{2-}	0.3	HPO_4^{2-}	0.55
HCO_3^-	0.6	$CaHCO_3^+$	0.4	$MgHCO_3^+$	0.5	$NaHCO_3$	0.25	$KHCO_3$	0.3	H_2CO_3	0.55
CO_3^{2-}	0.6	$CaCO_3$	0.4	$MgCO_3$	0.5	$NaCO_3^-$	0.25	KCO_3^-	0.3	HCO_3^-	0.55
HSO_4^-	0.6	$CaHSO_4^+$	0.4	$MgHSO_4^+$	0.5	$NaHSO_4$	0.25	$KHSO_4$	0.3	H_2SO_4	0.55
SO_4^{2-}	0.6	$CaSO_4$	0.4	$MgSO_4$	0.5	$NaSO_4^-$	0.25	KSO_4^-	0.3	HSO_4^-	0.55
$Glc–1–PH^-$	0.6	$CaGlc–1–PH^+$	0.4	$MgGlc–1–PH^+$	0.5	NaGlc–1–PH	0.25	KGlc–1–PH	0.3	$Glc–1–PH_2$	0.55
$Glc–1–P^{2-}$	0.6	CaGlc–1–P	0.4	MgGlc–1–P	0.5	$NaGlc–1–P^-$	0.25	$KGlc–1–P^-$	0.3	$Glc–1–PH^-$	0.55

Cl^-	0.365	$CaCl^+$	0.5	$MgCl^+$	0.5	NaCl	0.36	KCl	0.3	HCl	0.4
$RCOO^-$	0.6	$CaRCOO^+$	0.4	$MgRCOO^+$	0.5	NaRCOO	0.25	KRCOO	0.3	RCOOH	0.55
Arg	0.6	$CaArg^{2+}$	0.4	$MgArg^{2+}$	0.5	$NaArg^+$	0.25	$KArg^+$	0.3	$ArgH^+$	0.55
Asp^-	0.6	$CaAsp^+$	0.4	$MgAsp^+$	0.5	NaAsp	0.25	KAsp	0.3	AspH	0.55
Cys	0.6	$CaCys^+$	0.4	$MgCys^+$	0.5	NaCys	0.25	KCys	0.3	CysH	0.55
Glu^-	0.6	$CaGlu^+$	0.4	$MgGlu^+$	0.5	NaGlu	0.25	KGlu	0.3	GluH	0.55
His	0.6	$CaHis^{2+}$	0.4	$MgHis^{2+}$	0.5	$NaHis^+$	0.25	$KHis^+$	0.3	$HisH^+$	0.55
Lys	0.6	$CaLys^{2+}$	0.4	$MgLys^{2+}$	0.5	$NaLys^+$	0.25	$KLys^+$	0.3	$LysH^+$	0.55
Ser^-	0.6	$CaSer^+$	0.4	$MgSer^+$	0.5	NaSer	0.25	KSer	0.3	SerH	0.55
Thr^-	0.6	$CaThr^+$	0.4	$MgThr^+$	0.5	NaThr	0.25	KThr	0.3	ThrH	0.55
Tyr^-	0.6	$CaTyr^+$	0.4	$MgTyr^+$	0.5	NaTyr	0.25	KTyr	0.3	TyrH	0.55
$((SerP)_3H_2)^{-4}$	0.45	$((SerP)_3H_2Ca)^{-2}$	0.5	$((SerP)_3H_2Mg)^{-2}$	0.5	$((SerP)_3H_2Na)^{-3}$	0.25	$((SerP)_3H_2K)^{-3}$	0.3	$((SerP)_3H_3)^{-3}$	0.55
$((SerP)_3H)^{-5}$	0.45	$((SerP)_3CaH)^{-3}$	0.5	$((SerP)_3HMg)^{-3}$	0.5	$((SerP)_3HNa)^{-4}$	0.25	$((SerP)_3HK)^{-4}$	0.3	$((SerP)_3H_2)^{-4}$	0.55
$((SerP)_3)^{-6}$	0.45	$((SerP)_3Ca)^{-4}$	0.5	$((SerP)_3Mg)^{-4}$	0.5	$((SerP)_3Na)^{-5}$	0.25	$((SerP)_3K)^{-5}$	0.3	$((SerP)_3H)^{-5}$	0.55
$((SerP)_3Ca_2)^{-2}$	0.35	$((SerP)_3Ca_3)$	0.5	$((SerP)_3Ca_2Mg)$	0.5	$((SerP)_3Ca_2Na)^{-1}$	0.25	$((SerP)_3Ca_2K)^{-1}$	0.3	$((SerP)_3Ca_2H)^{-1}$	0.55
$((SerP)_3CaH)^{-3}$	0.35	$((SerP)_3Ca_2H)^{-1}$	0.5	$((SerP)_3CaHMg)^{-1}$	0.5	$((SerP)_3CaHNa)^{-2}$	0.25	$((SerP)_3CaHK)^{-2}$	0.3	$((SerP)_3H_2Ca)^{-2}$	0.55
$((SerP)_3Ca)^{-4}$	0.45	$((SerP)_3Ca_2)^{-2}$	0.5	$((SerP)_3CaMg)^{-2}$	0.5	$((SerP)_3CaNa)^{-3}$	0.25	$((SerP)_3CaK)^{-3}$	0.3	$((SerP)_3CaH)^{-3}$	0.55
$PSerH^-$	0.65	$PSerHCa^+$	0.5	$PSerHCa^+$	0.5	PSerHNa	0.25	PSerHK	0.3	$PSerH_2$	0.55
$PSer^{2-}$	0.65	PSerCa	0.5	PSerCa	0.5	$PSerNa^-$	0.25	$PSerK^-$	0.3	$PSerH^{-a}$	0.55
OH^-	0.28	$CaOH^+$	0.5	$MgOH^+$	0.5	NaOH	0.25	KOH	0.3	H_2O	0.55

Appendix 4: MATLAB scripts for Newton's and Jacobian functions

The following section is a MATLAB script for Newton's and Jacobian methods to calculate ion equilibria non–linearly for any dairy liquids.

```
function x=MyNewton(func,x,maxits,tol, lb, ub, flag)
%=============================================================
% solves a set of equations given by the function func using Newton's method
% Inputs: func file handle for function that gives f(y)
% x0: initial guess of vector x, same dimension as f
% tol: convergence tolerance
% Outputs: x: solution vector
%=============================================================
    if strcmp(flag, 'start')
    relaxation=0.5;
    else
    relaxation=1;
    end
    for k=1:maxits
    f=func(x);
    J=jacobian(func,x);
    deltax=-J\f;
    x=x+relaxation*deltax;
    x(x<lb)=lb(x<lb);      % limit to lower bound
    x(x>ub)=ub(x>ub);
    normx=norm(deltax);
    normf=norm(f);
        if normx<tol && normf < tol
        convergence=true;
        fprintf('%3i iterations: normf %5.3g ',k, normf)
        break
        end
        if k>=10
        dummy=1;
        end
    end
    if k>=maxits
    fprintf('Not converged after %3i iterations ',k)
    end
end

function J=jacobian(func, x)
%=============================================================
% Jacobian function generates a numerical Jacobian matrix of partial derivatives
% Call: J=jacobian(func, x)
% Inputs: func - function handle for function to return column
% Vector f=f(x), dimension m
% x: vector of values at which to evaluate the Jacobian dimension n
% Outputs: f: column vector for f(x)
```

```
% J: matrix of partial derivatives m rows by n columns
% Written by Ken Morison, 7 July 2004, and modified slightly
% by John Hannah, 11 August 2006
% Get unperturbed f(x)
%=============================================================
n=max(size(x));        % find the maximum dimension  of x
f0=func(x);      % evaluate function with unperturbed x
transposef=0;
    if size(f0,2)>size(f0,1)    % a row vector. Give warning and transpose
    disp('Warning from Jacobian.m. Your function should return f(x) as a column vector.
    Transpose your result')
    f0=f0';
    transposef=1;
    end
    for i=1:n   % x(i)
    deltax=x(i)*1e-7;
    x0=x(i);
        if abs(x0)< 1e-9     % for values of x close to zero, ensure a non-zero perturbation
        deltax=1e-9;
        end
    x(i)=x(i)+deltax;
    f=func(x);   % perturbed function
        if transposef==1     % f needs to be transposed
        f=f';          % transpose f
        end
    J(:,i)=(f-f0)./deltax;
    x(i)=x0;   % return to original value
    end
end   % end of Jacobian function
```

Appendix 5: MATLAB scripts for sodium chloride solution

The following section is a MATLAB script for the calculation of sodium chloride solution by using the free–ion approach.

```
function SolveNaClFreeionMSA
%=================================================================
% This function will solve the ion equilibria of sodium chloride (NaCl) solution for free–ion
approach.
% Written by Pariya Noeparvar.
% Last updated on 24/04/2018.
%=================================================================
close all
global y
global z
NaCl=1*[logspace(-1,0,100) logspace(0.01, 6.6,100)];    %  total amount of NaCl added, µmol/L
tol=1e-10;
maxits=1000;
    for i=1 : length(NaCl)
        if i==1
        % Initial guess
        %Cl          OH            Na          H            NaCl°          NaOH        HCl, µmol/L
        x=[NaCl(i); 0.40*NaCl(i); NaCl(i); 0.1*100; 0.5*NaCl(i); 0.5*NaCl(i);0.4*NaCl(i)];
        end
    x0=x ;     % use previous solution
    lb=zeros(length(x),1);
    ub=NaCl(i)*ones(length(x),1);
    ub(1)=NaCl(i);
    ub(2)=1e6;   % i.e. 1 mol/L  pH 14
    ub(4)=1e6;    % pH 0
    fanon=@(x) MyEquations(x, NaCl(i));
    x=MyNewton(fanon,x0,maxits, tol, lb, ub);
    xsol(:,i)=x;     % record last solution
    pH(i)=-log10(xsol(4,i)/1e6);
    Na(i)=xsol(3,i)/1e6;  % free sodium concentration, mol/L
    Cl(i)=xsol(1,i)/1e6;   %  free chloride concentration, mol/L
    y_Na(i)=y(3);   % Molar activity coefficient of free sodium
    y_Cl(i)=y(1);   % Molar activity coefficient of free chloride
    fprintf(' NaCl   pH  %5.2g  %5.2f  \n', NaCl(i), pH)
    IM(i)=0.5*sum((xsol(:,i)/1e6).*z.^2);   % Molar ionic strength, mol/L
    y_davies=Davies(z, IM);   % Activity coefficient by Davies theory
    y_DH=DH(z,IM);    % Activity coefficient by Debye-Hückel theory
    DH_Na=y_DH(3,:);   % Activity coefficient of free sodium by Debye-Hückel theory
    end
Exp_Na=[0 -0.1 -0.13    -0.27   -0.33 -0.4  -0.5  -0.48   -0.3  -0.1 0.1];  % Activity coefficient of free
sodium from Wilczek-Vera et al., 2004
sqrt_NaCl=[0 0.1 0.15  0.35   0.48   0.7   1    1.3   1.6   1.8   2];  % squared molar concentration of
NaCl, (mol/L)^½
```

```
Exp_Cl=[ 0  -0.1  -0.13  -0.3  -0.42  -0.5  -0.58  -0.62 -0.57 -0.49  -0.40 ];  % Activity coefficient of free chloride from Wilczek-Vera et al., 2004
plot(sqrt(NaCl/1e6), log(y_Na),'k')
hold on
xlabel('\surd NaCl concentration, (mol/L)^{1/2}')
ylabel('ln y, [-]')
plot(sqrt(NaCl/1e6), log(y_Cl),'k--')
plot(sqrt_NaCl, Exp_Na,'ko')
plot(sqrt_NaCl, Exp_Cl,'k^')
plot(sqrt(NaCl/1e6), log(y_Na_Davies),'k:')
plot(sqrt(NaCl/1e6), log(DH_Na), 'k.-')
legend('MSA theory, Na^+', 'MSA theory, Cl^-', 'Wilczek-Vera et al., 2004; Na^+','Wilczek-Vera et al., 2004; Cl^-', 'Davies thoery, Na^+ or Cl^-',' Debye-Hückel thoery, Na^+ or Cl^-','location','southwest')
ylim([-2.6 0.5])
end

function f=MyEquations(x, NaCl_initial)
global z
global y
global sigma
% Intrinsic association constant from Holt et al., 1981
Ka1=0.9/1e6;   % Na+ Cl- NaCl°
Ka2=0.2/1e6;   % Na+ OH- NaOH°
Ka3=10^-9.3/1e6;   % H+ Cl- HCl°
% Cl-  OH- Na+ H+ NaCl°NaOH° HCl°
z=[ -1; -1; 1; 1; 0; 0; 0];  % Charge number of ions
sigma=1e-9*[ 0.44;  0.28; 0.51; 0.226; 0.40;  0.4; 0.4];  % The effective size parameter, m
T=25+273.15;  % Temperature, K
logKw=-4787.3/T-7.1332*log10(T)-0.010365*T+22.801;    % Natural logarithm of the intrinsic association constant of water, Harned and Cook 1937
Kw=10^logKw;  % (mol/L)^2
Kw1=(55.5/Kw)/1e6;
Cl=x(1);
OH=x(2);
Na=x(3);
H=x(4);
NaCl_0=x(5);
NaOH=x(6);
HCl=x(7);
Na_t=NaCl_initial;  % Total concentration of Na, µmol/L
Cl_t=NaCl_initial;    % Total concentration of Cl, µmol/L
Density_soln=NaClDensityMolar((NaCl_initial)/1e6, 25);        % kg/m3
MW_NaCl=58.4/1000;  %  Molar mass of NaCl, kg/mol
MW_water=0.01802;   %Molar mass of water, kg/mol
C_H2O=(Density_soln-NaCl_initial*1e3/1e6*MW_NaCl)/MW_water*1e6/1000;      % mol/m3 converted to µmol/L
f=zeros(7,1);  % the function values
N_A=6.022e23;      % Avogadro's number, 1/mol
rho=x(1:7)/1e6*N_A*1000;  % The number of density, mol/m³
```

```
y=FreeIonMolarActCoeff(z, sigma, rho, (Na+Cl)/1e6);
a=y.*x(1:7);  % Molar activity of the species, µmol/L
f(1)=(Ka1*a(3)*a(1)-a(5))/1e3;      % Na+, Cl-, NaCl°
f(2)=(Ka2*a(3)*a(2)-a(6))/1e3;      % Na+, OH-, NaOH°
f(3)=(Ka3*a(1)*a(4)-a(7))/1e3;    % H+, Cl-, HCl°
f(4)=(Kw1*a(2)*a(4)-C_H2O)/1e9;   % Water equilibrium
f(5)=sum(z.*x(1:7))/sum(x(1:7))/1;  % Electroneutrality
f(6)=(Na_t-(Na+NaCl_0+NaOH))/1e0;   % Total sodium
f(7)=(Cl_t-(Cl+HCl+NaCl_0))/1e0;   % Total chloride
end

function y=FreeIonMolarActCoeff(z, sigma, rho, C_s)   % with considering epsilon_r as function
of Conc
% Mean Spherical aprroximation method: Elecrostatic+hard sphere contributions
% Ref: Van Boekel, 2008
% z in species charge
% sigma is species diameter in m.
% rho is number density,mol/m³
e_0=1.6e-19;   %Electron charge, Coulomb
epsilon_r=78.65-15.45*C_s +3.76*C_s^1.5; % Dielectric constant,[-]
KB=1.38e-23;     % Boltzmann constant, m².kg/s-²K^-1
epsilon_0=8.85e-12;   %Vacuum permitivitty, Farads/m
T=25+273.15;   % Absolute temperature, K
L_B=e_0^2/(4*pi()*epsilon_r*epsilon_0*KB*T);   %Bjerrum distance, m
kappa=sqrt(4*pi*L_B*sum(rho.*z.^2));
Gamma=sqrt(kappa^2/4);
sigma2=sigma.^2;
sigma3=sigma.^3;
Delta=1-(pi/6*sum(sum(rho.*sigma3)));
Omega=1+((pi/2*Delta)*sum((rho.*sigma3)./(1+Gamma*sigma)));
xi=(pi/(2*Omega*Delta))*sum((rho.*sigma.*z)./(1+Gamma*sigma));
% Electrostatic contribution
lny_es=-L_B*((Gamma*z.^2)./(1+Gamma*sigma)+xi*sigma.*((2*z-
xi*sigma2)./(1+Gamma*sigma)+(xi*sigma2)/3).^2);
y_es=exp(lny_es);
X_0=(pi/6)*sum(rho);
X_1=(pi/6)*sum(rho.*sigma);
X_2=(pi/6)*sum(rho.*sigma2);
X_3=(pi/6)*sum(rho.*sigma3);
F1=(3*X_2)/(1-X_3);
F2=(3*X_1/(1-X_3))+(3*X_2^2/(X_3*(1-X_3)^2))+(3*X_2^2*log(1-X_3)/X_3^2);
F3=(X_0-X_2^3/X_3^2)*(1/(1-X_3))+((3*X_1*X_2-(X_2^3/X_3^2))/(1-
X_3)^2)+(2*X_2^3/(X_3*(1-X_3)^3))-(2*X_2^3*log(1-X_3)/X_3^3);
% Hard sphere contribution
y_hs=exp(-log(1-X_3)+sigma.*F1+sigma.^2.*F2+sigma.^3.*F3);
y=exp(log(y_es)+log(y_hs));  % electrostatic contribution+hard sphere contribution
end
```

Appendix 6: Precipitation and dissolution rate constants

Following are the numerical values of precipitation and dissolution rate constants of potential milk solid phases such as DCPD, DCPA, OCP, WH, HAP, CDA, $Mg_3(PO_4)_2$, $CaCO_3$, TCCT, and TCCH, for which lack of sufficient data was found in literature except for $CaCO_3$. These values are required for the dynamic calculation of salt equilibria in milk or milk–like solutions.

Table A.6.1 Precipitation and dissolution rate constant of milk solid phases.

	Precipitation rate constant, min^{-1}	Dissolution rate constant, min^{-1}
DCPD	0.25	0.0001
DCPA	0.9	5
OCP	20	0.1[a]
WH	3	0.1[a]
HAP	4	0.01
CDA	5	0.001
$Mg_3(PO_4)_2$	1	0.01[a]
$CaCO_3$	0.0025 (Kazadi Mbamba, 2016)	0.1
TCCT	0.01	0.0004[a]
TCCH	0.2	0.5[a]

[a] these components had the saturation below 1 and had dissolution.

DCPA and DCPD values were based on the Section 3.7.2.3.

Appendix 7: Chemical structure of amino acids

The following is the amino acids exist in milk proteins regardless of dissociation state with the corresponding dissociation constants on both C– and N–terminuses heads.

Table A.8.1 Chemical structure of milk protein amino acids with the dissociation constants (Fennema, 1996; Belitz and Grosch, 1999; Mercadé-Prieto et al., 2007).

Amino acids	Chemical structure and dissociation constant	Type of the chain	The side group
Alanine	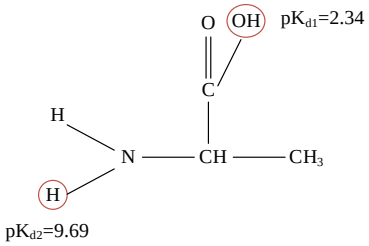	No dissociable and uncharged side chain	–
Arginine	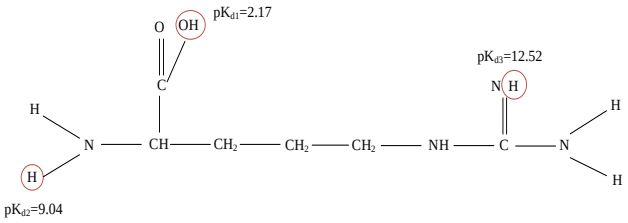	One dissociable positive charged (basic) side group	$–RNH_2$
Asparagine	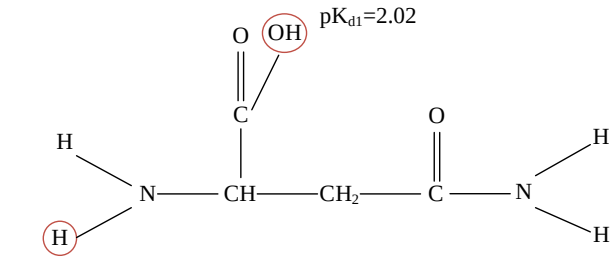	No dissociable and uncharged side chain	–
Aspartic acid	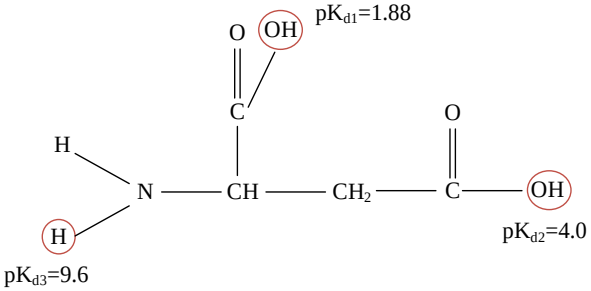	One dissociable negative charged (acidic) side group	–RCOOH

Cysteine	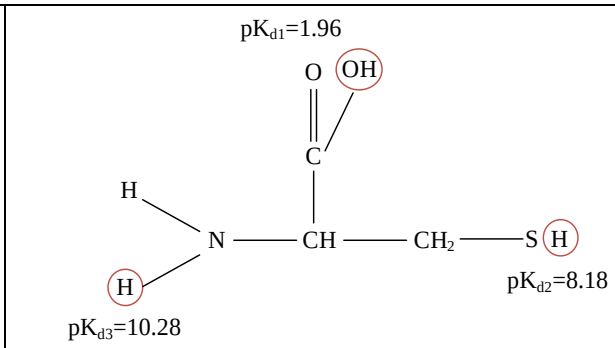	One dissociable negative charged (acidic) side group	–RSH
Glutamine	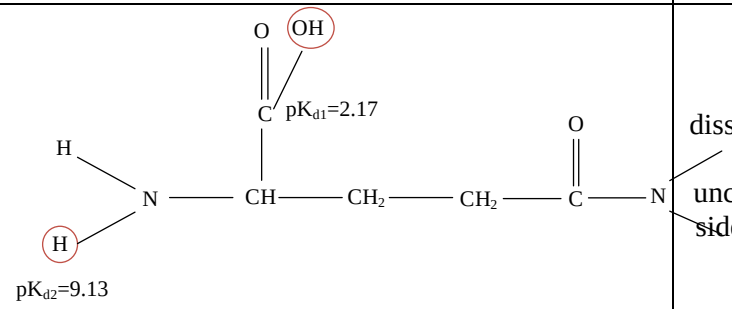	No dissociable and uncharged side chain	–
Glutamic acid	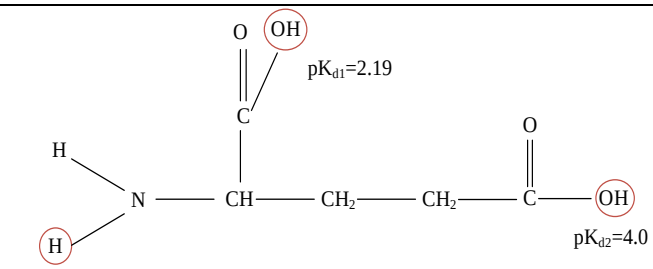	One dissociable negative charged (acidic) side group	–RCOOH
Glycine	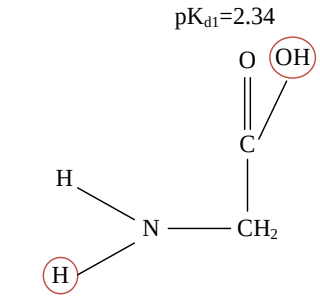	No dissociable and uncharged side chain	–
Histidine	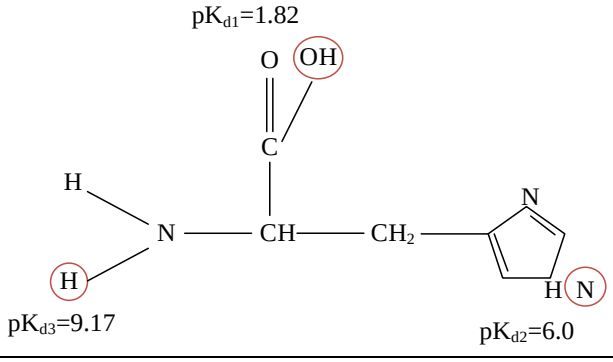	One dissociable positive charged (basic) side group	–RNH

Isoleucine	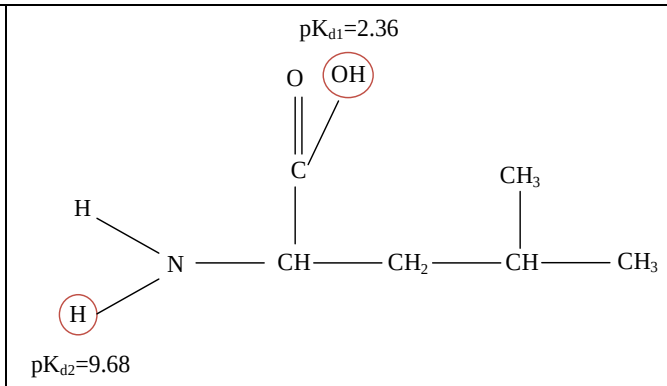	No dissociable and uncharged side chain	–
Leucine	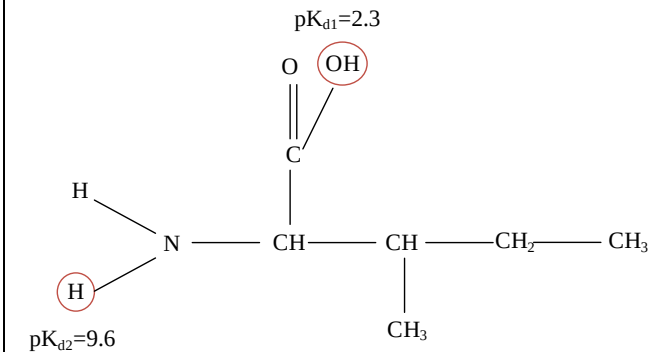	No dissociable and uncharged side chain	–
Lysine	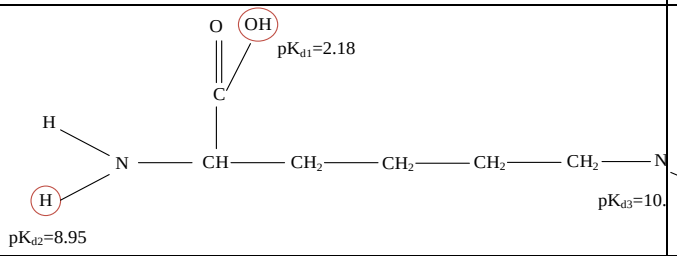	One dissociable positive charged (basic) side group	–RNH$_2$
Methionine	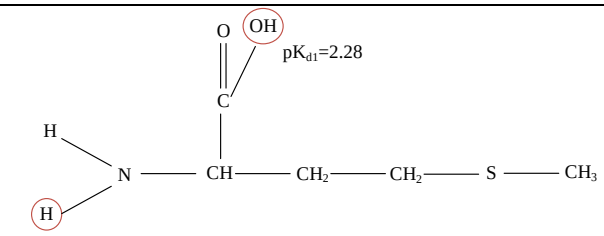	No dissociable and uncharged side chain	–
Phenylalanine	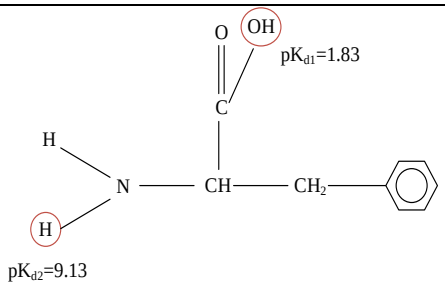	No dissociable and uncharged side group	–
Proline	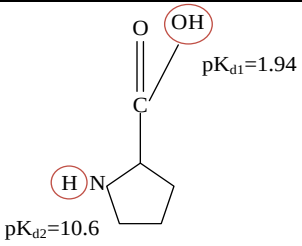	No dissociable and uncharged side group	–

Serine	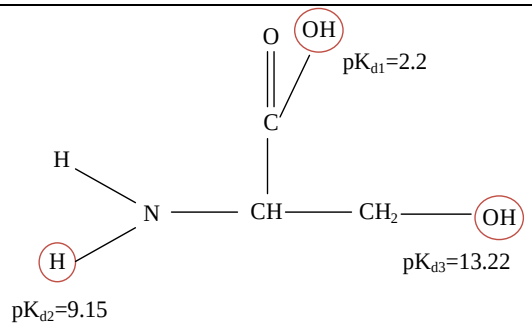	One dissociable negative charged (acidic)s side group	–RCOH
Threonine	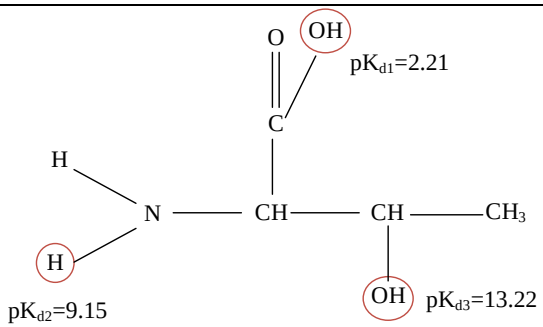	One dissociable negative charged (acidic) side group	–RCOH
Tryptophan	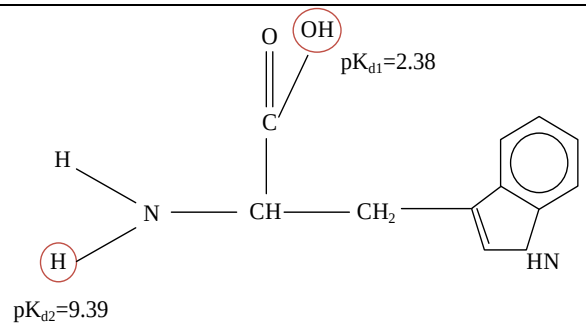	No dissociable and uncharged side group	
Tyrosine	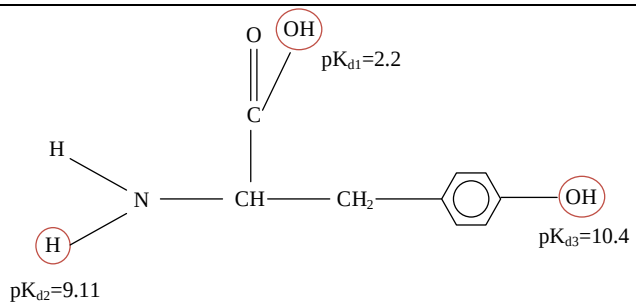	One dissociable negative charged (acidic) side group	–RCOH
Valine	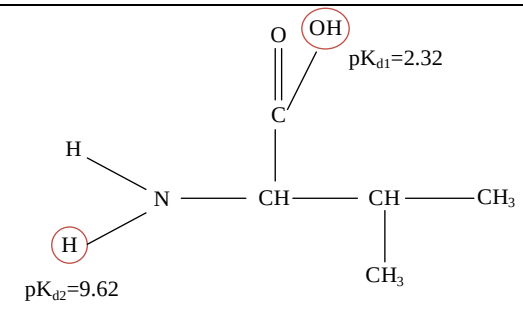	No dissociable and uncharged side group	–

The round red circles represents N–, C– terminuses and/or dissociable side groups.

Appendix 8: MATLAB scripts for milk solution with CPN

The following is the MATLAB scripts for the milk solution including CPN and saturations of the potential solid salts at equilibrium.

```
function SolveMILKCPNSaturation
%=========================================================
% This function will solve the ion equilibria of milk and CPN.
% Written by Pariya Noeparvar, 16 October 2018
% Last updated on 5 November 2018
%=========================================================
global z
global y
close all
nlog=100;
ConcRatio=1;
HCl=[logspace(-6, -1.0, nlog) zeros(1, nlog)]*1e6;    % µmol/L
NaOH=[zeros(1, nlog) logspace(-6, -1.0, nlog)]*1e6;
% There are 32 anions and 5 cations
n_A=32;
n_C=5;
% Association constant
[K_eq]=AssocConstants;
tol=1e-10;  % Tolerance
maxits=100;  % Max iteration
      for j=1 :  length(HCl)
          if j<= nlog
          i=nlog+1-j;
          else
          i=j;
          end
          %   Arg  Asp Cys Glu His Lys Ser Thr Tyr  SerP3
          AAperBLG=[3   10    5    16    2   15    7     8    4     0];  % Amino acid side groups per
          molecule of BLG
          AAperALA=[1    9    8    8     3    12   7     7    4     0 ];  % Amino acid side groups per
          molecule of ALA
          AAperBld=[  23  42  35   62   17  60   28  34    19  0];  % Amino acid side groups per molecule
          of Bld
          AAperAs1=[6  7   0   25     5  14   16  5    10         2 ];  % Amino acid side groups per
          molecule of As1Cas
          AAperAs2=[6  4   2   25     3  24   17  15    12       2];  % Amino acid side groups per molecule
          of As2Cas
          AAperBCas=[4  4      0   18   5  11   16  9    4        1];  % Amino acid side groups per molecule
          of BCas
          AAperkCas=[5  4       2   13   3  9   13  14    9       0];  % Amino acid side groups per molecule
          of kCas
          % Conc_BLG in milk: 0.0032 kg/kg  accroding to Wasltra Jenness 1984
          % Can be 0.003 kg/kg according to Elofsson et al., 1997
```

```
% Density of BLG=1.035 kg/L
% MW_BLG=18.4 kg/mol   According to Meissner et al., 2015 and Walstra and Jenness 1984

Conc_BLG_milk=0.0032*1.035*1e6/18.4;   % Concentration BLG in milk ,µmol/L
Conc_ALA_milk=0.0012*1.035*1e6/14.176;   % Concentration ALA in milk ,µmol/L
Conc_Bld_milk=0.0004*1.035*1e6/66.267;   % Concentration Bld in milk ,µmol/L
Conc_as1cas_milk=0.0107*1.035*1e6/23.618;   % Concentration as1_cas in milk ,µmol/L
Conc_as2cas_milk=0.0026*1.035*1e6/25.23;   % Concentration as2_cas in milk ,µmol/L
Conc_Bcas_milk=0.0093*1.035*1e6/23.983;   % Concentration Bcas in milk ,µmol/L
Conc_kcas_milk=0.0033*1.035*1e6/19.025;   % Concentration kcas in milk ,µmol/L
BLG=ConcRatio*Conc_BLG_milk;    % BLG conc, µmol/L
ALA=ConcRatio*Conc_ALA_milk;    % ALA conc, µmol/L
Bld=ConcRatio*Conc_Bld_milk;    % Bld conc, µmol/L
As1_Cas=ConcRatio*Conc_as1cas_milk;    % As1_Cas conc, µmol/L
As2_Cas=ConcRatio*Conc_as2cas_milk;    % As2_Cas conc, µmol/L
B_Cas=ConcRatio*Conc_Bcas_milk;    % B_Cas conc, µmol/L
k_Cas=ConcRatio*Conc_kcas_milk;    % k_Cas conc, µmol/L
% Total concentration of AA from all proteins in milk, µmol/L
Conc_AA_milk=sum(AAperBLG)*Conc_BLG_milk+sum(AAperALA)*Conc_ALA_milk+...
sum(AAperBld)*Conc_Bld_milk+sum(AAperAs1)*Conc_as1cas_milk+...
sum(AAperAs2)*Conc_as2cas_milk+sum(AAperBCas)*Conc_Bcas_milk+...
sum(AAperkCas)*Conc_kcas_milk;
% Concentration of each AA in milk, µmol/L
Arg_initial=AAperBLG(1)*BLG+AAperALA(1)*ALA+AAperBld(1)*Bld+AAperAs1(1)*As1_Cas+
AAperAs2(1)*As2_Cas+AAperBCas(1)*B_Cas+AAperkCas(1)*k_Cas;
Asp_initial=AAperBLG(2)*BLG+AAperALA(2)*ALA+AAperBld(2)*Bld+AAperAs1(2)*As1_Cas+
AAperAs2(2)*As2_Cas+AAperBCas(2)*B_Cas+AAperkCas(2)*k_Cas;
Cys_initial=AAperBLG(3)*BLG+AAperALA(3)*ALA+AAperBld(3)*Bld+AAperAs1(3)*As1_Cas+
AAperAs2(3)*As2_Cas+AAperBCas(3)*B_Cas+AAperkCas(3)*k_Cas;
Glu_initial=AAperBLG(4)*BLG+AAperALA(4)*ALA+AAperBld(4)*Bld+AAperAs1(4)*As1_Cas+
AAperAs2(4)*As2_Cas+AAperBCas(4)*B_Cas+AAperkCas(4)*k_Cas;
His_initial=AAperBLG(5)*BLG+AAperALA(5)*ALA+AAperBld(5)*Bld+AAperAs1(5)*As1_Cas+
AAperAs2(5)*As2_Cas+AAperBCas(5)*B_Cas+AAperkCas(5)*k_Cas;
Lys_initial=AAperBLG(6)*BLG+AAperALA(6)*ALA+AAperBld(6)*Bld+AAperAs1(6)*As1_Cas+
AAperAs2(6)*As2_Cas+AAperBCas(6)*B_Cas+AAperkCas(6)*k_Cas;
Ser_initial=AAperBLG(7)*BLG+AAperALA(7)*ALA+AAperBld(7)*Bld+AAperAs1(7)*As1_Cas+
AAperAs2(7)*As2_Cas+AAperBCas(7)*B_Cas+AAperkCas(7)*k_Cas;
Thr_initial=AAperBLG(8)*BLG+AAperALA(8)*ALA+AAperBld(8)*Bld+AAperAs1(8)*As1_Cas+
AAperAs2(8)*As2_Cas+AAperBCas(8)*B_Cas+AAperkCas(8)*k_Cas;
Tyr_initial=AAperBLG(9)*BLG+AAperALA(9)*ALA+AAperBld(9)*Bld+AAperAs1(9)*As1_Cas+
AAperAs2(9)*As2_Cas+AAperBCas(9)*B_Cas+AAperkCas(9)*k_Cas;
% Phosphoserines initial concentrations, µmol/L
SerP3_initial=1559;
SerP_initial=100;
% Cit ,  PO4, CO3, SO4, Cl, Phosphate esters, Carboxylate, µmol/L
Cit_initial=9500*ConcRatio;
PO4_initial=20600*ConcRatio;
CO3_initial=400*ConcRatio;
SO4_initial=1200*ConcRatio;
Cl_initial=30.4e3*ConcRatio;
Esters_initial=2600*ConcRatio;
RCOO_initial=3100*ConcRatio;
```

```
% Cations: Ca,  Mg,      Na,       K
Ca_initial=29000*ConcRatio;
Mg_initial=4900*ConcRatio;
Na_initial=22000*ConcRatio;
K_initial=38300*ConcRatio;
Lactose=147e3*ConcRatio;
All_components(j)=Conc_AA_milk*ConcRatio+Cit_initial+PO4_initial+CO3_initial+...
SO4_initial+ Cl_initial+HCl(j)+Esters_initial+RCOO_initial+Ca_initial+Mg_initial+...
Na_initial+NaOH(j)+K_initial; % all components concentration, µmol/L
% 32 anions for initial guesses
C_A=ConcRatio*[Cit_initial*[0.0001; 0.01; 0.1]; PO4_initial*[0.2;0.1; 0.0001];...
CO3_initial*[1; 0.01]; SO4_initial*[0.001; 1]; Esters_initial*ones(2,1); ...
Cl_initial+HCl(j); RCOO_initial;...
Arg_initial*ones(1,1)/3; Asp_initial*ones(1,1)/3;...
Cys_initial*ones(1,1)/3; Glu_initial*ones(1,1)/3;...
His_initial*ones(1,1)/3; Lys_initial*ones(1,1)/3;...
Ser_initial*ones(1,1)/2; Thr_initial*ones(1,1)/2; Tyr_initial*ones(1,1)/3;...
SerP3_initial*0.001*ones(6,1); SerP_initial*ones(2,1); ...
0.1/10];
% Initial guess for 5 cations
C_C=ConcRatio*[Ca_initial; Mg_initial; NaOH(j)+Na_initial; K_initial; 0.1*100];   % Ca Mg Na
K H
% Ion pairs initial guess
C_CA(1:n_A, 1:n_C)=min(max(1e-20*ones(n_A, n_C),C_A(1:n_A)*C_C'./(K_eq*1e-
6)),C_A(1:n_A)*ones(1,n_C)+ones(n_A,1)*C_C');
xx=reshape(C_CA,n_A*n_C,1);
C_CA_initial=[xx(1:24); xx(27:28); xx(30:129); xx(132); xx(135); xx(137); xx(139);
xx(141:152); xx(158)];
        if j==1
        %  Anions (32), Cation (5), ionpairs (180), CPN  TCCT DCPD DCPA  HAP, Lactose
        µmol/L,
        x0=[C_A; C_C; C_CA_initial;0.01; 0.1; 0.1; 0.1; 0.1; 0.1 ];
        x=x0;
        flag='start';   % Newton's method will use more relaxation for the first solution.
        end
        if j==nlog+1
        x=x00;
        end
x0=x ;     % use previous solution
lb=zeros(length(x),1);
ub=All_components(j)*ones(length(x),1);
ub(32)=1e6;    % OH- ie 1 mol/L
ub(37)=1e6;    % H+
fanon=@(x) MyEquations(x, All_components(j), Cit_initial, ...
PO4_initial, CO3_initial, SO4_initial, Esters_initial, HCl(j)+Cl_initial,...
RCOO_initial, Arg_initial, Asp_initial, Cys_initial, Glu_initial, His_initial, Lys_initial,  ...
Ser_initial, Thr_initial, Tyr_initial, SerP3_initial, SerP_initial, ...
Ca_initial, Mg_initial, Na_initial+NaOH(j), K_initial, Lactose);
x=MyNewton(fanon,x0,maxits, tol, lb, ub, flag);
flag='good';
        if j==1
```

```
            x00=x;  % retain solution for neutral condition for 2nd half with NaOH
            end
        xsol(:,i)=x;     % record last solution µmol/L
        ysol(:,i)=y;   % Activity coefficient
        pH(i)=-log10(xsol(37,i)/1e6);
        Sat_TCCT(i)=x(182);       % saturation of tri calcium citrate tetrahydrate
        Sat_DCPD(i)=x(183);   % saturation of DCPD
        Sat_DCPA(i)=x(184);
        Sat_HAP(i)=x(185);
        a=y(1:181).*x(1:181)/1e6;   % activities in mol/L
        pKsp_OCP=72.5;
        pKsp_WH=81.7;  % Whitlockite
        pKsp_CDA=85.1;  % calcium def HAP
        Sat_OCP(i)=a(33)^(8/14)*a(5)^(2/14)*a(6)^(4/14)/(10^-(pKsp_OCP/14));  % Ca(8) HPO4(2)
        PO4(4) % 8+2+4=14
        Sat_WH(i)=(a(33)^10*a(5)*a(6)^6/(10^-pKsp_WH))^(1/17);  % Ca(10) HPO4 PO4(6)
        Sat_CDA(i)=(a(33)^9*a(5)*a(6)^5*a(32)/(10^-pKsp_CDA))^(1/16);  % Ca(9) HPO4 PO4(5) OH
        fprintf(' HCl conc, µmol/L     pH         %5.6f     %5.2f  \n', HCl(, pH(i))
        % for debugging
        C_Asol=xsol(15:31,i)';   % the first nine amino acids
        C_Casol=xsol(52:65,i)';  % the ions pairs corresponding to amino acids(Ca)
        C_Mgsol=xsol(81:97,i)';  % the ions pairs corresponding to amino acids(Mg)
        C_Nasol=xsol(113:129,i)';  % the ions pairs corresponding to amino acids(Na)
        C_Ksol=xsol(145:161,i)';  % the ions pairs corresponding to amino acids(K)
        C_Hsol=xsol(170:180,i)';  % the ions pairs corresponding to amino acids(H)
        % General method of net charge of the molecule
        % this method is based on the activities of species
        Electroneutrality(i)=sum(z(15:31).*xsol(15:31,i))+sum(z(52:65).*xsol(52:65,i))+...
        sum(z(81:97).*xsol(81:97,i))+sum(z(113:129).*xsol(113:129,i))+...
        sum(z(145:161).*xsol(145:161,i))+sum(z(170:180).*xsol(170:180,i));
        NetChargePerMolecule(i)=Electroneutrality(i)/(As1_Cas+As2_Cas+B_Cas+k_Cas+BLG+ALA+
        Bld);
        CPN(i)=xsol(181,i)/1e3;
        SerP3free(i)=(xsol(24,i)+xsol(25,i)+xsol(26,i)+xsol(27,i)+xsol(28,i)+xsol(29,i)+...
        xsol(61,i)+xsol(62,i)+xsol(63,i)+xsol(90,i)+xsol(91,i)+xsol(92,i)+...
        xsol(93,i)+xsol(94,i)+xsol(95,i)+xsol(122,i)+xsol(123,i)+xsol(124,i)+...
        xsol(125,i)+xsol(126,i)+xsol(127,i)+xsol(154,i)+xsol(155,i)+xsol(156,i)+...
        xsol(157,i)+xsol(158,i)+xsol(159,i)+xsol(179,i))/1e3;  % mM
        Rel_SerP3H2(i)=xsol(24,i)/(1000*SerP3free(i));
        Rel_SerP3H(i)=xsol(25,i)/(1000*SerP3free(i));
        Rel_SerP3(i)=xsol(26,i)/(1000*SerP3free(i));
        Rel_SerP3Ca2(i)=xsol(27,i)/(1000*SerP3free(i));
        Rel_SerP3CaH(i)=xsol(28,i)/(1000*SerP3free(i));
        Rel_SerP3Ca(i)=xsol(29,i)/(1000*SerP3free(i));
        Rel_SerP3H2Ca(i)=xsol(61,i)/(1000*SerP3free(i));
        Rel_SerP3Ca3(i)=xsol(62,i)/(1000*SerP3free(i));
        Rel_SerP3Ca2H(i)=xsol(63,i)/(1000*SerP3free(i));
        Rel_SerP3H3(i)=xsol(179,i)/(1000*SerP3free(i));
        end
[PI_charge, PI_index]=min(abs(NetChargePerMolecule));
figure
```

```
plot(pH, CPN,'k')
xlabel('pH','fontsize',13)
ylabel('Concentration, mmol/L','fontsize',13)
hold on
plot(pH, SerP3free,'k--')
legend('CPN','(SerP)_3')
set(gca,'fontsize',13)
title('a')
figure
plot(pH, NetChargePerMolecule,'k')
hold on
plot(pH(PI_index),NetChargePerMolecule(PI_index),'ko','linewidth',3)
xlabel('pH','fontsize',13)
ylabel('Net charge/molecule','fontsize',13)
txt= ['   \leftarrow IEP=', num2str(pH(PI_index))];
text(pH(PI_index),NetChargePerMolecule(PI_index)+1.2,txt)
grid on
set(gca,'fontsize',13)
title('c')
figure
plot(pH, Sat_DCPD,'k')
hold on
plot(pH, Sat_DCPA,'k-.')
plot(pH, Sat_HAP,'k:')
plot(pH, Sat_TCCT,'k-x')
plot(pH, Sat_OCP,'k.-')
plot(pH, Sat_CDA,'k--')
plot(pH, Sat_WH,'k-^')
legend('DCPD','DCPA','HAP','TCCT','OCP','CDA','WH','location','northwest')
xlabel('pH','fontsize',13)
ylabel('Saturation','fontsize',13)
set(gca,'fontsize',13)
title('b')
figure
plot(pH, Rel_SerP3H3,'k->')
hold on
plot(pH, Rel_SerP3Ca,'k--')
plot(pH, Rel_SerP3H2Ca,'k')
plot(pH, Rel_SerP3Ca2,'k.-')
plot(pH, Rel_SerP3,'k:')
plot(pH, Rel_SerP3Ca3,'k-.')
xlabel('pH','fontsize',13)
ylabel('(SerP)_3 relative concentration','fontsize',13)
legend('(SerP)_3H_3','(SerP)_3Ca','(SerP)_3H_2Ca','(SerP)_3Ca_2','(SerP)_3','(SerP)_3Ca_3')
set(gca,'fontsize',13)
title('d')
end

function f=MyEquations(x, All_components, Cit_initial, PO4_initial, ...
CO3_initial, SO4_initial, Esters_initial, Cl_initial, RCOO_initial, Arg_initial,...
Asp_initial, Cys_initial, Glu_initial, His_initial,Lys_initial, Ser_initial, Thr_initial,...
Tyr_initial, SerP3_initial, SerP_initial, Ca_initial, Mg_initial, Na_initial, K_initial, Lactose)
```

```
global z
global y
% Ref:Fennema and Mercado, 2015
[Ka]=1e-6*AssocConstants;   %L/µmol
Ka_CPN=9e-62;  % (µmol/L)^-22
Ksp_TCCT=2.29e-18*(1e6)^5;    % (µmol/L)^5   Gao et al., 2010
Ksp_DCPD= 2.09e-7*(1e6)^2;   %  (µmol/L)^2  Mekmene et al., 2012
Ksp_DCPA=4.0e-7*(1e6)^2;
Ksp_HAP=1.58e-117*(1e6)^18;
z_A=[ -1 -2 -3 -1 -2 -3 -1 -2 -1 -2 -1 -2 -1 -1   0  -1   -1  -1   0    0   -1    -1  -1 -4 -5  -6 -2 -3 -4 -1 -2 -1];
z_C=[2  2 1   1  1];     %  Ca Mg  Na   K  H
z=[z_A z_C ...
1 0 -1 1 0 -1 1 0 1 0 1 0 1 1     2 1 1  1  2 2 1 1 1   -2 0 -1 1  0 1 ...
1 0 -1 1 0 -1    1 0 1 0 1 0 1 1     2 1 1  1  2 2 1 1 1   -2 -3 -4 0 -1 -2 1 0 1 ...
0 -1 -2 0 -1 -2 0 -1 0 -1 0 -1 0 0  1 0 0  0  1 1 0 0 0   -3 -4 -5 -1 -2 -3 0 -1 0 ...
0 -1 -2 0 -1 -2 0 -1 0 -1 0 -1 0 0  1 0 0  0  1 1 0 0 0   -3 -4 -5 -1 -2 -3 0 -1 0 ...
0 0 0 0 0 0 0  1 0 0  0  1 1 0 0 0 -3 0 -4 0]';
sigma=1e-9*[0.65 0.75 0.65 0.69 0.35 0.65 0.6*ones(1,17) 0.45 0.45 0.45 0.35 0.35 0.45 0.65 0.65
0.35  ...
0.65  0.4 0.45 0.45  0.33...
0.4*ones(1,20)  0.5*ones(1,9)...
0.5*ones(1,32)...
0.25*ones(1,32)...
0.3*ones(1,32)...
0.55*ones(1,18) 0.22 0.495]';         % m
H2Cit=x(1);
HCit=x(2);
Cit=x(3);
H2PO4=x(4);
HPO4=x(5);
PO4=x(6);
HCO3=x(7);
CO3=x(8);
HSO4=x(9);
SO4=x(10);
Ester_1=x(11);
Ester_2=x(12);
Cl=x(13);
RCOO=x(14);
Arg=x(15);
Asp_=x(16);
Cys_=x(17);
Glu_=x(18);
His=x(19);
Lys=x(20);
Ser_=x(21);
Thr_=x(22);
Tyr_=x(23);
SerP3H2=x(24);
SerP3H=x(25);
SerP3=x(26);
```

```
SerP3Ca2=x(27);
SerP3CaH=x(28);
SerP3Ca=x(29);
PSerH=x(30);
PSer=x(31);
OH=x(32);
Ca=x(33);
Mg=x(34);
Na=x(35);
K=x(36);
H=x(37);

CaH2Cit=x(38);
CaHCit=x(39);
CaCit=x(40);
CaH2PO4=x(41);
CaHPO4=x(42);
CaPO4=x(43);
CaHCO3=x(44);
CaCO3=x(45);
CaHSO4=x(46);
CaSO4=x(47);
Ca_Ester_1=x(48);
Ca_Ester_2=x(49);
CaCl=x(50);
CaRCOO=x(51);
ArgCa=x(52);
AspCa=x(53);
CysCa=x(54);
GluCa=x(55);
HisCa=x(56);
LysCa=x(57);
SerCa=x(58);
ThrCa=x(59);
TyrCa=x(60);
SerP3H2Ca=x(61);
SerP3Ca3=x(62);
SerP3Ca2H=x(63);
PSerHCa=x(64);
PSerCa=x(65);
CaOH=x(66);
MgH2Cit=x(67);
MgHCit=x(68);
MgCit=x(69);
MgH2PO4=x(70);
MgHPO4=x(71);
MgPO4=x(72);
MgHCO3=x(73);
MgCO3=x(74);
MgHSO4=x(75);
MgSO4=x(76);
```

```
Mg_Ester_1=x(77);
Mg_Ester_2=x(78);
MgCl=x(79);
MgRCOO=x(80);
ArgMg=x(81);
AspMg=x(82);
CysMg=x(83);
GluMg=x(84);
HisMg=x(85);
LysMg=x(86);
SerMg=x(87);
ThrMg=x(88);
TyrMg=x(89);
SerP3H2Mg=x(90);
SerP3HMg=x(91);
SerP3Mg=x(92);
SerP3Ca2Mg=x(93);
SerP3CaHMg=x(94);
SerP3CaMg=x(95);
PSerHMg=x(96);
PSerMg=x(97);
MgOH=x(98);
NaH2Cit=x(99);
NaHCit=x(100);
NaCit=x(101);
NaH2PO4=x(102);
NaHPO4=x(103);
NaPO4=x(104);
NaHCO3=x(105);
NaCO3=x(106);
NaHSO4=x(107);
NaSO4=x(108);
Na_Ester_1=x(109);
Na_Ester_2=x(110);
NaCl=x(111);
NaRCOO=x(112);
ArgNa=x(113);
AspNa=x(114);
CysNa=x(115);
GluNa=x(116);
HisNa=x(117);
LysNa=x(118);
SerNa=x(119);
ThrNa=x(120);
TyrNa=x(121);
SerP3H2Na=x(122);
SerP3HNa=x(123);
SerP3Na=x(124);
SerP3Ca2Na=x(125);
SerP3CaHNa=x(126);
SerP3CaNa=x(127);
```

```
PSerHNa=x(128);
PSerNa=x(129);
NaOH=x(130);
KH2Cit=x(131);
KHCit=x(132);
KCit=x(133);
KH2PO4=x(134);
KHPO4=x(135);
KPO4=x(136);
KHCO3=x(137);
KCO3=x(138);
KHSO4=x(139);
KSO4=x(140);
K_Ester_1=x(141);
K_Ester_2=x(142);
KCl=x(143);
KRCOO=x(144);
ArgK=x(145);
AspK=x(146);
CysK=x(147);
GluK=x(148);
HisK=x(149);
LysK=x(150);
SerK=x(151);
ThrK=x(152);
TyrK=x(153);
SerP3H2K=x(154);
SerP3HK=x(155);
SerP3K=x(156);
SerP3Ca2K=x(157);
SerP3CaHK=x(158);
SerP3CaK=x(159);
PSerHK=x(160);
PSerK=x(161);
KOH=x(162);
H3Cit=x(163);
H3PO4=x(164);
H2CO3=x(165);
H2SO4=x(166);
H_ester=x(167);
HCl=x(168);
RCOOH=x(169);
ArgH=x(170);
Asp=x(171);
Cys=x(172);
Glu=x(173);
HisH=x(174);
LysH=x(175);
Ser=x(176);
Thr=x(177);
Tyr=x(178);
```

```
SerP3H3=x(179);
PSerH2=x(180);
CPN=x(181);
a_H=x(182);
sat_TCCT=x(182);
sat_DCPD=x(183);
Sat_DCPA=x(184);
Sat_HAP=x(185);
Arg_t=Arg_initial;
Asp_t=Asp_initial;
Cys_t=Cys_initial;
Glu_t=Glu_initial;
His_t=His_initial;
Lys_t=Lys_initial;
Ser_t=Ser_initial;
Thr_t=Thr_initial;
Tyr_t=Tyr_initial;
Cit_t=Cit_initial;
PO4_t=PO4_initial;
CO3_t=CO3_initial;
SO4_t=SO4_initial;
Cl_t=Cl_initial;
Esters_t=Esters_initial;
RCOO_t=RCOO_initial;
Ca_t=Ca_initial;
Mg_t=Mg_initial;
Na_t=Na_initial;
K_t=K_initial;
SerP_t=SerP_initial;
SerP3_t=SerP3_initial;
Density_soln=MilkDensityMolar((All_components)/1e6, 25);        % kg/m3
MW_Milk=0.150;          % MW of milk components 18 Oct 2018.xlsx
MW_water=0.01802;
MW_Cl=35.46;    % g/mol
MW_NaOH=40/1000;
C_H2O=(Density_soln-All_components*(1e3/1e6)*MW_Milk)/MW_water*1e6/1000;      %
mol/m3 converted to µmol/L
f=zeros(182,1);
N_A=6.022e23;      % Avogadro's number
rho=[x(1:181)]/1e6*N_A*1000;  % mol base
y=FreeIonMolarActCoeff(z, sigma, rho, (SerP3)/1e6);
a=y.*x(1:182);  %µmol/L
scale=1e4;
% Ca
f(1)=(Ka(1,1)*a(33)*a(1)-a(38))/scale;
f(2)=(Ka(2,1)*a(33)*a(2)-a(39))/scale;
f(3)=(Ka(3,1)*a(33)*a(3)-a(40))/scale;
f(4)=(Ka(4,1)*a(33)*a(4)-a(41))/scale;
f(5)=(Ka(5,1)*a(33)*a(5)-a(42))/scale;
f(6)=(Ka(6,1)*a(33)*a(6)-a(43))/1e6;
f(7)=(Ka(7,1)*a(33)*a(7)-a(44))/scale;
```

```
f(8)=(Ka(8,1)*a(33)*a(8)-a(45))/scale;
f(9)=(Ka(9,1)*a(33)*a(9)-a(46))/1e3;
f(10)=(Ka(10,1)*a(33)*a(10)-a(47))/scale;
f(11)=(Ka(11,1)*a(33)*a(11)-a(48))/scale;
f(12)=(Ka(12,1)*a(33)*a(12)-a(49))/scale;
f(13)=(Ka(13,1)*a(33)*a(13)-a(50))/2e5;
f(14)=(Ka(14,1)*a(33)*a(14)-a(51))/scale;
f(15)=(Ka(15,1)*a(33)*a(15)-a(52))/scale;
f(16)=(Ka(16,1)*a(33)*a(16)-a(53))/scale;
f(17)=(Ka(17,1)*a(33)*a(17)-a(54))/scale;
f(18)=(Ka(18,1)*a(33)*a(18)-a(55))/1e3;
f(19)=(Ka(19,1)*a(33)*a(19)-a(56))/scale;
f(20)=(Ka(20,1)*a(33)*a(20)-a(57))/scale;
f(21)=(Ka(21,1)*a(33)*a(21)-a(58))/scale;
f(22)=(Ka(22,1)*a(33)*a(22)-a(59))/scale;
f(23)=(Ka(23,1)*a(33)*a(23)-a(60))/scale;
f(24)=(Ka(24,1)*a(33)*a(24)-a(61))/scale;
f(25)=(Ka(25,1)*a(33)*a(25)-a(28))/scale;
f(26)=(Ka(26,1)*a(33)*a(26)-a(29))/scale;
f(27)=(Ka(27,1)*a(33)*a(27)-a(62))/scale;
f(28)=(Ka(28,1)*a(33)*a(28)-a(63))/scale;
f(29)=(Ka(29,1)*a(33)*a(29)-a(27))/scale;
f(30)=(Ka(30,1)*a(33)*a(30)-a(64))/scale;
f(31)=(Ka(31,1)*a(33)*a(31)-a(65))/scale;
f(32)=(Ka(32,1)*a(33)*a(32)-a(66))/scale;
% Mg
f(33)=(Ka(1,2)*a(34)*a(1)-a(67))/scale;
f(34)=(Ka(2,2)*a(34)*a(2)-a(68))/scale;
f(35)=(Ka(3,2)*a(34)*a(3)-a(69))/scale;
f(36)=(Ka(4,2)*a(34)*a(4)-a(70))/scale;
f(37)=(Ka(5,2)*a(34)*a(5)-a(71))/scale;
f(38)=(Ka(6,2)*a(34)*a(6)-a(72))/1e6;
f(39)=(Ka(7,2)*a(34)*a(7)-a(73))/scale;
f(40)=(Ka(8,2)*a(34)*a(8)-a(74))/scale;
f(41)=(Ka(9,2)*a(34)*a(9)-a(75))/1e3;
f(42)=(Ka(10,2)*a(34)*a(10)-a(76))/scale;
f(43)=(Ka(11,2)*a(34)*a(11)-a(77))/scale;
f(44)=(Ka(12,2)*a(34)*a(12)-a(78))/scale;
f(45)=(Ka(13,2)*a(34)*a(13)-a(79))/1e6;
f(46)=(Ka(14,2)*a(34)*a(14)-a(80))/scale;
f(47)=(Ka(15,2)*a(34)*a(15)-a(81))/scale;
f(48)=(Ka(16,2)*a(34)*a(16)-a(82))/scale;
f(49)=(Ka(17,2)*a(34)*a(17)-a(83))/scale;
f(50)=(Ka(18,2)*a(34)*a(18)-a(84))/1e3;
f(51)=(Ka(19,2)*a(34)*a(19)-a(85))/scale;
f(52)=(Ka(20,2)*a(34)*a(20)-a(86))/scale;
f(53)=(Ka(21,2)*a(34)*a(21)-a(87))/scale;
f(54)=(Ka(22,2)*a(34)*a(22)-a(88))/scale;
f(55)=(Ka(23,2)*a(34)*a(23)-a(89))/scale;
f(56)=(Ka(24,2)*a(34)*a(24)-a(90))/scale;
f(57)=(Ka(25,2)*a(34)*a(25)-a(91))/scale;
```

```
f(58)=(Ka(26,2)*a(34)*a(26)-a(92))/scale;
f(59)=(Ka(27,2)*a(34)*a(27)-a(93))/scale;
f(60)=(Ka(28,2)*a(34)*a(28)-a(94))/scale;
f(61)=(Ka(29,2)*a(34)*a(29)-a(95))/scale;
f(62)=(Ka(30,2)*a(34)*a(30)-a(96))/scale;
f(63)=(Ka(31,2)*a(34)*a(31)-a(97))/scale;
f(64)=(Ka(32,2)*a(34)*a(32)-a(98))/scale;
% Na
f(65)=(Ka(1,3)*a(35)*a(1)-a(99))/scale;
f(66)=(Ka(2,3)*a(35)*a(2)-a(100))/scale;
f(67)=(Ka(3,3)*a(35)*a(3)-a(101))/scale;
f(68)=(Ka(4,3)*a(35)*a(4)-a(102))/scale;
f(69)=(Ka(5,3)*a(35)*a(5)-a(103))/scale;
f(70)=(Ka(6,3)*a(35)*a(6)-a(104))/1e6;
f(71)=(Ka(7,3)*a(35)*a(7)-a(105))/scale;
f(72)=(Ka(8,3)*a(35)*a(8)-a(106))/scale;
f(73)=(Ka(9,3)*a(35)*a(9)-a(107))/1e3;
f(74)=(Ka(10,3)*a(35)*a(10)-a(108))/scale;
f(75)=(Ka(11,3)*a(35)*a(11)-a(109))/scale;
f(76)=(Ka(12,3)*a(35)*a(12)-a(110))/scale;
f(77)=(Ka(13,3)*a(35)*a(13)-a(111))/scale;
f(78)=(Ka(14,3)*a(35)*a(14)-a(112))/scale;
f(79)=(Ka(15,3)*a(35)*a(15)-a(113))/scale;
f(80)=(Ka(16,3)*a(35)*a(16)-a(114))/scale;
f(81)=(Ka(17,3)*a(35)*a(17)-a(115))/scale;
f(82)=(Ka(18,3)*a(35)*a(18)-a(116))/1e3;
f(83)=(Ka(19,3)*a(35)*a(19)-a(117))/scale;
f(84)=(Ka(20,3)*a(35)*a(20)-a(118))/scale;
f(85)=(Ka(21,3)*a(35)*a(21)-a(119))/scale;
f(86)=(Ka(22,3)*a(35)*a(22)-a(120))/scale;
f(87)=(Ka(23,3)*a(35)*a(23)-a(121))/scale;
f(88)=(Ka(24,3)*a(35)*a(24)-a(122))/scale;
f(89)=(Ka(25,3)*a(35)*a(25)-a(123))/scale;
f(90)=(Ka(26,3)*a(35)*a(26)-a(124))/scale;
f(91)=(Ka(27,3)*a(35)*a(27)-a(125))/scale;
f(92)=(Ka(28,3)*a(35)*a(28)-a(126))/scale;
f(93)=(Ka(29,3)*a(35)*a(29)-a(127))/scale;
f(94)=(Ka(30,3)*a(35)*a(30)-a(128))/scale;
f(95)=(Ka(31,3)*a(35)*a(31)-a(129))/scale;
f(96)=(Ka(32,3)*a(35)*a(32)-a(130))/scale;
% K
f(97)=(Ka(1,4)*a(36)*a(1)-a(131))/scale;
f(98)=(Ka(2,4)*a(36)*a(2)-a(132))/scale;
f(99)=(Ka(3,4)*a(36)*a(3)-a(133))/scale;
f(100)=(Ka(4,4)*a(36)*a(4)-a(134))/scale;
f(101)=(Ka(5,4)*a(36)*a(5)-a(135))/scale;
f(102)=(Ka(6,4)*a(36)*a(6)-a(136))/1e6;
f(103)=(Ka(7,4)*a(36)*a(7)-a(137))/scale;
f(104)=(Ka(8,4)*a(36)*a(8)-a(138))/scale;
f(105)=(Ka(9,4)*a(36)*a(9)-a(139))/1e3;
f(106)=(Ka(10,4)*a(36)*a(10)-a(140))/scale;
```

```
f(107)=(Ka(11,4)*a(36)*a(11)-a(141))/scale;
f(108)=(Ka(12,4)*a(36)*a(12)-a(142))/scale;
f(109)=(Ka(13,4)*a(36)*a(13)-a(143))/1e6;
f(110)=(Ka(14,4)*a(36)*a(14)-a(144))/scale;
f(111)=(Ka(15,4)*a(36)*a(15)-a(145))/scale;
f(112)=(Ka(16,4)*a(36)*a(16)-a(146))/scale;
f(113)=(Ka(17,4)*a(36)*a(17)-a(147))/scale;
f(114)=(Ka(18,4)*a(36)*a(18)-a(148))/1e3;
f(115)=(Ka(19,4)*a(36)*a(19)-a(149))/scale;
f(116)=(Ka(20,4)*a(36)*a(20)-a(150))/scale;
f(117)=(Ka(21,4)*a(36)*a(21)-a(151))/scale;
f(118)=(Ka(22,4)*a(36)*a(22)-a(152))/scale;
f(119)=(Ka(23,4)*a(36)*a(23)-a(153))/scale;
f(120)=(Ka(24,4)*a(36)*a(24)-a(154))/scale;
f(121)=(Ka(25,4)*a(36)*a(25)-a(155))/scale;
f(122)=(Ka(26,4)*a(36)*a(26)-a(156))/scale;
f(123)=(Ka(27,4)*a(36)*a(27)-a(157))/scale;
f(124)=(Ka(28,4)*a(36)*a(28)-a(158))/scale;
f(125)=(Ka(29,4)*a(36)*a(29)-a(159))/scale;
f(126)=(Ka(30,4)*a(36)*a(30)-a(160))/scale;
f(127)=(Ka(31,4)*a(36)*a(31)-a(161))/scale;
f(128)=(Ka(32,4)*a(36)*a(32)-a(162))/scale;
% H
f(129)=(Ka(1,5)*a(37)*a(1)-a(163))/scale;
f(130)=(Ka(2,5)*a(37)*a(2)-a(1))/scale;
f(131)=(Ka(3,5)*a(37)*a(3)-a(2))/scale;
f(132)=(Ka(4,5)*a(37)*a(4)-a(164))/scale;
f(133)=(Ka(5,5)*a(37)*a(5)-a(4))/scale;
f(134)=(Ka(6,5)*a(37)*a(6)-a(5))/1e8;
f(135)=(Ka(7,5)*a(37)*a(7)-a(165))/scale;
f(136)=(Ka(8,5)*a(37)*a(8)-a(7))/1e5;
f(137)=(Ka(9,5)*a(37)*a(9)-a(166))/1e3;
f(138)=(Ka(10,5)*a(37)*a(10)-a(9))/scale;
f(139)=(Ka(11,5)*a(37)*a(11)-a(167))/scale;
f(140)=(Ka(12,5)*a(37)*a(12)-a(11))/scale;
f(141)=(Ka(13,5)*a(37)*a(13)-a(168))/1e6;
f(142)=(Ka(14,5)*a(37)*a(14)-a(169))/scale;
f(143)=(Ka(15,5)*a(37)*a(15)-a(170))/1e10;
f(144)=(Ka(16,5)*a(37)*a(16)-a(171))/scale;
f(145)=(Ka(17,5)*a(37)*a(17)-a(172))/1e5;
f(146)=(Ka(18,5)*a(37)*a(18)-a(173))/1e3;
f(147)=(Ka(19,5)*a(37)*a(19)-a(174))/scale;
f(148)=(Ka(20,5)*a(37)*a(20)-a(175))/1e8;
f(149)=(Ka(21,5)*a(37)*a(21)-a(176))/1e11;
f(150)=(Ka(22,5)*a(37)*a(22)-a(177))/1e11;
f(151)=(Ka(23,5)*a(37)*a(23)-a(178))/1e7;
f(152)=(Ka(24,5)*a(37)*a(24)-a(179))/scale;
f(153)=(Ka(25,5)*a(37)*a(25)-a(24))/scale;
f(154)=(Ka(26,5)*a(37)*a(26)-a(25))/scale;
% f(155)=(Ka(27,5)*a(36)*a(27)-a(63))/scale;
% f(156)=(Ka(28,5)*a(36)*a(28)-a(61))/scale;
```

```
% f(157)=(Ka(29,5)*a(36)*a(29)-a(28))/scale;      % Remove
f(155)=(Ka(30,5)*a(37)*a(30)-a(180))/scale;
f(156)=(Ka(31,5)*a(37)*a(31)-a(30))/scale;
f(157)=(Ka(32,5)*a(37)*a(32)-C_H2O)/1e7;
f(158)=sum(z(1:181).*x(1:181))/sum(x(1:181))/1e0;  % electroneutrality
f(159)=(SerP3_t-(3*SerP3H2+ 3*SerP3H+3*SerP3+3*SerP3Ca2+...
3*SerP3CaH+3*SerP3Ca+3*SerP3H2Ca+3*SerP3Ca3+3*SerP3Ca2H+...
3*SerP3H2Mg+ 3*SerP3HMg+3*SerP3Mg+3*SerP3Ca2Mg+...
3*SerP3CaHMg+3*SerP3CaMg+3*SerP3H2Na+3*SerP3HNa+...
3*SerP3Na+3*SerP3Ca2Na+3*SerP3CaHNa+3*SerP3CaNa+...
3*SerP3H2K+3*SerP3HK+3*SerP3K+3*SerP3Ca2K+3*SerP3CaHK+...
3*SerP3CaK+3*SerP3H3+CPN))/1e5;  % total SerP3
f(160)=(SerP_t-
(PSerCa+PSerHCa+PSerMg+PSerHMg+PSerHNa+PSerNa+PSerH+PSer+PSerH2+PSerHK+PSerK))/1e5;
% Total PSer
f(161)=(RCOO_t-(NaRCOO+RCOO+CaRCOO+MgRCOO+KRCOO+RCOOH))/1e5;  % total RCOO
f(162)=(Ca_t-(Ca+CaH2Cit+CaHCit+CaCit+CaH2PO4+CaHPO4+CaPO4+CaHCO3+CaCO3+...
CaHSO4+CaSO4+Ca_Ester_1+Ca_Ester_2+SerP3H2Ca+SerP3CaH+SerP3Ca+...
3*SerP3Ca3+2*SerP3Ca2H+2*SerP3Ca2+PSerHCa+PSerCa+CaRCOO+CaCl+CaOH+...
ArgCa+AspCa+CysCa+GluCa+HisCa+LysCa+SerCa+ThrCa+TyrCa+13.2*CPN))/1e5;  % total Ca
f(163)=(Mg_t-(Mg+MgH2Cit+MgHCit+MgCit+MgH2PO4+MgHPO4+MgPO4+MgHCO3+MgCO3+...
MgHSO4+MgSO4+Mg_Ester_1+Mg_Ester_2+SerP3H2Mg+SerP3HMg+SerP3Mg+...
3*SerP3Ca2Mg+2*SerP3CaHMg+2*SerP3CaMg+PSerHMg+PSerMg+MgRCOO+MgCl+MgOH+...
ArgMg+AspMg+CysMg+GluMg+HisMg+LysMg+SerMg+ThrMg+TyrMg+CPN))/scale; % Mg total
f(164)=(Na_t-(Na+NaH2Cit+NaHCit+NaCit+NaH2PO4+NaHPO4+NaPO4+NaHCO3+NaCO3+...
NaHSO4+NaSO4+Na_Ester_1+Na_Ester_2+SerP3H2Na+SerP3HNa+SerP3Na+...
3*SerP3Ca2Na+2*SerP3CaHNa+2*SerP3CaNa+PSerHNa+PSerNa+NaRCOO+NaCl+NaOH+
ArgNa+AspNa+CysNa+GluNa+HisNa+LysNa+SerNa+ThrNa+TyrNa))/scale; % Na total
f(165)=(K_t-(K+KH2Cit+KHCit+KCit+KH2PO4+KHPO4+KPO4+KHCO3+KCO3+...
KHSO4+KSO4+K_Ester_1+K_Ester_2+SerP3H2K+SerP3HK+SerP3K+...
3*SerP3Ca2K+2*SerP3CaHK+2*SerP3CaK+PSerHK+PSerK+KRCOO+KCl+KOH+...
ArgK+AspK+CysK+GluK+HisK+LysK+SerK+ThrK+TyrK))/1e6; % K total
f(166)=(Cit_t-(H2Cit+HCit+Cit+CaH2Cit+CaHCit+CaCit+MgH2Cit+MgHCit+MgCit+...
NaH2Cit+NaHCit+NaCit+KH2Cit+KHCit+KCit+H3Cit+1.3*CPN))/1e5;  % total Cit

f(167)=(Cl_t-(Cl+HCl+NaCl+CaCl+KCl+MgCl))/1e5;  % total Cl
f(168)=(PO4_t-(H2PO4+HPO4+PO4+CaH2PO4+CaHPO4+CaPO4+MgH2PO4+MgHPO4+MgPO4+...
NaH2PO4+NaHPO4+NaPO4+KH2PO4+KHPO4+KPO4+H3PO4+6.5*CPN))/scale;  % Total PO4
f(169)=(SO4_t-(HSO4+SO4+CaHSO4+CaSO4+MgHSO4+MgSO4+...
NaHSO4+NaSO4+KHSO4+KSO4+H2SO4))/scale;  % Total SO4
f(170)=(CO3_t-(HCO3+CO3+CaHCO3+CaCO3+MgHCO3+MgCO3+...
NaHCO3+NaCO3+KHCO3+KCO3+H2CO3))/scale;  % total CO3
f(171)=(Esters_t-(H_ester+Ester_1+Ester_2+Ca_Ester_1+Ca_Ester_2+...
Mg_Ester_1+Mg_Ester_2+Na_Ester_1+Na_Ester_2+K_Ester_1+K_Ester_2))/scale;  % total Esters
f(172)=(Arg_t-(Arg+ArgH+ArgCa+ArgMg+ArgNa+ArgK))/1e5;  % total Arg
f(173)=(Asp_t-(Asp_+Asp+AspCa+AspMg+AspNa+AspK))/1e5;  % total Asp
f(174)=(Cys_t-(Cys_+Cys+CysCa+CysMg+CysNa+CysK))/1e5;  % total Cys
f(175)=(Glu_t-(Glu_+Glu+GluCa+GluMg+GluNa+GluK))/1e5;  % total Glu
f(176)=(His_t-(His+HisH+HisCa+HisMg+HisNa+HisK))/1e5;  % total His
f(177)=(Lys_t-(Lys+LysH+LysCa+LysMg+LysNa+LysK))/1e5;  % total Lys
f(178)=(Ser_t-(Ser_+Ser+SerCa+SerMg+SerNa+SerK))/1e5;  % total Ser
f(179)=(Thr_t-(Thr_+Thr+ThrCa+ThrMg+ThrNa+ThrK))/1e5;  % total Thr
```

```
f(180)=(Tyr_t-(Tyr_+Tyr+TyrCa+TyrMg+TyrNa+TyrK))/1e5;  % total Tyr
f(181)=(Ka_CPN*a(33)^13.2*a(3)^1.3*a(5)^6.5*a(34)*SerP3-CPN)/1e0;  % here we are assuming
full activity of SerP3 and CPN
f(182)=(a(3)^2*a(33)^3/Ksp_TCCT-sat_TCCT)/1e0;
f(183)=(a(5)*a(33)/Ksp_DCPD-sat_DCPD)/1e0;
f(184)=(a(33)*a(5)/Ksp_DCPA-Sat_DCPA)/1e1;
f(185)=(a(33)^10*a(6)^6*a(32)^2/Ksp_HAP-Sat_HAP)/1e2;
f(186)=a_H-a(37);
end

function [K_eq]=AssocConstants
%  25 °C
% L/mol
T=25+273.15;
logKw=-4787.3/T-7.1332*log10(T)-0.010365*T+22.801;    % Harned and Cook 1937
Kw=10^logKw;  % mol/L
Kw1=55.5/Kw;    % 55.5 mol/L/1e-14  in normal association constant form
% Ca       Mg      Na       K      H
K_eq=[28        15        1         1         1380;   % H2Cit
876       402       10       10       6e4;      % HCit
1.65e5   1.11e5  20       16       2.57e6;   % Cit
11           12        1         1          200;     % H2PO4
642       838       17     13       2.87e7;   %HPO4
2.88e6  8.35e4  100     100     2.47e12;  % PO4
23           19        1         1          2.25e6;    % H2CO3
1.4e3     758      10       10         2.13e10;   % HCO3
10          10        1         1          10^-8;       % H2SO4
204       170      5         7          98;           % HSO4
10          10        1         1          10^-10;     % GlcPH
316       295      7         5          3.19e6;       % GlcP
9.4         5.6     0.9       1          10^-9.3;       % HCl
15          19       0.7      0.7        5.71e4;       % RCOO
0.1         0.1     0.1      0.1         1/10^(-12.52);   % Arg
0.1         0.1     0.1      0.1         1/10^(-3.6);     % Asp
0.1         0.1     0.1      0.1         1/10^(-8.50);     % Cys
0.1         0.1     0.1      0.1         1/10^(-4.0);     % Glu
0.1         0.1     0.1      0.1         1/10^(-6.00);     % His
0.1         0.1     0.1      0.1         1/10^(-10.95);  % Lys
0.1         0.1     0.1      0.1         1/10^(-13.22);  % Ser
0.1         0.1     0.1      0.1         1/10^(-13.22);  % Thr
0.1         0.1     0.1      0.1         1/10^(-9.60);     % Tyr
380       100        1         1         7.94e5;  %SerP3H2
380       100        1         1         7.94e5;  %SerP3H
3000    3000       1         1         1e7;   % SerP3
380       100        1         1         7.85e5;  %SerP3Ca2
380       100        1         1         7.94e5;  %SerP3CaH
380       100        1         1         7.94e5;  %SerP3Ca
10          10          1         1          200;   % HPSer
380       380     16.9      16.9      7.94e5;   % PSer
25.11    162.18  0.2       0.2       Kw1];              % OH
end
```